Distribution Agreement

In presenting this thesis or dissertation as a partial fulfillment of the requirements for an advanced degree from Emory University, I hereby grant to Emory University and its agents the non-exclusive license to archive, make accessible, and display my thesis or dissertation in whole or in part in all forms of media, now or hereafter known, including display on the world wide web. I understand that I may select some access restrictions as part of the online submission of this thesis or dissertation. I retain all ownership rights to the copyright of the thesis or dissertation. I also retain the right to use in future works (such as articles or books) all or part of this thesis or dissertation.

Signature:

_____ _____

Darian Williams Date

The Role of Mechanosensitive Kallikrein-Related Peptidase 10 in Endothelial Biology and Atherosclerosis

By

Darian Williams
Doctor of Philosophy

Graduate Division of Biological and Biomedical Science
Molecular and Systems Pharmacology

_____ [Advisor's signature]
Hanjoong Jo, PhD
Advisor

_____ [Member's signature]
John Hepler, PhD
Committee Member

_____ [Member's signature]
Morley Hollenberg, MD, PhD
Committee Member

_____ [Member's signature]
Stephen Traynelis, PhD
Committee Member

_____ [Member's signature]
Wilbur Lam, MD, PhD
Committee Member

Accepted:

_____
Kimberly Jacob Arriola, Ph.D, MPH
Dean of the James T. Laney School of Graduate Studies

_____
Date

The Role of Mechanosensitive Kallikrein-Related Peptidase 10 in Endothelial Biology and Atherosclerosis

By

Darian Williams
B.A., University of Colorado, Boulder, 2016

Advisor: Hanjoong Jo, PhD

An abstract of

A dissertation submitted to the Faculty of the James T.

Laney School of Graduate Studies of Emory University

in partial fulfillment of the requirements for the degree of

Doctor of Philosophy in Graduate Division of Biological and Biomedical Science

Molecular and Systems Pharmacology

October 26th, 2021

Abstract

The Role of Mechanosensitive Kallikrein-Related Peptidase 10 in Endothelial Biology and Atherosclerosis

By

Darian Williams

Introduction: Atherosclerosis preferentially occurs in arterial regions exposed to disturbed blood flow (*d-flow*), while regions exposed to stable flow (*s-flow*) are protected. The proatherogenic and atheroprotective effects of *d-flow* and *s-flow* are mediated in part by the global changes in endothelial cell gene expression, which regulates endothelial dysfunction, inflammation, and atherosclerosis. Previously, we identified Kallikrein-Related Peptidase 10 (KLK10, a secreted serine protease) as a flow-sensitive gene in arterial endothelial cells, but its role in endothelial biology and atherosclerosis was unknown.

Methods and Results: Here, we show that KLK10 is upregulated under *s-flow* conditions and downregulated under *d-flow* conditions using *in vivo* mouse models and *in vitro* studies with cultured endothelial cells (ECs). Single-cell RNA sequencing (scRNAseq) and scATAC sequencing (scATACseq) study using the partial carotid ligation mouse model showed flow-regulated KLK10 expression at the epigenomic and transcription levels. Functionally, KLK10 protected against *d-flow*-induced inflammation and permeability dysfunction in human artery ECs (HAECs). Further, treatment of mice *in vivo* with rKLK10 decreased arterial endothelial inflammation in *d-flow* regions. Additionally, rKLK10 injection or ultrasound-mediated transfection of KLK10-expressing plasmids inhibited atherosclerosis in *ApoE*$^{-/-}$ mice. Studies using pharmacological inhibitors and siRNAs revealed that the anti-inflammatory effects of KLK10 were mediated by a Protease Activated Receptors (PAR1/2)-dependent manner. However, unexpectedly, KLK10 did not cleave the PARs. Through a proteomics study, we identified HTRA1 (High-temperature requirement A serine peptidase 1), which bound and cleaved KLK10. Further, siRNA knockdown of HTRA1 prevented KLK10's anti-inflammatory and barrier protective function in HAECs, suggesting that HTRA1 regulates KLK10 function. Moreover, KLK10 expression was significantly reduced in human coronary arteries with advanced atherosclerotic plaques compared to those with less severe plaques.

Conclusion: KLK10 is a flow-sensitive endothelial protein and, in collaboration with HTRA1, serves as an anti-inflammatory, barrier-protective, and anti-atherogenic factor.

The Role of Mechanosensitive Kallikrein-Related Peptidase 10 in Endothelial Biology and Atherosclerosis

By

Darian Williams
B.A., University of Colorado, Boulder, 2016

Advisor: Hanjoong Jo, PhD

A dissertation submitted to the Faculty of the James T.

Laney School of Graduate Studies of Emory University

in partial fulfillment of the requirements for the degree of

Doctor of Philosophy in Graduate Division of Biological and Biomedical Science

Molecular and Systems Pharmacology

October 26th, 2021

Acknowledgments

I would like to first and foremost express my deepest appreciation to my advisor, Dr. Hanjoong Jo, who provided exceptional support and guidance in my journey to obtain my PhD. I joined Dr. Jo's biomedical engineering lab in November 2016 as a pharmacology student with no background in biomedical engineering. Dr. Jo took a chance on me and gave me the opportunity to work on an extremely exciting project with the potential for significant implications for the vascular and mechanobiology fields. Through thick and thin, Dr. Jo saw the best in me and his mentoring pushed me to strive to become the best scientist I could be. Without Dr. Jo's support, it is clear the success we have had with this project would not have been possible, so thank you.

I would next like to thank my committee members, Dr. Steven Traynelis, Dr. John Hepler, Dr. Wilbur Lam, and Dr. Morley Hollenberg for their insightful contribution to my PhD research. During every committee meeting, these professors gave their heartfelt support for me as a scientist and made it clear the impact they thought I could have on the field of Kallikreins and vascular biology. Their positive reinforcement and interest in my research drove me to reach higher standards for myself and my research.

Next, I must thank my collaborators both in the Jo lab and outside, who I had a great pleasure working with. Specifically, I would like to thank Dr. Marwa Mahmoud who laid the foundation for this project and enthusiastically welcomed me into the lab in 2016. I must also thank Dr. Sandeep Kumar and Dong-Wong Kang, both of whom were always available to help me through difficult research problems and help me complete countless animal studies. Additionally, Dr. Aitor Andueza provided significant contributions both experimentally and

intellectually. Lastly, thank you to everyone who has worked in the Jo lab, I am certain everyone in the lab in one way or another has contributed to this project or my development as a scientist.

Last but not least, I would like to give a special appreciation to my family and all the friends I have made during my time here at Emory. My parents, Christina and Eric Pagan, as well as my sister, Imani Williams, always believed in me, even during the times I did not believe in myself. Their guidance helped me through difficult times I could not be more appreciative. I must also thank Dr. David McAlister, who has been a role model to me ever since I was a kid. As an underrepresented PhD holder, David paved the path for me in biomedical research and instilled in me the values of hard work and dedication to my work. It is very clear to me without David, I would not be in the position I am today.

To finish, I would like to thank everyone who has been in my corner from the beginning, including family members, friends, those who have left us, and anybody I had the pleasure of spending time with at Emory. This experience would not be the same without you and I am sincerely appreciative of that.

TABLE OF CONTENTS

LIST OF FIGURES

LIST OF TABLES

SUMMARY

Atherosclerosis preferentially occurs in arterial regions exposed to disturbed blood flow (*d-flow*), while regions exposed to stable flow (*s-flow*) are protected. The proatherogenic and atheroprotective effects of *d-flow* and *s-flow* are mediated in part by the global changes in endothelial cell gene expression, which regulates endothelial dysfunction, inflammation, and atherosclerosis. Previously, we identified Kallikrein-Related Peptidase 10 (KLK10, a secreted serine protease) as a flow-sensitive gene in arterial endothelial cells, but its role in endothelial biology and atherosclerosis was unknown. Here, we show that KLK10 is upregulated under *s-flow* conditions and downregulated under *d-flow* conditions using *in vivo* mouse models and *in vitro* studies with cultured endothelial cells (ECs). Single-cell RNA sequencing (scRNAseq) and scATAC sequencing (scATACseq) study using the partial carotid ligation mouse model showed flow-regulated KLK10 expression at the epigenomic and transcription levels. Functionally, KLK10 protected against *d-flow*-induced inflammation and permeability dysfunction in human artery ECs (HAECs). Further, treatment of mice *in vivo* with rKLK10 decreased arterial endothelial inflammation in *d-flow* regions. Additionally, rKLK10 injection or ultrasound-mediated transfection of KLK10-expressing plasmids inhibited atherosclerosis in *ApoE*$^{-/-}$ mice. Studies using pharmacological inhibitors and siRNAs revealed that the anti-inflammatory effects of KLK10 were mediated by a Protease Activated Receptors (PAR1/2)-dependent manner. However, unexpectedly, KLK10 did not cleave the PARs. Through a proteomics study, we identified HTRA1 (High-temperature requirement A serine peptidase 1), which bound and cleaved KLK10. Further, siRNA knockdown of HTRA1 prevented KLK10's anti-inflammatory and barrier protective function in HAECs, suggesting that HTRA1 regulates KLK10 function. Moreover, KLK10 expression was significantly reduced in human coronary arteries with advanced

atherosclerotic plaques compared to those with less severe plaques. KLK10 is a flow-sensitive endothelial protein and, in collaboration with HTRA1, serves as an anti-inflammatory, barrier-protective, and anti-atherogenic factor.

1. INTRODUCTION

Atherosclerosis is a chronic inflammatory disease of the arterial vessel which underlies the occurrence of myocardial infarction, ischemic stroke, and peripheral arterial disease [6]. The disease is characterized by the initial development of a lesion in the arterial wall called a "fatty streak," which contains lipid-rich macrophages [7, 8]. Sustained chronic exposure to pro-inflammatory molecules from leukocytes and lipids increases vascular dysfunction and the narrowing of the arterial lumen, leading to the development of an atheromatous plaque [9]. In severe cases, the atheromatous plaque can occlude blood flow or rupture, leading to a myocardial infarction or stroke (Figure 1.1).

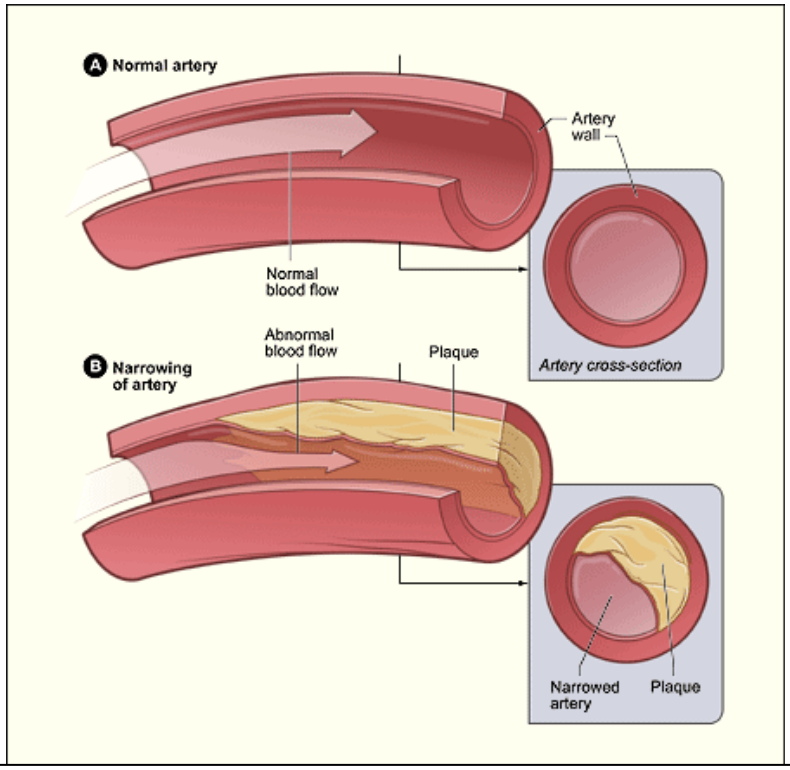

Figure 1.1 **Atherosclerotic disease progression.** (a) Depiction of a healthy artery with normal blood flow. (b) Depiction of a diseased artery with an atheromatous plaque and occluded blood flow. Insets show cross sections from the healthy and diseased artery. Adapted from vascularsurgery.ucsf.edu

Major risk factors for the development of atherosclerosis include unhealthy blood cholesterol levels (specifically high LDL and low HDL cholesterol), high blood pressure, smoking, insulin resistance, diabetes, obesity, lack of physical activity, unhealthy diet, older age, and a familial history of early heart disease[10]. Many of these risk factors can be mitigated with heart-healthy lifestyle changes such as better diet and increased exercise, however, in cases where these changes are not sufficient to decrease atherosclerosis, medications such as cholesterol lowering statins[11] or the new PCSK9 inhibitors[12, 13] can be used. Alternatively, in the most severe cases a medical procedure or intervention involving stents may be necessary[14].

Despite the success of stents and cholesterol lowering drugs for decreasing the incidence of atherosclerosis, heart attacks and ischemic strokes continue to be the leading causes of death in the Western world., killing more than 500,000 people anually[15, 16]. One major issue with current cholesterol lowering drugs is that they must still be taken in conjunction with a heart healthy lifestyle, indicating factors other than cholesterol still contribute to atherosclerosis progression[17]. Therefore, new therapeutics are still needed that target atherosclerosis at the source of the disease.

It is well-known that atherosclerosis preferentially occurs in branched or curved regions of the vasculature exposed to disturbed blood flow (*d-flow*), while areas of stable blood flow (*s-flow*) are protected from atherosclerosis[18-20]. Dysfunction of the endothelial cells (EC) in lesion-prone areas is an important contributor to the development of atherosclerosis, however, the underlying mechanisms by which blood flow regulates endothelial dysfunction and atherosclerosis are still unclear. Using the partial carotid ligation (PCL) mouse model of atherosclerosis and transcriptomic studies, our laboratory previously identified hundreds of endothelial cell genes that

change by *d-flow* in the left carotid artery (LCA) compared to the *s-flow* in the right carotid artery (RCA), termed flow-sensitive genes[3, 21]. Among the flow-sensitive genes were well-known mechanosensitive genes Krüppel-like Factor 2 (KLF2)[22], Krüppel-like Factor 4 (KLF4)[23], bone morphogenetic protein 4[24], hypoxia inducible factor-1a pathway regulating gene UBE2c[25, 26], sterol regulatory element binding protein 2[27], PPAP2B[28], ZBTB46[29], JCAD/KIAA1462[30], JMJD2b[31], endothelial nitric oxide synthase (eNOS)[32], and several flow-sensitive microRNAs[33]. Interestingly, Kallikrein related-peptidase 10 (*KLK10)*, a secreted serine protease, was identified as one of the most flow-sensitive; with high expression under *s-flow* and low expression under *d-flow* conditions[3]. However, its role in endothelial function and atherosclerosis has never been explored.

Because KLK10 is upregulated under *s-flow* conditions where atherosclerosis and inflammation are prevented, **we hypothesize that KLK10 mediates the beneficial effect of *s-flow* on the endothelium by inhibiting several aspects of endothelial dysfunction. Furthermore, we hypothesize loss of KLK10 under *d-flow* conditions promotes endothelial dysfunction and atherosclerosis.**

In Aim 1, we studied the regulation of KLK10 expression by flow in the PCL mouse model and in Human Aortic Endothelial Cells (HAECs) exposed to shear stress *in vitro*. Using qPCR, western blotting, and immunostaining, we found KLK10 to be upregulated by *s-flow* and downregulated by *d-flow* at the mRNA and protein level. Single-cell RNA sequencing (scRNAseq) and scATAC sequencing (scATACseq) study using the PCL mouse model revealed flow regulated

KLK10 expression at the epigenomic and transcription levels by altering the chromatin accessibility of the KLK10 promoter region.

In Aim 2, we tested the hypothesis that KLK10 inhibits endothelial dysfunction and atherosclerosis. Using human recombinantly-derived KLK10 (rKLK10) and KLK10 overexpressing plasmids, we studied the functional effects of KLK10 on endothelial permeability, inflammation, apoptosis, tube formation, monocyte adhesion, proliferation, and migration. KLK10 inhibited endothelial inflammation, permeability, migration, tube formation, and monocyte adhesion, but not proliferation or apoptosis. Due to the importance of inflammation, barrier permeability, and monocyte adhesion in the development of atherosclerosis, we focused on these dysfunctions for the subsequent studies. In atherosclerosis studies, administration of rKLK10 or KLK10 overexpressing plasmids in PCL mice decreased plaque burden and atherosclerosis severity compared to control mice.

Lastly, In Aim 3, we studied the mechanism by which KLK10 inhibits endothelial inflammation, permeability, and atherosclerosis. Preliminary data indicated that the ability of KLK10 to inhibit monocyte adhesion could be blocked by inhibiting or silencing the G-protein Coupled Receptors (GPCRs) Protease Activated Receptor-1 (PAR1) and Protease-Activated Receptor-2 (PAR2). These are receptors that are activated by site-specific cleavage of their extracellular N-terminal domain. However, follow-up studies revealed KLK10 does not bind or cleave either receptor, suggesting there was an unidentified protein that directly binds to KLK10 and mediates signaling through the PARs. Using affinity-pulldown techniques, we identified direct KLK10 binding proteins, with a specific focus on another serine protease, High-Temperature

Requirement A1 (HTRA1). Further mechanistic studies found HTRA1 cleaves KLK10 and siRNA-mediated knockdown of HTRA1 abrogated the anti-inflammatory and barrier protective functions of KLK10.

Overall, this dissertation will address the contribution of blood flow within the vasculature to the development of atherosclerosis and highlight the potential of the shear-sensitive endothelial protein KLK10 as a therapeutic target for the treatment of atherosclerosis.

1.1 Vascular hemodynamics and shear stress in endothelial biology

Although atherosclerosis development can be primarily attributed to the several risk factors described above, one major factor that predisposes specific regions of the vasculature to increased atherosclerosis susceptibility is blood flow. Early on, investigators postulated that vascular hemodynamics might play a role in atherogenesis[34], which was followed by the observation that atherosclerotic plaques tend to occur at sites of low and oscillating wall shear stress[35]. It has since been widely demonstrated that atherosclerotic plaques preferentially develop in regions of the vasculature exposed to disturbed blood flow (*d-flow*), typically at the branched and curved arterial regions[18-20]. Conversely, straight sections of the artery exposed to stable blood flow (*s-flow*) are protected from developing atherosclerosis[18-20] (Figure 1.2). *D-flow* is characterized by flow patterns with low-magnitude and oscillatory shear stress (OS) of approximately ±5 dynes/cm^2, whereas *s-flow* is characterized by high-magnitude, unidirectional laminar shear stress (LS) of 15 dynes/cm^2 [19, 36-38]. *D-flow* induces, while *s-flow* prevents, endothelial dysfunction including inflammation, endothelial-mesenchymal transition, thrombosis, vasoconstriction, and barrier dysfunction, which in turn lead to atherosclerosis in conjunction with additional risk factors such as hypercholesterolemia [19, 39].

As the primary cell lining the lumen of the vasculature and being in direct contact with the blood, Endothelial Cells (ECs) sense the mechanical forces associated with these different blood flow profiles and convert them into chemical signaling pathways that alter cellular gene expression[40]. This process is referred to as mechanotransduction, i.e., the conversion of a mechanical stimulus into chemical activity[41]. In the following subsection, I will address various previously described mechanosensors involved in mediating the effects of shear stress on the endothelium, with a focus on the mechanosensor Integrin α5.

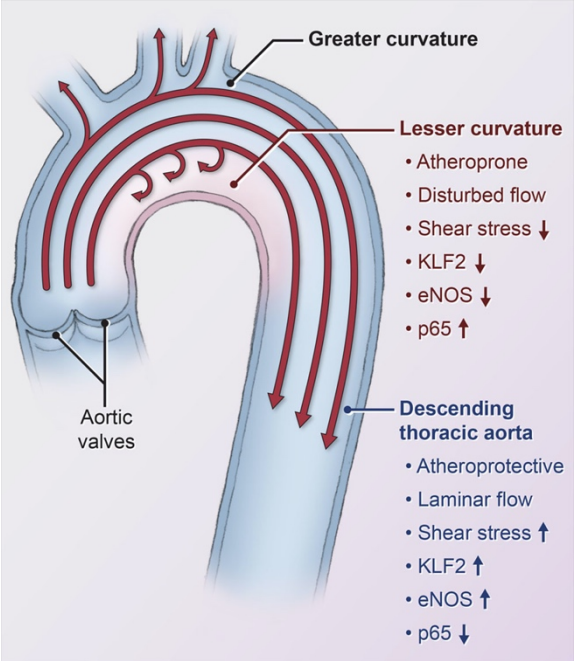

Figure 1.2 **Hemodynamics in the aortic arch.** Depiction of the aortic arch including blood flow dynamics through the greater curvature, lesser curvature, and descending thoracic aorta. Adapted with permission from Ku et al. 2019. [1]

1.2 Mechanosensors in the endothelium

ECs respond to shear stress primarily through numerous mechanosensors present on the cell surface, cell-cell junction, cell-matrix adhesion sites, and actin cytoskeletal structure, which transduce the mechanical cues into cell signaling events and ultimately changes in gene expression [42-44]. While these flow-dependent changes are relatively well described, the cell and molecular mechanisms by which d-flow and s-flow induce these different endothelial responses are still unclear. Are there specialized mechanosensors that detect d-flow versus s-flow, or does one mechanosensor respond differently to different flow conditions? This section covers the editorial published in Circulation Research: **Demos C*, Williams D*, Jo H. Disturbed Flow Induces Atherosclerosis by Annexin A2-Mediated Integrin Activation. Circ Res. 2020 Sep 25;127(8):1091-1093[45].** * Demos C and Williams D are co-first authors in this paper.

1.2.1 Previously described mechanosensors and their response to shear stress

Some of the most well-characterized mechanosensors are the PECAM-1 (platelet endothelial cell adhesion molecule 1), VE-cadherin (vascular endothelial-cadherin), and VEGFR-2 (vascular endothelial growth factor receptor) mechanosensory complex, PlxnD1 (Plexin D1), Piezo1, integrins, and NOTCH1[39, 40, 46]. Purinergic receptor calcium channels, G-proteins, glycocalyx, primary cilia, cytoskeleton, and caveolae can also function as mechanosensors[40, 46, 47]. The PECAM-1, VE-cadherin, and VEGFR-2 mechanosensory complex transduces laminar shear stress into the activation of PI3K (phosphoinositide 3-kinase) and AKT, stimulating nitric oxide (NO) production from eNOS (endothelial NO synthase). LS (laminar shear stress or s-flow) also induces integrin αvβ3 activation, which leads to endothelial alignment to the direction of flow[48-50]. Whether the PECAM-1 complex also responds to OS is unknown.

Two mechanosensors, Piezo1 and Plexin D1 (PlxnD1), have been identified to respond to both LS (s-flow) and OS (d-flow) differentially. PlxnD1 is a semaphorin guidance receptor which responds to both flow conditions [51]. EC-specific loss of PlxnD1 inhibits the site-specific atherosclerosis development in the aortic arch exposed to d-flow, while increasing the plaque development in the straight thoracic aortas exposed to s-flow [51]. This result suggests dual roles of PlxnD1 serving as a mechanosensor for both s-flow and d-flow. D-flow induces a conformational change of PlxnD1, which triggers complex formation with neuropilin-1 and VEGFR2 to mediate the AKT, ERK, focal adhesion kinase (FAK) and eNOS activation pathway. This suggests that PlxnD1 interacts with the PECAM1/VEGFR2/VE-cadherin mechanosensory complex to mediate the s-flow effect, but it is unclear if this is also involved in the d-flow response. Interestingly, the PlxnD1 flow response is dependent on the Gq/G11 pathway, but not on Piezo1. This implicates Gq/G11 as a possible hub where the two different mechanosignaling pathways diverge in response to various shear stress profiles. Piezo1 is a calcium-permeable, nonselective cation channel that has been well-characterized as a mechanosensor responding to both s-flow and d-flow. Upon activation by either flow condition, Piezo1 triggers the same initial mechanosignaling response of an influx of calcium, which in turn activates in parallel Gq/G11-mediated endothelial responses [46]. P2Y2 purinergic receptors and PAR1/2 all do activate Gq-PLC-IP3 and Ca++[52]. So, it is possible that anything that increase Ca++ (Piezo1-Ca++ influx, or GPCR-Gq-PLC-Ca++) are required. However, depending on the flow pattern, ECs read these initial mechanosensing and mechanotranduction responses as either atheroprotective signaling by activating the PI3K-eNOS pathway or as pro-atherogenic signaling through activation of the integrin, FAK-mediated NFκB pathway [50, 53]. Recent studies have shown that Piezo1 predominantly responds to OS to increase

calcium influx, which leads to the Gq/G11-dependent activation of integrin α5 [46]. Integrin α5 translocates into lipid rafts in response to OS, a process which is necessary for integrin activation and ligation into α5β1 [54]. Once activated, integrin α5β1 promotes the FAK-dependent NFκB activation and expression of proinflammatory cell adhesion proteins VCAM1 and ICAM1 [46, 54]. However, it was unknown how OS causes translocation and activation of integrin α5β1.

1.2.2 Piezo-dependent activation of ANXA2

Zhang et al demonstrate that the translocation and activation of integrin α5β1 induced by d-flow is mediated by Piezo1-dependent activation of ANXA2, leading to endothelial inflammation and atherosclerosis [55]. For this study, the authors employed a series of elegant and comprehensive approaches using proteomics, biophysics, genetic models, and novel *in vivo* EC-targeted gene modification methods. They first carried out a proteomics study to identify proteins that bind to integrin α5, and identified ANXA2 as a potential binding protein. Subsequent validation studies clearly established that ANXA2 indeed binds to integrin α5, and this interaction was essential in mediating the translocation and activation of the integrin into the lipid rafts in response to OS in ECs. Through a series of biophysical and molecular imaging studies using various constructs of ANXA2 and integrin α5, they showed that ANXA2 undergoes conformational changes in a phosphorylation/dephosphorylation-dependent manner in response to OS. ANXA2 is in a closed conformation when it is phosphorylated at Tyr-24 (pY24) but opens when dephosphorylated by PTP1B phosphatase in response to OS. Upon dephosphorylation at Y24, the C-terminal domain of ANXA2 is released from the N-terminus, allowing the cytoplasmic domain of the integrin α5 to bind to the C-terminal of ANXA2. The binding of ANXA2 to integrin

α5 then triggers its translocation to the lipid rafts, where the integrin is activated and stimulates the FAK-dependent endothelial inflammation pathway.

The mechanism by which ANXA2 is dephosphorylated by PTP1B activation is mediated by calcium influx through Piezo1 in response to OS. Since ANXA2 and PTP1B were known to be calcium sensitive, Zhang et al tested the role of calcium influx through the mechanosensor Piezo1. In studies using various siRNAs and the Piezo1 activator YODA1, they showed that OS activated PTP1B through Piezo1-mediated calcium flux. Through detailed biochemical studies including a mass spectrometry, they confirmed the dephosphorylation of ANXA2 at Y24 by PTP1B.

To validate the *in vitro* observations regarding the role of PTP1B, ANXA2 and integrin α5 in endothelial inflammation and atherosclerosis, they carried out several elegant and innovative *in vivo* studies using genetic and molecular interventions at various points in this pathway. For these studies, they employed the partial carotid ligation model of atherosclerosis [4]. In this model, ligation of three of four distal branches of common carotid artery induces d-flow, which leads to robust endothelial dysfunction and atherosclerosis within two weeks [4]. They first showed that the loss of ANXA2 inhibits atherosclerosis development using ApoE_ANXA2 double knockout mice. Further, they showed that the atheroprotective effect of ANXA2 knockout was reversed by infecting the carotids with lentiviral-ANXA2-wildtype. Moreover, infection with constitutively dephosphorylated lentiviral-ANXA2^{Y24F} mutant made the atherosclerosis even worse than the wildtype, consistent with the *in vitro* finding. In addition, infection of the carotids with lentiviral-PTP1B shRNA dramatically knocked down endothelial level of PTP1B, resulting in significant prevention of atherosclerosis in ApoE knockout, but not in ApoE_ANXA2 double knockout mice.

These results clearly validate the role of PTP1B and ANXA2 in d-flow-induced endothelial inflammation and atherosclerosis.

It is noteworthy to highlight the critical technical advancement and innovative approaches developed and demonstrated in this study. The use of lentiviral constructs to overexpress and knockdown key target genes, ANXA2 wild type and Y24F mutants and PTP1B shRNA in carotid artery ECs in the partial carotid ligation model of flow-induced atherosclerosis is remarkable in its tissue-targetability and overexpression and knockdown efficiencies. These approaches should be helpful to other investigators in the field in studying the role of many other genes, especially flow-sensitive genes, in endothelial function and atherosclerosis *in vivo.*

In summary, the report by Zhang et al demonstrates the novel mechanism by which d-flow induces integrin α5-dependent activation through the Piezo1-PTP1B-ANXA2 pathway, underlining the importance of this process in mechanotransduction (Figure 1.3). While these new insights provides deeper understanding of the differential activation mechanisms by which s-flow and d-flow lead to atheroprotective and proatherogenic responses, respectively, there still remain several outstanding unresolved questions. While s-flow and d-flow both stimulate initial calcium influx via Piezo1, what determines the divergence of proatherogenic and antiatherogenic pathways such as the activation of PTP1B or protein kinases regulating ANXA2? Although there are multiple mechanosensors, only a few have been tested for their ability to respond to d-flow versus s-flow. While it is likely that many mechanosensors respond in a coordinated manner, it still remains an open question. New insights provided by the current study also illustrate novel therapeutic opportunities for atherosclerosis.

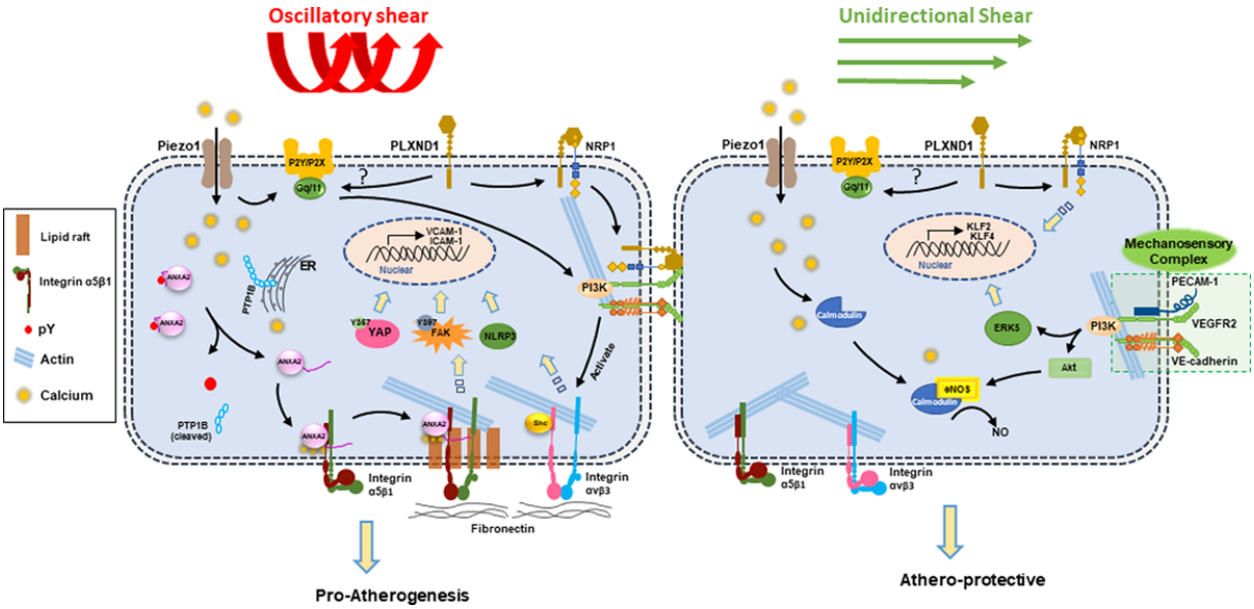

Figure 1.3. **Disturbed blood flow (D-flow) and stable flow (s-flow) induce differential mechanosensing and mechanotransduction**. D-flow is sensed by Piezo1 and Plexin D1, which lead to activation of integrins and proatherogenic signaling responses. D-flow induces calcium influx through Piezo1, which activates PTP1B (protein-tyrosine phosphatase 1B)-dependent ANXA2 (annexin A2) dephosphorylation. ANXA2 then binds integrin α5 which is translocated to the lipid raft and activated, leading to stimulation of FAK (focal adhesion kinase)-dependent endothelial inflammation and atherosclerosis.

1.3 Regulation of flow-sensitive non-coding genes

A large number of endothelial genes that change in response to flow are referred to as *flow-sensitive genes*, also known as mechanosensitive genes [56-63]. The majority of these flow-sensitive genes are protein-coding genes, such as the atheroprotective *Klf2* [64], *Klf4* [65], Timp3, and *eNOS* [63], which are upregulated by the stable flow. *D-flow* also upregulates a number of pro-atherogenic genes, including vascular cell adhesion molecule-1 (*VCAM-1*) [62, 66], matrix metalloproteinases (*MMPs*) [67], and bone morphogenic protein-4 (*BMP4*), which mediate inflammatory, proliferative, and apoptotic responses in vascular endothelium [42, 68, 69]. While the role of flow-sensitive coding genes (proteins) and post-translational modification proteins by flow have been extensively studied

for their role in atherosclerosis [42, 56, 57, 60, 70-77], the role of flow-sensitive non-coding genes in atherosclerosis is still emerging [78].

Non-coding genes are transcribed into functional RNAs; however, these RNAs do not code for proteins, i.e., non-coding RNAs (ncRNAs). Non-coding RNAs regulate a myriad of physiological process by acting as regulators of gene expression at the transcriptional, post-transcriptional, and epigenetic level [79]. Here, we will discuss two main categories of ncRNAs; the short ncRNAs (< 30 nucleotides) and the long noncoding RNAs (> 200 nucleotides) or lncRNAs. Short ncRNAs consist of microRNAs (miRNAs), siRNAs, piRNAs, and other subgroups. Due to the limited information on other subgroups of the short ncRNAs, the discussion will focus on the most well-studied group: miRNAs. Here, we review and update the current knowledge of flow-sensitive miRNAs and functionally essential lncRNAs for their role in vascular biology and atherosclerosis. **This section covers the review paper published in Vascular Pharmacology: Kumar S, Williams D, Sur S, Wang JY, Jo H. "Role of flow-sensitive microRNAs and long noncoding RNAs in vascular dysfunction and atherosclerosis."** ***Vascul Pharmacol.*** **2019;114:76-92**. [80]

1.3.1 Biogenesis, transcription, and processing of miRNAs

miRNAs are short noncoding RNAs that regulate gene expression at the post-transcriptional level [81, 82]. Typical miRNAs are transcribed by RNA polymerase II (RNA pol II) in the nucleus as pri-miRNAs, which are trimmed into 70–100 nucleotides (nt) hairpin-shaped precursor—pre-miRNA by the Drosha–DGCR8 complex [83-86]. Pre-miRNA is exported into the cytoplasm with the assistance of Ran-GTP and Exportin-5 complex [87, 88]. After that, the pre-

miRNA is cleaved by Dicer in association with its partners argonaute (AGO) and Trans-Activation Responsive RNA-Binding protein (TRBP) to produce a double-stranded 20–25 nt miRNA [89]. The fully processed miRNA duplex is then incorporated into a multicomponent protein complex known as an RNA-induced silencing complex (RISC). During this process, one strand of the miRNA duplex is selected as the mature miRNA (or miRNA-5p) while the other strand, known as miRNA* (passenger strand or miRNA-3p) which is typically rapidly degraded [90]. Mature miRNA-5p then further facilitates the cleavage of target mRNA and/or its translational repression via precise mechanisms [91-93]. The seed sequence (the nucleotides in position 2–8 of miRNA) binds to regions at the 3′UTR of its target mRNAs via complementary pairing [94]. *In silico* analyses have revealed that ~60% of protein-coding genes harbor miRNA target sites in their 3′UTR and that a single miRNA can typically modulate the expression of hundreds of genes. Not only are specific miRNA genes highly conserved in animals, but their target sites in the 3′UTR of genes are also under positive evolutionary selection. MiRNAs play an essential role in development and organogenesis and more importantly in vascular functions [95-99].

1.3.2 Role of miRNAs in vascular dysfunction and atherosclerosis

MiRNAs are frequently dysregulated in vascular pathologies such as atherosclerosis [100-104], and tremendous effort exists that aim to develop novel diagnostic markers and therapeutics for the treatment of atherosclerosis. Changes in miRNA expression levels due to blood flow have the potential to affect networks of genes regulating endothelial and vascular smooth muscle cell function, inflammation, and atherosclerosis. The flow-sensitive microRNAs play essential roles in the regulation of vascular dysfunction and atherosclerosis. Here, we broadly categorize these miRNAs based on their response to flow: (1) miRNAs upregulated by *s-flow* or downregulated by

d-flow (2) miRNAs downregulated by *s-flow* or upregulated by *d-flow*. MicroRNAs such as miR-10a, 23b, and 101 are either upregulated by *s-flow*/LS or downregulated by *d-flow*/OS, while microRNAs such as miR-17~92 cluster, 92a, 663, 712, and 205 are either upregulated by *d-flow*/OS or downregulated by *s-flow*/LS. Other microRNAs for which the information on flow-sensitivity is not explicit include miR-21, 155, 126, 143, and 145.

1.3.3 miRNAs upregulated by s-flow or LS

These miRNAs are either increased by *s-flow/LS* (atheroprotective flow) or decreased by *d-flow/OS* (pro-atherogenic flow) in endothelial cells and are shown to reduce vascular inflammation and atherosclerosis.

1. **miR-10a**: Stable blood flow upregulates the expression of miR-10a in the endothelium. Loss of miR-10a results in activation of NFκB via MAP3K7 and βTRC, both of which promote IκB degradation and p65 translocation, resulting in endothelial inflammation in a porcine model of atherosclerosis, suggesting that differential expression of miR-10a regulates a pro-inflammatory endothelial phenotype [105]. Expression of miR-10a in the athero-susceptible aorta has recently been shown to be rescued by retinoic acid receptor-α (RARα) and retinoid X receptor-α (RXRα) agonists, leading to inhibition of GATA6/VCAM-1 signaling and inflammatory cell infiltration [106]. Recently, it was shown that induction of miR-10a by administration of RARα/RXRα-specific agonists prevents inflammation and atherosclerosis in $ApoE^{-/-}$ mice, providing further support for the role of flow-sensitive miR-10a as an athero-protective miRNA and potential therapeutic target [107].
2. **miR-23b**: Pulsatile LS or *s-flow* upregulates the expression of miR-23b in the

endothelium. Increased levels of miR-23b suppressed endothelial proliferation by reducing E2F transcription factor 1 (E2F1) expression and Rb phosphorylation [108]. Also, miR-23b was shown to inhibit cyclin-dependent kinase-activating kinase (CAK) complex thereby suppressing cell cycle progression and reducing the basal transcription of RNA Pol II [109]. Furthermore, miR-23b was recently implicated as a novel regulator of vascular smooth muscle cell (VSMC) phenotype switching following vascular injury [110]. Here, miR-23b inhibited VSMC proliferation and migration while promoting expression of VSMC markers genes such as smooth muscle alpha (α)-2 actin (*ACTA2*) and smooth muscle myosin heavy chain 11 (*MYH11*). Transcription factor forkhead box O4 (FOXO4) was also identified as a direct target of miR-23b in VSMCs [110]. Together, these studies suggest miR-23b is a flow-sensitive miRNA involved in maintaining cellular quiescence, regulating cell identity and cell cycle in a flow-dependent context.

3. **miR-101**: LS increases the expression of miR-101, which then targets the mTOR gene, leading to cell cycle arrest in vascular endothelial cells [111]. Overexpression of miR-101 reduced the G1/S transition of the cell cycle in ECs subjected to LS [111]. However, expression of miR-101 is also regulated in other cell types and by various stress stimuli. For example, miR-101 is also upregulated in response to hypoxia, where it targets Cul3, a scaffold protein in the E3 ligase complex. Without Cul3, the transcription factor Nrf2 enters the nucleus and promote expression of angiogenesis-related genes [112]. In addition, in THP-1 monocytes and hepatocytes, miR-101 has also been reported to suppress ATP-binding cassette transporter A1 (ABCA1) expression under normal and inflammatory conditions [113]. Together, these findings suggest that miR-101 might

regulate cellular functions in endothelium in a flow-dependent manner and may also play a context-specific role in other cell types.

1.3.4 miRNAs upregulated by d-flow or OS

These miRNAs are either increased by *d-flow*/OS or decreased by *s-flow*/LS in endothelial cells and associated with vascular dysfunction and pro-atherogenic responses.

1. **miR-17~92:** The miR-17~92a cluster comprises several miRs, including miR-17, 18a, 19a 19b, 20a, and 92a. These miRs have been studied extensively for flow-dependent regulation and their role in atherosclerosis. The miR-17~92 cluster is regulated by shear stress in that some members (miR-17, miR-19b, miR-20a, miR-92a) were downregulated by pulsatile LS [114]. Interestingly, *s-flow* increased the expression of miR-19a, and its transient overexpression leads to a significant decrease in the cyclinD1 mRNA and protein levels, leading to cell cycle arrest at the G1/S stage [108]. However, a recent study showed that miR-19a also has a pro-inflammatory phenotype by targeting the gene high mobility group box transcription protein 1 (HMGB1) *in vitro* and *in vivo* [115]. HMGB1 is a repressor of macrophage migration inhibiting factor (MIF), and increased expression of miR-19a under OS conditions. This leads to higher levels of MIF resulting in the release of pro-inflammatory cytokines TNFα and Interleukin-6 (IL-6) [115]. Furthermore, miR-19a is upregulated in CD19+ B-cells from patients with atherosclerosis, where it has been shown to suppress the anti-inflammatory cytokine interleukin-10 (IL-10) [116]. Interestingly, miR-19a was also shown to be regulated by hypoxic conditions. Hypoxia-inducible factor (HIF)-1α is increased in atherosclerotic lesions and is associated with atherosclerotic plaque inflammation. *In vivo*, endothelial HIF-1α promoted atherosclerosis by upregulating miR-19a, which indirectly caused an increase in expression of Chemokine Ligand 1 (CXCL1)

[116, 117]. Together, current evidence suggests that miR-19a regulates aspects of chemokine and cytokine expression under inflammatory and hypoxic conditions in both ECs and CD19+ B cells. Subsequent studies showed that miR-92a was downregulated by LS and was upregulated by OS [118]. These *in vitro* findings are consistent with *in vivo* studies showing that ECs in the athero-prone porcine aortic arch area have increased miR-92a levels as compared to those of the athero-resistant thoracic aorta [118]. Regarding its function, overexpression of miR-92a prevented angiogenesis in a mouse model of limb ischemia by targeting the integrin subunit alpha 5 [119]. Further studies demonstrate that miR-92a exerts its proatherogenic effect by inhibiting KLF2-mediated thromboembolic and eNOS expression, as well as KLF4-induced expression of E-selectin, eNOS, VCAM-1, and MCP1 [120]. Recently, miR-92a was shown to silence the integral membrane protein Phosphatidic Acid Phosphatase type 2B (PPAP2B) under OS conditions *in vivo*, resulting in an increased inflammatory response to circulating lipids [28]. Moreover, SOCS5 has been identified as a miR-92a target that is involved in the regulation of endothelial inflammation via activation of the JAK-STAT pathway [121]. Thus, miR-92a appears to target genes corresponding to several pro-angiogenic proteins [119] and inhibition of miR-92a in a preclinical study of porcine limb ischemia and myocardial infarction enhanced blood vessel growth and functional recovery of damaged tissue [122]. Taken together, inhibiting selected members of the miR-17~92 cluster can be an effective anti-atherogenic strategy.

2. **miR-663:** MiR-663 was identified as one of the most upregulated miRNAs from a microarray study using HUVECs exposed to OS conditions compared to the LS [123]. Overexpression of miR-663 induced EC inflammation, suggesting its potential pro-atherogenic role [123]. This study further identified several transcription factors including

KLF4, CEBPB, and ATF3 as potential targets of miR-663 under the OS condition. These transcription factors regulate multiple genes involved in the inflammatory responses in endothelium. Furthermore, inhibiting miR-663 with miR-663-LNA restores KLF4 expression in ECs under OS condition, suggesting that *d-flow* induced miR-663 is critically involved in the tweaking of the KLF4 expression in endothelium [123]. Furthermore, miR-663 was upregulated in HUVECs exposed to pro-atherogenic oxidized phospholipids and was found to play a permissive role in the induction of VEGF and activation of ATF4 branch of unfolded protein response in ECs [124, 125]. Interestingly, however, miR-663 regulates VSMC phenotypic switching by targeting the transcription factors JunB/Myosin Light chain 9 [126-128]. These results suggest that miR-663 has a context-dependent and cell type-specific role in the pathophysiological process, as overexpression of this human-specific microRNA using an adenoviral construct reduced neointimal formation in a mouse model of neointimal hyperplasia [129]. In order to be developed as a potential therapeutic candidate for atherosclerosis, future work is needed to delineate the cell-specific effects of miR-663.

3. **miR-712 and miR-205 family:** MiR-712 and miR-205 were identified as pro-atherogenic miRNAs induced by disturbed flow. MiR-712 was first reported from a miRNA array study using endothelial-enriched RNAs obtained from the mouse model of flow-induced atherosclerosis, known as the partial carotid ligation model [66]. Interestingly, miR-712 is murine-specific, and miR-205 was identified as its homolog in humans and other vertebrates from a seed-sequence matching study [130]. miR-205 shares the same "seed sequence" with miR-712 and both have increased expression under *d-flow*. The miR-712/205 family activates endothelial inflammation and permeability changes in a flow-dependent manner. The pro-inflammatory and pro-atherogenic effects of miR-712/miR-

205 were mediated in large part by tissue inhibitor of metalloproteinase-3 (TIMP3) [130]. Loss of TIMP3 by miR-712 resulted in activation of matrix metalloproteinases (MMPs) and a disintegrin and metalloproteinases (ADAMs), ultimately leading to endothelial inflammation, hyperpermeability, and atherosclerosis [131] as well as in abdominal aortic aneurysm [132]. We also showed that targeting this miRNA using anti-miR-712 injected either systemically as the naked form was able to prevent atherosclerosis in a mouse model of atherosclerosis [130]. Furthermore, we demonstrated that anti-miR-712 could be delivered specifically to the inflamed artery endothelial cells in mice by encapsulating anti-miR-712 inside the cationic lipid nanoparticles decorated with the VCAM1-targeting peptide [133]. The VCAM1-targeting lipid nanoparticles containing anti-miR-712 was able to inhibit atherosclerosis in the partial ligation model of mouse atherosclerosis, compared to the control group demonstrating the specific effect of the nanoparticle approach as a targeted therapeutic method. Interestingly, the mechanism of biogenesis for miR-712 (murine-specific miRNA) and miR-663 (primate-specific miRNAs) also share a familiar yet unexpected source, the internal transcribed spacer region of pre-ribosomal RNA (*RN45s*) gene [130], suggesting that mechanism of generation of flow-sensitive microRNAs is conserved in multiple species. It is interesting to note that two of the most disturbed flow/OS-induced miRNAs (miR-712 in mice and miR-663 in human ECs) are generated from this unusual, atypical source, especially what is considered to be a rubbish portion of *RN45s* region [130]. The pathobiological implication of this unusual biogenesis of this flow-sensitive miR-712 and miR-663 from the interspace translational regions of the ribosomal RNA gene is unknown at present. These miRNAs may be used as biomarkers and therapeutic candidates for atherosclerosis.

1.3.5 Other flow-sensitive microRNAs

Some flow-sensitive microRNAs, such as miR-21, and 155, have been implicated in both anti- and pro-atherogenic responses. This may reflect the fact that a single miRNA can target numerous target mRNAs, some of which mediate pro-atherogenic responses in one cell type or organ, while others act oppositely in different cell types, tissues or in various context-dependent manner. Therefore, the overall response of miRs in the whole body *in vivo* is likely to depend on cellular context, cell type, and environment [134].

1. **miR-21:** MiR-21, a flow-sensitive miRNA, has been extensively studied for its role in atherosclerosis. MiR-21 was initially shown to be upregulated by LS in HUVECs [135]. However, other study showed that the pro-atherogenic OS upregulated miR-21, which targeted peroxisome-proliferator-activated receptor α (PPARα) leading to the enhanced expression of the pro-inflammatory VCAM-1 [136]. Consistent with its role as a pro-atherogenic miRNA, miR-21 is up-regulated in human atherosclerotic plaques [137], arterial endothelium exposed to *d-flow* in the mouse PCL model [66, 138], and in peripheral blood mononuclear cells from patients with coronary heart disease [139]. In coronary heart disease patients, miR-21 level negatively correlated with the number of circulating regulatory T (Treg) cells [139], which is known to play a protective role against atherosclerosis. Interestingly, miR-21 is induced by high glucose in macrophages and targets programmed cell death 4 (PDCD4), reducing macrophage apoptosis. Also, miR-21 is upregulated in tissues from patients with abdominal aortic aneurysm [140], serum from patients with cerebrovascular disease [141], and may also serve as a marker of plaque stability [103]. MiR-21 was the first miRNA shown to regulate VSMC growth and survival by silencing expression of phosphatase and tensin homolog (PTEN) and increased

expression of B-cell leukemia/lymphoma 2 (BCL2), ultimately promoting cell survival and proliferation [142-144]. Further, it was shown that inhibition of PTEN by miR-21 upregulates AKT signaling and protects against ischemia-reperfusion and hypoxia-reperfusion-induced cardiomyocyte apoptosis, giving its clinical relevance [145]. Also, trimetazidine, an anti-ischemic and antioxidant agent, was shown to prevent the ischemia/reperfusion-induced cardiomyocyte apoptosis by up-regulating miR-21 [146]. Together, this evidence suggests that miR-21 seems to be upregulated by disturbed flow/OS and mostly plays a pro-atherogenic role in ECs. However, it also appears to serve a protective role for injured or diseased VSMCs and cardiomyocytes, highlighting the complex roles of miR-21 in cardiovascular pathobiology.

2. **miR-155:** MiR-155, a flow-sensitive miR, has been extensively studied in atherosclerosis and coronary artery disease, but its role has been reported as both pro- and anti-atherogenic. Initially, miR-155 expression was found to be abundantly expressed in the intima of the thoracic aorta, which is naturally exposed to *s-flow in vivo* [147]. It was also found to be increased by LS in HUVECs; suggesting it may be an anti-atherogenic flow-sensitive miRNA [147]. It was further shown to inhibit NF-kB signaling in HUVECs by targeting p65 under inflammatory conditions [148]. Consistent with this idea, hematopoietic deficiency of miR-155 induced atherosclerosis and decreased plaque stability by increasing myeloid inflammatory cell recruitment to the plaque regions [149]. Furthermore, miR-155 was shown to prevent pro-inflammatory signaling in macrophages, and dendritic cells via inhibition of MAPK310, a member of the pro-inflammatory Mitogen-Activated Protein-Kinase (MAPK) signaling pathway [150]. However, in contrast, other studies showed evidence suggesting that miR-155 mediates pro-atherogenic responses [151,

[152]. MiR-155 was shown to directly target eNOS mRNA in HUVECs and impair endothelium-dependent vascular relaxation in human arteries [153]. Leukocyte-specific miR-155 directly repressed expression of negative regulators of pro-inflammatory cytokine signaling such as B-cell Lymphoma 6 (BCL6), Suppressor of cytokine signaling (SOCS1) [154], and Src homology 2 domain-containing inositol-5-phosphatase (SHIP-1) [155, 156]. Another study showed that genetic knockdown of miR-155 ameliorated atherogenesis in ApoE$^{-/-}$ mice by reducing inflammatory responses of macrophages and increasing macrophage cholesterol efflux [152]. Similar to miR-19a, miR-155 also promotes foam cell formation by targeting HMGB1 in macrophages [157]. Also, tissue-specific genetic knockdown of miR-155 in bone marrow-derived cells suppressed atherogenesis in ApoE$^{-/-}$ mice [152]. MiR-155 appears to play the pro-inflammatory role in macrophages but the anti-inflammatory role in ECs. It is interesting to note that miR-155 is induced by pro-inflammatory stimuli, such as TNFa [158] and oxidized LDL [157, 159]. In these cases, it may function in a negative feedback loop to mitigate inflammation from pro-inflammatory stimuli. A recent study further showed that miR-155 targets calcium-regulated heat stable protein 1 (CARHSP1), which regulates the stability of TNFa [160], further reinforcing the role of miR-155 as a negative feedback regulator. Together, these conflicting results suggest that miR-155 has differential effects on atherosclerosis depending on the specific cell-types and pathobiological contexts. Cell-type and context-specific modulation of miR-155 by using appropriated targeted delivery methods [133, 161] may be useful to overcome this conundrum.

1.3.6 Long non-coding RNAs (LncRNAs) in Atherosclerosis

The lncRNAs are a group of non-coding RNAs with a length of more than 200 nucleotides that play a role in the regulation of gene expression at the post-transcriptional, transcriptional, and chromatin levels [162, 163]. Recently first flow-sensitive and endothelial-enriched lncRNA, STEEL, was reported [164], opening the possibility that there would be many other flow-sensitive lncRNAs that play essential roles in vascular pathobiology to be discovered. Given its relative paucity of data on flow-sensitive lncRNAs, here we review the emerging roles of other lncRNAs that have been studied in vascular dysfunction and atherosclerosis [165, 166]. We also noted that Chen et al. performed a lncRNA and mRNA array study using HUVECs exposed to low shear stress (2 dyn/cm^2) for a short duration (2 hours) [167]. Although the study reported 149 differentially expressed lncRNAs by the brief shear exposure, the findings from the study needs to be further validated.

1. **STEEL:** The spliced-**t**ranscript **e**ndothelial-***e***nriched **l**ncRNA (STEEL) is the first flow-sensitive lncRNA enriched in ECs. Recently, Man et al. showed that expression of STEEL is decreased by atheroprotective flow (steady LS) compared to the atheroprone flow (*d-flow* or OS) in a KLF2-dependent mechanism [164]. Functionally, they showed that endothelial expression of STEEL stimulated vessel network formation and maturation. Knockdown of STEEL decreased many shear sensitive genes including KLF2 and eNOS. Interestingly, however, overexpression of KLF2 downregulated STEEL expression, suggesting the feedback inhibition of STEEL by KLF2. Additional studies using chromatin immunoprecipation showed that STEEL is enriched in the nucleus where it binds to PARP1 at the KLF2 and eNOS genomic loci, suggesting its epigenetic regulatory mechanism [164]. Although the role of STEEL in atherosclerosis is yet to be studied, this finding opens the

possibility that there may be many other flow-dependent lncRNAs waiting to be discovered for their roles in cardiovascular pathobiology.

2. **LASSIE:** A KLF2-dependent lncRNA Lassie (lncRNA activated by shear stress in the endothelium) was reported to be increased by shear stress in HUVECs [168]. This abstract reported that Lassie improved survival and angiogenic potential of endothelial cells; however, further studies are needed to validate the report and molecular mechanisms.
3. **SENCR:** SENCR was discovered as a new vascular cell-enriched lncRNA by Miano and colleagues by an RNA-Seq study [169, 170]. It is abundantly expressed in both endothelial and smooth muscle cells, and no orthologues have been identified outside of human/chimp lineages. Studies using the SECNR knockdown approach in human coronary artery smooth muscle cells (HCASMCs) showed that its target genes include Myocardin, a critical contractile transcriptional factor, which in turn stabilizes contractile phenotype while inhibiting motile responses [169]. In embryonic stem cells, SENCR stimulates their commitment to ECs during development [170]. In HUVECs, SENCR increases angiogenic responses, which may be mediated by downregulating expression of migratory and angiogenic genes such as CCL5, CEACAM1, and CX3CL1, suggesting them as its target genes [170]. They further showed that SENCR expression was significantly reduced in EC isolated from patients with coronary artery disease compared to the healthy subjects [170], indicating its implication in atherosclerosis.

1.3.7 Circulating miRNAs as Biomarkers for Atherosclerosis

A biomarker, or biological marker, typically refers to a quantifiable indicator of a biological state or pathological condition [171]. Circulating miRNAs have tremendous potential as a

disease biomarkers as differential plasma miRNA levels have been described for many pathophysiological conditions, including atherosclerosis [172]. Here, we will review those studies that have shown evidence suggesting diagnostic and prognostic potentials for one or a few circulating miRNAs as specific biomarkers of atherosclerosis. Since multiple miRNAs are also secreted into the circulation, these can be used as potential circulating biomarkers. For example, miR-146a levels are increased in the serum of patients with acute coronary syndrome [173]. The peripheral blood levels of miR-92a, miR-126, and miR-222 in this study were markedly decreased in both atherosclerotic and pre-atherosclerotic patients compared to healthy controls, although the decease of miR-92a and miR-222 in pre-atherosclerotic patients was not as significant as that in atherosclerotic patients [173]. In patients with acute myocardial infarction (MI), circulating levels of muscle-enriched miRNAs (miR-1, -133a, and 499) and the cardiac-specific miR-208a were significantly increased in human patients [174]. This study especially suggested miR-208a as an early detection marker of acute MI. MiR-221/22 levels decrease while miR-21 and miR-130a increase in the plasma patients with peripheral arterial disease [175]. The opposite effects of miR-221/222 on the proliferation, migration, and apoptosis of endothelial cells and vascular smooth muscle cells may have significant therapeutic implications in many vascular diseases such as atherosclerosis and restenosis following angioplasty [176]. Interestingly, the plasma level of liver-specific miR-122 was increased significantly after acute MI or cardiogenic shock [177, 178], suggesting their potential as a biomarker.

Circulating extracellular miRNAs are carried in various ways including exosomes, microvesicles, and complexes bound to low and high density lipoprotein particles as well as protein complexes such as AGO2-miRNAs [179-182]. These circulating miRNAs are biologically active,

altering gene expression in recipient cells [183]. Therefore, miRNAs are considered as newly described forms of intercellular communication. For example, as discussed above, extracellular vesicles or exosomes enriched with miR-143/145, which are secreted from HUVECs in response to shear stress, can be taken up by VSMCs where the miRNAs regulate their target genes [184]. Conversely, ECs can be targeted by exogenous miRNAs secreted by other cells such as blood monocytes. For example, miR-150 containing microvesicles released from monocytes from atherosclerotic patients was shown to increase the proliferation of endothelial cells [185]. Similarly, apoptotic bodies enriched in miR-126 can be taken by HUVECs and promote atherosclerosis regression by inducing CXCL12 expression through CXCR4 [186]. There is a tremendous interest to understand the mechanisms underlying miRNA incorporation into exosomes, delivery, and targeting and recognition machinery.

It is important to note that circulating miRNAs will typically have systemic effects regulating many cells and tissues and are not likely to be specific for atherosclerosis. For example, miR-92a, miR-126, and miR-222 are not specific only for cardiovascular diseases. The levels of miR-92 also increase in the context of other diseases such as hypertension [187], colorectal cancer [188], and have been shown to play an essential role in diagnosis and prognosis of other diseases [189]. Similarly, upregulated levels of miR-126 are also associated with an immune imbalance in children with acute asthma [190], and exosomal miR-126 can be used as a circulating biomarker in non-small-cell lung cancer [191] and hepatocellular carcinoma [192]. Likewise, the potential of miR-222 is currently being explored as a biomarker in various diseases including cancer and inflammatory diseases [193-197]. Although many studies have shown one or a few circulating miRNAs as specific biomarkers of atherosclerosis, it is likely that a panel of circulating miRNAs instead of one or a

few miRNAs, combined with other better-established biomarkers may be of better diagnostic and prognostic value. Also, specific and systematic large-scale clinical studies will be required to identify the real potential of these circulating miRNAs as diagnostic and prognostic biomarkers.

The role of lncRNAs as potential biomarkers in cardiovascular disease especially in atherosclerosis is still in its infancy, and much work remains to be done. In diabetic patients, circulating levels of lncRNA predicting cardiac remodeling (LIPCAR) were associated with diastolic function [198]. Similarly, circulating levels of MIAT and SENCR were directly associated with left ventricular mass to the left ventricular end-diastolic volume ratio, a well-known cardiac remodeling marker suggesting that lncRNAs are independent predictors of diastolic function and cardiac remodeling [199]. Although a large number of studies suggest that circulating ncRNAs promise to serve as a minimally invasive diagnostic and prognostic biomarker for various types of cardiovascular disease, the lack of consistency in these studies has been a significant concern in this field[200-209]. Therefore, reliable, accurate, and sensitive detection of circulating ncRNAs and validation is a prerequisite for their use as a biomarker in clinical applications. Several methodological factors including sample collection and processing, as well as assay performance and ncRNA quantification, can influence the quality of the resulting data and need critical considerations. It is important to note that platelets and platelet microvesicles contain significant amounts of microRNAs and efficiently contribute to the pool of circulating miRNAs. These platelet-related miRNAs such as miR-223, miR-126, miR-197, miR-191, miR-21, miR-150, miR-155, miR-140, miR-96, miR-98 are a potential source of confusion in biomarker assays and need to be carefully excluded and analyzed [210, 211]. Despite these potential technical limitations, It is an exciting future direction to determine the correlation between circulating levels of lncRNAs and

atherosclerosis as well as the underlying mechanisms by which they are carried in circulation and delivered to target cells. These studies would reveal the potential of the circulating lncRNAs as diagnostic biomarkers and therapeutic targets.

1.3.8 MiRNAs and lncRNAs as therapeutic targets in atherosclerosis

Since multiple miRNAs and lncRNAs are involved in the regulation of several vital processes in every stage of atherosclerosis initiation and progression, and perhaps regression, modulation of miRNA expression could have beneficial effects in prevention, reduction, and regression of atherosclerosis. Both the gain-of-function and loss-of-function approaches are used to examine the role of miRNAs as anti-atherogenic therapeutics. MicroRNA overexpression (gain-of-function) has been used as an anti-atherogenic therapeutic strategy. MiR-145 overexpression in VSMCs promotes a reduction in atherosclerotic plaque size in the most common sites of plaque formation such as aortic sinuses, ascending aortas, and brachiocephalic arteries [212]. Furthermore, miR-145 enhances plaque stability through an increase in the number of VSMCs, collagen content and fibrous cap area associated with a decrease in the number of macrophages and necrotic area. In contrast, suppression of pro-atherogenic miRNAs is also of potential therapeutic strategy for atherosclerosis. Several studies used antagomiRs or anti-miRs (synthetic antisense oligonucleotides) to lower the expression of proatherogenic miRNAs, such as miR-712, miR-205, miR-92a, and miR-33 have demonstrated efficacy as anti-atherogenic therapies [120, 121, 130, 213, 214]. With the advancements in the synthesis of modified oligonucleotide technology, these miRNAs can be targeted with either miRNA mimics to increase repression of target genes or miRNA inhibitors (anti-miRs or antagomiRs) to prevent miRNA repressing its target gene(s). These

approaches have shown great promise as potential therapies, and some of them are in clinical phase trial stages of drug development [215-217].

Although a growing number of lncRNAs are implicated in vascular function [78, 218, 219], it is unclear how they participate in the pathophysiological processes. Their potential as therapeutic targets has often been raised, and there are a few compelling examples of *in vivo* modulation of lncRNAs. However, modulating lncRNAs has been a challenging task to date. This is further complicated by the fact that many of the lncRNAs are not conserved between mice and humans. The widespread use of RNA-Sequencing methods reveals a rapidly expanding a number of potential new candidates for therapy. LncRNAs potentially represent a powerful tool for personalized medicine due to their specific expression patterns associated with distinct pathologies. There remain several limitations and challenges that need to be addressed before lncRNAs can genuinely reach the clinical application. Foremost is target specificity, given the pleiotropic implications of a single lncRNA in pathophysiological processes. Although lncRNAs may show dysregulation specific to certain diseases, they exhibit various functions in the organism and some lncRNAs may act through more than one mechanism [220]. Second, the low conservation of lncRNAs across evolution makes both the identification of human lncRNAs and their clinical testing challenges, because rodents may not be an adequate model for these studies.

Here, we summarized the current knowledge of flow-sensitive miRNAs and lncRNAs, as well as their essential roles in the regulation of endothelial function and atherosclerosis. These studies demonstrate that lncRNAs and flow-sensitive microRNAs are crucial mediators of endothelial function and atherosclerosis. However, our knowledge of these noncoding RNAs,

especially lncRNAs, their regulation, and their functions is still in its infancy and further investigation is warranted to identify other RNAs and explore their biological roles, mechanisms, and potential therapeutic applications. There have been some promising results from recent Phase II clinical trials indicating the safety, feasibility, and therapeutic potential of anti-miRs for the treatment of diseases.

In animal studies, some anti-miRs targeting flow-sensitive microRNAs such as miR-712, miR-205, or miR-155, have demonstrated their potential as anti-atherogenic therapies. This encourages the development of miRNA therapeutics for the treatment of atherosclerosis in humans. Despite these encouraging results, the development of miRNA therapeutics must overcome several significant challenges. First, there is a significant need to identify more athero-miRs (miRNAs with consistent pro- or anti-atherogenic effects) that could be used as reliable and safe anti-atherogenic therapeutic targets. Second, there is an urgent need to develop better and more specific miRNA modulators. The current methods to inhibit miRNAs include anti-miR/antagomiR and miR-sponge, both of which directly bind to miRNAs, thereby affecting all of their target genes (~ hundreds of genes) indiscriminately, potentially causing undesirable effects. Therefore, to minimize the potentially undesirable effects of anti-miR, antago-miR, or miR-sponge treatment, better strategies should be developed to deliver these inhibitors. These include targeted delivery of miRNA therapeutics specifically to cells and tissues of interest with minimal delivery to non-target cells to lower potential side effects. For example, we showed that anti-miR-712 could be delivered to inflamed endothelial cells by targeting VCAM1 on the endothelial cells by using nanoparticles coated with the VCAM1-targeting peptide [133]. Also, designing more specific

inhibitors such as target site blockers that can specifically block a unique and desired mRNA-miRNA interaction without affecting the expression of off-target genes [221].

In summary, ncRNAs robustly regulate vascular physiology and pathophysiology (Figure 1.4). These non-coding RNAs also regulate several aspects of atherosclerosis including vascular dysfunction and inflammation and lipid metabolism. Although many lncRNAs have been identified to date, only a handful have been studied for their association with atherosclerosis. Further advancements in the field of lncRNAs research will not only lead to identification of newer molecular pathways leading to disease process but also provide improved therapeutic candidates for targeting atherosclerosis.

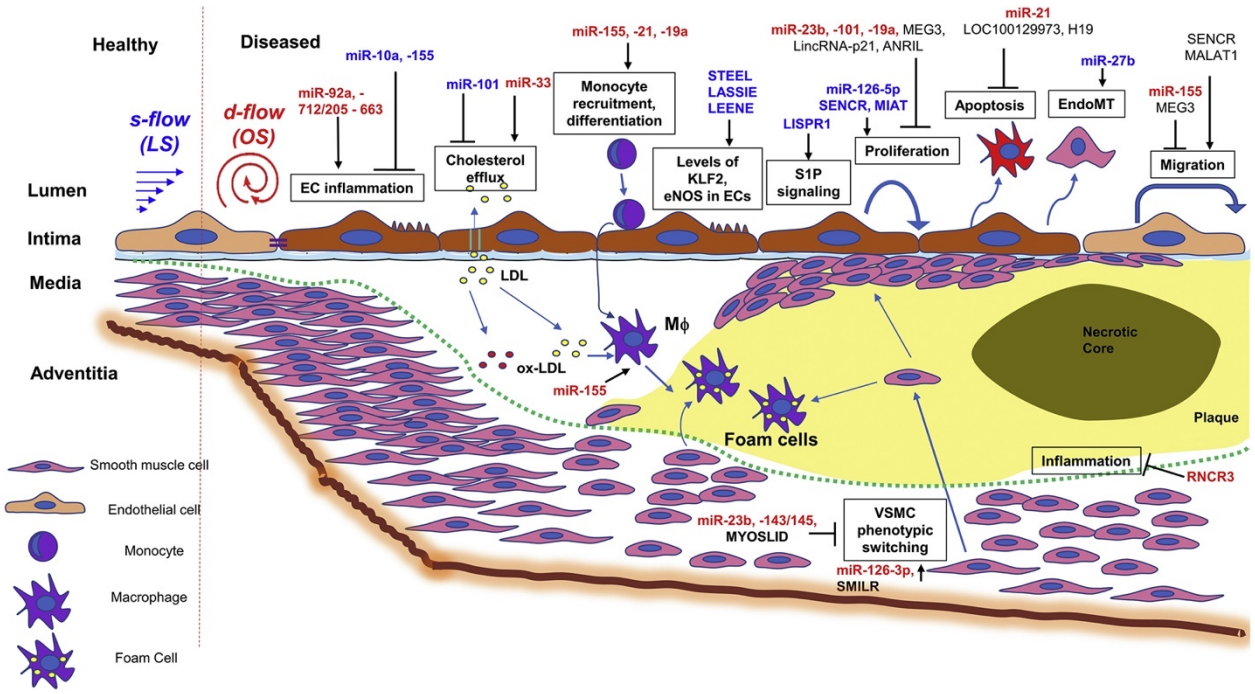

***Figure 1.4*. Flow-sensitive miRNAs and lncRNAs in vascular dysfunction and atherosclerosis**: The microRNAs and long non-coding RNAs that are regulated by flow and are implicated in vascular dysfunction and atherosclerosis through regulating gene targets in endothelial cells, smooth muscle cells, and monocytes/macrophages are shown.

1.4 *In vivo* models of atherosclerosis

A number of small and large animal models have been used to study atherosclerosis[222, 223]. Typically, large animals display characteristics that are more relatable to humans but have several downsides including cost and limited genetic modifiability. Smaller animal models such as mice also have downsides as they don't recapitulate the disease as seen in humans, however, they are cheap, display ease of genetic manipulation and develop atherosclerosis in a relatively short time period. For these reasons, murine models of atherosclerosis have become the most extensively used animal model.

The two most frequently used mouse models of atherosclerosis are the ApoE$^{-/-}$ and LDLR$^{-/-}$ mice. Knockdown of either the lipoprotein ApoE or the LDL receptor will lead to increased blood cholesterol and hypocholesterolemia when the mice are fed a high-fat diet consisting of 1.25% cholesterol, 15% fat and 0.5% cholic acid. After approximately 15 weeks, mice will develop intermediate lesions at *d-flow* regions. After 20 weeks and beyond, fibrous plaques are evident containing smooth muscle cells, extracellular matrix and an overlying fibrous cap[223]. While these models most effectively recapitulate atherosclerosis as it occurs in humans, lacking from these mouse models is a means for directly linking *d-flow* to atherogenesis.

To develop a mouse model in which *d-flow* can be acutely induced and studied for its contribution to atherosclerosis development, my advisor, Dr. Hanjoong Jo, developed the partial carotid ligation (PCL) mouse model (Figure 1.5). In this model, three of the four caudal branches of the left common carotid artery are ligated (LCA) [external carotid artery (ECA), internal carotid artery (ICA), and occipital artery (OA), the superior thyroid artery (STA) was left open]. The right common carotid artery (RCA) is left intact and serves as an internal control. As soon as one day after the surgery, *d-flow* will be induced in the LCA and within two weeks, PCL mice on a high-fat diet will develop robust atherosclerosis only in the LCA. Over this course of time, endothelial genes that change in response to *d-flow,* can be identified by isolating endothelial-enriched RNA from the LCA and comparing transcript expression profile to endothelial-enriched RNA from the control RCA.

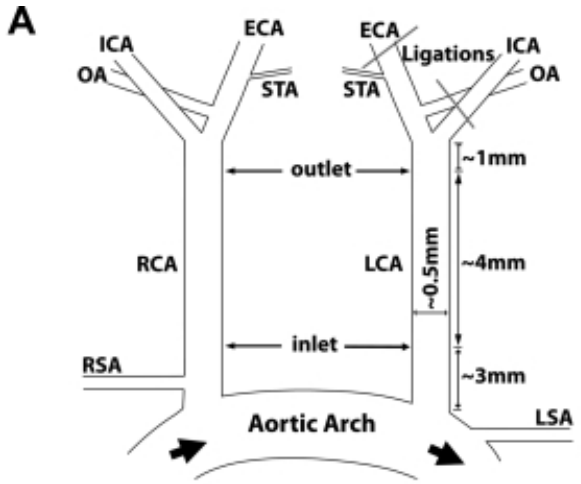

Figure 1.5. **Partial carotid ligation mouse model.** (a) Depiction of the aortic arch, the left common carotid artery (LCA), the right common carotid artery (RCA) and the ligations performed on three of the four caudal branches of the LCA [external carotid artery (ECA), internal carotid artery (ICA), and occipital artery (OA)]. The superior thyroid artery (STA) was left open. Adapted from Nam et al. 2009[4].

1.5 *In vitro* models of shear stress

While *in vivo* models of atherosclerosis offer the most physiologically relevant means to assess the effects of shear stress on endothelial biology and atherosclerosis, *in vitro* models of shear stress provide a method to simplify the complex shear stress dynamics in the vasculature and study local hemodynamic conditions that ECs experience *in vivo*. Several *in vitro* shear systems have been previously developed[224], of which the cone-and-plate viscometer and parallel-plate flow chamber have become the most popular (Figure 1.6).

1. *Cone-and-plate viscometer*: One of the first and most characterized *in vitro* models of shear stress is the cone-and-plate viscometer[225, 226]. In this system, shear stress is applied to cultured cells in a stationary plate by a rotating cone. A modified version was later introduced[227], which included a speed-controlled motor with variable rotational velocities. More recently, our lab has developed a modified cone-and-plate

which is housed in a standard incubator and programmed shear stress profiles can be controlled by computer[24, 228] (Figure 1.6a)

2. *Parallel-plate flow chamber:* Another *in vitro* model is the parallel-plate flow chamber, developed originally by Frangos, McIntire, and colleagues[229, 230]. In this system, a flow chamber consisting of a polycarbonate plate, a rectangular Silastic gasket, and a glass slide (or cover slip) with the attached EC monolayer were held together by a vacuum maintained at the periphery of the slide. Flow was driven either by the hydrostatic pressure head between the two reservoirs to produce steady flow or via cam-driven clamps upstream of the chamber to produce pulsatile flow. Although the cone-and-plate and the parallel-plate flow chamber systems are the most commonly used *in vitro* shear systems, microfluidic chambers have become more recently used as they allow for high throughput experiments. This method was pioneered and commercialized by Schaff et al. [231-233] (Figure 1.6b,c)

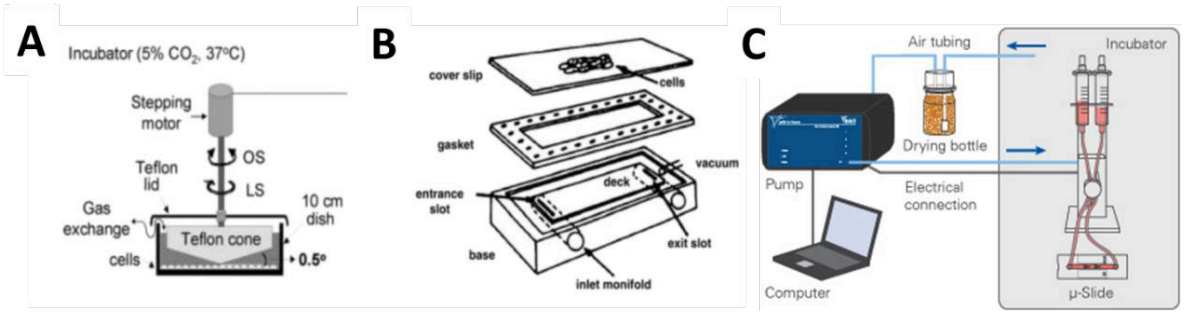

Figure 1.6. **In vitro models of shear stress. A**) Cone-and-plate viscometer. Adapted from Jo et al. (1991). **B**)Parallel plate flow chamber. Adapted from Lawrence et al. (1987). **C**) Ibidi shear stress system.

1.6 KLK10 and the Kallikreins

Flow regulates the expression of hundreds of endothelial cell genes[3, 21]. A large number of endothelial genes that change in response to flow are referred to as *flow-sensitive genes*, also known as mechanosensitive genes [56-63]. The majority of these flow-sensitive genes are protein-coding genes, such as the atheroprotective *Klf2* [64], *Klf4* [65], Timp3, and *eNOS* [63], which are upregulated by the stable flow. *D-flow* also upregulates a number of pro-atherogenic genes, including vascular cell adhesion molecule-1 (*VCAM-1*) [62, 66], matrix metalloproteinases (*MMPs*) [67], and bone morphogenic protein-4 (*BMP4*), which mediate inflammatory, proliferative, and apoptotic responses in vascular endothelium [42, 68, 69].

To identify which genes are regulated by flow *in vivo*, our lab previously carried out a gene array study using endothelial RNAs obtained from carotid arteries exposed to *d-flow* vs. *s-flow* using our partial carotid ligation (**PCL**) model of mouse atherosclerosis [62]. Among hundreds of flow-sensitive genes including the well-known KLF2, **KLK10 was identified as the most flow-sensitive gene** (based on fold-change comparing *s-flow*/*d-flow*) in the study [62], but its function in ECs has never been reported. This dissertation will define its function in EC biology and atherosclerosis.

1.61 Kallikrein physiology

Human kallikreins were initially discovered at high levels in the pancreas and given the name *kallikreas* in Greek, meaning "of the pancreas". There are 16 different Kallikrein-related peptides: one plasma kallikrein (PKK) encoded by the *KLKB1* gene on chromosome 4q35 and 15 tissue kallikreins (KLK1-15) encoded in tandem on chromosome 19q13.4[234]. This cluster of tissue

KLKs represent the largest contiguous cluster of serine proteases in the human genome[235]. As serine proteases, these enzymes use a serine residue as the final catalytic triad residue to catalyze reactions. Other types of proteases include aspartic-, threonine-, cysteine-, and metalloproteases, which are also categorized according to the residue involved in their catalytic activity. Interestingly, although both serine proteases, tissue KLKs differ in many aspects from the plasma kallikrein, including different molecular weight, gene structure, substrate specificity, and function[236]. While plasma kallikrein is known for its role in anticoagulation pathway and bradykinin release resulting in vasodilation [237], tissue KLKs are best studied for their role in cancer. For example, the prostate-specific-antigen (PSA) is KLK3[238]. Also, expression of KLK5, 6, 14 is increased in ovarian cancer[239, 240].

KLK10 was initially identified as normal epithelial cell-specific 1 (NES1) protein[241], where it was found to be expressed in normal mammary and prostate epithelial cells, but markedly reduced in established breast and prostate cancer cell lines[242]. Follow-up studies suggested a potential tumor suppressor role for KLK10 with its expression downregulated in breast, prostate, testicular, and lung cancer[242-246]. The mechanisms underlying the potential tumor suppressor function have not been described. Further studies, however, showed a more complex story as KLK10 is overexpressed in ovarian, pancreatic, and uterine cancer[247-250]. Since KLK10 level can be easily measured in blood, studies have shown abnormal serum levels of KLK10 in patients with breast, prostate, or ovarian cancer[251, 252], suggesting its tissue-specific pathophysiological roles.

Now, there is growing evidence that certain KLKs are involved in tumorigenesis by activating proteolytic processes that associate with the neoplastic phenotype. For example, many

tissue KLKs participate in key proteolytic processes involved in cancer proliferation, growth, survival, angiogenesis, growth, and apoptosis (Figure 1.7)[5]. The pro- or anti- angiogenic effect of tissue KLKs are particularly of interest for the study of endothelial biology and atherosclerosis. KLK1 and -4 promote angiogenesis by cleaving light molecular weight kininogen to kinin or by activating metalloproteinases 2 and 9 to their active forms, thereby potentiating ECM hydrolysis and enhancing endothelial cell migration and neovascularization[253, 254]. Other kallikrein-related peptidases (KLK2 and KLK4) can stimulate the urokinase plasminogen activator (uPA)/uPA receptor system, which also leads to metalloproteinase activation and ECM degradation[255]. KLK12 may also promote angiogenesis by the conversion of the membrane-bound platelet-derived growth factor B (PDGF-B) precursor into a soluble form that modulates secretion of the angiogenic vascular endothelial growth factor A (VEGF-A)[256]. KLKs3, -6, and -13, have the opposite action by blocking VEGF and/or fibroblast growth factor 2 (FGF2) or generating angiostatin-like fragments from plasminogen, which are potent inhibitors of angiogenesis *in vitro.*

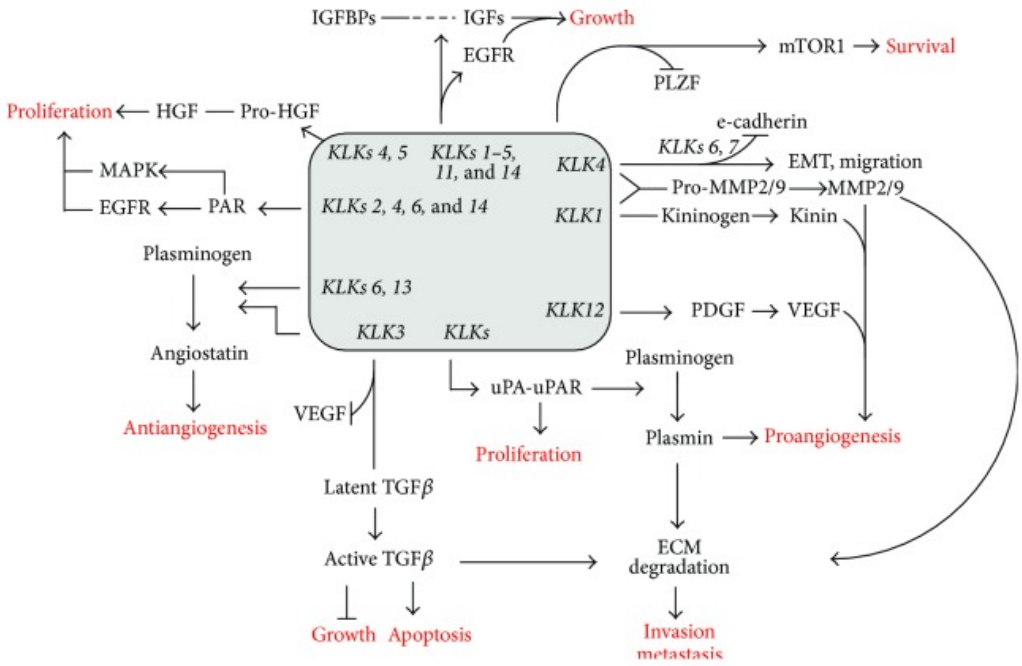

Figure 1.7. **Involvement of Kallikrein-related peptidases in cancer**. Adapted with permission from Stefanini, Ana Carolina B et al 2015. [5]

While much of the focus on kallikreins explores their roles in various cancers, recent literature has made it clear that KLKs play diverse biological and pathophysiological roles that are still emerging (Figure 1.8). For example, KLK5, -7, and -14 have been shown to cleave protease activated receptor 1, -2, and -4, thereby promoting skin inflammation and desquamation, while inhibiting the expression of adhesion factors[5]. KLK1 has been shown to protective against hypertension, cardiac, renal injury, and ischemic stroke through cleavage of low molecular weight kininogen. KLK6 is increased in in neuroinflammatory diseases including Parkinson's disease and Multiple sclerosis, where the protease contributes to increased demyelination through its proteolytic activities. KLK3 promotes semen liquefaction. A number of KLKs are involved in immune responses that regulate inflammatory diseases such as psoriasis, acne rosacea, and

amelogenesis imperfecta. Lacking from this information is the role of KLK10 in general biology and various pathologies, which has not been studied for reasons I will discuss next.

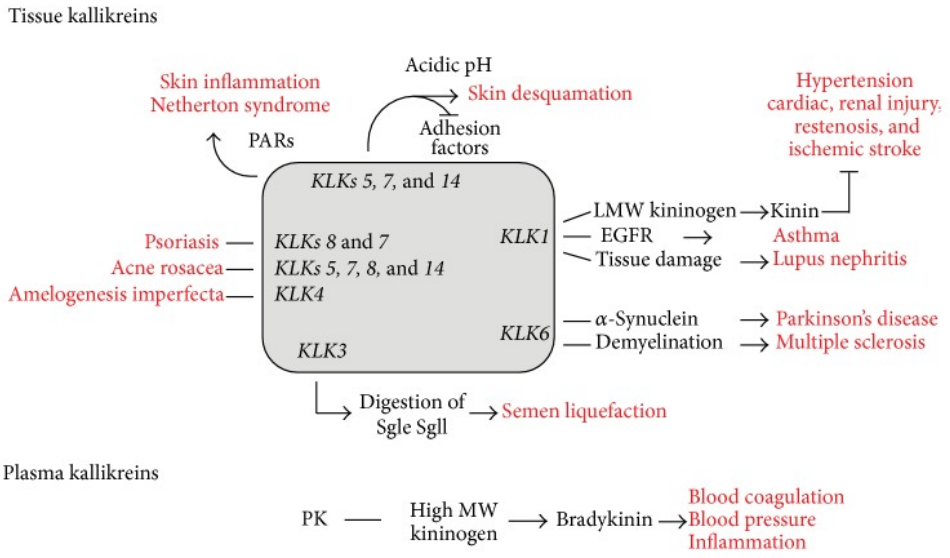

Figure 1.8. **Physiological and pathophysiological roles of kallikrein related peptidases**. Adapted with permission from Stefanini, Ana Carolina B et al 2015. [5]

1.62 Regulation of Kallikrein Enzymatic Activity

Several regulatory mechanisms protect cells and tissues from harmful proteolysis by KLKs. This includes the regulation of both the activation and inhibition of KLKs by endogenous proteases and inhibitors.

1. **Regulation of KLK activation.** KLKs are produced as inactive full-length pre-proproteins. In order to be secreted out of the cell, KLK pre-peptide sequences must be removed by intracellular proteases, typically during protein folding in the endoplasmic reticulum (ER). Once secreted outside the cell, the KLK exists as an

inactive zymogen and the pro-peptide sequences must be removed by extracellular proteases to activate the KLK[257]. This complex activation process often involves other KLKs and other serine proteases in activation cascades that exquisitely regulate each other's' activities[258]. Interestingly however, KLKs may function independently of their protease activity[259]. For example, certain KLKs have been shown to bind but not cleave their substrates, thereby potentially regulating the accessibility or bioavailability of their substrates[234]. In the case of KLK10 little is known about activation, natural substrates and regulation, except for the non-prime specificity and its relatively slow cleavage of some pro-KLK peptides[258, 260]. KLK10 is least homologous to other KLK family members and is a unique member containing a mutation at the catalytic site motif 3 (Gly^{193} to Ser^{193}) that is highly conserved in all other human KLKs[235]. This mutation may be responsible for the inability to identify specific substrate sequences of KLK10, unlike other KLKs[235, 259]. In contrast to all other KLKs, KLK10 exhibits some unique features on its N-terminal domain, being the only KLK with a charged N-terminal residue in position 16 (Glutamate) according to chymotrypsin numbering. All other KLKs possess a hydrophobic residue (Ile or Val), which inserts into the activation pocket, in order to form the stabilizing salt bridge to the highly conserved Asp194[261]. Disruption of this salt bridge typically results in complete loss of KLK activity [260]. This finding along with the unusual N-terminal sequence and the observation that KLK10 lacks protease activity in certain biological samples, such as ascites fluid from ovarian cancer patients, led to the assumption that it is not a functional serine protease as opposed to the other KLKs[262, 263]. Interestingly, Debela et al. also found expression

of recombinant E.coli-derived KLK10 with a three residue longer N-terminus starting at Leucine 13 was active against fluorogenic substrates[260]. These findings support the hypothesis that KLK10 may play an important and unique role in endothelial biology and atherosclerosis that others KLKs do not.

2. **Inhibition of KLKs.** Once activated, KLKs must not be allowed to constantly exert their proteolytic functions. Overexpression or increased activity of KLKs is associated with a number of inflammatory disease and may also be associated with the development of cancer (KLK3 is PSA). To prevent KLK enzymatic processes, the cell is equipped with a number of natural and synthetic inhibitors. Examples of natural inhibitors include metal ions such as Zn^{2+} which can inhibit most KLKs with an approximate IC50 range of 2 μM- to 24 μM [261]. Examples of proteinaceous inhibitors include Serine Protease Inhibitors (SERPINs) and lympho-epithelial Kazal-type inhibitor (LEKTI). Certain exogenous inhibitors also exist, of which sulfonyfluorides (PMSF) and diisopropylfluorophosphate (DIFP). These inhibitors covalently bind to the serine residue in the catalytic triad, permanently inhibiting their targets from catalyzing reactions. PMSF and DIFP are potent, non-specific, irreversible, and highly toxic. Lastly, synthetically derived peptide and antibody inhibitors have become increasingly more common as a therapeutic approach to inhibit specific KLKs based on their substrate specificity. Two early approaches to peptide-based KLK inhibitors used a chemical modification of low-molecular-weight kininogen peptide into a highly specific KLK1 inhibitor, and of a semenogelin-2 peptide into a potent KLK3 inhibitor[264-266].

Therapeutic Relevance of KLKs

As I have discussed, the KLK network is involved in a number of intricate signaling pathways and protein-protein interactions that regulate important biological systems, suggesting dysregulation of KLKs plays a key role in various disease pathology. Therefore, therapeutic approaches to targeting KLKs may provide a novel means to treat or prevent these diseases. KLKs can be inhibited by several types of inhibitors, including peptide, protein, and antibody inhibitors, KLK-activated prodrugs, interfering RNAs, and small molecule inhibitors. Further, recent studies have highlighted the potential for development of KLK-based immunotherapies (also described as therapeutic vaccines) for prostate cancer.

While the potential for therapeutic targeting of kallikreins has made significant progress, several roadblocks have risen as well. First, our understanding of the complex proteolytic networks that KLKs govern is far from complete. How will inhibition or targeting of one kallikrein affect the activation or functional role of other KLKs? Disruption of the KLK network could have more detrimental than beneficial consequences, therefore, a deep understanding of the role of individual KLKs in their respective disease contexts is necessary. Second, common to all closely-related enzymatic families, is the problem of designing inhibitors with extremely high specificity. This is especially a problem with small molecule inhibitors as the active sites of KLKs are well conserved, meaning that one inhibitor targeted to one KLK could be prone to inhibit other KLKs. Improved resolution of KLK crystal structures to identify KLK-specific protein structures will provide substantial help in this regard. Interestingly, Debela et al recently identified the crystal structure of KLK10, stating " it appears that the KLK10 conformation represents neither a typical zymogen nor an active protease" [267]. This data along with future insights into the activation of KLK10,

specific substrates that KLK10 acts on, and the diseases KLK10 are involved will allow for the development of therapies specifically targeted towards KLK10.

In this dissertation I will cover many of these topics, with a specific focus on our approach of KLK10-based protein therapies for the inhibition of endothelial inflammation and atherosclerosis.

2. SPECIFIC AIMS AND HYPOTHESES

2.1 Significance and Impact

Atherosclerosis is an inflammatory disease characterized by the initial development of a lesion in the arterial wall, called a "fatty streak", which contains lipid rich macrophages[1,2]. Sustained chronic exposure to pro-inflammatory molecules from white blood cells and lipids increases EC dysfunction and the severity of the initial lesion, leading to the development of an atheromatous plaque[1,2]. In the most severe cases, the atheromatous plaque can block or occlude blood flow, leading to a myocardial infarction or stroke depending on the location of the blockage. Despite the success of statins and stents for lowering the incidence of atherosclerosis, heart attacks and ischemic strokes continue to be the leading causes of death in the U.S.[3]. Therefore, new therapeutics for the treatment of atherosclerosis are still needed.

One area of research that shows promise in being able to identify novel therapeutics for atherosclerosis looks into how blood flow affects atherogenesis. Previous studies established that atherosclerosis preferentially occurs in areas of disturbed blood flow (d-flow)[4,5,6]. D-flow, characterized as low, oscillatory shear stress (OS) promotes the development of atherosclerosis by increasing EC dysfunction through the suppression of atheroprotective genes, while increasing expression of pro-atherogenic and pro-inflammatory genes[7,8,9]. In contrast, stable blood flow (s-flow) with characteristic high, unidirectional laminar shear stress (LS) promotes EC quiescence and atheroprotection by upregulating anti-atherogenic genes and suppressing pro-atherogenic genes[7,8,9].

2.2 Rationale

Our laboratory previously demonstrated that PCL surgery in mouse causes *d-flow* with characteristic low and oscillatory shear stress (**OS**), which in turn rapidly induces robust atherosclerosis within two weeks, directly demonstrating a causal relationship between *d-flow* and atherosclerosis [62, 66]. In addition, we have also developed a method of isolating intimal RNA in sufficient purity and quantity from these mouse carotid arteries following ligation[66]. This method allows for easy and rapid endothelial-enriched RNA isolation that is virtually free of contamination from vascular smooth muscle cells (αSMA) and leukocytes (CD11b, CD45) as determined by qPCR analysis using RNA from the LCA and contralateral RCA samples as a built-in control (*with s-flow*). Using these methods, we performed mRNA array studies to determine expression patterns of mechanosensitive endothelial genes (mRNAs) [268]. We also established an additional method to isolate mRNA from the endothelial layer of the greater curvature (**GC,** naturally atheroresistant, *s-flow* region) and lesser curvature (**LC**, naturally athero-prone, *d-flow* region) of the aortic arch. It is important to note that numerous studies from others and us have confirmed that the molecular and macroscopic changes occurring in the surgically induced *d-flow* region of the LCA are similar to that in LC of aortic arch exposed to naturally occurring *d-flow* [62, 130]. This mouse model and endothelial RNA/DNA preparation method has been widely adopted by numerous groups and have been cited by >200 times [62, 66, 132, 269-272]. Here, we will use these methods to determine the role of KLK10 in endothelial cell (**EC**) biology and atherosclerosis.

KLK10 is a member of the kallikrein family of serine proteases. There are 16 different Kallikrein related peptides: one plasma kallikrein (KLK1b) encoded on chromosome 4q35 and 15 tissue kallikreins (KLK1-15) encoded in tandem on chromosome 19q13.4[13]. These proteases are

produced as inactive full-length pre-pro peptides, which are then enzymatically cleaved and secreted to produce the mature, active form. It is important to note that each KLK has unique tissue and cell expression patterns and functions, although how these distinct expression patterns and unique functions are regulated remains unclear[14]. While plasma kallikrein is known for its role in anticoagulation pathway and bradykinin release resulting in vasodilation[14], tissue KLKs play diverse biological and pathophysiological roles such as tumorigenic, tumor suppressor, skin-barrier function, innate immunity, and hypertension[13]. KLKs are best known as cancer biomarkers. For example, the prostate-specific-antigen (PSA) is KLK3. Also, expression of KLK5, 6, 14 is increased in ovarian cancer[15,16]. In contrast, KLK10 levels is decreased in plasma samples of patients with breast, prostate or stomach cancer[17], however, it has not yet been studied in the context of endothelial biology or atherosclerosis. Interestingly, KLK10 is least homologous to other KLK family members and is a unique member containing a mutation at the catalytic site motif 3 (Gly^{193} to Ser^{193}) that is highly conserved in all other human KLKs[18]. This mutation may be responsible for the inability to identify specific substrate sequences of KLK10, unlike other KLKs[18,19]. Therefore, KLK10 may play a novel and unique role in endothelial biology and atherosclerosis.

Upon identifying KLK10 as a highly flow-sensitive protein, our lab has begun investigating the function of KLK10 as a possible regulator of endothelial function and atherosclerosis.

2.3 Innovation

This dissertation has numerous innovations in the novel hypotheses and ideas, and experimental approaches. The role of KLK10 in ECs has never been reported to our knowledge. The overall hypothesis proposed here is novel that *s-flow* increases expression and secretion of endothelial KLK10, which then serves as an anti-inflammatory and barrier-protective protein. We also propose a further novel hypothesis that KLK10 works via not just PAR1-, but also by PAR2-biased agonisms. Initially, it was puzzling to us that how PAR1, which is well known as the thrombin receptor that induces EC inflammation and barrier disruption, could be the receptor for KLK10 since it induces the exact opposite responses in ECs (anti-inflammation and barrier protection). Here, we will test the new concept whether KLK10 induces the "PAR1/2-biased agonisms" like APC as discussed above. Recently, a recombinant APC drug (Xigris) was pulled from the market due to increased bleeding and lack of benefits [273], but an alternatively modified APC is undergoing clinical trials as a supplemental therapy for stroke patients [274-276], raising the importance of novel approaches like ours. If successful, our study with KLK10 may become a potential anti-atherogenic therapeutic target. Technically, we propose several novel and innovative approaches. EC-targeted AAVs for overexpression of KLK10 *in vivo*: To modify KLK10 levels in mouse ECs *in vivo*, we will use ultrasound-mediated gene delivery to overexpress KLK10 plasmids. This will be compared to another simple approach of rKLK10 protein injection in mouse. Our PCL model is one of the most robust and well-accepted approaches to study flow-dependent regulation of EC genes, EC function and atherosclerosis using ApoE$^{-/-}$ mice. Recently, we have improved this model further by combining the PCL model with a single AAV-PCSK9 injection that induces hyperlipidemia and atherosclerosis in C57Bl6 mice within 2-3 weeks [277]. With this model, we no longer have to use ApoE$^{-/-}$ or LDLR$^{-/-}$ background to study atherosclerosis,

eliminating the need to generate double knockouts such as PAR1$^{-/-}$ on ApoE$^{-/-}$ background to test the role of PAR1$^{-/-}$.

2.4 Project Objective

The overall goal of this project was to determine the role of KLK10 in shear-stress mediated regulation of endothelial biology. We explore the functional roles of KLK10 on endothelial inflammation, permeability, migration, apoptosis, tube formation, and monocyte adhesion. Further, we examine the role of KLK10 in atherosclerosis using acute and chronic mouse models of atherosclerosis. Lastly, we seek to understand the mechanism of action explaining the regulation of KLK10 by shear stress and the functional effects of KLK10 on endothelial biology.

2.5 Overall Hypothesis

Because KLK10 is upregulated under *s-flow* conditions where atherosclerosis and inflammation are low, **we hypothesize that KLK10 mediates the beneficial effect of *s-flow* on the endothelium by inhibiting several aspects of endothelial dysfunction. Furthermore, we hypothesize loss of KLK10 under *d-flow* conditions promotes endothelial dysfunction and atherosclerosis.**

2.6 Specific Aim 1: Determine the regulation of KLK10 by flow and the role of KLK10 in flow-mediated EC dysfunction

Hypothesis: *KLK10 is upregulated under s-flow and downregulated under d-flow. When upregulated under s-flow, KLK10 decreases monocyte adhesion, EC inflammation, and enhances endothelial barrier function.*

This aim expands on our effort to establish and validate KLK10 as flow-sensitive and anti-inflammatory following a microarray screen of flow-sensitive genes. To test KLK10 flow-sensitivity *in vivo*, we utilized the PCL surgery that allows us to induce atherosclerosis in the Left Carotid Artery (LCA) of mice, while the Right Carotid Artery (RCA) remains healthy and serves as an internal control. KLK10 was observed to be downregulated in the LCA and upregulated in the RCA by qPCR and immunostaining; validating the initial microarray study. Additional studies employing single-cell RNA sequencing (scRNAseq) and scATAC sequencing (scATACseq) using the partial carotid ligation mouse model showed flow-regulated KLK10 expression at the epigenomic and transcription levels. The cone and plate viscometer system was also used to expose endothelial cells to s-flow or d-flow *in vitro*. qPCR and western blot showed KLK10 mRNA and protein flow-sensitivity matching microarray and *in vivo* studies. In a parallel study using human coronary arteries, we found KLK10 expression correlates with atherosclerotic plaque severity, with KLK10 expression being lowest in patients with early plaques (AHA grade 1-3) compared to high expression in patients with advanced plaques (AHA grade 4-6).

Preliminary studies indicated KLK10 to inhibit several aspects of endothelial dysfunction important in atherogenesis, with a specific focus on inflammation and permeability. We have expanded on our initial studies to assess whether has a protective function, or an anti-inflammatory function. To test this hypothesis, we have treated ECs with rKLK10 before or after the addition of

TNFα or exposure to *d-flow* and performed several different endothelial functional assays. Results from these experiments indicated that KLK10 lowered TNFα-induced and disturbed-flow induced monocyte adhesion, permeability, and inflammation. We have also used siRNA to knockdown KLK10 to test if loss of KLK10 decreases the anti-inflammatory effect of *s-flow*. We have observed loss of KLK10 increases monocyte adhesion under *s-flow* compared to cells that have been exposed to *s-flow* and treated with a scrambled siRNA. Lastly, we tested whether the anti-inflammatory and barrier-protective effects of KLK10 could be translated to mice by assessing inflammation in the lesser curvature regions of the aortic arch exposed to *d-flow* following injections of rKLK10.

2.7 Specific Aim 2: Assess the mechanisms by which KLK10 controls EC function

A paper published by Dr. Hollenberg's group indicated certain kallikreins to signal through Protease Activated Receptor (PARs). Therefore, we hypothesized that if KLK10 signals through the PARs, we would observe a loss of the anti-inflammatory effect when we treat ECs with rKLK10 and use inhibitors or siRNAs for those receptors. Preliminary experiments done earlier in the lab focused on PAR1 and PAR2. Results from these initial experiments showed inhibition or knockdown of PAR1 or PAR2 reduced the anti-inflammatory effect of rKLK10. Aim 2 continues with the hypothesis that KLK10 signals through PAR1 and PAR2.

The PARs are G-protein Coupled Receptors that are activated by site-specific cleavage on their extracellular domain. Therefore, we hypothesized that the anti-inflammatory effect of KLK10 was mediated by cleavage of either PAR1 or PAR2. To test for cleavage, we have employed two methods: 1) PAR1/2 synthetic peptide cleavage assay, and 2) PAR1/2 SEAP reporter assay. The synthetic peptide cleavage assay allows us to test whether KLK10 cleaves synthetic peptides

corresponding to the extracellular domain of PAR1/2. The PAR1/2 SEAP reporter assay relies on PAR1/2-SEAP fusion reporter constructs in which the secreted alkaline phosphatase protein has been fused to the N-terminal portion of the extracellular peptide of PAR1 or PAR2. Here, cleavage of either PAR1 or PAR2 by KLK10, Thrombin, or Trypsin can be detected by an increase in SEAP in the media. Results from both experimental approaches did not show rKLK10 to cleave PAR1 or PAR2, while Thrombin and Trypsin (positive controls) did show cleavage.

Second, if KLK10 signals through PAR1 or PAR2, it should increase the activity of downstream secondary signaling messengers, such as G-proteins or β-arrestins. We hypothesized KLK10 to signal through a β-arrestin pathway due to previous literature indicating other serine proteases signaling through this pathway and also having an anti-inflammatory effect (Activated Protein C). To test this hypothesis, we performed a time-course signaling assay treating ECs with rKLK10 or Thrombin and using phospho-specific antibodies for certain downstream signaling partners involved in the G-protein and β-arrestin pathways. We looked at p38 and ERK1/2 for G-protein signaling, and AKT and JNK for β-arrestin signaling. Thrombin induced p38 and ERK1/2 signaling as previously published, while KLK10 had no effect on either of these pathways. KLk10 and Thrombin both reduced AKT phosphorylation, although differently. KLK10 did not affect JNK signaling, while Thrombin activated it.

While KLK10 shows biological activity (Aim 1), it does not show cleavage of PAR1 or PAR2. However, the anti-inflammatory effect is still lost when PAR1 or PAR2 are inhibited. Therefore, we updated Aim 2 and tested the hypothesis that KLK10 is acting indirectly through PAR1 or PAR2 by binding or cleaving other signaling partners in the media or on the cell

membrane. To continue the search for KLK10-binding proteins or receptor, I performed a ligand-receptor capture experiment using the TriCEPS moiety purchased commercially. The TriCEPS moiety has three arms; one binds KLK10, the other binds glycosylated proteins on the cell membrane, and the last arm contains a visualization/functional biotin group. After coupling rKLK10 the TRIceps, it will be added to the cells and after binding between KLK10 and its receptor has occurred, the cells will be collected, lysed and submitted for mass spec proteomics.

2.8 Specific Aim 3: Test the role of KLK10 in atherosclerosis

Hypothesis: *Reduction of KLK10 by d-flow causes EC inflammation and barrier disruption, leading to atherosclerosis. Providing KLK10 by rKLK10 or s-flow triggers the PAR1/2-biased agonisms, which in turn inhibits EC inflammation and barrier disruption and subsequent atheroprotection.*

In this aim we have decided to focus on the use of two AAVs to overexpress KLK10 in our mouse models of atherosclerosis; a liver-specific rAAV9 and an EC-targeted rAAV2. The liver-specific rAAV9 showed injection of the AAV into WT mice increased expression of the mCherry reporter and KLK10 mRNA in the liver, but not KLK10 protein. We have since found this may be due to a premature stop codon mutation that occurred during production and packaging of the virus. For these reasons, we have updated Aim 3 to take alternative approaches to test the effect of KLK10 on *in vivo* inflammation and atherosclerosis while we work out issues with AAV

As an alternative approach to overexpress KLK10 in mice, we looked to overexpress a KLK10 plasmid *in vivo* using ultrasound-mediated gene delivery. This is a minimally invasive, non-viral and clinically translatable method of gene therapy that combines plasmid DNA with microbubbles and sonoporation to enhance membrane permeability and plasmid uptake in various

tissues. For this study, we hypothesized injections of KLK10 plasmid/microbubbles into the hindlimbs of PCL mice with ultrasound would overexpress KLK10 in the skeletal muscle and the blood, ultimately inhibiting atherosclerosis development. Using the luciferase reporter on the plasmid, we visualized overexpression of the plasmids prior to sacrificing the mice. All the mice showed bioluminescence in the hindlimb, although to varying degrees. We then sacrificed the mice and isolated the aortic arch and the carotids to assess atherosclerosis development. The mice injected with KLK10 plasmid showed a decrease in gross plaque burden, as well as plaque area, compared to the control. There were no differences in the lipid profile between KLK10 mice and control mice. From this study, we concluded overexpression of KLK10 is able to inhibit atherosclerosis development.

2.9 Potential Significance

Atherosclerosis is the major underlying cause of heart attack, ischemic stroke, and peripheral arterial disease. Despite the dramatic success of drugs and devices such as statins and stents in lowering the cardiovascular disease incidence and mortality, these atherosclerotic diseases continue to be a top cause of death in the world. This demonstrates that the current therapeutics alone are not sufficient in preventing and treating atherosclerosis, and those new classes of therapeutics such as anti-inflammatory therapeutics are needed. By studying the role of flow-sensitive genes (mRNAs and miRNAs) in EC biology and atherosclerosis, we have been able to identify a few potential anti-atherogenic therapeutics such as anti-miR-712/205 family and TIMP3 [58, 130, 132, 133]. This dissertation will show us how KLK10, one of the most flow-sensitive genes, could regulate vascular inflammation and atherosclerosis and serve as a potential anti-atherogenic therapeutic.

3. MATERIALS AND METHODS

3.1 Cell Culture

3.1.1 HAECs

Human Aortic Endothelial Cells (HAECs) were isolated from heart donor patients (*n*= 15) (according to an Institutional Review Board-approved protocol at Emory University and Georgia Institute of Technology) using a brief collagenase digestion and gentle scraping method [62]. Confluent cells were sorted for endothelial purity in the following manner: HAECs were incubated in 5 µl of DiI-acetylated LDL (acLDL; BTI) per 1 ml of complete media for 4 h before cell sorting using FACS Aria I (BD Biosciences). Human Aortic Endothelial Cells (HAECs) purchased from Lonza were used as positive controls. Human aortic SMCs (HASMCs) were used as a negative control.

Cells were cultured in 100 mM dishes (Falcon 353003) coated with 0.1% gelatin (Sigma Aldrich G9391) for 1 hr at 37°C. The media composition is MCDB131 (MediaTech) supplemented with 0.002 µg/ml FGF, 0.010 µg/ml EGF, 0.001 µg/ml VEGF, 0.002 µg/ml IGF, 50 µg/ml ascorbic acid, 0.001 mg/ml hydrocortisone, 1% bovine brain extract, 10% fetal bovine serum (FBS, Hyclone), 1% L- glutamine, and 1% penicillin-streptomycin. as we described[33]. All HAECs were grown at 5% CO2 and 37°C and used between passages 5 and 9.

3.1.2 HUVECs

Human Umbilical Vein Endothelial Cells were purchased from BD Biosciences and cultured in 100 mm dishes (Falcon 353003) coated with 0.1% gelatin (Sigma Aldrich G9391) for 1 hr at 37°C. The media composition is M199 media (Cellgro) supplemented with 20% FBS

(Hyclone), 1% bovine brain extract, 10 mM L-glutamine, and 0.75 U/mL heparin sulfate as we described[278]. All HUVECs were grown at 5% CO2 and 37°C and used between passages 5 and 9.

3.1.3 HEK293 cells

Human embryonic kidney cells 293 (HEK293) were purchased from ATCC and cultured in uncoated 100 mm plates with media composed of DMEM (4.5g/L glucose), 10% FBS, 1% L-glutamine, and 1% penicillin-streptomycin at 5% CO2 and 37°C. Cells were not passaged more than 25 times.

3.1.3 THP1 human monocytes

THP-1 human monocytes were obtained from ATCC and maintained in uncoated T75 flasks containing RPMI-1640 medium supplemented with 10% FBS and 0.05 mM 2-mercaptoethanol at 5% CO2 and 37°C as we described[278]. Cells were not passaged more than 25 times.

3.2 Shear Stress Experiments

3.2.1 Cone and Plate Viscometer

Briefly, HAECs or HUVECs were cultured to 100% confluency and then subjected to shear stress in our cone-and-plate viscometer for 24 hr. Cells subjected to laminar shear stress (LS) experienced a unidirectional shear stress of 15 dyn/cm^2, whereas cells subjected to oscillatory shear stress (OS) experienced an oscillating shear stress of 5 dyn/cm^2 at 1Hz. Alignment of ECs under LS was visually confirmed by phase-contrast microscopy. Cells were scraped in 600 μL HBSS (Corning 45000-462) and pelleted by centrifugation at 5000 rpm for 1 minute. One third

was resuspended with Qiazol (Qiagen 79306) and the rest was resuspended in phosphate-buffered RIPA with glycerol (Boston Bioproducts BP-421) and protease inhibitor (Sigma Aldrich 11697498001).

3.2.2 Ibidi Parallel Plate Pump System

As an alternative method of applying shear stress to endothelial cells, we employed the Ibidi parallel pump system (Ibidi, Munich, Germany) which moves media parallel to endothelial cells grown on a channel slide. For our studies, we used the Ibidi μ-slides I 0.4 mm slides (Ibidi, 80176). These μ-slides hold a volume of 100 μL, with a channel height of 400 μm and a cell culture surface area of 2.5 cm^2 (5 mm width × 50 mm 55 length). Prior to cell growth, μ-slides were coated with 0.1% gelatin for 1 hr at 37°C with 5.0% CO2 to improve cell adhesion. Cells (3.3×10^5) were loaded onto coated slides, grown until confluency, and exposed to LS (15 dyn/cm^2) or OS (5 dyn/cm^2 at 1Hz).

The Ibidi pump system was set up per the company's instructions and proprietary software was used to control the level of shear applied to cells by controlling total media flow rate through the channels of known dimensions. We used the red type perfusion tubing set that connects to the μ-slide and can induce shear stress of 4-40 dyn/cm^2. Sterile filters (Syringe Filter PES .22um Sterile 50, 0.22-μm pore size, EMD millipore) were used to filter the air entering the tubing system, via an air pressure pump, which applied the force required to maintain the flow rate of the media through the tubing and across the μ-slide. The air pressure pump responds to the company's proprietary software and provides air to the perfusion sets at the designated pressure with a range

of −100 mbar to +100 mbar. The air pumped into the system came from the incubator itself and thus contained 5% CO2.

3.3 Partial Carotid Ligation and endothelial RNA enrichment

3.3.1 Partial Carotid Ligation

All animal studies were performed with male C57BL/6 or *ApoE*$^{-/-}$ mice (Jackson Laboratory), were approved by Institutional Animal Care and Use Committee by Emory University, and were performed in accordance with the established guidelines and regulations consistent with federal assurance. All studies using mice were carried out with male mice at 6-10 weeks to reduce the sex-dependent variables. For partial carotid ligation studies, mice at 10 weeks were anesthetized and 3 of 4 caudal branches of Left Common Carotid Artery (LCA; left external carotid, internal carotid, and occipital artery) were ligated with 6-0 silk suture, but the superior thyroid artery was left intact. Development of *d-flow* with characteristic low and oscillating shear stress in each mouse was determined by ultrasound. All ultrasound measurements were taken using a VEVO 770 high-resolution in vivo microimaging ultrasound system with a 30-MHz mouse probe (Visualsonics). Mice were anesthetized with inhaled isoflurane, and body temperature was maintained on a heated stage for the duration of studies. Levels of anesthesia, heart rate, temperature, and respirations were continuously monitored. Pulse wave Doppler mode was used at the inlet, midpoint, and outlet of the common carotid arteries for measuring flow velocity, *M*-mode for vessel dimensions, and *B*-mode for vessel length. All measurements were gated to an electrocardiogram and respiration. Following the partial ligation, mice were either continued to be fed chow-diet for 2 days or high-fat diet for atherosclerosis studies for 3 weeks as specified in each study.

3.3.2 Endothelial RNA enrichment from the carotid arteries

Endothelial-enriched RNA was prepared from the LCA and the contralateral right common carotid artery (RCA) control following 48 hrs after the partial ligation. Mice were sacrificed by CO_2 inhalation according to Emory University's IACUC protocol and pressure perfused with saline containing heparin (10 U/ml) via the left ventricle after severing the inferior vena cava. The LCA and the RCA were then isolated and carefully cleaned of periadventitial fat. The carotid lumen was quickly flushed (few seconds) with 150 µl of QIAzol lysis reagent (QIAGEN) using a 29-gauge insulin syringe in a microfuge tube. The eluate was then used for intimal RNA isolation using an miRNeasy mini kit (QIAGEN) according to the manufacturer's instructions. The carotid artery left over after flushing with QIAzol was used to prepare RNA from media and adventitia. Media and adventitia was snap-frozen in liquid nitrogen, pulverized by mortar and pestle, and lysed in QIAzol lysis reagent (700 µl per carotid), and RNA was isolated using the miRNeasy mini kit.

3.4 En face preparation and immunohistochemical staining of mouse arteries

3.4.1 En face immunostaining of the aortic arch

For *en face* immunostaining, C57BL/6 mice were euthanized under CO_2 and the aortas were pressure-fixed with 10% formalin saline. The aortas were carefully cleaned *in situ* and the aortic arch as well as thoracic aortas were dissected and opened longitudinally. The aortas were then permeabilized using 0.1% Triton-X100 in PBS for 15 minutes, blocked for 2 hrs with 10% donkey serum, and incubated with primary antibodies overnight at 4°C followed by Alexa Fluor-conjugated secondary antibodies (ThermoFisher Scientific, 1:500) for 2 hrs at room temperature

the following day. The lesser curvature (LC) and greater curvature (GC) of each arch were separated and mounted on glass slides with VectaShield that contained DAPI (Vector Laboratories). *En face* images were collected as a Z-stack with a Zeiss LSM 800 confocal microscope.

3.4.2 Immunostaining of mouse frozen sections

For mouse frozen section staining studies, fresh mouse aortas (C57BL/6 or *ApoE*$^{-/-}$ mice) were euthanized under CO_2 and the aortas were pressure-fixed with 10% formalin saline. Aortas were then placed in Tissue-Tek OCT compound, snap-frozen in liquid nitrogen, and sectioned at 7 μm. Sections from aortas were permeabilized using 0.1% Triton-X100 in PBS for 15 minutes, blocked for 2 hrs with 10% donkey serum, and incubated with primary antibodies overnight at 4°C followed by Alexa Fluor-conjugated secondary antibodies (ThermoFisher Scientific, 1:500) for 2 hrs at room temperature the following day. Slides were then mounted using VectaShield that contained DAPI (Vector Laboratories) and imaged on a Zeiss LSM 800 confocal microscope.

3.5 Immunohistochemical staining of human coronary sections

For human coronaries arteries, 2 mm cross sections of the left anterior descending arteries were obtained from de-identified human hearts not suitable for cardiac transplantation donated to LifeLink of Georgia. The de-identified donor information is shown in Supplementary Table 1. Tissues were fixed in 10% neutral buffered formalin overnight, embedded in paraffin, and 7 μm sections were taken, and stained as we described[279, 280]. Sections were deparaffinized and antigen retrieval was performed using a pressure cooker as described previously[279, 280]. Sections were then permeabilized using 0.1% Triton-X100 in PBS for 15 minutes, blocked for 2hrs with 10% goat

serum, and incubated with primary antibodies overnight at 4°C followed by Alexa Fluor-conjugated secondary antibody for 2 hrs at room temperature the following day. Nuclei were counter-stained with DAPI (Vector Laboratories, Burlingame, Calif). Hematoxylin and Eosin staining (American Mastertech) was performed according to the manufactures recommendation and plaque area quantification using ImageJ software (NIH) was done as we described[279, 280].

3.6 Quantitative real-time polymerase chain reaction (qPCR)

Total RNAs from mouse organs or cell cultures were isolated using RNeasy Mini Kit (Qiagen 74106) and reverse transcribed to cDNA using High-Capacity cDNA Reverse Transcription Kit (Applied Biosystems 4368814). qPCR was performed for genes of interests using VeriQuest Fast SYBR QPCR Master Mix (Affymetrix 75690) with custom designed primers and 18S as house-keeping control as we previously described[33]. The qPCR conditions were 10 min at 95°C, followed by 40 cycles of 95°C for 5 s and 60°C for 30 s. Primers used for human and mouse samples are listed in Table 3.1.

Primer (custom)	Sequence
h_KLK10 For	GAGTGTGAGGTCTTCTACCCTG
h_KLK10 Rev	ATGCCTTGGAGGGTCTCGTCAC
m_KLK10 For	CGC TAC TGA TGG TGC AAC TCT
m_KLK10 Rev	ATA GTC ACG CTC GCA CTG G
H/M 18S For	AGGAATTGACGGAAGGGCACCA
H/M 18S Rev	GTGCAGCCCCGGACATCTAAG
h_VCAM1 For	GATTCTGTGCCCACAGTAAGGC
h_VCAM1 Rev	TGGTCACAGAGCCACCTTCTTG
h_ICAM1 For	AGCGGCTGACGTGTGCAGTAAT
h_ICAM1 Rev	TCTGAGACCTCTGGCTTCGTCA
h_HTRA1 For	GACAGGCCAAAGGAAAAGCC
h_HTRA1 Rev	GCTCCTGAGATCACGTCTGG

Table 3.1. **Primer gene targets and primer sequences.**

3.7 Recombinant KLK10 production in CHO-K1 cells and treatment of endothelial cells *in vitro*

We initially used human recombinant KLK10 (rKLK10; Ala34-Asn276 with a 6x N-terminal His tag) produced in E.coli (Ray Biotech, 230-00040-10) for functional studies. Follow-up studies were carried out using human rKLK10 produced in CHO-K1 cells using a full-length expression vector (pcDNA 3.4, Met1-Asn276). rKLK10 with a 6x C-terminal His tag was affinity purified using HisPur Ni-NTA Resin (Thermo Scientific) per the manufacturer's instruction using the conditioned medium and dialyzed in PBS to reach a final concentration of 0.88 mg/mL. To ensure similar properties from the two different rKLK10 formulations, human rKLK10 produced

in the mammalian CHO-K1 cells validated the initial results from e.coli-derived KLK10. Amino acid sequencing analysis of the purified rKLK10 by mass spectrometry showed that our rKLK10 preparation was a mature form expressing Ala34-Asn276.

3.8 Transfection of nucleic acids *in vitro*

Cells were transiently transfected with a human KLK10-encoding plasmid (pCMV6-KLK10-Myc-DDK; Origene RC201139) at 0.1-1 μg/mL or as a control a GFP plasmid (PmaxGFP, Lonza, Cat. No. D-00059) using Lipofectamine 3000 (Invitrogen, Cat. No. L3000008) as we described[33]. Alternatively, cells were transfected with KLK10 siRNA (25 nM; Dharmacon; J-005907-08), PAR1 (50 nM; Dharmacon; L-005094-00-0005), PAR2 (50 nM; Dharmacon; L005095-00-0005), HTRA1 (50 nm; Dharmacon L-006009-00-0010) or control non-targeting siRNA (25 or 50 nM; Dharmacon; Cat. No. D-001810-10-20) using Oligofectamine (Invitrogen, Cat. No. 12252011) as we described[33].

3.9 Endothelial Functional Assays

3.9.1 Endothelial migration assay

Endothelial migration was measured by the endothelial scratch assay, as we described[281]. Briefly, HUVECs were treated with rKLK10 at increasing doses overnight and cell monolayers were scratched with a 200-μL pipette tip. The monolayer was washed once, and the medium was replaced with 2% serum media. After 6 hrs, the number of cells migrated into the scratch area were quantified microscopically using NIH ImageJ.

3.9.2 Endothelial TUNEL apoptosis assay

Endothelial apoptosis was determined using the TUNEL apoptosis assay, as we described[282]. Briefly, HUVECs were treated with rKLK10 at increasing doses overnight and the cells were fixed using 4% paraformaldehyde for 15 minutes and permeabilized with 0.1% Triton X-100 for 15 minutes. TUNEL staining was then performed using a commercially available kit (Roche, 12156792910) and the number of TUNEL-positive cells were counted using NIH ImageJ.

3.9.3 Endothelial tube formation assay

Endothelial tube formation was measured using a Matrigel tube formation assay, as we described[281]. Briefly, HUVECs were seeded in a growth factor reduced Matrigel (BD Bioscience) coated 96-well plate and incubated with rKLK10 (100 ng/mL) for 6hrs at 37°C. Tubule formation was quantified microscopically by measuring tubule length using NIH ImageJ.

3.9.4 Endothelial ki67 proliferation assay

Endothelial proliferation was determined using Ki67 immunohistochemistry, as we described[29]. Briefly, HUVECs were treated with rKLK10 at increasing doses overnight and the cells were washed twice with PBS, fixed using 4% paraformaldehyde for 15 minutes, and permeabilized with 0.1% Triton X-100 for 15 minutes. After blocking with 10% Goat Serum for 2hrs at RT, cells were incubated overnight at 4°C with rabbit anti-Ki67 primary antibody (Abcam ab15580, 1:100). The following day, cells were washed three times with PBS, incubated for 2hrs at RT protected from light with Alexa-fluor 647-labeled goat anti rabbit IgG (1:500 dilution), and counterstained with DAPI. The number of Ki67 positive cells were counted using NIH ImageJ.

3.9.5 Endothelial FITC-Avidin permeability assay

Endothelial permeability was determined by FITC-avidin binding to biotinylated gel, as previously described[283]. Briefly, HAECs were seeded on biotinylated-gelatin and treated with rKLK10 overnight followed by thrombin (5 U/mL) for 4hrs or OS for 24hrs as described above. Following the completion of the experiments, FITC-avidin was added to the cells and fluorescent intensity was measured using NIH ImageJ.

3.9.6 Endothelial monocyte adhesion assay

Monocyte adhesion to ECs was determined using THP-1 monocytes (ATCC TIB-202) as we described[33]. In brief, THP-1 cells (1.5×10^5 cells/mL) were labeled with a fluorescent dye 2',7'-bis(carboxyethyl)-5 (6)-carboxyfluorescein-AM (Thermo Fisher Scientific B1150; 1 mg/mL) in serum-free RPMI medium (Thermo Fisher Scientific 11875093) for 45 minutes at 37°C. After exposure to flow or other experimental treatments, the ECs were washed in RPMI medium before adding 2',7'-bis(carboxyethyl)-5 (6)-carboxyfluorescein-AM–loaded THP-1 cells. After a 30-minute incubation at 37°C under no-flow conditions, unbound monocytes were removed by washing the endothelial dishes 5× with HBSS and cells with bound monocytes were fixed with 4% paraformaldehyde for 10 minutes. Bound monocytes were quantified by counting the number of labeled cells at the endothelium under a fluorescent microscope.

3.10 Preparation of whole-cell lysate and immunoblotting

At the completion of the study, cells were put on ice and washed 3× with ice-cold HBSS and lysed with RIPA buffer containing protease inhibitors (Boston Bioproducts BP-421)[33]. The protein content of each sample was determined by Pierce BCA protein assay. Aliquots of cell

lysate (25 μg) were resolved on 10% to 12% SDS-polyacrylamide gels and subsequently transferred to a polyvinylidene difluoride membrane (Millipore). The membrane was blocked using 5% milk in TBST for 1hr and incubated with the following primary antibodies overnight at 4°C in 1% BSA in TBST at the concentration recommended by the manufacturer. The following day, HRP-conjugated secondary antibody was added for 1 hr at RT in 1% BSA in TBST and protein expression was detected by enhanced chemiluminescence (ECL) method using a western blot imager (iBright, Thermo Fisher Scientific).

3.11 rKLK10 treatment and KLK10 overexpression in C57BL/6 and ApoE-/- mice

Treatment with rKLK10 was first performed in C57BL/6 mice by administering rKLK10 (0.006-0.6 mg/kg) by tail-vein once.. Three days later mice were euthanized by CO_2 inhalation and *en face* preparation of the aorta was performed as we described[33]. Alternatively, *ApoE*$^{-/-}$ on a high-fat diet containing 1.25% cholesterol, 15% fat and 0.5% cholic acid were given the partial carotid ligation surgery and rKLK10 or vehicle was administered by tail-vein once every three days for three weeks as we described[33]. Following the completion of the study, mice were euthanized by CO_2 inhalation and the aortas were excised, imaged, and sectioned for IHC[33].

KLK10 plasmid overexpression was performed using ultrasound-mediated sonoporation method of gene therapy as reported[284-286]. Briefly, perfluoropropane microbubbles encapsulated by DSPC and DSPE-PEG2000 (9:1 molar ratio) were made using the shaking method as previously described[284-286]. KLK10 plasmid expressing secreted KLK10 and luciferase (pCMV-Igκ-KLK10-T2A-Luc) from GENEWIZ or luciferase plasmid (pCMV-Luc) from Invitrogen (50 μg each) was then mixed with the microbubbles ($5x10^5$) and saline to reach 20 μl total volume.

Following partial carotid ligation, *ApoE*$^{-/-}$ mice on a high-fat diet were injected intramuscularly to the hind-limbs with the plasmid-microbubble solution. The injected areas of the hind-legs were then exposed to ultrasound (0.35 W/cm^2) for 1 minute, and repeated 10 days later. At the completion of the study, 3 weeks after the partial ligation, mice were anesthetized, administered with luciferin (IP; 3.75 mg) and imaged for bioluminescence on a Bruker *In Vivo* Xtreme X-ray Imaging System. Mice were then euthanized by CO_2 inhalation and the aortas were excised, imaged, and sectioned for staining as described above.

3.12 PAR cleavage assays

3.12.1 Synthetic Peptide Cleavage Assay

Synthetic peptides corresponding to the extracellular domain of PAR1 (AA Ala22-Thr102) and PAR2 (AA Ile26-Thr75) were assembled by automated Fmoc/tBu-solid-phase synthesis (model CS336X; CSBio) followed by cleavage in trifluoroacetic acid (TFA)/phenol/thioanisole/ethanedithiol/water (10:0.75:0.5:0.25:0.5, w/w; 25 °C, 90 minutes) and precipitation with diethyl ether. The crude peptides were purified by reversed-phase high-pressure liquid chromatography and were obtained in the form of their TFA salts. Their masses as well as masses of their theoretical Lys-C protease (Promega) fragments, obtained upon digestion, were confirmed by electrospray-ionization mass spectrometry (maXis ESI-TOF; Bruker). PAR1 and PAR2 peptides (100 μM) were then incubated with rKLK10 (100 ng/mL), thrombin (5 U/mL), or trypsin (5 U/mL) for 30 minutes at 37°C and analyzed by Tricine-SDS-PAGE followed by Coomassie stain[287].

3.12.2 PAR1 and PAR2 alkaline phosphatase reporter assay

PAR1/2-Alkaline Phosphatase (AP) constructs made as previously described[288-290] were transfected into HAECs (1 μg/mL) for 24hrs using Lipofectamine 3000. Cells were treated with rKLK10 (100 ng/mL), thrombin (5 U/mL), or trypsin (5 U/mL) for 30 minutes. Conditioned media were then collected and analyzed for secreted alkaline phosphatase activity (SEAP) using a commercial kit (T1015, Invitrogen) and a microplate reader[288-290].

3.13 KLK10 affinity pulldown using TRICEPS

Affinity pulldown using TRICEPS-biotin was performed as described previously[291]. Briefly, HAECs were grown to confluency on a 15 cm^2 dish and were oxidized using 1.5 mM sodium metaperiodate (NaIO4) for 15min at 4°C. rKLK10, glycine, or Transferrin (300 μg each) was coupled to 150 μg of TRICEPS v.3.0 (DualSystems Biotech) for 1.5hr in 25 mM HEPES pH 8.2 at room temp and added to the HAECs for 1.5hr at 4°C. For flow cytometry and immunostaining experiments, cells were fixed with 4% paraformaldehyde and incubated with Streptavidin-PE for 1hr followed by flow cytometry or confocal microscopy. For the identification of KLK10 binding proteins, cells were scraped and lysed, followed by affinity pulldown and submitted to DualSystems Biotech for LC-MS/MS tandem mass spectrometry analysis as previously described[291].

3.14 Proximity Ligation Assay

Duolink In Situ Red Starter Kit Mouse/Rabbit Proximity Ligation Assay was purchased from Millipore Sigma (DUO92101) and was performed according to the manufactures protocol using KLK10 and HTRA1 antibodies described above.

3.15 rKLK10:HTRA1 cleavage assay and mass spectrometry analysis of KLK10 cleavage products

rKLK10 (500 ng, described above) was incubated with wild-type human recombinant (rHTRA1) (500 ng, Origene TP322362**)** or kinase-inactive rHTRA1 containing an S328A mutation (500 ng Origene TP700208**)** for 18hrs at 37°. Cleavage products were reduced with dithiothreitol (5 mM) for 30min at room temp followed by alkylation with iodoacetamide (25 mM) for 30min at room temp in the dark and run on a 12% SDS-PAGE gel followed by Coomassie G-250 staining. Gel pieces corresponding to 35, 33, and 17kDa KLK10 proteins were excised from Coomassie-stained gels for tryptic digestion and mass spectrometry.

3.16 In-gel digestion

Gel pieces were cut into smaller pieces for efficient destaining and digestion. The pieces were covered with 50 mM ammonium bicarbonate/acetonitrile (1:1, v/v) and were incubated with occasional vortexing for 5 min, after which the solution was discarded. This destaining step was repeated depending on the staining intensity. Subsequently, neat acetonitrile was added and the pieces were incubated with occasional vortexing for 10 min or until gel pieces became white and dry. The acetonitrile was discarded and the gel pieces were dried under vacuum. For digestion, the gel pieces were covered with trypsin solution (10 ng/μL) in 50 mM ammonium bicarbonate and were incubated overnight at 37 °C. Next day, the supernatant containing the tryptic peptides were saved and the gel pieces were used for further extraction of peptides. Gel pieces were completely covered with the extraction buffer containing (1:1, v/v) 5% formic acid/50% acetonitrile and were incubated with occasional vortexing for 10 min. The extraction was repeated one more time followed by incubation with neat acetonitrile. The extracted peptides were dried under vacuum.

3.17 Mass Spectrometry

Dried peptides were resuspended in 10 µL of loading buffer (0.1% trifluoroacetic acid, TFA) and 2 µL was loaded onto a self-packed 25 cm (100 µm internal diameter packed with 1.7 µm Water's CSH beads) and was separated using Dionex 3000 RSLCnano liquid chromatography system. The liquid chromatography gradient started at 1% buffer B (buffer A: 0.1% formic acid in water, buffer B: 0.1 % formic acid in acetonitrile) and ramps to 5% in 0.1 minute. This was followed by a 25 min linear gradient to 40% B and finally a 5 minute 99% buffer B flush. The mass spectrometry data were acquired on an Orbitrap Fusion Tribrid Mass Spectrometer (ThermoFisher Scientific). The spectrometer was operated in data dependent mode in top speed with a cycle time of 3 seconds. Survey scans were collected in the Orbitrap with a 60,000 resolution, 400 to 1600 m/z range, 400,000 automatic gain control (AGC), 50 ms max injection time and RF lens at 60%. Higher energy collision dissociation (HCD) tandem mass spectra were collected in the ion trap with a collision energy of 35%, an isolation width of 1.6 m/z, AGC target of 10000, and a max injection time of 35 ms. Dynamic exclusion was set to 30 seconds with a 10 ppm mass tolerance window.

3.18 Protein identification

Mass spectrometry data was analyzed according to a published protocol[292]. Spectra were searched using Proteome Discoverer 2.1 against human Uniprot (Swiss-Prot only) database (20,381 target sequences). Searching parameters included fully tryptic restriction and a precursor mass tolerance (± 20 ppm). Methionine oxidation (+15.99492 Da), asaparagine and glutamine deamidation (+0.98402 Da) and protein N-terminal acetylation (+42.03670) were variable modifications (up to 3 allowed per peptide); cysteine was assigned a fixed carbamidomethyl

modification (+57.021465 Da). Percolator was used to filter the peptide spectrum matches to a false discovery rate of 1%.

3.19 Serum lipid analysis

Serum lipid analysis was performed at the Cardiovascular Specialty Laboratories (Atlanta, GA) using a Beckman CX7 biochemical analyzer for total cholesterol, triglycerides, HDL and LDL as we reported[33].

3.20 KLK10 ELISAs

KLK10 secreted into the conditioned cell culture media from HAECs exposed to shear stress was measured by using a human KLK10 ELISA kit (MyBioSource, MBS009286). Secreted KLK10 in mouse plasma was measured by using a mouse KLK10 ELISA kit (Antibodies-online, ABIN628061).

3.21 Single-cell RNAseq and ATACseq

3.21.1 Mouse partial carotid ligation (PCL) surgery

To induce *d-flow*, PCL surgery was performed. Briefly, mice were initially anesthetized with 3.5% isoflurane and subsequently maintained on 1.5% isoflurane during the entire procedure. The LCA bifurcation was exposed by blunt dissection and three of four caudal LCA branches (left external carotid, internal carotid, and occipital arteries) were ligated with 6-0 silk sutures, leaving the superior thyroid artery intact. The contralateral RCA was left untouched and served as an internal control. Following surgery, analgesic buprenorphine (0.1 mg kg^{-1}) was administrated. At 2 days (2D-R and 2D-L) and 2 week post-partial ligation (2W-R and 2W-L), LCAs and RCAs

were dissected out and a luminal enzymatic digestion of the carotids was performed to isolate endothelial-enriched single-cell preparations. Single-cell preparations from LCAs and RCAs from 12 mice were pooled to prepare single-nuclei for scATACseq study, while LCAs and RCAs from 10 additional mice were pooled to obtain single cells for scRNaseq study. Both studies were performed back-to-back.

3.21.2 Single-cells and single-nuclei isolation and library preparation for scRNaseq and scATACseq analyses

After euthanizing the mice using CO_2, the LCAs and RCAs were dissected, cleaned, and perfused with normal saline solution before a dissociation buffer was injected. The dissociation buffer was slightly modified from a previously reported recipe[293] by including 600 U ml^{-1}Type II Collagenase and 60 U ml^{-1} DNase I in 0.5% fetal bovine serum (FBS) of 1X phosphate-buffered saline (PBS). Immediately after the introduction of dissociation buffer into the carotid lumens, the ends of the RCAs and LCAs were clamped and dissected out. The explanted carotids were incubated in 35-mm dishes containing HEPES-buffered saline solution (HBSS) at 37 °C. After 45 min, the LCA and RCA lumens were flushed with the dissociation buffer into a 1.5 mL Eppendorf tube. The flushings were washed with ice-cold PBS and centrifuged for 5 min at 500 x g and were further incubated with accutase for 5 min at 37 °C to prepare single-cells.

For scRNaseq, single-cells were resuspended in 1% BSA in PBS, counted and immediately processed at the Emory Integrated Genomics Core (EIGC) using a 10x Genomics Chromium device for single-cell encapsulation, barcoding, and RNA preparation. Subsequently, the cDNA libraries were prepared and sequenced on Illumina NextSeq® to a depth of 15,000 unique molecule identifier (UMI) per cell. UMI counts for each cellular barcode were quantified and used to

estimate the number of cells successfully captured and sequenced. For scATACseq, single-cells were washed with 0.04% BSA and incubated in a lysis buffer containing 10 mM Tris-HCl, 10 mM NaCl, 3 mM $MgCl_2$, 0.1% Tween-20, 0.1% NP40, 0.01% digitonin and 1% BSA in nuclease-free Water. After 5 min, the lysates were washed with wash buffer (10 mM Tris-HCl, 10 mM NaCl, 3 mM $MgCl_2$, and 0.1% Tween-20) and the nuclei were resuspended in a Nuclei Buffer® (10x Genomics), and were immediately processed at the EIGC for scATAC sequencing. The nuclei (~7,000 each) from 2D (R and L) and 2W (R and L) were individually incubated with ATAC Buffer and ATAC Enzyme (Tn5 transposase, 10x Genomics) to form a transposition mix for 60 min at 37°C following manufacturer's protocol. A mild detergent condition was chosen to keep the nuclei intact during tagmentation. Then a master mix composed of Barcoding Reagent, Reducing Agent B and Barcoding Enzyme was added. The resulting mixtures were loaded onto a Chromium Chip and single-nuclei gel emulsions with barcoding were prepared following the manufacturer's instructions. The Cell Ranger Single-Cell Software suite was then used for demultiplexing, barcode processing, alignment, and initial clustering of the raw scATACseq and scRNaseq profiles.

3.21.3 scRNAseq data analysis

We analyzed the scRNaseq data with Seurat R package. Briefly, the scRNaseq data files were processed with Cell Ranger Software where the sequencing reads were aligned to mouse reference genome using STAR aligner. A read was considered exonic, if at least 50% of it mapped to an exon, intronic (if it was non-exonic and intersected an intron), or intergenic otherwise. For reads that aligned to a single exonic locus but also aligned to 1 or more non-exonic loci, the exonic locus was prioritized and the read was considered to be confidently mapped to the exonic locus.

Cell Ranger also aligned exonic reads to annotated transcripts. An annotated transcript that aligned to the same strand was considered to be confidently mapped to the transcriptome. These confidently mapped reads were used for unique molecular identifier (UMI) counting and subsequent analysis to generate h5 files. The h5 file of each sample was then processed with Seurat R package for further analysis. First, a quality check was performed to remove low-quality cells and doublets by selecting the cells containing unique feature counts of over 200 or less than 7,600, and cells with lower than 10% of mitochondrial counts. All datasets were merged, normalized, scaled, clustered, and visualized by UMAP. As an independent validation, the scRNaseq analysis was also carried using Partek Flow® analysis software following the same filtering criteria. Both Partek Flow and Seurat analyses provided consistent and nearly identical results.

3.21.4 Single-cell ATACseq data analysis

The sequencing data for the scATAC study were processed by Cell Ranger (CR) Software. Briefly, to avoid barcode misidentification, each 16-nucleotide barcode was compared against a 'whitelist' of correct barcode sequences, and the frequency of each whitelist barcode is counted. The barcodes with less than 2 nucleotide mismatches were corrected and included for further analysis. Prior to the alignment of the sequences to a mouse reference sequence (mm10), the *cutadapt* tool was used to trim the barcodes using default parameters. Reads with less than 25 bp were not included in further analysis. Fragments were then identified as reading pairs if their MAPping Quality (MAPQ) scores were larger than 30 on both reads, not mitochondrial, and not chimerically mapped. Once the fragments were filtered, fragments.tsv.gz file was created marking the start and end of the fragment after adjusting the 5′ ends of the read-pair to account for transposition. The file was position-sorted and ran through the SAMtools tabix command with

default parameters. Peak calling was also performed with Cell Ranger using the sites as determined by the ends of the fragments in the position-sorted fragments.tsv.gz file, which counts the number of transposition events at each base-pair along the genome. A signal threshold was set up based on an odds-ratio of 1/5 that determines whether a region is a peak signal or noise. Consequently, not all cut sites were within a peak region. Peaks within 500 bp of each other were merged to produce a position-sorted BED file of peaks. Finally, the Peak-Barcode Matrix was produced which consisted of the counts of fragment ends within each peak region for each barcode. This raw Peak-Barcode Matrix captures the enrichment of open chromatin accessibility per barcode.

3.22 Statistical analyses

Statistical analyses were performed using GraphPad Prism software. All of the n numbers represent biological replicates. Error bars depict the standard error of means (SEM). Initially, the data sets were analyzed for normality using the Shapiro-Wilk test ($P<0.05$) and equal variance using the F test ($P>0.05$). Data that followed a normal distribution and possessed equal variance were analyzed using 2-tailed Student t test or 1-way ANOVA, where appropriate with Bonferroni post hoc test as needed. In the case where the data showed unequal variances, an unpaired t test with Welch correction was performed or Brown-Forsythe and Welch ANOVA for multiple comparisons. In the case where the data failed the Shapiro-Wilk test ($P>0.05$), a nonparametric Mann-Whitney U test was conducted for pairwise comparisons or the Kruskal-Wallis for multiple groups was performed. For animal experiments, we carried out a priori power analysis (G*Power3 analysis at d=2.0, α=0.05, power=0.95, one-tail t-test) based on our previous experience using the PCL model to determine the number of animals needed to achieve statistically significant results.

Outliers were determined and excluded by calculating interquartile range (IQR) and multiplying 1.5 x IQR.

4. DETERMING THE ROLE OF KLK10 IN FLOW-MEDIATED EC DYSFUNCTION

4.1 Introduction

Determining the mechanisms by which flow regulates endothelial biology and atherosclerosis is critical for the development of novel therapeutics that targets the disease at the molecular level. As I have described in the Introduction, flow regulates endothelial function through the flow-sensitive coding and non-coding genes. Using the PCL mouse model of atherosclerosis and transcriptomic studies, we previously identified hundreds of flow-sensitive genes in endothelial cells (ECs) that change by *d-flow* in the left carotid artery (LCA) compared to the *s-flow* in the right carotid artery (RCA)[3, 21]. Among the flow-sensitive genes were well-known mechanosensitive genes Krüppel-like Factor 2 (KLF2)[22], Krüppel-like Factor 4 (KLF4)[23], bone morphogenetic protein 4[24], hypoxia inducible factor-1a pathway regulating gene UBE2c[25, 26], sterol regulatory element binding protein 2[27], PPAP2B[28], ZBTB46[29], JCAD/KIAA1462[30], JMJD2b[31], endothelial nitric oxide synthase[32], and several flow-sensitive microRNAs[33]. Interestingly, Kallikrein related-peptidase 10 (*KLK10)*, a secreted serine protease, was identified as one of the most flow-sensitive; with high expression under *s-flow* and low expression under *d-flow* conditions[3] (Figure 4.1).

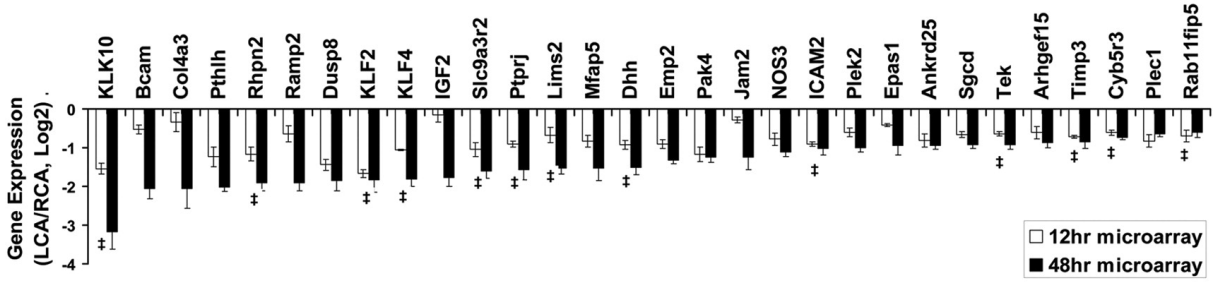

Figure 4.1. **Flow-sensitive genes identified in the PCL mouse model by microarray 12hr and 48hr post-ligation.** Values are expressed at Log2 FC LCA/RCA. Adapted from Ni, C. et al. [3].

Following the initial identification of KLK10 as flow-sensitive, a subsequent publication by Sangwung, P et al provided insight into the mechanisms by which flow regulates KLK10 expression[294]. In this paper, the researchers found endothelial-specific deletion of flow-sensitive transcription factors *klf2* and *klf4* significantly reduced the expression of KLK10 in endothelial cells. Under normal conditions, *Klf2* and *klf4* are upregulated by *s-flow.* Therefore, this finding supports the hypothesis of a mechanism where *Klf2* and *klf4* are upregulated by *s-flow* and in-turn increase transcription of the *KLK10* gene. KLF2 and KLF4 are generally known as atheroprotective transcription factors as they regulate the expression of key anti-inflammatory gene such as eNOS and thrombomodulin[294]. Further, endothelial-specific double knockout of *klf2* and *klf4* promotes atherosclerosis. For these reasons, it is logical to hypothesize as a target of KLF2 and KLF4, KLK10 mediates the atheroprotective effects of *s-flow* on the endothelium through inhibition of several different endothelial dysfunctions. In this study, we tested the hypothesis KLK10 regulates EC function by evaluating its role in endothelial inflammatory response, tube formation, migration, proliferation, and apoptosis, which play critical roles in the pathogenesis of atherosclerosis (Figure 4.2).

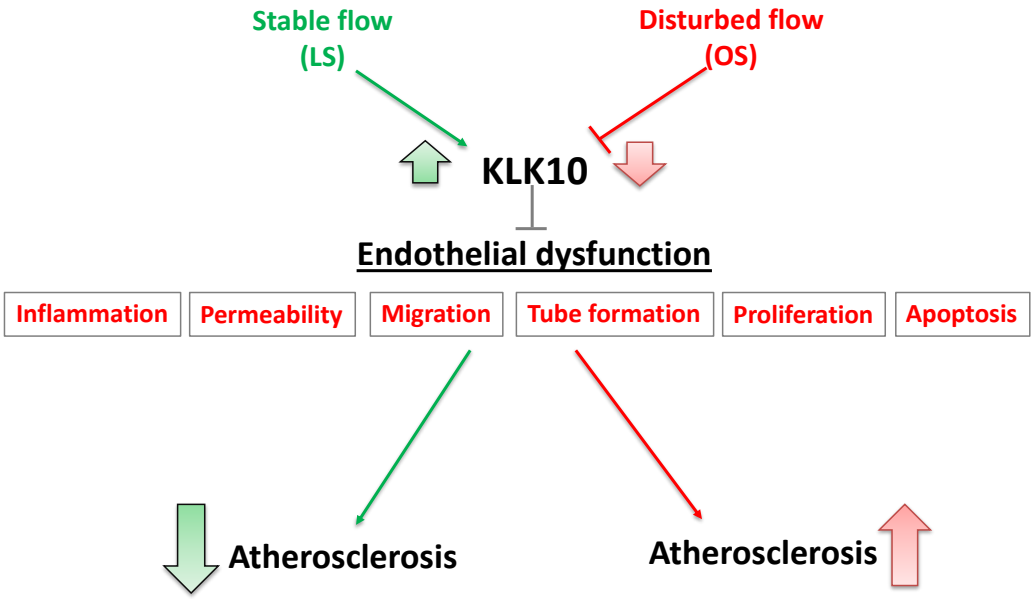

Figure 4.2. **Initial working hypothesis.** KLK10 expression is increased by stable flow (laminar shear stress) and inhibited by disturbed flow (oscillatory shear stress). When upregulated under stable flow, KLK10 inhibits several aspects of endothelial dysfunction including inflammation, permeability, migration, tube formation, proliferation, and apoptosis.

4.2 Results

4.2.1 KLK10 expression is increased by s-flow and decreased by d-flow in the carotid arteries of PCL mice.

Before exploring the functional roles of KLK10 in endothelial cells, we first sought to validate our previous mouse PCL DNA microarray data (Figure 4.1). To do so, we first examined the regulation of KLK10 by flow at the mRNA and protein level *in vivo* using the PCL mouse model (Figure 4.3). Following the flushing of endothelial RNAs from the carotid arteries, qPCR analysis of mouse KLK10 mRNA found KLK10 to be decreased by 90% at the mRNA level in the LCA compared to RCA. This finding was supported by immunostaining of mouse frozen tissue

sections which also showed a significant decrease in KLK10 protein expression at the endothelial layer, indicated by CD31 immunostaining.

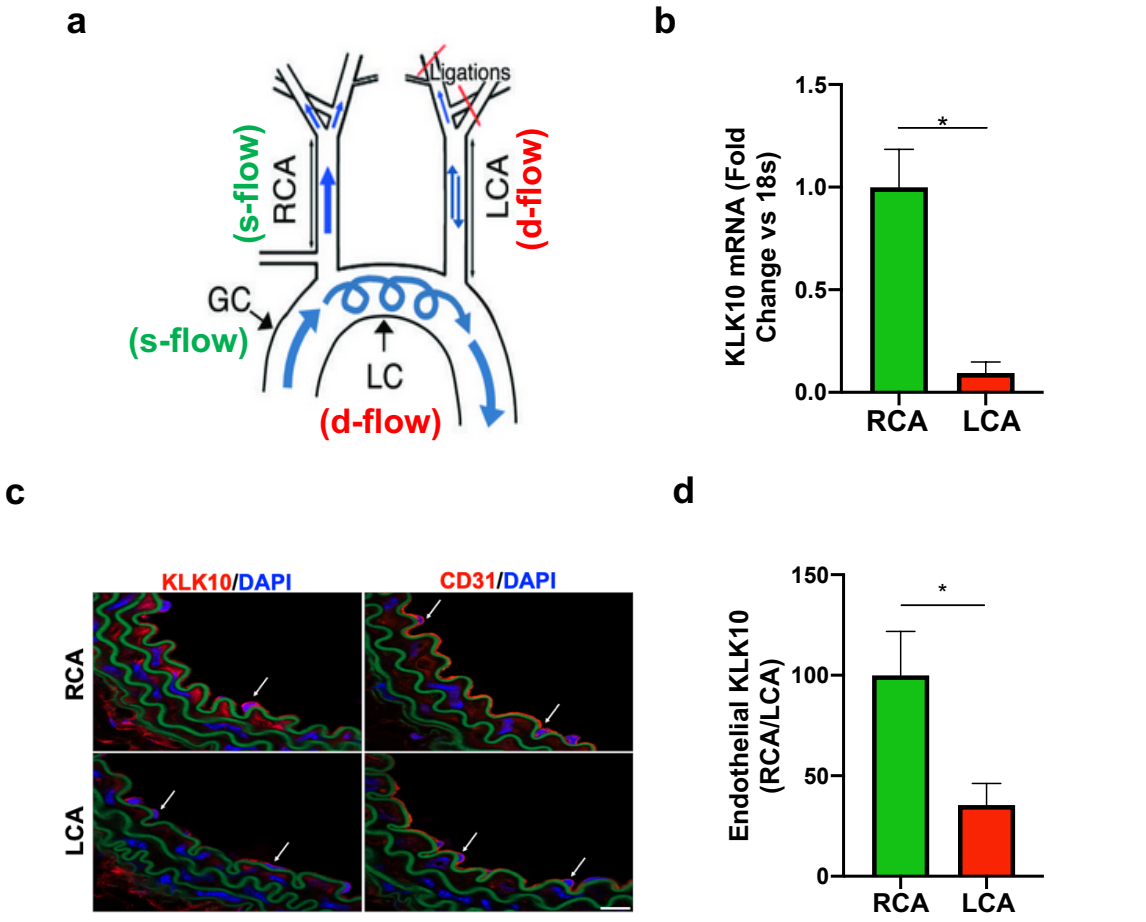

***Figure 4.3*. KLK10 is upregulated by *s-flow* and inhibited by *d-flow* in the PCL mouse model.** (a) Depiction of the partial carotid ligation (PCL) surgery and flow-sensitive regions in the aortic arch: right carotid artery (RCA; *s-flow*), left carotid artery (LCA; *d-flow*), greater curvature (GC: *s-flow*), and lesser curvature (LC; *d-flow*). Two days following the PCL of C57BL/6 mice, RCA and LCA were collected to prepare for endothelial-enriched RNA preparation used for KLK10 qPCR (b) and frozen section imaging (c-d). Shown are confocal images of immunostaining with KLK10 or CD31 antibodies (red) and counterstained with DAPI (blue) Scale bar=200 μm. Arrows indicate endothelial cells (c). Quantification of endothelial KLK10 fluorescence normalized to the % of the RCA. All data is represented as Mean±SEM, Paired two-tailed t-Test. n=6.*P≤0.05.

Being able to validate the flow-sensitivity of KLK10 in the PCL mouse model, we also wanted to examine KLK10 expression in regions of the vasculature naturally exposed to *d-flow*. To do so, we performed *en face* immunostaining of the greater and lesser curvature of the aortic arch (depicted in Figure 4.3a) in C57BL/6 mice with no surgical intervention. KLK10 protein expression was reduced in the lesser curvature (LC; the athero-prone aortic arch region that is naturally and chronically exposed to *d-flow*) compared to the greater curvature region (GC; the athero-protected aortic arch region that is naturally and chronically exposed to *s-flow)* as shown by *en face* immunostaining (Figure 4.4). In this experiment, VE-Cadherin staining was used as a marker for endothelial cells.

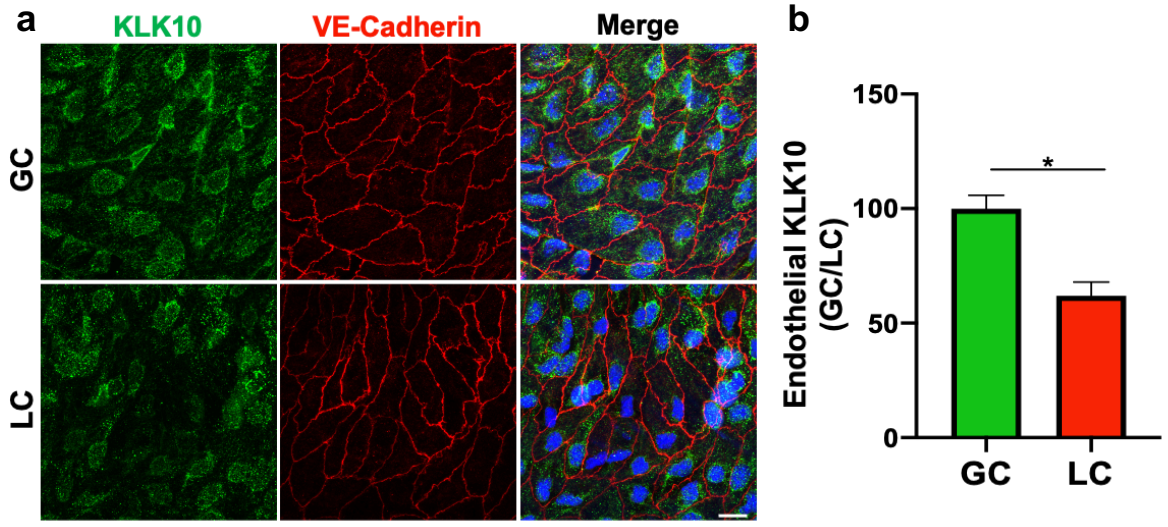

***Figure 4.4*. KLK10 is upregulated in greater curvature and inhibited in the lesser curvature.** (a) Confocal images of e*n-face* immunostaining of the LC and GC from C57BL/6 mice stained with anti-KLK10 (green) and anti-VE-Cadherin (red) antibody are shown. Counterstained with DAPI (blue). Scale bar=20 μm. (b) Quantification of endothelial KLK10 fluorescence normalized to the % of the GC. All data is

We next tested whether flow can regulate KLK10 expression *in vitro* using human aortic ECs (HAECs) exposed to unidirectional laminar shear (LS at 15 dynes/cm^2) or oscillatory shear (OS at ±5 dynes/cm^2 at 1 Hz) for 24h using the cone and plate viscometer, mimicking *s-flow* and *d-flow* conditions *in vivo*, respectively[24, 279]. KLK10 mRNA, protein in cell lysates, and secreted protein in the conditioned media were decreased by OS and increased by LS (Figure 4.5), confirming the role of KLK10 as a flow-sensitive gene and protein *in vivo* and *in vitro*.

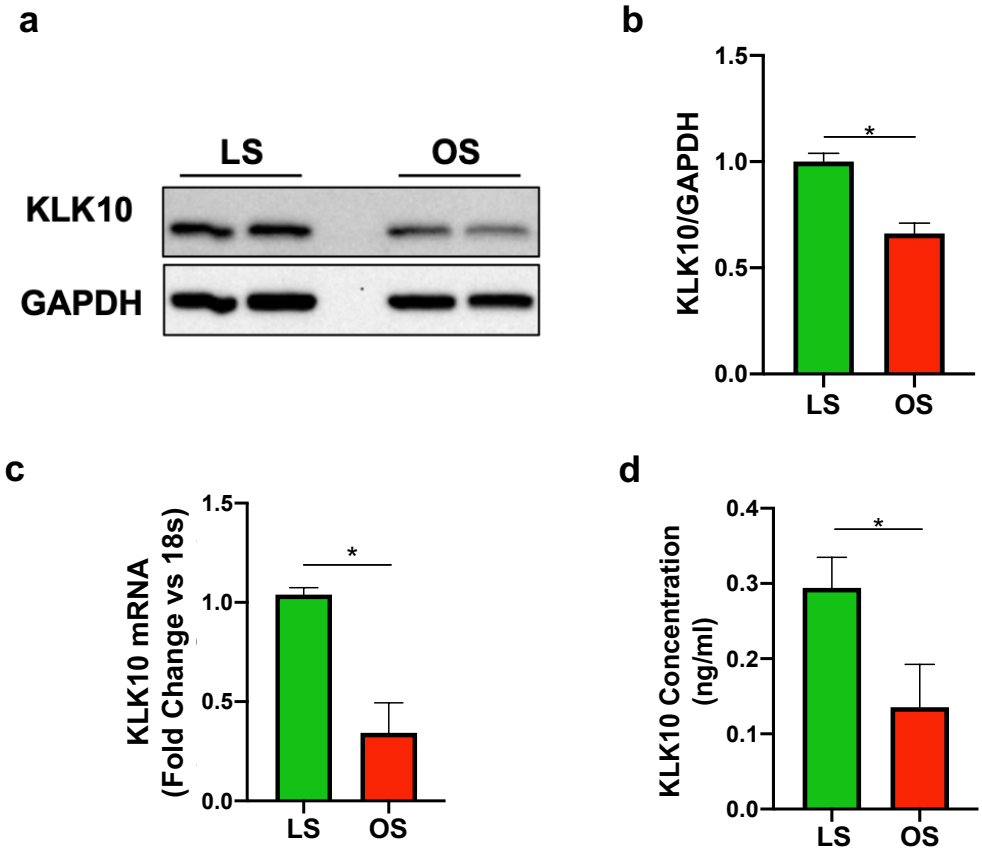

***Figure 4.5*. KLK10 is upregulated by *s-flow* and inhibited by *d-flow in vitro*.** (a) HAECs subjected to 24hr of unidirectional laminar shear (LS; 15 dynes/cm^2) or oscillatory shear (OS; ±5 dynes/cm^2) were used to measure expression of KLK10 protein in cell lysates by western blot (a,b) KLK10 mRNA by qPCR (c), and (d) KLK10 protein secreted to the conditioned media by ELISA. All data is represented as

We further confirmed the flow-dependent expression of KLK10 by re-analyzing the single-cell RNA sequencing (scRNAseq) and ATAC sequencing (scATACseq) data sets that we recently published using the PCL model[2]. For the scRNAseq and scATACseq study, single-cells and -nuclei obtained from the LCAs and RCAs, respectively, at 2 days or 2 weeks after the PCL were used. As described previously, the carotid artery wall cells were identified as EC clusters (E1-E8), smooth muscle cells (SMC), fibroblasts (Fibro), monocytes/macrophages (Mo1-4), dendritic cells (DC) and T-cells[2] (Figure 4.6). E2 and E3 represent athero-protected endothelial populations exposed to *s-flow* in the RCA, whereas E5 and E7 represent ECs exposed to acute *d-flow* (for 2 days). E6 and E8 populations represent athero-prone ECs exposed to chronic *d-flow* in the LCA (2 weeks).

As shown in the scRNAseq data analysis (Figure 4.6a), KLK10 expression is highest in *s-flow* (E2 and E3) and decreases in response to acute (E5 and E7) and chronic (E6 and E8) *d-flow*. It also shows KLK10 expression is specific to ECs and not expressed in other cell types studied in the carotid. Similarly, scATACseq data (Figure 4.6b) showed that the KLK10 promoter region is open and accessible (indicating active transcription status) in *s-flow* conditions but closed and inaccessible (indicating inactive transcription status) under *d-flow* conditions. Together, both the scRNAseq and scATACseq results demonstrate that KLK10 expression is potently regulated by flow at the epigenomic and transcriptome level, supporting the *in vitro* and *in vivo* results shown above.

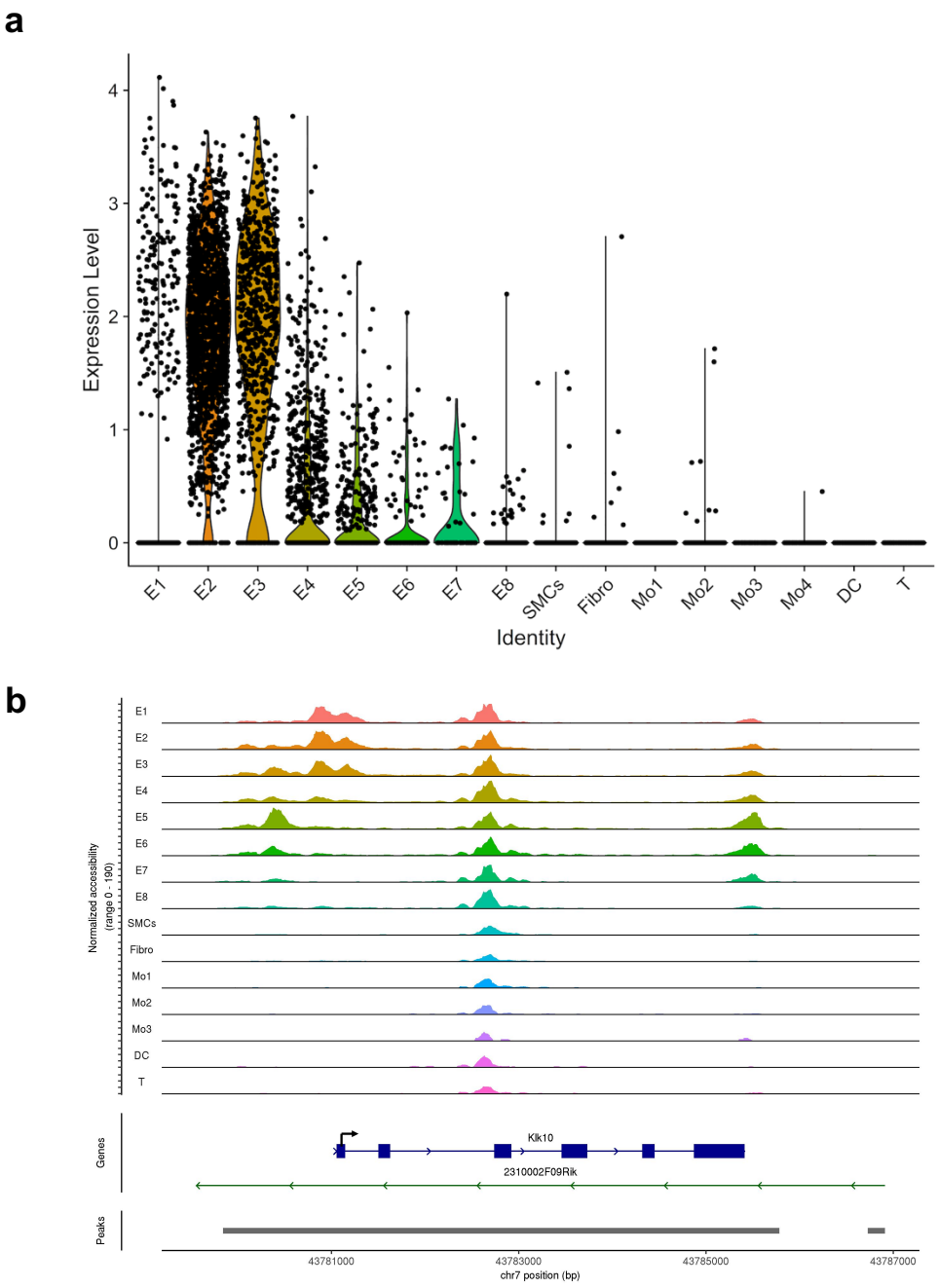

***Figure 4.6*. Flow regulates KLK10 expression through epigenetic modifications.** (a) Single-cell RNA sequencing (scRNAseq) and (b) single-cell ATAC sequencing (scATACseq) data sets were re-analysed[2]. We found a flow-dependent response to KLK10 mRNA expression and chromatin accessibility, respectively, in ECs in the RCAs and LCAs at 2 days and 2 weeks after the PCL. KLK10 expression in ECs (E1-E8), smooth muscle cells (SMCs), fibroblasts (Fibro), monocytes/macrophages (Mo1-4), dendritic (DC), and T cells (T) are shown as we previously reported. E2 and E3 represent ECs exposed to *s-flow* conditions, while E5 and E7 clusters represent ECs exposed to acute (2 days) *d-flow.* E6 and E8 represent ECs exposed to chronic (2 weeks) *d-flow*.

Lastly, as a means of translational validation, we examined if KLK10 expression is altered in human coronary artery tissue sections with varying degrees of atherosclerotic plaques (n=40 individuals, de-identified patient characteristics are listed in Appendix Table A1. KLK10 (Figure 4.7a) and CD31 (Figure 4.7b) immunostaining demonstrated that KLK10 expression was significantly reduced at the endothelial layer in arteries with significant plaques (Grade 4-6) than less-diseased arteries (Grades 1-3) (Figure 4.7).

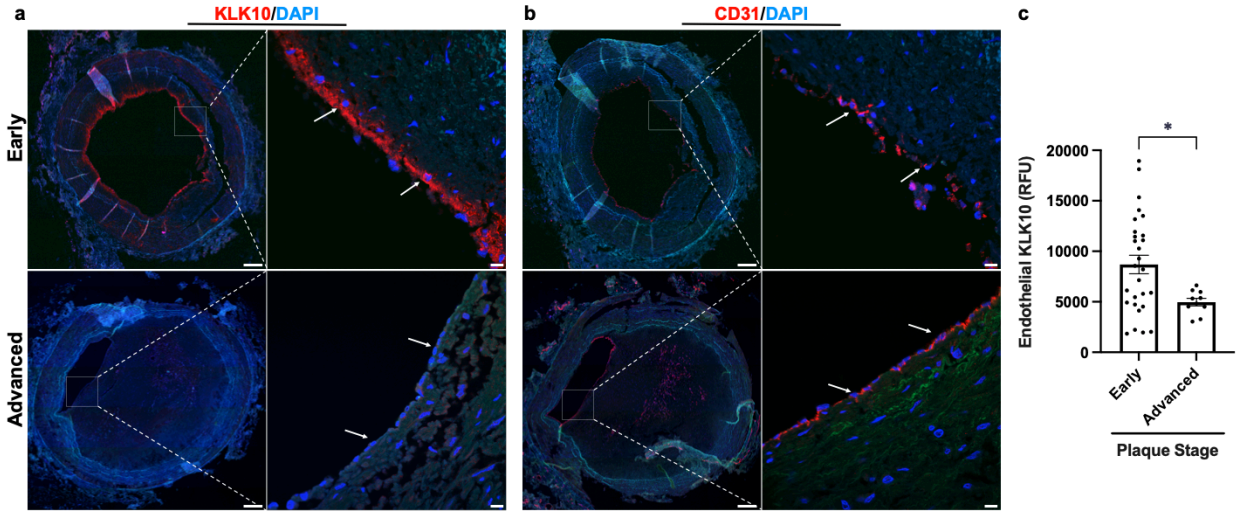

Figure 4.7. **KLK10 expression is decreased in human coronary arteries with advanced atherosclerotic plaques** (a) Human coronary artery sections with varying degrees of atherosclerotic lesions were stained with KLK10 antibody (red) and DAPI (blue). Scale bar low mag=500 µm, scale bar; high mag=50 µm. Arrows indicate endothelial cells. (b) Consecutive arterial sections from the same patients were stained with CD31 antibody (red) and DAPI (blue). (c) Quantification of endothelial KLK10 fluorescent intensity in lower stage plaques (AHA grades 1-3) and advanced stage plaques (AHA grade 4-6). Data are from 40 different patients. Two-tailed t-test. Mean±SEM *P≤0.05.

4.2.2 KLK10 Inhibits Several Aspects of Endothelial Dysfunction

Having established KLK10 as flow-sensitive at multiple levels, we next tested the hypothesis that KLK10 mediates the atheroprotective and anti-inflammatory effects of *s-flow* on the endothelium through inhibition of endothelial dysfunction. We first tested if KLK10 regulates EC function by evaluating its role in tube formation, migration, proliferation, and apoptosis, which play critical roles in the pathogenesis of atherosclerosis. Here, we performed a dose-curve study where we treated Human Umbilical Vein Endothelial Cells (HUVECs) with increasing concentrations of human recombinant KLK10 for 24hrs (rKLK10) followed by the scratch assay (migration), TUNEL assay (apoptosis), KI67 assay (proliferation), and the Matrigel tube formation assay. Treatment of HUVECs with rKLK10 significantly inhibited endothelial migration in a dose-dependent manner, but not proliferation or apoptosis (Figure 4.8a-c). The greatest effect was observed was with 100 ng/mL rKLK10, which also significantly inhibited tube formation (Figure 4.8d).

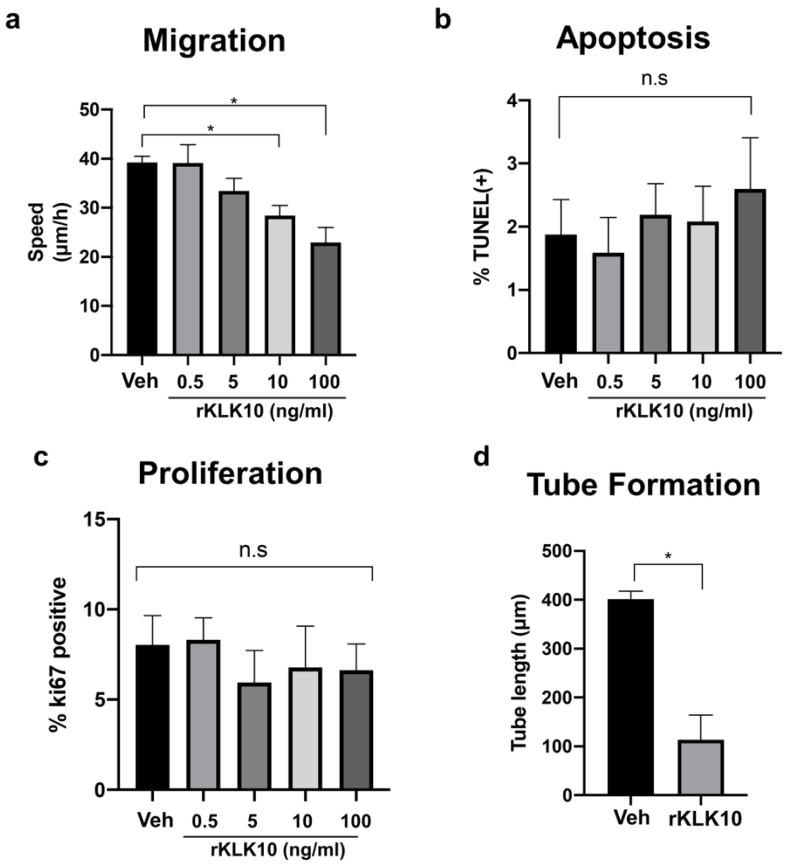

Figure 4.8. **KLK10 inhibits endothelial migration and tube formation, but not apoptosis or proliferation.** (a) Human umbilical vein endothelial cells (HUVECs) were treated with rKLK10 from 0.5-100 ng/mL and (a) the scratch assay was performed to measure the rate at which endothelial cells migrated across the scratch; (b) apoptosis was assessed by TUNEL staining; (c) proliferation was assayed by ki67 immunostaining. (d) HUEVCs were grown on Matrigel and treated with rKLK10 at 100 ng/mL or vehicle and tube length was measured in ImageJ. One-way ANOVA with Bonferroni correction for multiple comparisons where appropriate (a-c) or paired two-tailed t-test (d). Mean±SEM. n=4 *P≤0.05.

Next, we tested the effect of KLK10 on monocyte adhesion to the endothelium. Under *d-flow* and under inflammatory conditions, endothelial cells will upregulate the expression of cellular adhesion molecules VCAM1 and ICAM1[295]. Circulating monocytes recognize these adhesion molecules through cell-cell interactions and bind the endothelial cell, leading to monocyte

infiltration and macrophage formation[295]. For this set of experiments, we took two approaches: 1) a dose-curve study where we treated Human Aortic Endothelial Cells (HAECs) with increasing concentrations of rKLK10, and 2) an overexpression study where we transfected KLK10-overexpressing plasmids into HAECs. After 24hrs of rKLK10 treatment or transfection, we treated the cells with the pro-inflammatory cytokine TNFα (5 ng/mL for 4hrs) followed by the monocyte adhesion assay (Figure 4.9). Both rKLK10 and KLK10-overexpressing plasmids showed dose-dependent decreases in monocyte adhesion, indicating KLK10 protects ECs from inflammatory stimuli such as TNFα. Interestingly, heat-inactivation (HI) of rKLK10 caused a loss-of-effect on the inhibition of monocyte adhesion, implicating the importance of the enzymatic activity or native conformation of KLK10. This topic will be discussed in further detail in Chapter 6.

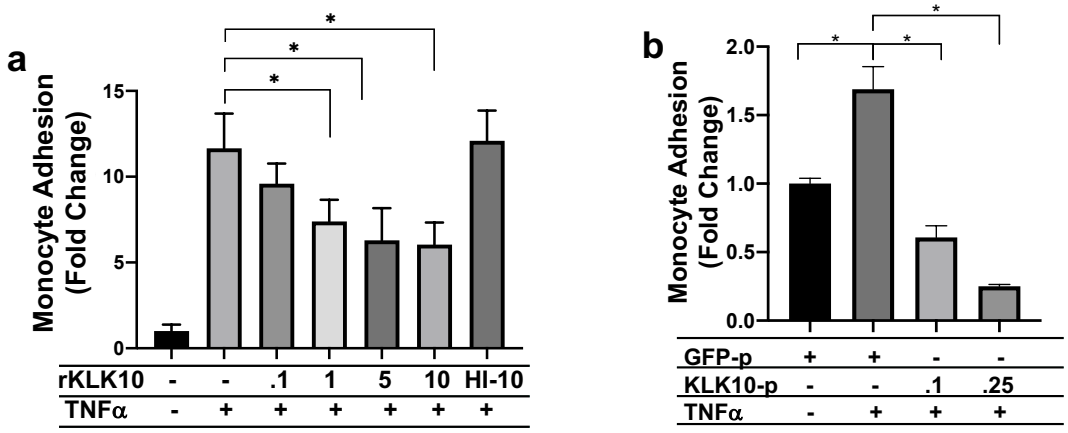

Figure 4.9. **KLK10 inhibits TNFα-induced monocyte adhesion to the endothelium.** (a) THP1 monocyte adhesion assay was carried out in HAECs transfected with 0.1 µg or 0.25 µg of KLK10 plasmid (KLK10-p) or GFP plasmid (GFP-p) for 48hrs followed by TNFα treatment (5 ng/mL for 4hr). Data is represented as fold change in monocyte adhesion normalized to GFP-p control. (b) THP1 monocyte adhesion assay was carried out in HAECs treated with rKLK10 (0.1-10 ng/mL) or heat-inactivated rKLK10 (HI-10) for 24hrs followed by TNFα treatment (5 ng/mL for 4hr). Data is represented as fold change in monocyte adhesion normalized to vehicle control. Mean±SEM. n=6 *P≤0.05.

Following the hypothesis that KLK10 inhibits monocyte adhesion, we further explored the ability of KLK10 inhibit the expression of the cellular adhesion molecules VCAM1 and ICAM1 which mediate monocyte adhesion to the endothelium. First, we performed another dose-response assay in HAECs where we treated the cells with rKLK10 for 24hrs followed by TNFα the next day. At the completion of the experiment, we collected total mRNA and cellular lysate to assess the expression VCAM1 and ICAM1 by qPCR and western blot, respectively. rKLK10 treatment decreased the expression of the VCAM1 and ICAM1 at both the mRNA and protein level (Figure 4.10), indicating KLK10 is inhibiting signaling pathways that promote the transcriptional activation of *VCAM1* and *ICAM1* genes. Importantly, this finding rules out one hypothesis that KLK10 could be directly acting on VCAM1 and ICAM1 proteins at the endothelial membrane.

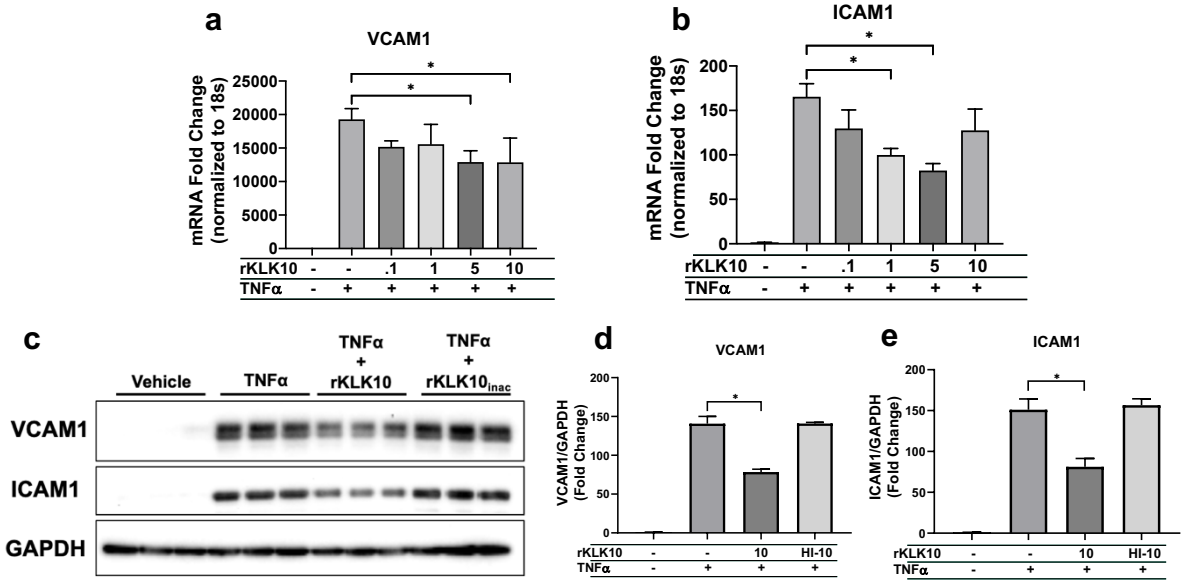

***Figure 4.10*. KLK10 inhibits expression of VCAM1 and ICAM1 from TNFα at the mRNA and protein level.** (a) HAECs were treated with rKLK10 (0.1-10 ng/mL for 24hrs) followed by TNFα treatment (5 ng/mL for 4hr) and expression of inflammatory marker VCAM1 and ICAM1 expression were assessed by qPCR (a,b) or western blot (c-e). Data is normalized to housekeeper genes 18s and GAPDH and represented as fold change of the vehicle control. Mean±SEM. n=3. *P≤0.05.

While encouraging, so far the main effects we have seen from KLK10 are an ability to inhibit endothelial inflammation and monocyte adhesion in response to TNFα treatment. This raises the question, does KLK10 also protect against *d-flow* induced inflammation and monocyte adhesion *in vitro* and *in vivo*? To test this question *in vitro*, we treated HAECs with rKLK10 overnight and exposed them to shear stress (LS or OS) using the cone-and-plate viscometer for 24hrs. KLK10 treatment significantly reduced OS-induced inflammation (indicated by VCAM1 expression) and monocyte adhesion at a concentration of 10 ng/mL (Figure 4.11).

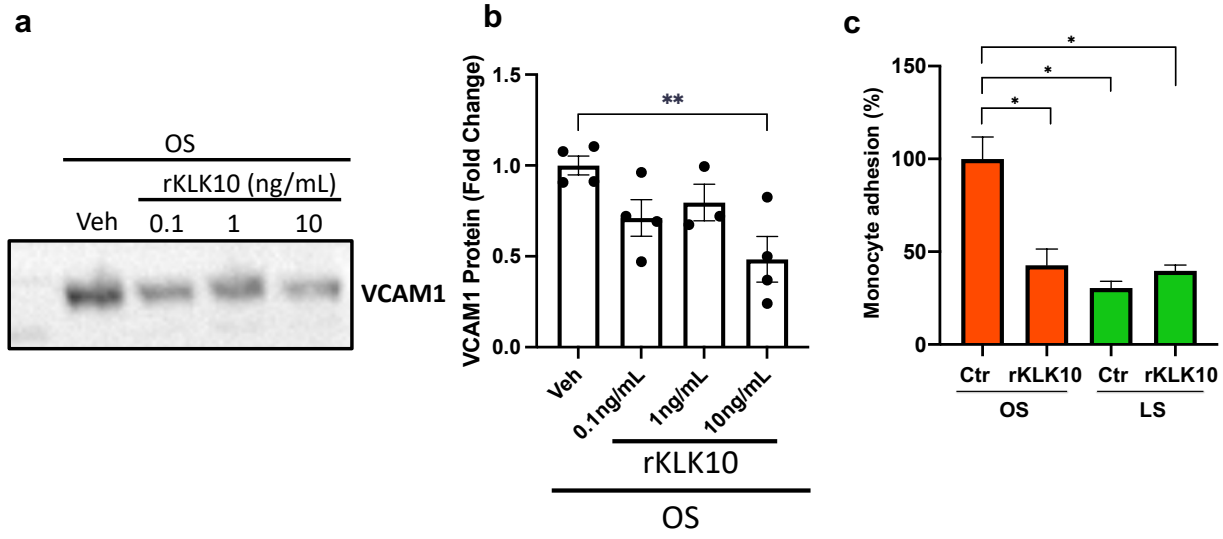

***Figure 4.11*. KLK10 inhibits *d-flow* induced expression of VCAM1 and monocyte adhesion.** (a,b) HAECs were treated with rKLK10 at the indicated concentrations and subjected to OS (±5 dynes/cm^2) for 24hrs. Cellular lysate was then collected and analyzed by SDS-PAGE for VCAM1 expression. (c)Monocyte adhesion assay was conducted on HAECs subjected to 24hr of either LS (15 dynes/cm^2) or OS (±5 dynes/cm^2). Data is represented as % of monocyte adhesion normalized to the control OS condition. Mean±SEM, One-way ANOVA with Bonferroni correction for multiple comparisons. n=4.*P≤0.05

We next tested if rKLK10 could affect the endothelial inflammation in naturally flow-disturbed LC of the aortic arch in mice (Figure 4.12). Treatment with rKLK10 *in vivo* (intravenous injection every 2 days for 5 days at 0.6 mg/kg) dramatically reduced VCAM1 expression in the *d-flow* (LC) region in the aortic arch of these mice. We also observed a dose-dependent effect of rKLK10 on VCAM1 expression (Figure 4.12).

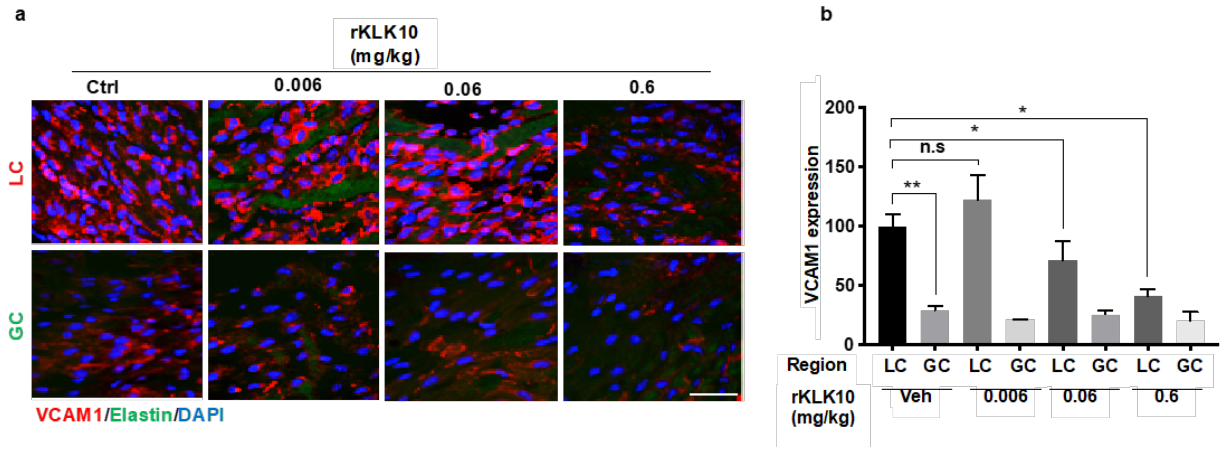

Figure 4.12. **rKLK10 inhibits VCAM1 expression in the d-flow region of the mouse aortic arch in a dose-dependent manner.** (a) Mice (male, C57/BL6) were administered 0.0006-0.6 mg/kg rKLK10 or vehicle by IV injection and inflammation was assessed by *en face* immunostaining of VCAM1 at the Lesser Curvature (LC) and the Greater Curvature (GC) of the aortic arch. Red=VCAM1, Blue=DAPI, Green=Elastin. Scale bar=50 um (b) Quantification of VCAM1 staining in A normalized to the LC. n=6. Two-way ANOVA with Bonferroni correction for multiple comparisons. Mean±SEM. *P≤0.05, **P ≤ 0.01.

The last functional assay we tested was endothelial permeability using a FITC-Avidin permeability assay (Ch. 3.9.5). In this experiment, we tested if rKLK10 treatment can protect the permeability barrier function of ECs. As a positive control, thrombin treatment increased the permeability of HAECs as measured by increased binding of fluorescently labeled (FITC)-Avidin to biotin-gelatin as reported previously[283]. Overnight rKLK10 pre-treatment prevented the permeability increase induced by thrombin in HAECs (Figure 4.13a). Similarly, rKLK10

reduced the permeability induced by OS (Figure 4.13b), further demonstrating the protective role of KLK10 in endothelial barrier function.

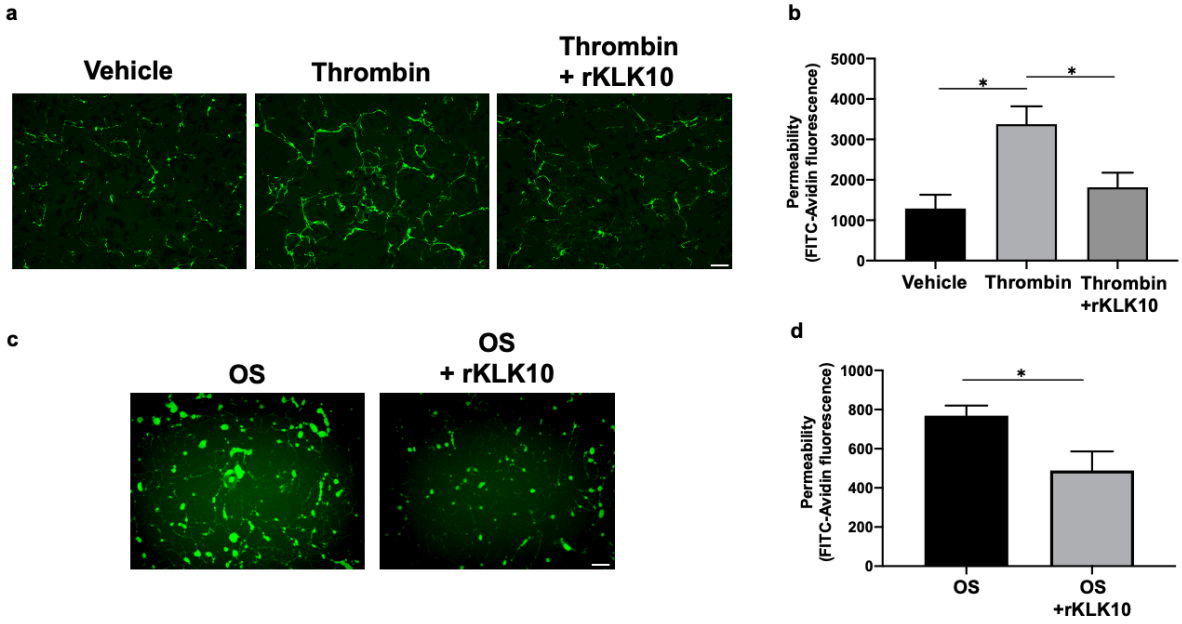

***Figure 4.13*. KLK10 protects endothelial permeability against thrombin and OS.** (a) HAECs were grown to confluency on biotinylated gelatin and were treated with rKLK10 (10 ng/mL) or vehicle overnight followed by thrombin (5 U/mL for 30 minutes). Endothelial permeability was then measured by the binding of FITC-avidin to the biotinylated gelatin. (b) Quantification of endothelial permeability measured as FITC-Avidin fluorescence. (c) HAECs were grown to confluency on biotinylated gelatin and were subjected OS (±5 dynes/cm^2) with rKLK10 (10 ng/mL) or vehicle for 20hrs. Endothelial permeability was then measured by the binding of FITC-avidin to the biotinylated gelatin. Scale bar=100 µm. All data is represented as Mean±SEM, n=4-6. One-way ANOVA with Bonferroni correction (b) or paired two-tailed T-Test (d).*P≤0.05.

4.3 Summary

In this chapter we have tested the hypothesis that shear stress regulates the expression of KLK10 and in-turn, KLK10 regulates several endothelial dysfunctions associated with atherosclerosis. Studies from this aim identified KLK10 is indeed regulated by flow; *s-flow* promotes, while *d-flow* inhibits expression, and secretion of KLK10 in ECs *in vitro* and *in vivo*. Interestingly, Single-cell RNA sequencing (scRNAseq) and scATAC sequencing (scATACseq) studies using the PCL mouse model revealed that flow regulated KLK10 expression at the epigenomic and transcription levels. These results proved to be translatable to humans, as KLK10 expression was also found to be decreased in human coronary arteries with advanced plaques compared to coronaries with early-stage plaques. These results clearly support the proposed role of KLK10 as a shear-sensitive gene and protein. For these reasons, we continued to study the involvement of KLK10 in endothelial dysfunction associated with disturbed blood flow. Because KLK10 is upregulated by *s-flow* and has been indicated as a target of the atheroprotective transcription factors *KLF2* and *KLF4*[294], we hypothesized KLK to mediate the beneficial effects of *s-flow* and inhibit endothelial dysfunction associated with *d-flow*. We tested a panel of endothelial dysfunctions and found KLK10 inhibited permeability, migration, tube formation, inflammation and monocyte adhesion, but not proliferation or apoptosis. Further in-depth analysis revealed KLK10 inhibits inflammatory pathways induced by either TNFα or *d-flow*, while inhibiting permeability pathways associated with thrombin or *d-flow.* We validated our *in vitro* findings on inflammation *in vivo* and found rKLK10 treatment to inhibit inflammation at the lesser curvature (naturally exposed to *d-flow*) in a dose-dependent manner. These findings are summarized in the updated working hypothesis (Figure 4.14)

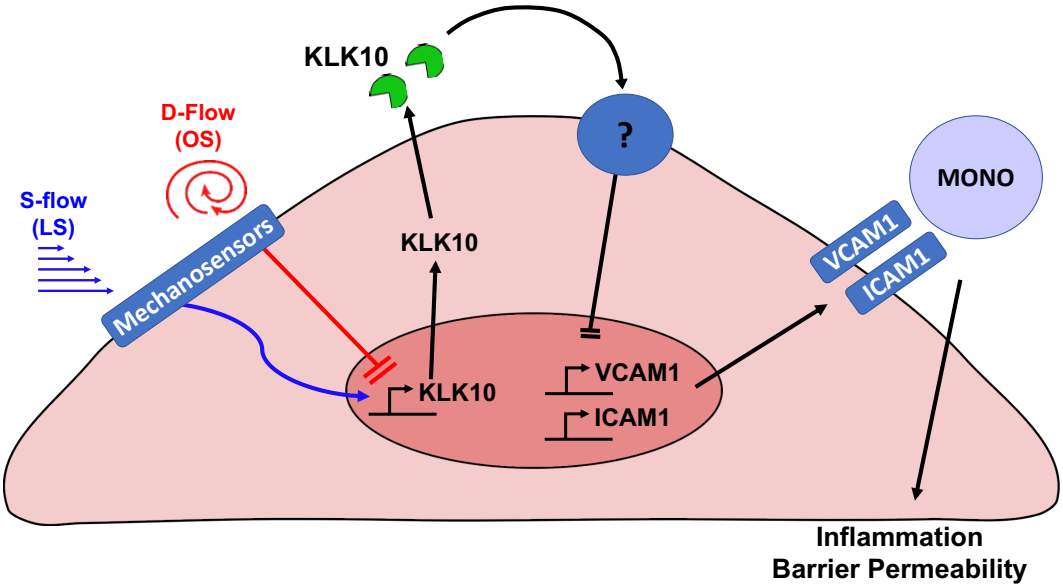

***Figure 4.14*. Aim 1 Updated Working Hypothesis.** KLK10 is upregulated by *s-flow* and downregulated by *d-flow*. Under *s-flow* KLK10 is secreted out of the cell and interacts with an unknown receptor on the endothelial membrane to inhibit expression of VCAM1 and ICAM1. Inhibition of VCAM1 and ICAM1 expression prevents subsequent monocyte adhesion, barrier permeability, and inflammation.

4.4 Discussion

The findings from this study provide a basis for an important role of KLK10 in endothelial biology and atherosclerosis. KLK10 shows shear-sensitivity at multiple levels (genetic, mRNA, and protein) that are consistent with previously observed results in a DNA microarray. Further, scRNAseq and scATACseq experiments in the PCL mouse model indicated flow modifies the chromatin structure of the *KLK10* gene, thereby regulating transcription factors accessibility to the promoter region. Therefore, not only have we established KLK10 as being regulated by flow, but we have also determined the mechanism by which flow regulates KLK10 expression. Further, based on decreased expression of KLK10 in human coronary arteries with advanced plaques, it may be suggested a similar mechanism is occurring in humans with atherosclerosis, however, more

mechanistic studies must be completed before that conclusion can be made. As a flow-sensitive gene, the results from this study indicate KLK10 mediates the atheroprotective effects of *s-flow* on the endothelium by inhibiting endothelial dysfunction. KLK10 had the greatest effects on inflammation, permeability, and monocyte adhesion but did not affect endothelial proliferation or apoptosis, indicating its functional role is less likely to do with maintaining endothelial cell cycle but rather combating pro-inflammatory stimuli such as TNFα or *d-flow.* These findings must be taken into account when studying the mechanism of action for the functional effects of KLK10. KLK10 is a secreted serine protease, therefore, it is highly likely that it is exerting its effects through an unidentified receptor or binding partner present on the endothelial membrane, thereby inhibiting inflammation, permeability and monocyte adhesion.

One of the most important findings from this aim is the potential therapeutic effect of rKLK10. rKLK10 treatment and KLK10 overexpression inhibited endothelial inflammation *in vitro* and injections of rKLK10 to C57BL/6 mice inhibited *d-flow*-induced inflammation in the lesser curvature of the aortic arch. Therefore, it is logical to hypothesize that rKLK10 treatment or overexpression could inhibit atherosclerosis development in a mouse model of atherosclerosis. This point of discussion will serve as the basis for the next chapter.

5. ASSESSING THE THERAPETIC POTENTIAL OF KLK10 IN ATHEROSCLEROSIS

5.1 Introduction

Observing KLK10 to have significant protective effects against EC barrier permeability, monocyte adhesion, and inflammation, we hypothesized these individual protective effects on endothelial cells would lead to an overall anti-atherogenic in mouse models of atherosclerosis. To test this hypothesis, we employed two complimentary approaches to probe the therapeutic potential of KLK10 in the PCL mouse model: 1) intravenous injections of rKLK10, and 2) ultrasound-mediated gene delivery of KLK10-overexpressing plasmids. Intravenous injections of rKLK10 have already proven to have a therapeutic effect on the inhibition of *d-flow*-induced inflammation, therefore it is logical to hypothesize these injections can also be used for the treatment of atherosclerosis. For this study, we performed the PCL surgery on ApoE$^{-/-}$ mice fed a high-fat diet (HFD) and injected rKLK10 (0.6 mg/kg) once every 3 days for 3 weeks.

Ultrasound-mediated gene delivery is a relatively new technique for overexpressing genes *in vivo* that we decided to use following failures with AAVs. This is a minimally invasive, non-viral and clinically translatable method of gene therapy that combines plasmid DNA with microbubbles and sonoporation to enhance membrane permeability and plasmid uptake in various tissues[296, 297]. For this study, we hypothesized injections of KLK10 plasmid/microbubbles into the hindlimbs of PCL mice followed by ultrasound would overexpress KLK10 in the skeletal muscle, which would be secreted into the blood and ultimately inhibit atherosclerosis development (Figure 5.1). For this study, we used a custom-designed mouse KLK10 plasmid (pCMV-Igκ-KLK10-T2A-Luc). This plasmid is driven by a strong PCMV promoter and contains an Igκ sequence fused to the N-terminal domain of KLK10 to enhance the secretion of KLK10. Immediately after the

KLK10 sequence is a self-cleaving p2a sequence followed by luciferase reporter. Following translation of the protein, the p2a will self-cleave[298], leaving luciferase in the cell while KLK10 is secreted into the blood.

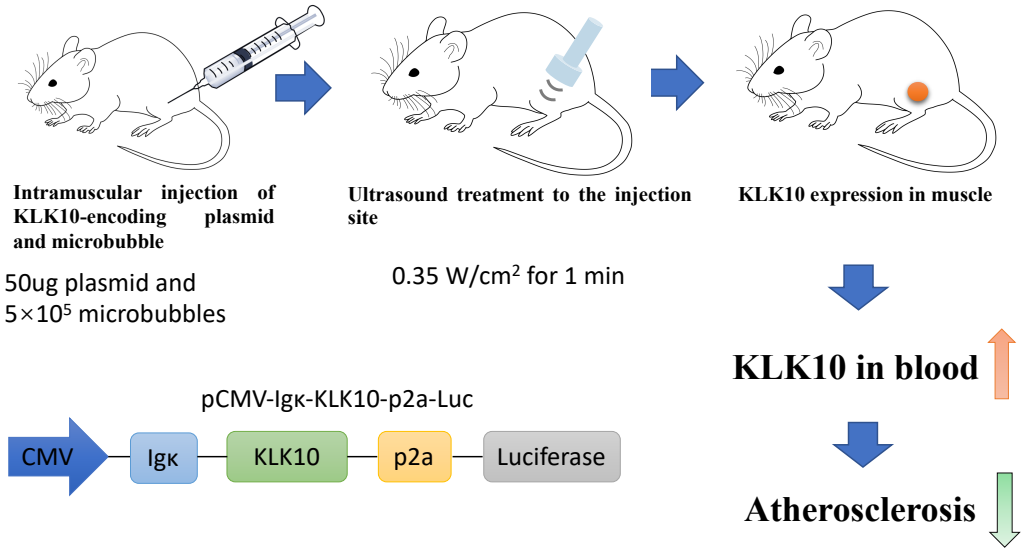

Figure 5.1. **KLK10 Ultrasound-mediated gene delivery hypothesis and study design** (a) A mixture of KLK10 plasmid (50 ug) and microbubbles ($5x10^5$) are injected into the hindlimbs of $ApoE^{-/-}$ mice and the site of injection is exposed to ultrasound (0.35 W/cm^2) for 1 min. We hypothesize this will lead to KLK10 expression in the muscle, which will be secreted into the blood and inhibit atherosclerosis in $ApoE^{-/-}$ mice on a high fat diet. (b) KLK10 or control plasmid with microbubbles were injected into the hindlimbs of $ApoE^{-/-}$ mice and 5 days later the PCL surgery was performed, and mice were put on a high-fat diet. Injections of plasmid and microbubbles were repeated once every 10 days (day 0, 10, 20) and bioluminescent imaging was performed one day prior

5.2 Results

5.2.1 Treatment with rKLK10 inhibits atherosclerosis in ApoE$^{-/-}$ mice

Following encouraging results from our *in vivo* test of rKLK10 on inflammation in the lesser curvature of the aortic arch, we next tested if rKLK10 treatment could inhibit atherosclerosis in ApoE$^{-/-}$ mice given the PCL surgery and put on an HFD. For this study, we performed the PCL surgery on ApoE$^{-/-}$ mice fed a high-fat diet (HFD) and injected rKLK10 (0.6 mg/kg) or vehicle by tail-vein once every 3 days for 3 weeks (Figure 5.2).

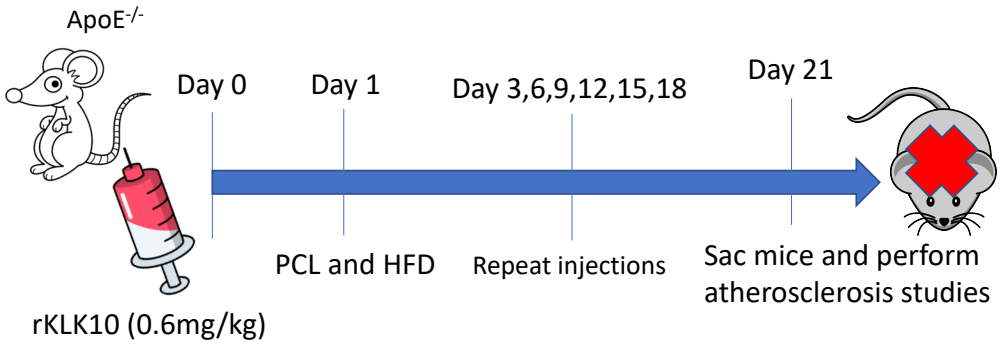

***Figure 5.2*. Acute rKLK10 therapy in ApoE$^{-/-}$ PCL mice study design.**

At the completion of the study, we dissected out the carotid arteries to assess plaque burden and performed histological/immunochemistry assessments of frozen sections from the carotids. Injection with rKLK10 (twice per week at 0.6 mg/kg for 3 weeks post-PCL surgery) significantly reduced atherosclerosis development (Figure 5.3a), indicated by a ~50% reduction in measured plaque area from H&E staining of the carotid arteries (Figure 5.3b,c).

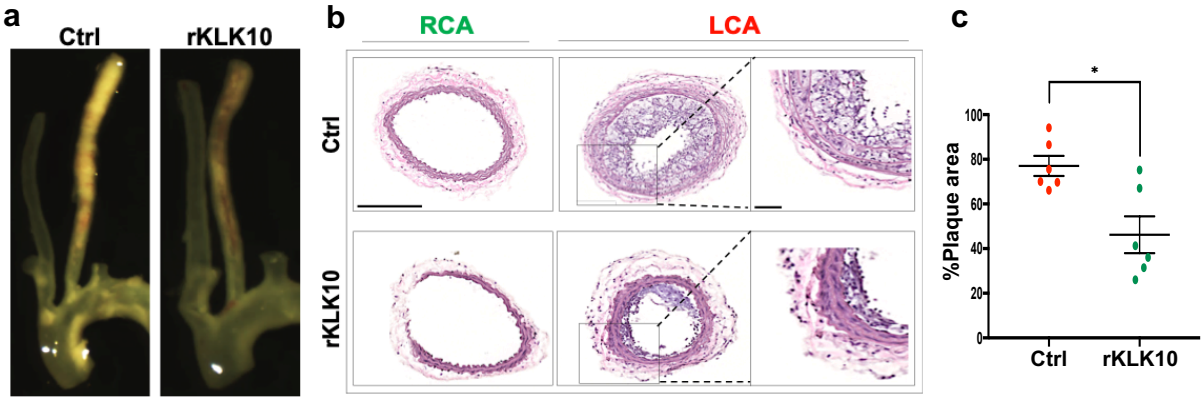

***Figure 5.3*. Treatment with rKLK10 inhibits atherosclerosis development.**
a) *ApoE*$^{-/-}$ were subjected to partial carotid ligation and high fat diet feeding. The mice received either rKLK10 (0.6 mg/kg) or vehicle injection every three days for the duration of three weeks. LCA show plaque development, which was reduced by rKLK10 as shown by dissection microscopy. Frozen sections from the LCA and RCA were stained with (b) H&E and (c) for CD68 in LCA. DAPI (blue). Scale bar low mag=250 µm, high mag=50 µm. All data is represented as Mean±SEM, *P≤0.05, Paired two-tailed t-test. N=6.

Next, to determine the composition of immune cells within the plaques, we stained frozen carotid artery sections (LCA) with the macrophage marker CD68. Based on previous monocyte adhesion data performed *in vitro,* we hypothesized decreased monocyte adhesion to the endothelium *in vivo* would lead to decreased accumulation of macrophages within the plaque. Following this hypothesis, rKLK10 treated mice showed decrease macrophage accumulation within the plaque, indicated by decreased CD68 immunofluorescence (Figure 5.4).

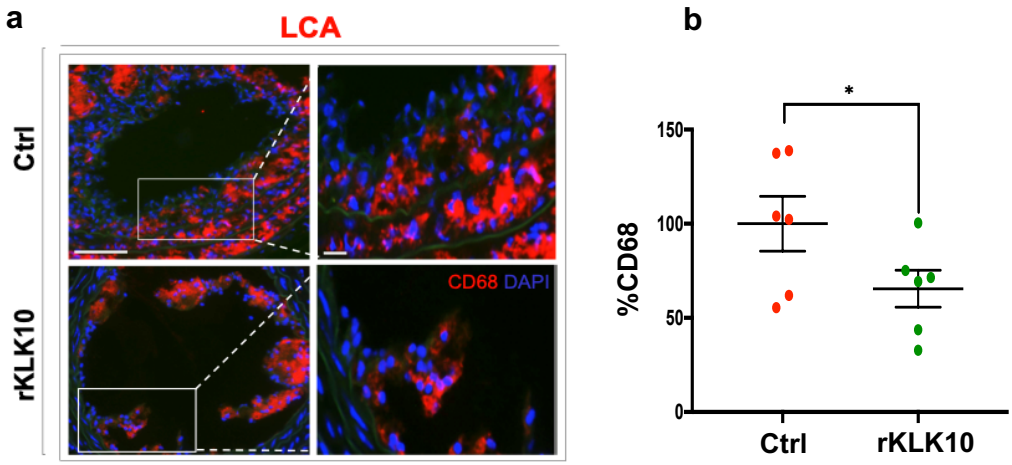

***Figure 5.4*. rKLK10 inhibits macrophage accumulation within the plaque.**
a) *ApoE*$^{-/-}$ were subjected to partial carotid ligation and high fat diet feeding. The mice received either rKLK10 (0.6 mg/kg) or vehicle injection every three days for the duration of three weeks. LCA show plaque development, which was reduced by rKLK10 as shown by dissection microscopy. Frozen sections from the LCA and RCA were stained with (b) H&E and (c) for CD68 in LCA. DAPI (blue). Scale bar low mag=250 µm, high mag=50 µm. All data is represented as Mean±SEM, *P≤0.05, Paired two-tailed t-test. N=6.

In addition to these atherosclerotic analyses, we also collected serum from the mice to assess a panel of lipids including total cholesterol, LDL cholesterol, HDL cholesterol, and triglycerides. The goal of this lipid analysis was to confirm the mice had similar levels of circulating lipids and to determine if the inhibition of atherosclerosis observed in KLK10-treated mice was due to decreased levels of lipids. KLK10 treatment had no effect on circulating lipid levels (Figure 5.5), indicating the observed inhibition of atherosclerosis in the mice treated with rKLK10 is actually due to the effects of KLK10. Together, these results so far support the hypothesis of KLK10 as an atheroprotective therapeutic target for the treatment of atherosclerosis.

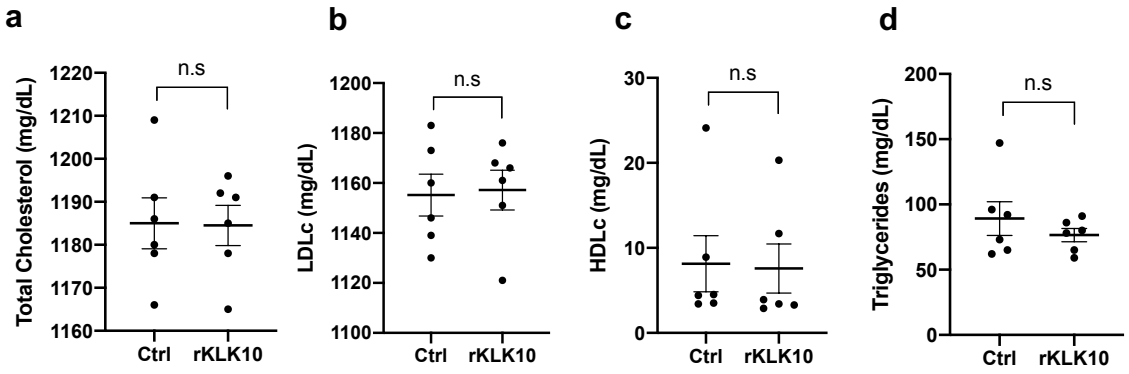

Figure 5.5. **Treatment with rKLK10 has no effect on circulating lipids.**
Plasma lipid analysis of (a) total cholesterol, (b) LDL cholesterol, (c) HDL cholesterol, or (d) triglycerides showed no effect of rKLK10 compared to control. All data is represented as Mean±SEM, *P≤0.05, Paired two-tailed t-test. N=6

5.2.2 Ultrasound-mediated overexpression of KLK10 inhibits atherosclerosis in ApoE$^{-/-}$ mice

As an alternative approach to studying the therapeutic efficacy of KLK10, we next sought to test whether overexpression of KLK10 *in vivo* could inhibit atherosclerosis development in a similar manner as rKLK10 treatment. To do so, we employed ultrasound-mediated gene delivery as a method to overexpress KLK10 plasmids in the hind-limbs of ApoE$^{-/-}$ mice given the PCL surgery. For this study, we injected either KLK10 plasmid (pCMV-Igκ-KLK10-T2A-Luc) or luciferase plasmid (pCMV-Luc) as a control along with microbubbles to the hind-limbs of *ApoE*$^{-/-}$ mice and sonoporated the legs with ultrasound as previously described[284-286]. The plasmid injection and sonoporation was repeated 10 days later to ensure sustained protein expression for the duration of the study (Figure 5.6).

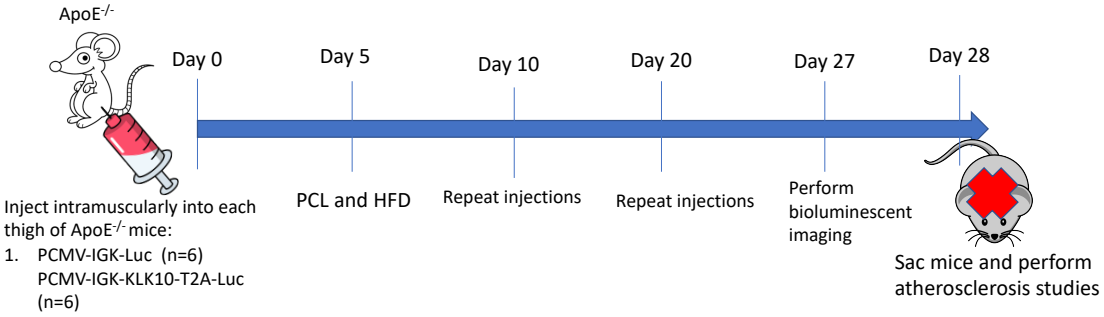

***Figure 5.6*. Ultrasound-mediated gene delivery of KLK10 plasmids study design.**

Since both the control and KLK10 plasmids contain luciferase reporters, we were able to perform bioluminescent imaging prior to the completion of the study to ensure the plasmids were being expressed as expected. Both the luciferase control and KLK10-luciferase plasmids demonstrated similar levels of bioluminescence in the hindlimbs at the site of injection/ultrasound exposure (Figure 5.7a). We then dissected out the carotid arteries to assess plaque burden and plaque area via H&E staining. Mice overexpressing the KLK10 plasmid showed marked decreases in atherosclerosis, indicated by gross plaque burden (Figure 5.7b,c) and plaque area measured from H&E staining (Figure 5.7d,e). Taken together, these data conclusively support the role of KLK10 as an atheroprotective factor. However, lacking from these data is the direct link between increased KLK10 levels in the blood and decreased atherosclerosis.

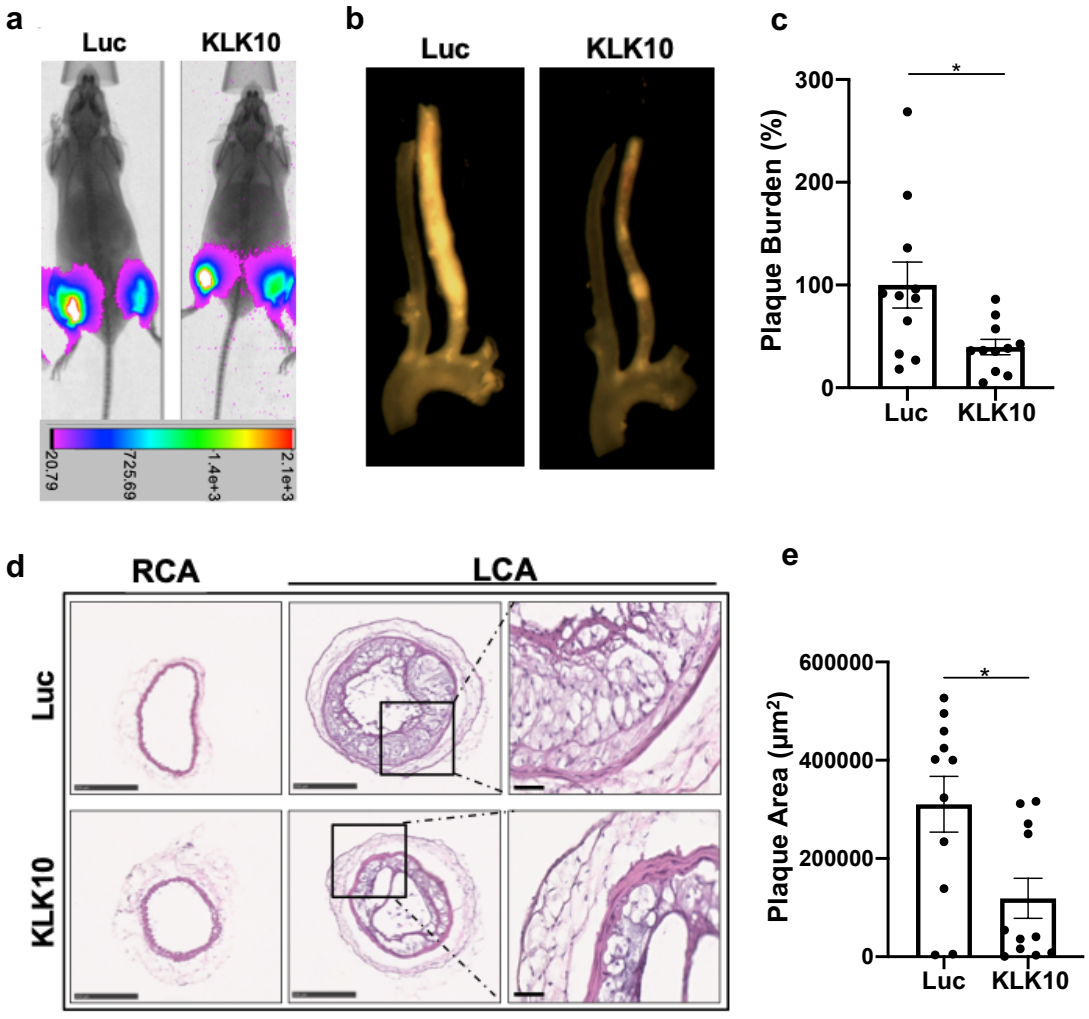

Figure 5.7. **Ultrasound-mediated overexpression of KLK10 plasmid inhibits atherosclerosis development.**
(a) Bioluminescent imaging of *ApoE*$^{-/-}$ PCL mice on a high-fat diet injected with Luciferase control plasmid or KLK10-Luciferase plasmid, measured in photons/second. (b) Gross plaque images of excised carotid arteries and (c) quantification of plaque burden normalized to the % of the Luciferase control. (d) H&E staining of sections from the LCA and RCA of mice injected with Luciferase control plasmid or KLK10-Luciferase plasmid. Scale bar low mag=250 µm, high mag=50 µm. (e) Quantification of plaque area measured in µm^2. All data is represented as Mean±SEM, *P≤0.05, Paired two-tailed t-test. N=4-11.

To measure KLK10 levels in the blood, we purchased an ELISA kit targeted towards mouse KLK10 (described in Ch. 3.20). Circulating KLK10 levels in the mice measured by ELISA at the time of sacrifice were measured in the range of 5-10 ng/mL and unexpectedly showed no measurable difference between the luciferase and KLK10 groups (Figure 5.8a). This may be due to a waning plasmid expression at the sacrifice time. However, we found higher levels of KLK10 staining at the endothelial layer in the LCA and RCA (Figure 5.8b,c), as well as in the lung tissue samples as shown by western blot (Figure 5.8d,e)

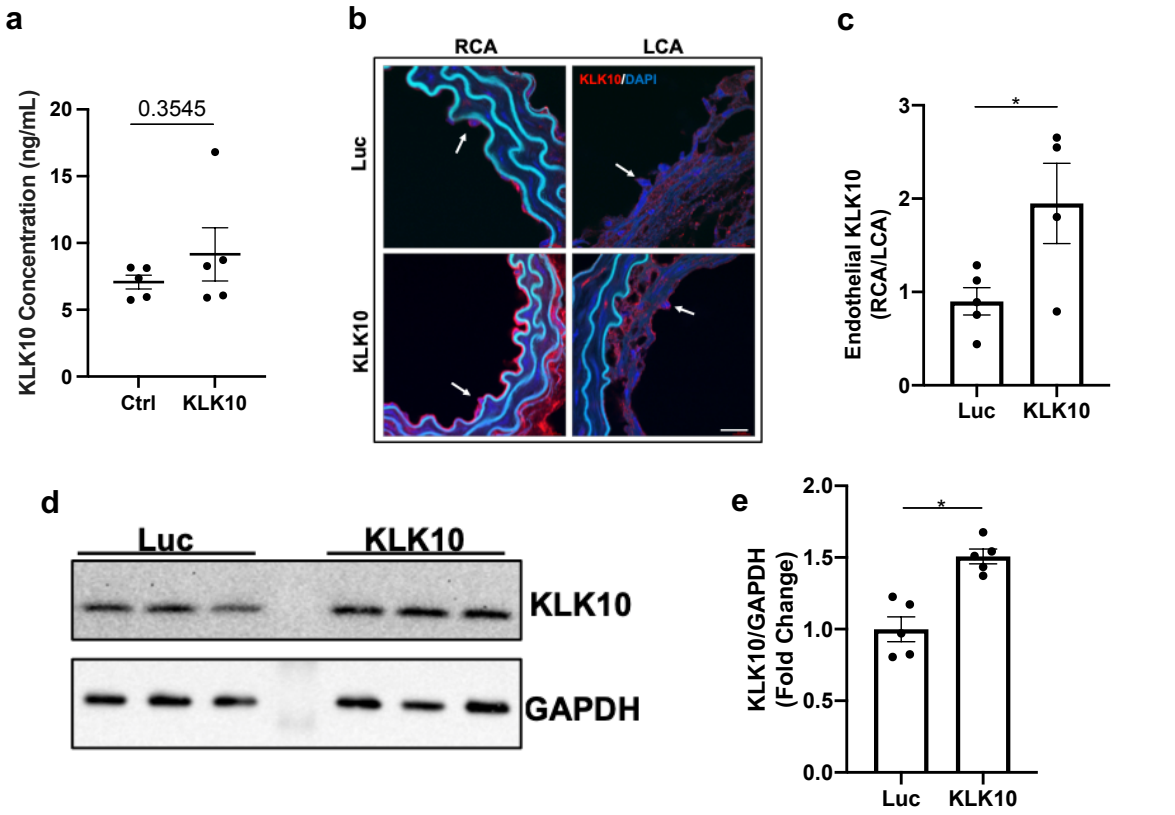

***Figure 5.8*. KLK10 is overexpressed at the endothelium and in the lungs of KLK10-injected mice.** (a) Immunostaining of sections from the RCA and LCA were further stained with anti-KLK10 (red) and DAPI (blue). Arrows indicate the endothelial layer. Scale bar=20 μm. (b) Quantification of endothelial KLK10 fluorescence represented as fold change normalized to Luciferase control. (c) Western blot assessing KLK10 expression in lung tissue from mice injected with control luciferase plasmid or KLK10 plasmid. GAPDH was used as a loading control. (d) Quantification of KLK10 expression in normalized to GAPDH and Luciferase control. All data is represented as Mean±SEM, *P≤0.05, Paired two-tailed t-test. N=4-5.

5.3 Summary

In this chapter we have tested the therapeutic efficacy of KLK10 for treating atherosclerosis in ApoE$^{-/-}$ mice given the PCL surgery. We employed two different approaches: 1) tail-vein injections of rKLK10, and 2) ultrasound-mediated gene delivery of KLK10-overexpressing plasmids. Remarkably, both approaches showed that KLK10 can inhibit atherosclerosis. In the rKLK10 study, we identified rKLK10 treatment causes decreased CD68 expression in the plaque, suggesting the mechanism behind KLK10 atheroprotective effects may be due an inhibition of macrophage accumulation within the plaque. This hypothesis follows our *in vitro* data showing KLK10 reduces monocyte adhesion. Additionally, analysis of circulating lipids ruled out any changes in cholesterol, triglycerides, LDcL, or hLDLc. In the ultrasound-mediated gene delivery study, we not only showed that KLK10 overexpression works to treat atherosclerosis, but we also demonstrated the viability of this approach for overexpressing plasmids containing luciferase reporters such as KLK10. With the luciferase reporters on the KLK10 and control plasmids, we successfully visualized expression of each plasmid at the site of injection and ultrasound exposure. Although we were unable to detect significantly increased levels of KLK10 in the plasma at the completion of the study, we did find increased levels of KLK10 in the lungs and at the endothelium of the carotids. Together with the bioluminescent imaging, there is a sufficient amount of evidence to suggest that the inhibition of atherosclerosis is due to overexpression of KLK10 protein. With data from both studies, we conclude KLK10 is an anti-atherogenic factor with high therapeutic potential.

5.4 Discussion

This chapter presents exciting findings regarding the potential therapeutic effect of KLK10 for the treatment of atherosclerosis. Using two completely independent approaches, we showed that either rKLK10 or KLK10 overexpression can inhibit atherosclerosis. Both means are potential therapeutic approaches, as recombinant protein injections are routinely performed in humans[299] and ultrasound already exists in the clinic as a diagnostic tool and treatment application with the development of ultrasound contrast agents[300]. One potential benefit of the ultrasound-mediated gene delivery is the ability to visualize expression of the plasmid. A patient can be injected one time and expression can be monitored over time to determine when the next injection is needed. Further, this approach has several benefits over other genetic approaches including the ability to track bioavailability, monitoring expression of the plasmid, and limited dosing[300].

The current limitation of our study is the lack of data supporting the hypothesis that KLK10 expression is increased in the blood of the treated mice. We hypothesize KLK10 expression had waned at the completion of the study since the last injection was performed 8 days prior to the end of the study. This could be tested by performing a time course analysis of KLK10 protein levels in the blood after injection and ultrasound exposure. Additionally, these types of studies would also allow us to determine the longest length of time needed before the next injection. Another explanation for the lack of increased blood levels of KLK10 is an inaccurate ELISA kit. We have not ruled out the possibility that this ELISA is not specific to KLK10, as mouse KLK10 shares a high percentage of sequence similarity between other members of the KLK family. Therefore, more testing needs to be done with this ELISA before

we can conclude KLK10 levels are not increased in the blood. Further, there is no logical explanation of how KLK10 can be increased in the lungs and at the endothelium without KLK10 being increased in the blood circulating within those tissues.

The question that remains following these studies assessing the functional and atheroprotective roles of KLK10 is the mechanism is for KLK10's effects. This topic will be the focus of the upcoming chapter.

6. INVESTIGATING THE KLK10 MECHANISM OF ACTION

6.1 Introduction

So far we have seen that the flow-sensitive protease KLK10 regulates endothelial biology and acts as an atheroprotective factor in the PCL mouse model. Remaining from these studies is the explanation for how KLK10 regulates endothelial biology and atherosclerosis. This chapter will cover the aim to determine the molecular mechanisms underlying the effects of KLK10.

Protease Activated Receptors (PARs) 1, 2 and 4 have been shown to mediate the effects of some KLKs (e.g. KLK5, 6, and 14)[301, 302]. Therefore, we tested if the anti-inflammatory effect of KLK10 could be mediated by PARs. PARs are established sensors of tissue injury and vascular leakage that regulate EC activation, inflammation and permeability[20,21]. PAR1 is well-known as the thrombin receptor, playing a key role in thrombosis[22]. The PARs are members of the G-protein Coupled Receptor (GPCR) family that are activated by site-specific cleavage of their extracellular N-terminal domain, which exposes a new N-terminal sequence that acts as a tethered ligand for the 7-transmembrane domain[20,23]. The interaction between the shortened N-terminal domain and the 7-transmembrane domain facilitates recruitment of G-proteins to the C-terminal domain, which are activated and act as secondary messengers to alter cell signaling[24].

PARs are cleaved and activated by a large number of serine proteases, that include Thrombin, Activated Protein C (APC), and Trypsin[20]. Thrombin cleavage of PAR1 to drive coagulation is particularly well characterized. In the coagulation cascade, Thrombin cleaves PAR1, inducing recruitment of $G_{12/13}$, G_q, and G_i family G-proteins[23] and activation of pro-inflammatory signaling pathways such as the p38 MAP Kinases, ERK1/2 MAP Kinases and the

Rho transcription factors[25,26,27]. This ultimately increases platelet binding to ECs as well as EC barrier permeability, connecting tissue damage to both hemostatic and inflammatory responses. It is interesting to note that APC also cleaves PAR1, like thrombin, but induces the opposite effects by a mechanism known as a *biased agonism*[28,29]. While thrombin activation of PAR1 induces EC inflammation, APC activation of PAR1 inhibits EC inflammation. Mechanistically, APC cleaves PAR1 at a site distinct from Thrombin and causes PAR1 to recruit β-arrestins instead of G-proteins[30,31], which then activate PI3K/AKT and Rac1 signaling pathways[32], leading to cyto-protective effects[33]. Given the ongoing clinical trials using APC as a supplemental therapy for stroke patients[31,34,35] and a previous failure of Xigris (rAPC from Eli Lilly), highlights the potential importance of KLK10 as novel anti-atherogenic therapy. As shown in Figure 1, *we hypothesize that KLK10 inhibits EC inflammation and protects barrier function by inducing β-arrestin biased signaling pathway in a PAR1 and PAR2-dependent mechanism*.

Since our gene array and qPCR data showed that mouse artery ECs express PAR1 and PAR2, but not PAR3 and PAR4[3, 21], we tested whether PAR1 and PAR2 mediate the KLK10 effect in ECs under OS condition by using two independent approaches - specific pharmacological inhibitors and siRNAs. For PAR1, we used the chemical inhibitor SCH79797 which is a selective PAR1 antagonist[303]. Based on preliminary toxicity studies, we found a concentration of 0.1 μM as being sufficient to prevent any cell death while still falling within a reported efficacious range[304]. For PAR2, we used the Vertex inhibitor FSLLRY-NH2. This is a peptide antagonist that specifically binds the PAR2 extracellular domain and prevents proteases from cleaving at their respective sites. Because this is a peptide inhibitor and not a chemical inhibitor, we used a higher concentration of 10 μM, which is also the IC50[305].

6.2 Results

6.2.1 PAR1 and PAR2 mediate the monocyte adhesion effect of KLK10

To test the hypothesis that PAR1 and PAR2 mediate the KLK10 effect in ECs, we used two independent approaches - specific pharmacological inhibitors and siRNAs. HAECs were first exposed to OS for 16h to induce an endothelial inflammatory response and treated with either the PAR1 inhibitor (SCH79797, 0.1μM) or PAR2 inhibitor (FSLLRY-NH2, 10μM). Both PAR inhibitors prevented the anti-inflammatory effect of KLK10 (Figure 6.1a), suggesting the role of PAR1/2 in mediating the KLK10 effect. The siRNAs for PAR1 and PAR2 also prevented the anti-inflammatory effect of KLK10, as shown by the monocyte adhesion assay (Figure 6.1b). When both PAR1 and PAR2 were knockdown together by the siRNAs, no additive effect was observed.

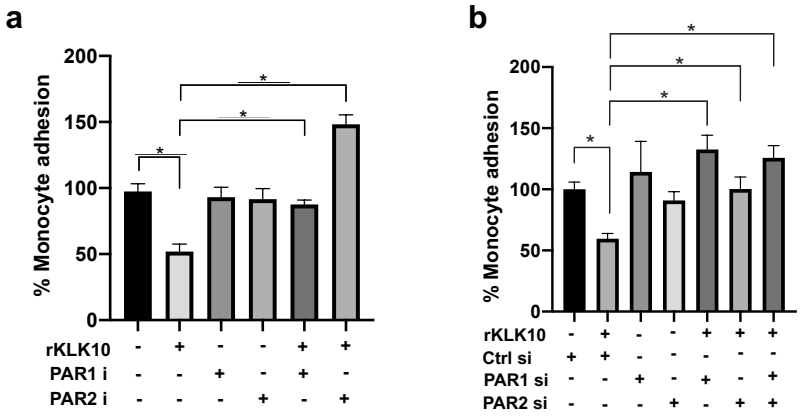

Figure 6.1. **KLK10 inhibits endothelial inflammation in a PAR1/2-dependent manner.** (a) THP1 monocyte adhesion assay was conducted in HAECs subjected to OS (±5 dynes/cm^2) for 24hrs with rKLK10 and PAR1 (SCH79797, 0.1 μM) or PAR2 inhibitor (FSLLRY-NH2, 10 μM). Data is normalized to the % of vehicle control. (b) THP1 monocyte adhesion assay was conducted in HAECs subjected to OS (±5 dynes/cm^2) for 24hrs with rKLK10 and PAR1/2 siRNA or control siRNA. Data is normalized to the % of vehicle control siRNA. All data is represented as Mean±SEM, *P≤0.05, Paired two-tailed t-test. N=5.

Since PARs are activated by site-specific cleavage of their extracellular N-terminal domain[306, 307], we tested if KLK10 can also cleave PAR1 and PAR2 to further define the mechanism of action. For this study, we used two independent approaches. First, a secreted

alkaline phosphatase (SEAP) reporter fused to the N-terminal domain of either PAR1 or PAR2 (PAR1-AP or PAR2-AP) was expressed in HAECs as reported previously[288-290]. As expected, treatment with thrombin (PAR1 agonist) increased activity of SEAP from the PAR1-AP, indicating the cleavage of the PAR1 N-terminus in response to the canonical agonist (Figure 6.2a). Similarly, trypsin (PAR2 agonist) also increased the SEAP activity in PAR2-AP expressing HAECs. Unexpectedly, however, treatment with rKLK10 did not induce the SEAP activity, indicating it did not cleave the PAR1 or PAR2. Next, as an alternative approach, we tested if KLK10 overexpression using the plasmid vector could cleave PAR1-AP or PAR2-AP in HAECs. Consistent with the rKLK10, KLK10 overexpression also failed to cleave either PAR1-AP or PAR2-AP, while thrombin and trypsin were still able to cleave the receptors (Figure 6.2b).

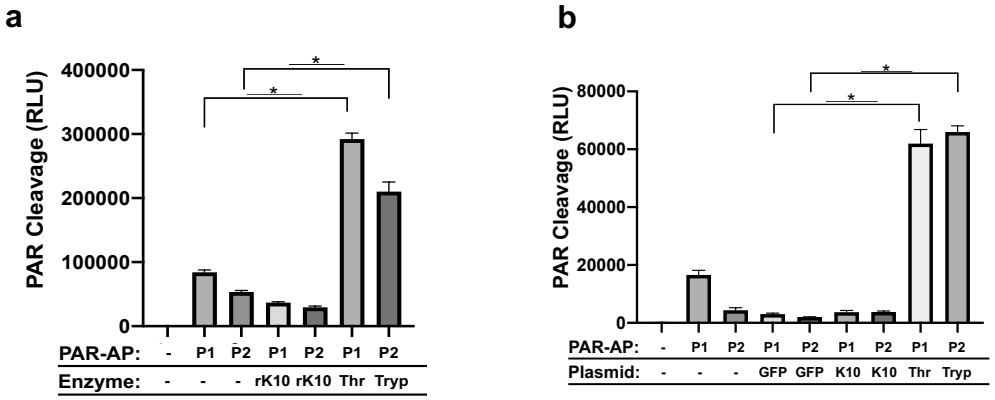

***Figure 6.2*. KLK10 does not cleave PAR1-AP or PAR2-AP.** (a) PAR cleavage assay in which HAECs were transfected with PAR1-AP or PAR2-AP plasmids and treated with rKLK10 (100 ng/mL), thrombin (5 U/mL) or trypsin (5 U/mL) for 1hr. Conditioned media was then assayed for alkaline phosphatase activity. (b) PAR cleavage assay in which HAECs were co-transfected with PAR1-AP or PAR2-AP plasmids and KLK10 plasmids. Conditioned media was then assayed for alkaline phosphatase activity. All data is represented as Mean±SEM, *P≤0.05, Paired two-tailed t-test. N=4.

Next, as an alternative, independent approach, we carried out a peptide cleavage assay using the synthetic N-terminal peptides corresponding to amino acid sequence 22-102 of PAR1 ($PAR1^{22-102}$) and 26-75 of PAR2 ($PAR2^{26-75}$), which contain canonical cleavage-activation sites for known proteinase agonists[306, 307]. Again, as expected, thrombin and trypsin efficiently cleaved the PAR1 and PAR2 peptides, respectively, as demonstrated by the Coomassie staining of Tricine-SDS PAGE gel (Figure 6.3). However, rKLK10 failed to cleave the peptides. These results demonstrate that neither rKLK10 nor KLK10 overexpressed by the expression vector can cleave and activate PAR1 or PAR2 receptors.

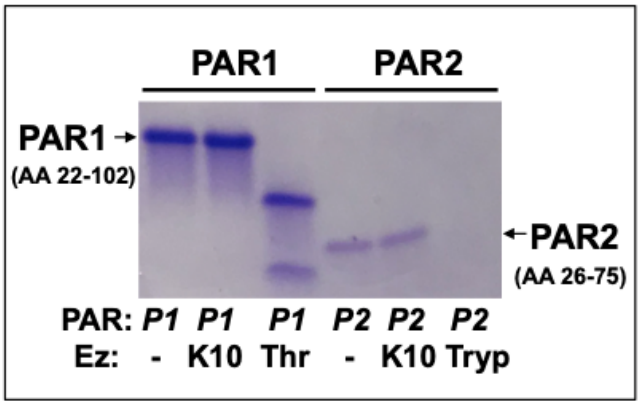

***Figure 6.3*. KLK10 does not cleave PAR1 or PAR2 synthetic peptides.**
Synthetic peptides (100 μM) corresponding to the N-terminal extracellular domains of PAR1 (AA22-102) or PAR2(AA26-75) were incubated with rKLK10 (100 ng/mL), thrombin (5 U/mL) or trypsin (5 U/mL) for 1hr at 37°C in 50 mM Tris, 150 mM NaCl, pH 8.0 and peptide products were analyzed by Tricine SDS-PAGE.

Observing KLK10 to not cleave PAR1 or PAR2, we next tested whether rKLK10 has enzymatic activity by incubating rKLK10 with an FP-biotin serine proteinase Activity-Based Probe, followed by streptavidin-HRP western blotting. rKLK10 was labelled with FP-biotin (Figure 6.4), indicating that KLK10 is indeed an active serine proteinase. Of importance, labeling

by the activity-based probe was lost when rKLK10 was heat-inactivated, suggesting its 3D conformation is necessary for its enzymatic activity and the anti-inflammatory effect. Taken together, these results demonstrate that KLK10 inhibits endothelial inflammation in a PAR1/2-dependent manner, but without directly cleaving the PARs.

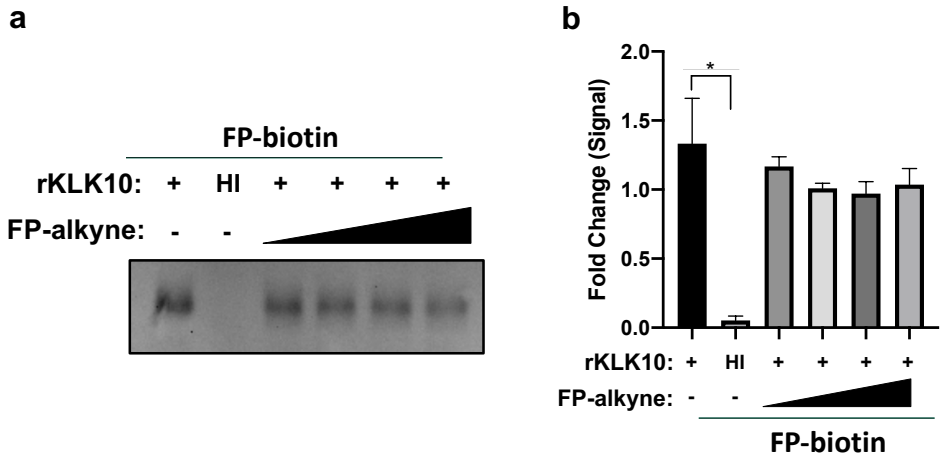

***Figure 6.4*. KLK10 shows enzymatic activity using FP-biotin activity-based probe.** (a) KLK10 enzymatic activity was measured by incubating rKLK10 (60 ng) with FP-Biotin (50 μm) and increasing concentrations of FP-alkyne competitive inhibitor (50-500 μm) followed by streptavidin-HRP western blotting. FP-biotin was also incubated with heat-inactivated (HI) rKLK10. (b) Quantification of KLK10 enzymatic activity represented as fold change normalized to FP-Biotin+rKLK10. All data is represented as Mean±SEM, *P≤0.05, One-Way Anova with Bonferroni Correction. N=6

6.2.2 TRICEPS-affinity pulldown indicates KLK10 binds to VEGFA, HTRA1, and VATB2

Thus far, our results indicated that KLK10 induces anti-inflammatory effects in a PAR1/2-dependent manner without cleaving them. Therefore, we hypothesized that KLK10 binds to another protein which mediates the PAR1/2-dependent anti-inflammatory effect. To test this hypothesis, we carried out an affinity pulldown assay using rKLK10 conjugated to TRICEPS-biotin to identify KLK10 binding proteins in HAECs followed by mass spectrometry[291, 308]. The

TRICEPs moiety has three arms; one binds KLK10, the other binds glycosylated proteins on the cell membrane, and the last arm contains a visualization/functional biotin group. After coupling rKLK10 to TRICEPs, it will be added to the cells and after binding between KLK10 and its receptor has occurred, the cells will be collected, lysed and submitted for mass spec proteomics. Using glycine conjugated TRICEPS and streptavidin-PE alone as negative controls, we found that rKLK10 coupled to TRICEPS specifically bound to the endothelial membrane as determined by flow cytometry (Figure 6.5a,b) and immunostaining (Figure 6.5c,d)

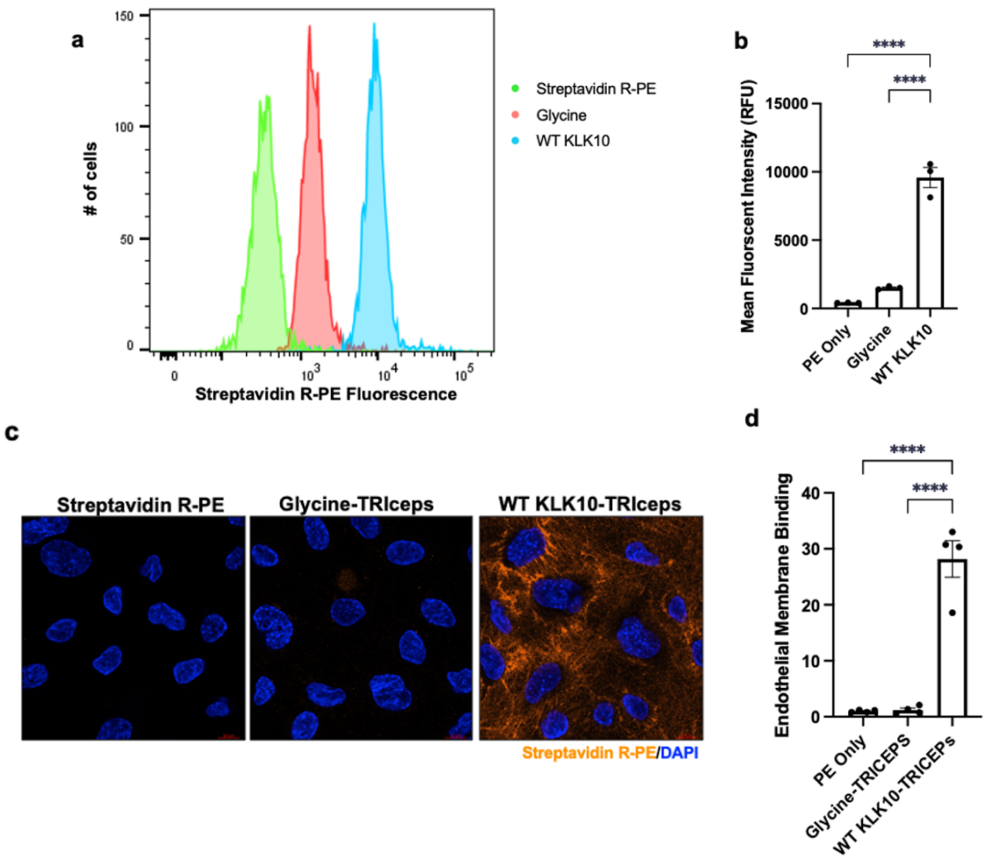

***Figure 6.5*. KLK10-coupled TRICEPS binds the endothelial membrane.** WT rKLK10-coupled TRICEPS was added to HAECs and binding to the membrane was assessed by flow cytometry (a,b) and immunostaining (c,d) using Streptavidin-PE which binds to the biotin on TRICEPS. Glycine-coupled TRICEPS and Streptavidin-PE alone were used as a negative controls. n=3-4. One-way ANOVA with Bonferroni correction for multiple comparisons where appropriate. Mean±SEM. *P≤0.05.

To identify KLK10-binding proteins in HAECs, rKLK10 conjugated to TRICEPS-biotin was pulled down using Streptavidin followed by mass spectrometry. As a positive control, Transferrin conjugated to TRICEPS-biotin was used since it was previously shown to bind the Transferrin receptor TFR1[291, 308]. Mass spectrometry data showed that Transferrin bound to TRF1, as expected (Figure 6.6). In contrast, KLK10 bound to HTRA1, VEGFA (Vascular Endothelial Growth Factor A), and VATB2 (ATPase H+ Transporting V1 Subunit B2), as well as KLK10 itself. Of the three KLK10 binding proteins, we selected HTRA1 for further study because of its potential clinical significance and novelty. All KLK10-binding proteins identified from the mass spectrometry analysis are listed in Appendix Table A2.

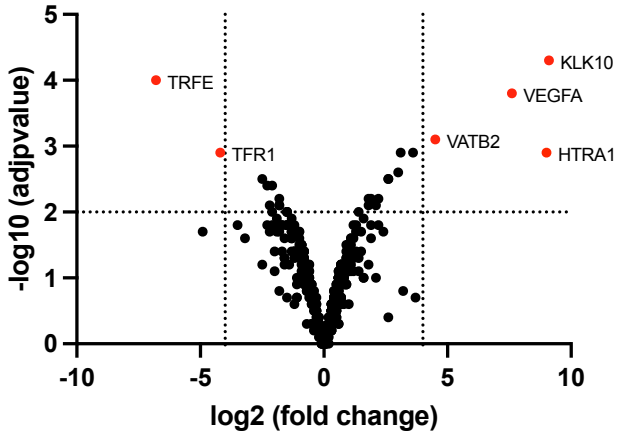

***Figure 6.6*. KLK10 binds to VEGFA, HTRA1, and VATB2.** Volcano plot depicting proteins that bind to KLK10 compared to the Transferrin (TRFE) control in HAECs using a TRICEPS affinity pulldown method, followed by mass spectrometry. Three KLK10 binding proteins (HTRA1, VEGFA, were VATB2) in addition to KLK10 itself were identified as highlighted in red. n=3. One-way ANOVA with Bonferroni correction for multiple comparisons where appropriate. Mean±SEM. *P≤0.05.

6.2.3 HTRA1 binds and cleaves KLK10, regulating it anti-inflammatory and barrier protect effects

HTRA1 is a serine protease associated with two diseases: CARASIL (Cerebral Autosomal Recessive Arteriopathy with Subcortical Infracts and Leukoencephalopathy) and AMD (Age-related Macular Degeneration). While CARASIL is associated with loss-of-function mutations of HTRA1[309, 310], AMD is associated with gain-of-function mutations[311, 312], suggesting the importance of regulating HTRA1 activity in a tight range in pathobiology[310, 313-315]. We further validated the binding identified by the mass spectrometry study between KLK10 and HTRA1 by the Proximity Ligation Assay in HAECs exposed to LS or OS (Figure 6.7a,b). We found that KLK10 and HTRA1 are bound to each other in both LS and OS conditions, with no significant difference between the groups.

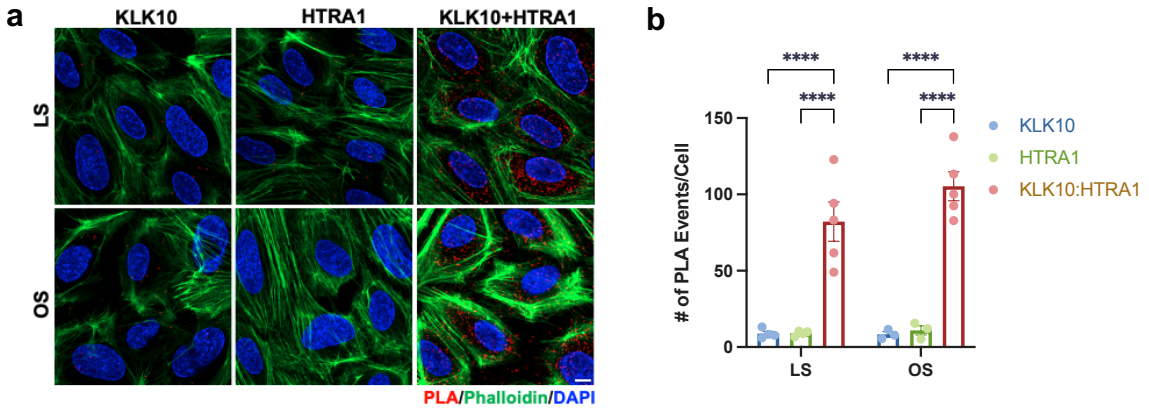

Figure 6.7. **Proximity Ligation Assay demonstrates KLK10 binds to HTRA1 in HAECs.** (a) The binding of KLK10 and HTRA1 as indicated by red staining was demonstrated by the proximity ligation assay (PLA) using KLK10 and HTRA1 antibodies in HAECs subjected to 48hr of LS or OS. HAECs were then counterstained with Phalloidin D (green) and DAPI (blue). (b) Quantification of the number of PLA interactions per cell is shown, n=5. One-way ANOVA with Bonferroni correction for multiple comparisons where appropriate. Mean±SEM. *P≤0.05.

Next, we tested if HTRA1 has functional importance in the anti-inflammatory and barrier protective function of KLK10 by using the HTRA1 siRNA in HAECs exposed to OS. The siRNA-

mediated knockdown of HTRA1 significantly reduced the KLK10's protective effects on VCAM1 induction (Figure 6.8a-c), shear-induced permeability (Figure 6.7d), and p65 NFκB nuclear localization (Figure 6.8e-f). These results demonstrate that HTRA1 regulates the anti-inflammatory and barrier-protective effects of KLK10. Interestingly, we found that HTRA1 was upregulated by OS in HAECs (Figure 6.8a,c), indicating HTRA1 itself is shear sensitive. These results show KLK10 and HTRA1 expression are inversely regulated by flow.

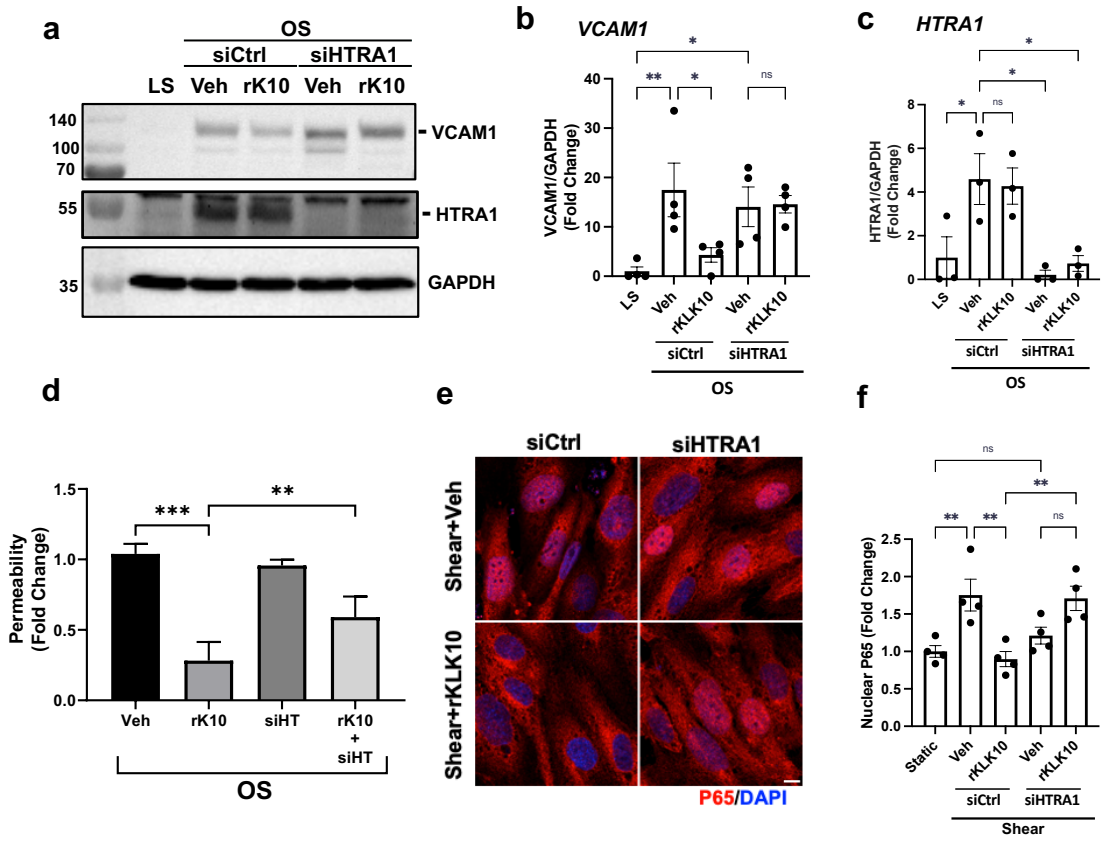

Figure 6.8. **Knockdown of HTRA1 prevents the anti-inflammatory and barrier protective effects of KLK10.** (a-f) HAECs pre-treated with HTRA1 siRNA (50 nM) and were exposed to OS in the presence of rKLK10 (10 ng/mL) for 24hrs, followed by (a-c) Western blots using antibodies to VCAM1, HTRA1, and GAPDH control or (d) the FITC-avidin permeability assay. (e,f) HAECs pre-treated with HTRA1 siRNA were exposed to LS (15 dynes/cm^2) in the presence of rKLK10 (10 ng/mL) for 1hr to induce p65 nuclear localization and immunostained with p65 antibody (red) and DAPI (blue). Quantification of nuclear p65 levels is shown as fold-change over static control, n=4. One-way ANOVA with Bonferroni correction for multiple comparisons where appropriate. Mean±SEM. *P≤0.05.

6.2.4 HTRA1 cleaves KLK10 at the N-terminal and C-terminal regions

Since HTRA1 is a serine protease, we tested if HTRA1 cleaves KLK10. To test this hypothesis, we incubated rKLK10 (A34-N276, 35kDa) with recombinant WT or catalytically inactive HTRA1 mutant (S328A), and analyzed the KLK10 cleavage products by western blot and Coomassie staining. Incubation of rKLK10 (35kDa form) with WT rHTRA1 generated two cleaved KLK10 fragments at 33kDa and 17kDa, while incubation with the inactive rHTRA1 mutant continued to have the intact 35kDa KLK10 band (Figure 6.9a). The mass spectrometry analysis of the tryptic peptides produced from digesting these three bands with trypsin revealed that all three were indeed KLK10 proteins. The tryptic digestion mapping analysis of the mass spectrometry data (Figure 6.9b and Appendix Figure A1) suggested that the 35kDa protein was the intact rKLK10 (A34-N276). In contrast, the 33kDa and 17kDa fragments showed evidence for cleavages at the N-terminus and two different C-termini. The 33kDa form contained L43-K264 (missing A34-R42 at the N-terminus and Y265-N276 at the C-terminus), while the 17kDa form showed L43-K199 (missing A34-R42 at the N-terminus and E200-R220 at the C-terminus). These missing tryptic peptides at both the N- and C-terminal regions of KLK10 may contain potential cleavage sites by HTRA1.

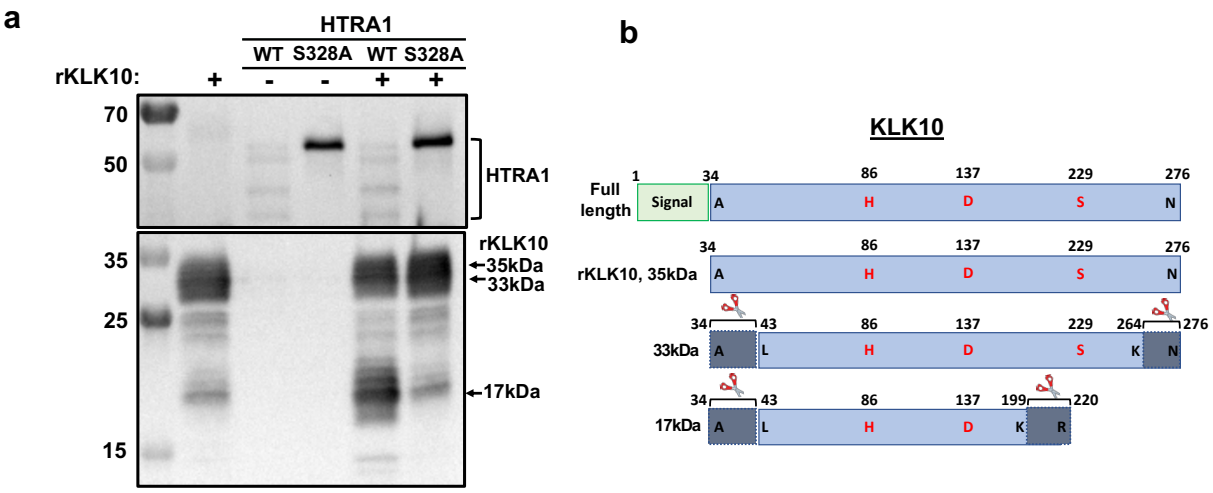

Figure 6.9. **HTRA1 cleaves KLK10 at distinct sites on the N- and C-terminal domains of KLK10** (a) KLK10 (500 ng) and rHTRA1 (500 ng; WT or S328A mutant) were incubated for 18hrs, and cleaved proteins were analyzed by western blot using KLK10 and HTRA1 antibodies. (b) Mass spectrometry analysis of tryptic peptides generated from HTRA1 cleavage of rKLK10 revealed the intact rKLK10 (A34-N276) along with KLK10-33kDa (L43-N276) and KLK10-17kDa (L43-K199) cleaved proteins. Bracketed regions indicate HTRA1 cleavage locations. H, D, and S indicate conserved catalytic triad amino acids

6.3 Summary

In this chapter, we have identified a clear mechanism of action underlying the anti-inflammatory and barrier-protective effects of KLK10. Using pharmacological inhibitors and siRNAs, we found that PAR1/2 mediated the anti-inflammatory effect of KLK10. Unexpectedly however, despite having measurable enzymatic activity, KLK10 did not cleave the PAR1/2, suggesting a non-canonical activation mechanism. Through a TRICEPs-affinity pulldown assay, we found direct KLK10-binding proteins including VEGFA, HTRA1, and VATB2. Because HTRA1 is a GWAS gene and has been implicated in a number of vascular diseases including CARASIL and AMD[309, 311], we further studied its role in the KLK10 mechanism of action. The proximity ligation confirmed binding of KLK10 and HTRA1. Additionally, we found a novel

mechanism by which HTRA1 regulates KLK10's anti-inflammatory and barrier protective functions. Knockdown of HTRA1 in HAECs exposed to OS blocked KLK10 from inhibiting inflammation (VCAM1, p65 nuclear translocation) and barrier permeability. HTRA1 cleaves KLK10 at distinct sites at the N- and C-terminal domains, which is most likely a key step in regulating the functional effects of KLK10. These findings are summarized in the updated working hypothesis (Figure 6.10).

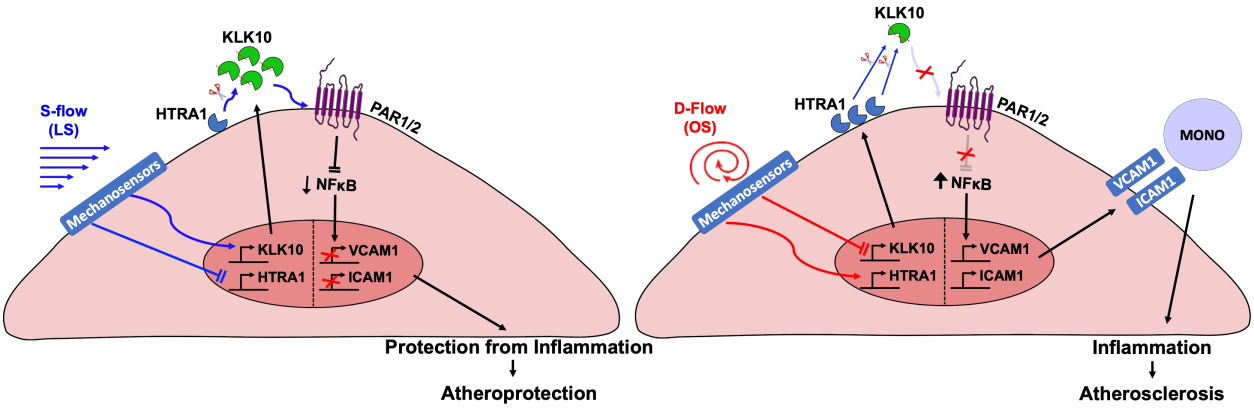

***Figure 6.10*. Working hypothesis: Flow-sensitive KLK10 inhibits inflammation and atherosclerosis in a HTRA1- and PAR1/2-dependent mechanism.** KLK10 is upregulated by *s-flow* and downregulated by *d-flow*. HTRA1 is also a secreted serine protease with inverse regulation by flow relative to KLK10. Under *s-flow* conditions when KLK10 is expression is high and HTRA1 expression is low, HTRA1 may cleave and activates KLK10, which in turn activates non-canonical PAR1/2 pathway to inhibit NF□B-mediated expression of VCAM1 and ICAM1, thereby decreasing monocyte adhesion and atherosclerosis. Under *d-flow* conditions when KLK10 is expression is low and HTRA1 expression is high, HTRA1 cleaves KLK10 to prevent its anti-inflammatory and anti-atherogenic pathway.

6.4 Discussion

Our data reveal a novel effect of KLK10 through an unexpected action mechanism in endothelial cell function. KLK10 expression is downregulated in breast, prostate, testicular, and lung cancer[242-246] but overexpressed in ovarian, pancreatic, and uterine cancer[247-250]. These suggest that abnormal, either too low or too high, levels of KLK10 are associated with various pathophysiological conditions. Alternatively, KLK10 activity may be regulated by its binding proteins, such as HTRA1.

HTRA1 may play a critical role in regulating KLK10 function and atherosclerosis. In this study, we showed that HTRA1 binds, cleaves, and regulates KLK10 function in endothelial function. The balance between HTRA1 and KLK10 may have much wider implications in pathophysiology of other diseases including CARASIL, AMD, and various cancer. Interestingly, genome-wide association studies have identified loss-of-function mutations in the HTRA1 gene in a rare cerebral arteriopathy, CARASIL, while gain-of-function mutations of HTRA1 is associated with AMD[310, 313-315]. These two opposite consequences of HTRA1 in different disease conditions suggest that HTRA1 activity should be tightly regulated. It is interesting that shear stress regulates the expression of both KLK10 and HTRA1, but in an opposite direction. Since *s-flow* induced KLK10^{high}/HTRA1^{low} while *d-flow* led to KLK10^{low}/HTRA1^{high}, the KLK10 versus HTRA1 balance could affect KLK10 cleavage status and subsequent activity under different flow conditions. The pathophysiological significance of the KLK10/HTRA1 balance in atherosclerosis and other diseases is an important future question.

We found that HTRA1 cleaves rKLK10 (35kDa form) to generate 33kDa and 17kDa cleavage products. The 33kDa and 17kDa forms displayed potential cleavage regions both at the N-terminus and two different C-termini (Figure 6.9a,b). Additional studies are required to identify the exact cleavage sites within these regions in ECs and tissues. Interestingly, however, the 17kDa form loses one of the residues involved in the catalytic triad (S229), which may lead to the loss of KLK10 activity. The functional importance of these KLK10 fragments needs to be determined in the future.

Mechanistically, our data using the PAR inhibitors and siRNAs (Figures 6.1a,b) show that PAR1/2 mediate the anti-inflammatory effect of KLK10 in ECs. Since PAR1/2 can be activated by KLKs 5, 6, and 14[301, 302], it came as a surprise that KLK10 was not able to cleave and activate the PARs directly in our study using several independent approaches (Figure 6.2 and 6.3). This was demonstrated by SEAP-PAR1/2 or N-Luciferase-PARs 1/2 cleavage assay in response to either rKLK10 or the KLK10 expression vector, as well as the cleavage assays using the PAR1/2 peptides representing the canonical cleavage sites. Nonetheless, the activity-based probe analysis showed that KLK10 was indeed catalytically active. Of note, KLK10 lost its enzymatic activity and the anti-inflammatory effect upon heat-denaturation, indicating the importance of the 3D conformation for its enzyme activity and biological activity.

Taken together, our results show that KLK10's anti-inflammatory effect in ECs does not require the direct cleavage of PAR1/2. Instead, HTRA1 binds, cleaves, and possibly activates KLK10, regulating its anti-inflammatory response in a non-canonical PAR1/2-dependent manner (Figure 6.10). The interaction of KLK10 and HTRA1 leads to inhibition of the NFκB activation

and endothelial inflammation through the non-canonical PAR1/2-dependent manner, and atherosclerosis (Figure 6.10). The mechanism by which KLK10 and HTRA1 interaction regulates the PAR signaling pathway is an important unanswered question.

7. Discussion

7.1 Summary

In this dissertation, we have studied the role of KLK10 in endothelial mechanobiology and atherosclerosis. Here, we describe that *s-flow* promotes, while *d-flow* inhibits, expression and secretion of KLK10 in ECs *in vitro* and *in vivo*. Single-cell RNA sequencing (scRNAseq) and scATAC sequencing (scATACseq) studies using the partial carotid ligation mouse model showed flow-regulated KLK10 expression at the epigenomic and transcription levels. These findings were further supported by immunochemistry analysis of human coronary arteries where we found KLK10 expression to be decreased in arteries with advanced plaques compared to arteries with early plaques. Additionally, we found for the first time that KLK10 can inhibit endothelial inflammation, endothelial barrier dysfunction, and reduce migration and tube formation, but not apoptosis or proliferation. Importantly, treatment of ECs *in vitro* with rKLK10 or a KLK10 expression plasmid inhibited endothelial inflammation induced by *d-flow* or TNFα. Moreover, treatment with rKLK10 or overexpression of KLK10 by ultrasound-mediated plasmid expression inhibited endothelial inflammation and atherosclerosis development *in vivo*. We found that PAR1/2 mediated the anti-inflammatory effect of KLK10. Unexpectedly, however, but KLK10 did not cleave the PAR1/2, suggesting a non-canonical activation mechanism. Indeed, we found a novel mechanism by which HTRA1 regulates KLK10's anti-inflammatory and barrier protective functions. Our findings also indicate that KLK10 is likely to be important in human atherosclerotic plaque development. The protective effects of rKLK10 or plasmid-driven KLK10 expression on endothelial inflammation, barrier function, and atherosclerosis suggest its therapeutic potential for atherosclerosis treatment.

Our data reveal a novel effect of KLK10 through an unexpected action mechanism in endothelial cell function. KLK10 expression is downregulated in breast, prostate, testicular, and lung cancer[242-246] but overexpressed in ovarian, pancreatic, and uterine cancer[247-250]. These suggest that abnormal, either too low or too high, levels of KLK10 are associated with various pathophysiological conditions. Alternatively, KLK10 activity may be regulated by its binding proteins, such as HTRA1.

HTRA1 may play a critical role in regulating KLK10 function and atherosclerosis. In this study, we showed that HTRA1 binds, cleaves, and regulates KLK10 function in endothelial function. The balance between HTRA1 and KLK10 may have much wider implications in pathophysiology of other diseases including CARASIL, AMD, and various cancer. Interestingly, genome-wide association studies have identified loss-of-function mutations in the HTRA1 gene in a rare cerebral arteriopathy, CARASIL, while gain-of-function mutations of HTRA1 is associated with AMD[310, 313-315]. These two opposite consequences of HTRA1 in different disease conditions suggest that HTRA1 activity should be tightly regulated. It is interesting that shear stress regulates the expression of both KLK10 and HTRA1, but in an opposite direction. Since *s-flow* induced $KLK10^{high}/HTRA1^{low}$ while *d-flow* led to $KLK10^{low}/HTRA1^{high}$, the KLK10 versus HTRA1 balance could affect KLK10 cleavage status and subsequent activity under different flow conditions. The pathophysiological significance of the KLK10/HTRA1 balance in atherosclerosis and other diseases is an important future question.

We found that HTRA1 cleaves rKLK10 (35kDa form) to generate 33kDa and 17kDa cleavage products. The 33kDa and 17kDa forms displayed potential cleavage regions both at the

N-terminus and two different C-termini (Figure 6.9a,b). Additional studies are required to identify the exact cleavage sites within these regions in ECs and tissues. Interestingly, however, the 17kDa form loses one of the residues involved in the catalytic triad (S229), which may lead to the loss of KLK10 activity. The functional importance of these KLK10 cleavage products needs to be determined in the future.

Mechanistically, our data using the PAR inhibitors and siRNAs (Figures 6a and 6b) show that PAR1/2 mediate the anti-inflammatory effect of KLK10 in ECs. Since PAR1/2 can be activated by KLKs 5, 6, and 14[301, 302], it came as a surprise that KLK10 was not able to cleave and activate the PARs directly in our study using several independent approaches (Figure 6). This was demonstrated by SEAP-PAR1/2 or N-Luciferase-PAR1/2 cleavage assay in response to either rKLK10 or the KLK10 expression vector, as well as the cleavage assays using the PAR1/2 peptides representing the canonical cleavage sites. Nonetheless, the activity-based probe analysis showed that KLK10 was indeed catalytically active. Of note, KLK10 lost its enzymatic activity and the anti-inflammatory effect upon heat-denaturation, indicating the importance of the 3D conformation for its enzyme activity and biological activity.

Taken together, our results show that KLK10's anti-inflammatory effect in Ecs does not require the direct cleavage of PAR1/2. Instead, HTRA1 binds, cleaves, and possibly activates KLK10, regulating its anti-inflammatory response in a non-canonical PAR1/2-dependent manner (Figure 6.10). The interaction of KLK10 and HTRA1 leads to inhibition of the NFκB activation and endothelial inflammation through the non-canonical PAR1/2-dependent manner, and

atherosclerosis (Figure 6.10). The mechanism by which KLK10 and HTRA1 interaction regulates the PAR signaling pathway is an important unanswered question.

7.2 Conclusions

In conclusion, we show that KLK10 is a flow-sensitive protein that is upregulated by *s-flow* and downregulated by *d-flow* in ECs. Our results also demonstrate that KLK10, working with HTRA1, is a key mediator of the anti-inflammatory and anti-atherogenic effects of *s-flow* in a PAR1/2-dependent manner. The current study also raises numerous new and unexpected questions regarding the role and mechanisms of KLK10 and HTRA1 in vascular pathophysiology. Further, KLK10 and HTRA1 may serve as potential anti-atherogenic therapeutic targets.

7.3 Future Directions

In Aim 1, we identified KLK10 as a shear-sensitive endothelial protein that is regulated by flow through epigenetic modifications of the *KLK10* promoter regions. Lacking from this study are experiments to identify the upstream mechanosensing and mechanotransduction pathways that lead to the epigenetic modification of *KLK10*. What mechanosensors are involved in this pathway and how do they respond to LS vs OS shear stress? Further, how do these pathways affect the chromatin state of the *KLK10*? It is possible the mechanotransduction pathways involve previously described mechanosensors like Piezo1, PlexinD1, or integrins. However, there may also be novel undescribed mechanosensors involved which will require further studies to identify. Regulation of chromatin state and epigenetic modifications typically occurs through histone modifying enzymes such as histone methyltransferases and histone de-acetylases. Interestingly, our group has previously identified a large number of histone modifying enzymes that are shear-sensitive[2]. These

shear-sensitive transferases are potential candidates that could regulate KLK10 chromatin state and they can be identified through chromatin immunoprecipitation studies in the PCL mouse model.

In aim 2, we studied the functional roles of KLK10 in endothelial biology with a focus on endothelial inflammation, barrier permeability, and monocyte adhesion. We also tested the therapeutic potential of KLK10 in the PCL mouse model of atherosclerosis. Using multiple independent approaches, KLK10 displayed high therapeutic potential with the ability to inhibit TNFα and *d-flow*-induced inflammation, as well as atherosclerosis in an acute study. The next steps for this aim will be testing other means of overexpressing KLK10 *in vivo*, for example, through AAVs. AAVs overexpressing KLK10 could offer multiple advantages over rKLK10 injections or ultrasound mediate gene delivery, including the need for only a single injection that can cause sustained expression of the protein and also the ability to modify AAVs to target a specific cell-type of interest, such as Ecs. Further, we must also test the therapeutic potential of KLK10 in other models of atherosclerosis. The PCL surgery is an acute model of *d-flow* induced atherosclerosis. Does KLK10 also inhibit atherosclerosis in chronic models of atherosclerosis, such as $ApoE^{-/-}$ mice on a HFD for 3 months? The development of AAVs capable of overexpressing KLK10 in Ecs for long periods of time will greatly help in exploring this topic. Stemming from these studies is also the question, if rKLK10 treatment or KLK10 overexpression inhibits atherosclerosis, does knockout of KLK10 in mice promote atherosclerosis? To answer this question, we have already started the process of developing KLK10 knockout mice using CRISPR-Cas9 based technologies. These mice can be given the PCL surgery and studied in acute studies or given a HFD for 3 months and studied in chronic studies.

In aim 3, we investigated the mechanism of action for anti-inflammatory and barrier protective effects of KLK10. These studies clearly showed KLK10 acts in a non-canonical PAR1/2 mechanism involving HTRA1. One key point remaining from these studies are experiments to define how KLK10 and HTRA1 work together to signal through the PARs. KLK10 alone did not cleave PAR1 or PAR2, but it is possible that KLK10 and HTRA1 work together to cleave the receptor. Another explanation is that KLK10 and HTRA1 acts as inhibitors of PAR1/2 signaling, possibly through competitive inhibition of proteases that typically act through the PARs. Underlying these important topics is the aspect of HTRA1 cleavage of KLK10. Importantly, what are the functional consequences for this cleavage? It has been controversial whether KLK10 protein possesses enzymatic activity. KLK10 immunopurified from ascites fluids of ovarian cancer patients showed no enzymatic activity[262]. In contrast, KLK10 containing fraction obtained by size-exclusion chromatography using ascites fluid of ovarian cancer patients showed some enzymatic activity[316], although it did not exclude the possibility of the activity coming from other enzymes. When mature KLK10 was expressed as standard form starting at Glu-46 in e.coli, it was not active, but the extended N-terminal form starting at Leu-43 was active[260]. In our studies, we used two different rKLK10s (Ala^{34}-Asn^{276} produced in e. coli and Ala^{31}-Asn^{276} produced in CHO cells) and one KLK10 expression plasmid expressing full-length human KLK10 sequence (Met^{1}-Asn^{276}) (see materials and Methods). One potential difference in enzymatic activity may be related to the different N-terminal sequences contained in each KLK10. While KLK10 starting at Leu43 showed enzymatic activity, those starting at Ala^{31}, Ala^{34}, and Glu^{46} did not. Interestingly, KLK10 immunopurified from ovarian cancer patients had the A34 N-terminus and was inactive [262]. In addition, expression of the full-length human KLK10 sequence produced the pro-KLK10 starting at the expected site starting at Ala^{31}. The KLK10 starting at Leu43 displays enzymatic activity, but

it has not been shown to be expressed under pathophysiologically relevant conditions. We propose that KLK10 produced in physiologically relevant conditions start either at Ala31 or Ala34, which do not display enzymatic activity but has biological activity. It is possible that KLK10 may be cleaved at other N-terminus such as Leu^{43} under certain pathological conditions, revealing its enzymatic activity.

Lastly, it remains to be seen whether HTRA1 mediates the anti-atherogenic effect of KLK10 *in vivo*. To study this point, we need to repeat our atherosclerosis studies in $HTRA1^{-/-}$ mice. These mice have been produced in other labs and may be possible to obtain through a future collaboration. It is also possible that the other KLK10 binding proteins including VEGFA and VATB2 play a role in KLK10's regulation of endothelial biology, which will need to be studied further.

APPENDIX

	Age (Mean ± StDev)	Stroke	Hypertension	Diabetes	Smoking
Total (n=40)	52.25 ± 13.35	15	26	8	17
Sex					
Male (n=27)	53.21 ± 11.15	10	16	5	12
Female (n=13)	51.93 ± 16.22	5	10	3	5
Race					
White (n=21)	54.95 ± 13.14	8	12	3	9
Black (n=17)	49.72 ± 14.17	7	14	5	7
Hispanic (n=2)	44 ± 5.66	0	0	0	1

***Table A.1*. De-identified human characteristics.** Hearts were not suitable for cardiac transplantation donated to LifeLink of Georgia used in Figure 4.7.

Table A.2. KLK10-TRICEPs affinity pulldown mass spectrometry analysis

Protein Name	Accession	# of peptides	Log2 (KLK10/GLY)	Adjpvalue(KLK10/Gly)	-log10 (adjpvalue(KLK10/Gly)	Log2 (KLK10/TRFE)	Adjpvalue(KLK10/TRFE)	-log10 (adjpvalue(KLK10/TRFE)	Log2 (TRFE/GLY)	Adjpvalue(TRFE/Gly)	-log10 (adjpvalue(TRFE/GLY
ILVBL	A1L0T0	7	2.5	4.0E-03	2.4	-0.9	5.8E-02	1.2	3.4	6.2E-04	3.2
RP1BL	A6NIZ1	2	-0.8	1.7E-01	0.8	-0.4	4.7E-01	0.3	-0.4	1.1E-01	1.0
A2ML1	A8K2U0	9	-1.5	1.4E-01	0.9	0.1	7.4E-01	0.1	-1.6	1.1E-01	1.0
ADAS	O00116	2	-0.1	9.9E-01	0.0	-0.6	2.2E-01	0.7	0.5	2.1E-01	0.7
CLIC1	O00299	6	0.0	7.5E-01	0.1	0.6	1.6E-01	0.8	-0.6	1.2E-01	0.9
ACATN	O00400	13	2.8	4.0E-03	2.4	-0.8	8.5E-02	1.1	3.5	7.1E-04	3.1
PLOD2	O00469	10	0.8	1.4E-01	0.9	0.2	5.5E-01	0.3	0.6	1.6E-01	0.8
RNT2	O00584	3	-1.3	5.1E-02	1.3	-0.1	8.8E-01	0.1	-1.2	1.0E-02	2.0
PODXL	O00592	3	-3.1	4.0E-03	2.4	-1.2	4.0E-02	1.4	-1.9	3.9E-03	2.4
CYR61	O00622	13	2.2	4.0E-03	2.4	1.8	6.6E-03	2.2	0.4	1.7E-01	0.8
COPE	O14579	2	-0.4	9.9E-01	0.0	0.0	9.6E-01	0.0	-0.4	9.7E-01	0.0
AP3D1	O14617	2	-0.7	3.4E-01	0.5	0.5	3.8E-01	0.4	-1.1	6.0E-02	1.2
NRP1	O14786	17	0.8	6.2E-02	1.2	-0.5	1.2E-01	0.9	1.3	4.0E-03	2.4
PSA7	O14818	7	-0.3	5.2E-01	0.3	0.5	1.8E-01	0.8	-0.8	3.7E-02	1.4
PLXB2	O15031	4	-0.5	4.2E-01	0.4	-2.2	1.9E-02	1.7	1.7	3.8E-03	2.4
PGRC2	O15173	3	-0.2	6.3E-01	0.2	-1.0	4.5E-02	1.3	0.8	3.2E-01	0.5
SURF4	O15260	2	-0.2	8.2E-01	0.1	0.2	5.1E-01	0.3	-0.4	4.9E-01	0.3
MOT4	O15427	11	4.7	4.0E-03	2.4	-0.5	2.6E-01	0.6	5.3	5.0E-04	3.3
MRP4	O15439	4	0.4	4.2E-01	0.4	-1.2	3.6E-02	1.4	1.6	8.4E-02	1.1
FLRT2	O43155	2	-1.0	6.2E-02	1.2	-0.4	2.9E-01	0.5	-0.6	5.0E-02	1.3
KLK10	O43240	14	7.6	4.1E-03	2.4	9.1	4.6E-05	4.3	-1.6	1.4E-01	0.9
E41L2	O43491	3	-0.3	7.4E-01	0.1	-0.6	1.1E-01	1.0	0.3	3.3E-01	0.5
ACTN4	O43707	28	-0.5	2.0E-01	0.7	-0.1	6.5E-01	0.2	-0.3	2.2E-01	0.7
MCAT	O43772	12	2.2	9.5E-03	2.0	-0.8	1.2E-01	0.9	3.0	1.1E-03	2.9
PM34	O43808	3	1.1	4.5E-01	0.3	-1.8	6.9E-03	2.2	2.9	4.6E-02	1.3
CALU	O43852	14	-0.7	1.5E-01	0.8	0.0	9.4E-01	0.0	-0.8	2.1E-02	1.7
NDUS5	O43920	3	-1.2	5.6E-02	1.3	0.0	9.6E-01	0.0	-1.1	2.9E-02	1.5
PEPL	O60437	19	0.7	9.3E-01	0.0	1.9	2.5E-02	1.6	-1.2	3.4E-01	0.5
NRP2	O60462	5	0.0	8.0E-01	0.1	1.3	2.1E-02	1.7	-1.3	1.1E-02	2.0
MPZL2	O60487	4	2.9	4.0E-03	2.4	-0.5	1.6E-01	0.8	3.4	8.4E-04	3.1
ACSL4	O60488	2	0.9	5.1E-02	1.3	-1.3	2.1E-02	1.7	2.1	1.2E-03	2.9
PLIN3	O60664	4	0.3	4.5E-01	0.3	0.6	1.3E-01	0.9	-0.2	3.6E-01	0.4
MOT2	O60669	2	2.4	8.6E-02	1.1	-1.1	9.4E-02	1.0	3.6	2.8E-02	1.6
CTND1	O60716	8	0.3	4.9E-01	0.3	0.0	9.1E-01	0.0	0.3	3.4E-01	0.5
S19A2	O60779	2	3.0	8.2E-03	2.1	-0.9	2.9E-02	1.5	3.9	2.3E-03	2.6
H2B1L	O60814	2	-0.1	6.8E-01	0.2	0.7	5.7E-02	1.2	-0.8	1.8E-02	1.7
PLXA2	O75051	11	-0.9	1.2E-01	0.9	-1.6	4.8E-02	1.3	0.6	8.1E-02	1.1
HIP1R	O75146	2	-1.6	2.0E-01	0.7	-1.3	2.7E-02	1.6	-0.3	5.8E-01	0.2
MPU1	O75352	2	0.1	8.6E-01	0.1	0.3	5.1E-01	0.3	-0.2	6.0E-01	0.2
SC22B	O75396	4	0.5	3.8E-01	0.4	-0.7	6.1E-02	1.2	1.2	1.7E-02	1.8
FACE1	O75844	8	2.7	4.0E-03	2.4	-0.4	2.2E-01	0.7	3.1	1.2E-03	2.9
TOM70	O94826	2	-0.6	3.6E-01	0.4	-1.4	6.6E-02	1.2	0.8	4.1E-02	1.4
SC31A	O94979	6	-0.1	8.0E-01	0.1	0.1	7.9E-01	0.1	-0.2	4.5E-01	0.3
SCEL	O95171	2	-6.7	2.1E-01	0.7	-3.5	1.6E-02	1.8	-3.2	5.6E-01	0.3
SC24A	O95486	2	2.4	6.0E-02	1.2	-1.3	3.6E-02	1.4	3.7	1.1E-02	2.0
ACSL3	O95573	2	0.8	6.6E-02	1.2	-0.1	7.3E-01	0.1	0.9	2.1E-02	1.7
CAVN2	O95810	8	-0.2	9.5E-01	0.0	-0.1	6.7E-01	0.2	-0.1	8.4E-01	0.1
CLIC3	O95833	2	-1.7	2.6E-01	0.6	-1.5	1.9E-01	0.7	-0.2	5.0E-01	0.3
RECK	O95980	19	1.8	1.4E-02	1.9	-1.4	1.4E-02	1.8	3.2	1.2E-03	2.9
NDUBA	O96000	2	-0.6	2.4E-01	0.6	0.9	1.4E-01	0.9	-1.5	3.8E-03	2.4
NB5R3	P00387	4	-0.1	8.6E-01	0.1	-0.5	1.6E-01	0.8	0.4	1.8E-01	0.7
COX2	P00403	2	1.1	2.9E-01	0.5	0.8	1.1E-01	1.0	0.3	9.8E-01	0.0
AATM	P00505	18	-0.6	6.4E-01	0.2	0.6	9.4E-02	1.0	-1.2	1.3E-01	0.9
CAH2	P00918	2	2.2	8.4E-01	0.1	0.2	9.5E-01	0.0	1.8	7.2E-01	0.1
IGHG1	P01857	2	0.4	6.6E-01	0.2	2.1	9.2E-02	1.0	-1.7	1.6E-01	0.8
CO1A1	P02452	6	0.7	8.3E-01	0.1	1.2	2.7E-02	1.6	-0.5	3.5E-01	0.5
LMNA	P02545	36	0.2	7.7E-01	0.1	-0.2	6.6E-01	0.2	0.3	8.8E-01	0.1
FINC	P02751	53	1.2	2.2E-02	1.7	-0.1	7.5E-01	0.1	1.4	6.8E-03	2.2
FETUA	P02765	3	1.3	1.5E-02	1.8	0.7	9.7E-02	1.0	0.6	8.2E-02	1.1
ALBU	P02768	13	0.4	1.7E-01	0.8	0.6	9.1E-02	1.0	-0.2	7.4E-01	0.1
TFR1	P02786	21	0.9	7.2E-02	1.1	-4.2	1.2E-03	2.9	5.1	5.0E-04	3.3
TRFE	P02787	54	0.8	7.5E-02	1.1	-6.8	1.1E-04	4.0	7.6	6.9E-05	4.2
GLCM	P04062	2	-0.4	5.4E-01	0.3	0.3	5.4E-01	0.3	-0.7	3.6E-01	0.4
ANXA1	P04083	20	0.0	8.5E-01	0.1	0.6	9.4E-02	1.0	-0.6	1.3E-01	0.9
K2C1	P04264	52	-1.0	1.4E-01	0.9	1.0	7.6E-02	1.1	-2.0	1.7E-02	1.8
VWF	P04275	2	-1.4	2.2E-01	0.7	0.0	9.6E-01	0.0	-1.4	1.6E-01	0.8
SEMG1	P04279	3	-0.3	9.9E-01	0.0	2.6	3.8E-01	0.4	-2.9	3.0E-02	1.5
G3P	P04406	12	-0.1	6.4E-01	0.2	0.3	2.3E-01	0.6	-0.5	5.5E-02	1.3
CPNS1	P04632	3	1.7	9.5E-03	2.0	2.2	6.6E-03	2.2	-0.5	9.4E-02	1.0
RPN1	P04843	8	-0.7	7.4E-02	1.1	-0.9	3.2E-02	1.5	0.2	6.6E-01	0.2
RPN2	P04844	2	-1.1	1.3E-01	0.9	-0.4	2.4E-01	0.6	-0.7	2.4E-01	0.6
GNAI2	P04899	11	0.6	1.3E-01	0.9	0.9	4.7E-02	1.3	-0.3	9.8E-01	0.0
AT1A1	P05023	11	-0.1	9.8E-01	0.0	-0.3	2.3E-01	0.6	0.3	3.0E-01	0.5
AT1B1	P05026	2	-2.9	3.2E-02	1.5	-0.7	4.5E-01	0.3	-2.2	2.7E-03	2.6
A4	P05067	3	-0.3	9.3E-01	0.0	0.4	2.9E-01	0.5	-0.7	7.4E-01	0.1
ITB3	P05106	13	1.1	3.2E-02	1.5	-1.8	8.2E-03	2.1	2.8	7.5E-04	3.1
S10A8	P05109	3	-0.8	1.1E-01	0.9	0.9	4.8E-02	1.3	-1.7	3.8E-03	2.4
PAI1	P05121	4	1.0	7.2E-02	1.1	0.4	3.3E-01	0.5	0.7	7.8E-02	1.1
ICAM1	P05362	12	-1.9	9.5E-03	2.0	-1.3	1.4E-02	1.9	-0.5	1.5E-01	0.8
ITB1	P05556	24	-1.8	1.4E-02	1.8	-0.8	7.6E-02	1.1	-1.0	2.4E-02	1.6
GELS	P06396	8	0.7	8.0E-01	0.1	0.4	2.6E-01	0.6	0.4	5.9E-01	0.2
S10A9	P06702	3	-0.3	3.7E-01	0.4	0.7	9.1E-02	1.0	-1.0	2.4E-02	1.6
S10A6	P06703	2	0.9	2.2E-01	0.7	1.6	9.4E-02	1.0	-0.7	2.9E-01	0.5
ENOA	P06733	27	0.0	9.5E-01	0.0	0.7	9.4E-02	1.0	-0.7	2.3E-02	1.6
G6PI	P06744	9	-0.2	4.7E-01	0.3	0.6	1.0E-01	1.0	-0.8	1.7E-02	1.8
ITAV	P06756	22	-0.9	6.6E-02	1.2	-1.1	2.1E-02	1.7	0.1	5.1E-01	0.3
H2B2E	P06899	2	-0.6	1.3E-01	0.9	0.5	1.6E-01	0.8	-1.1	1.2E-02	1.9
PDIA1	P07237	25	0.5	2.0E-01	0.7	0.4	2.4E-01	0.6	0.0	6.1E-01	0.2
CATD	P07339	7	-1.4	5.7E-02	1.2	0.6	9.4E-02	1.0	-2.0	1.3E-02	1.9
ANXA2	P07355	25	-0.2	9.9E-01	0.0	0.7	9.2E-02	1.0	-0.8	7.5E-02	1.1
TRY1	P07477	2	-0.9	1.9E-01	0.7	0.3	4.3E-01	0.4	-1.2	5.3E-02	1.3
SAP	P07602	4	-1.1	1.5E-01	0.8	0.3	2.9E-01	0.5	-1.4	5.0E-02	1.3
PROF1	P07737	8	-0.4	6.9E-01	0.2	0.6	1.4E-01	0.8	-1.0	5.9E-02	1.2
SYEP	P07814	13	1.1	6.3E-02	1.2	-0.1	6.8E-01	0.2	1.2	1.5E-02	1.8
CATB	P07858	8	-0.8	1.3E-01	0.9	0.4	1.7E-01	0.8	-1.2	1.4E-02	1.9
HS90A	P07900	11	0.0	9.0E-01	0.0	0.2	5.3E-01	0.3	-0.2	4.5E-01	0.3
QCR6	P07919	2	-1.9	9.7E-02	1.0	-1.2	2.7E-01	0.6	-0.7	3.5E-02	1.5
LAMB1	P07942	2	3.2	4.0E-03	2.4	2.6	3.4E-03	2.5	0.6	8.2E-02	1.1
TSP1	P07996	20	0.6	9.7E-02	1.0	0.2	5.2E-01	0.3	0.4	9.6E-02	1.0

4F2	P08195	8	-2.2	1.4E-02	1.8	-1.2	4.9E-02	1.3	-1.0	4.1E-02	1.4
HS90B	P08238	13	0.3	4.4E-01	0.4	0.3	2.4E-01	0.6	0.0	7.1E-01	0.1
SRPRA	P08240	2	2.8	1.1E-02	2.0	1.1	2.5E-02	1.6	1.7	2.3E-02	1.6
CY1	P08574	3	-1.3	1.1E-01	0.9	0.1	9.0E-01	0.0	-1.3	8.7E-03	2.1
MET	P08581	2	0.5	3.8E-01	0.4	-1.3	2.7E-02	1.6	1.7	9.6E-03	2.0
ITA5	P08648	16	-0.9	6.0E-02	1.2	-0.7	5.7E-02	1.2	-0.2	5.1E-01	0.3
VIME	P08670	30	0.3	3.1E-01	0.5	0.5	1.4E-01	0.9	-0.2	9.4E-01	0.0
LEG1	P09382	6	0.5	3.8E-01	0.4	0.8	1.0E-01	1.0	-0.3	2.3E-01	0.6
HMGB1	P09429	7	-0.4	6.6E-01	0.2	0.2	7.1E-01	0.2	-0.6	2.6E-01	0.6
SPRC	P09486	2	-1.1	2.0E-01	0.7	-1.1	1.9E-01	0.7	0.1	7.2E-01	0.1
HMOX1	P09601	3	0.0	6.8E-01	0.2	-1.2	2.1E-02	1.7	1.2	3.1E-01	0.5
COX6C	P09669	3	-0.3	5.7E-01	0.2	0.9	1.3E-01	0.9	-1.2	2.0E-02	1.7
UCHL1	P09936	3	0.0	6.8E-01	0.2	0.9	3.6E-02	1.4	-0.9	2.2E-01	0.7
PTPRF	P10586	16	1.0	7.2E-02	1.1	-1.3	1.4E-02	1.8	2.3	2.7E-03	2.6
THIO	P10599	4	-0.2	4.5E-01	0.3	0.7	8.9E-02	1.0	-0.9	1.2E-02	1.9
COX5B	P10606	4	-0.7	3.7E-01	0.4	0.5	3.1E-01	0.5	-1.2	3.0E-02	1.5
TPI1	P10646	2	-3.6	1.4E-02	1.9	-3.2	2.5E-02	1.6	-0.4	3.4E-01	0.5
CH60	P10809	23	-0.7	1.5E-01	0.8	0.2	4.6E-01	0.3	-1.0	3.1E-02	1.5
HSP7C	P11142	21	-0.2	5.9E-01	0.2	0.2	4.6E-01	0.3	-0.4	9.6E-02	1.0
RALA	P11233	3	-0.3	7.4E-01	0.1	0.5	1.9E-01	0.7	-0.8	1.2E-01	0.9
ADT3	P12236	3	0.5	1.5E-01	0.8	-0.4	1.9E-01	0.7	0.9	1.4E-02	1.9
TPR	P12270	6	0.0	9.0E-01	0.0	-1.1	1.2E-01	0.9	1.0	2.7E-02	1.6
PIP	P12273	3	-0.8	2.6E-01	0.6	1.1	2.7E-02	1.6	-1.9	1.7E-02	1.8
ACTN1	P12814	21	0.1	6.0E-01	0.2	0.2	5.6E-01	0.2	-0.1	9.0E-01	0.0
ACE	P12821	2	1.9	1.9E-02	1.7	3.1	1.2E-03	2.9	-1.1	2.3E-02	1.6
XRCC6	P12956	11	0.1	6.6E-01	0.2	0.1	8.5E-01	0.1	0.0	6.3E-01	0.2
COX41	P13073	2	-1.2	1.8E-01	0.7	-0.5	5.0E-01	0.3	-0.7	1.7E-01	0.8
ICAM2	P13598	5	-1.0	4.8E-02	1.3	-0.8	5.7E-02	1.2	-0.2	4.6E-01	0.3
K1C10	P13645	34	-1.2	8.6E-02	1.1	0.6	2.3E-01	0.6	-1.9	2.4E-02	1.6
CD59	P13987	4	-1.2	7.4E-02	1.1	-0.8	9.2E-02	1.0	-0.4	3.6E-01	0.4
MIF	P14174	2	0.0	9.4E-01	0.0	0.5	1.6E-01	0.8	-0.5	2.1E-01	0.7
CD99	P14209	2	0.5	1.5E-01	0.8	-0.8	6.1E-02	1.2	1.4	7.9E-03	2.1
GLU2B	P14314	6	-0.4	6.9E-01	0.2	0.0	9.3E-01	0.0	-0.4	5.0E-01	0.3
HCLS1	P14317	3	-0.1	9.7E-01	0.0	0.5	1.9E-01	0.7	-0.6	2.9E-01	0.5
NID1	P14543	10	0.3	2.9E-01	0.5	-0.3	2.5E-01	0.6	0.7	2.3E-02	1.6
KPYM	P14618	27	0.0	9.8E-01	0.0	0.6	7.7E-02	1.1	-0.6	3.0E-02	1.5
ENPL	P14625	27	0.2	5.8E-01	0.2	0.1	8.4E-01	0.1	0.2	5.7E-01	0.2
IDE	P14735	16	1.3	9.8E-01	0.0	1.4	1.1E-02	2.0	-0.2	5.0E-01	0.3
PLAK	P14923	23	-0.9	1.8E-01	0.8	1.0	5.3E-02	1.3	-1.8	3.8E-02	1.4
AMPN	P15144	9	-2.6	2.8E-02	1.5	-0.4	5.7E-01	0.2	-2.1	2.4E-03	2.6
PVR	P15151	4	-0.9	7.9E-02	1.1	-0.2	6.5E-01	0.2	-0.7	6.5E-02	1.2
RAC2	P15153	2	0.5	2.0E-01	0.7	0.8	7.6E-02	1.1	-0.3	4.7E-01	0.3
MCP	P15529	5	-0.5	3.5E-01	0.5	-0.8	4.8E-02	1.3	0.3	3.1E-01	0.5
VEGFA	P15692	2	5.5	8.9E-02	1.1	7.6	1.8E-04	3.8	-2.0	2.4E-01	0.6
DESP	P15924	119	-0.9	2.0E-01	0.7	1.0	6.0E-02	1.2	-1.9	5.0E-02	1.3
CD44	P16070	5	-2.7	4.0E-03	2.4	-0.6	7.5E-02	1.1	-2.1	1.9E-03	2.7
PECA1	P16284	34	0.1	7.6E-01	0.1	-1.0	2.7E-02	1.6	1.1	1.1E-02	2.0
AT2A2	P16615	6	0.3	5.8E-01	0.2	0.0	9.0E-01	0.0	0.2	5.0E-01	0.3
ITA2	P17301	24	0.3	3.6E-01	0.4	-0.6	8.2E-02	1.1	0.9	1.4E-02	1.9
CAN2	P17655	3	0.8	1.0E-01	1.0	1.3	2.1E-02	1.7	-0.5	1.1E-01	0.9
EGLN	P17813	17	-1.0	6.3E-02	1.2	-1.0	4.4E-02	1.4	-0.1	9.3E-01	0.0
LEG3	P17931	4	-0.3	4.2E-01	0.4	0.4	2.7E-01	0.6	-0.6	2.2E-01	0.7
PTN1	P18031	3	2.4	1.4E-02	1.9	0.7	5.8E-02	1.2	1.6	2.3E-02	1.6
ITB5	P18084	6	0.0	8.8E-01	0.1	-1.3	1.6E-02	1.8	1.3	4.0E-03	2.4
VINC	P18206	25	0.0	8.9E-01	0.1	0.0	9.4E-01	0.0	0.1	6.8E-01	0.2
ATP5J	P18859	2	-1.1	2.8E-01	0.5	-0.3	3.0E-01	0.5	-0.8	4.6E-01	0.3
CADH2	P19022	4	-1.1	6.3E-02	1.2	-0.8	9.2E-02	1.0	-0.3	3.5E-01	0.5
VCAM1	P19320	5	-0.6	7.9E-02	1.1	-0.8	3.7E-02	1.4	0.2	4.6E-01	0.3
NDUV2	P19404	2	-1.3	3.3E-02	1.5	0.0	1.0E+00	0.0	-1.3	1.4E-02	1.9
COX5A	P20674	2	-1.0	1.4E-01	0.9	0.7	1.3E-01	0.9	-1.6	1.4E-02	1.9
VATB2	P21281	2	3.7	1.8E-01	0.7	4.5	7.1E-04	3.1	-0.7	3.7E-01	0.4
FLNA	P21333	83	0.3	3.0E-01	0.5	0.3	2.9E-01	0.5	0.0	7.3E-01	0.1
AOFA	P21397	4	0.2	3.9E-01	0.4	-0.1	6.8E-01	0.2	0.4	1.4E-01	0.9
5NTD	P21589	13	0.6	1.3E-01	0.9	-1.5	1.0E-02	2.0	2.0	2.7E-03	2.6
VDAC1	P21796	4	-0.3	3.4E-01	0.5	0.2	4.6E-01	0.3	-0.5	1.4E-01	0.9
SDHB	P21912	10	-1.4	4.4E-02	1.4	0.0	9.6E-01	0.0	-1.4	1.8E-02	1.7
CD9	P21926	3	1.4	2.2E-02	1.7	-0.8	5.8E-02	1.2	2.2	1.4E-03	2.9
COMT	P21964	2	-0.4	4.1E-01	0.4	0.2	6.6E-01	0.2	-0.5	7.4E-02	1.1
UBA1	P22314	10	0.2	9.4E-01	0.0	0.3	3.0E-01	0.5	-0.2	4.1E-01	0.4
ROA2	P22626	11	-0.9	1.6E-01	0.8	0.3	3.5E-01	0.5	-1.2	5.0E-02	1.3
TGM1	P22735	9	-1.4	5.6E-02	1.3	0.2	3.7E-01	0.4	-1.6	2.2E-02	1.7
PPIB	P23284	12	0.0	8.3E-01	0.1	0.0	9.2E-01	0.0	-0.1	8.3E-01	0.1
PTPRB	P23467	22	-0.9	6.6E-02	1.2	-1.2	1.6E-02	1.8	0.3	1.5E-01	0.8
PTPRG	P23470	2	2.3	2.7E-01	0.6	3.2	1.5E-01	0.8	-0.9	4.8E-01	0.3
THAS	P24557	8	1.7	3.7E-02	1.4	-2.3	1.6E-02	1.8	4.1	1.0E-03	3.0
ZA2G	P25311	4	-0.8	1.8E-01	0.7	1.2	7.6E-02	1.1	-1.9	9.6E-03	2.0
ITA3	P26006	4	-1.7	8.5E-02	1.1	-0.2	8.5E-01	0.1	-1.5	1.0E-02	2.0
MOES	P26038	11	0.1	6.0E-01	0.2	0.3	4.6E-01	0.3	-0.2	9.9E-01	0.0
HMGB2	P26583	3	-0.6	4.2E-01	0.4	0.3	6.4E-01	0.2	-0.9	5.0E-02	1.3
PTBP1	P26599	10	0.0	8.4E-01	0.1	0.2	4.9E-01	0.3	-0.2	6.3E-01	0.2
1433T	P27348	4	0.1	5.5E-01	0.3	1.4	5.0E-02	1.3	-1.3	1.2E-01	0.9
CALR	P27797	15	-0.7	1.3E-01	0.9	0.3	4.3E-01	0.4	-1.0	9.3E-03	2.0
CALX	P27824	20	-0.7	1.1E-01	1.0	0.0	9.4E-01	0.0	-0.7	3.7E-02	1.4
PSA5	P28066	8	2.2	7.7E-03	2.1	-0.8	6.6E-02	1.2	2.9	1.4E-03	2.9
GRN	P28799	10	-0.9	7.5E-02	1.1	0.1	8.2E-01	0.1	-1.0	2.3E-02	1.6
CTGF	P29279	17	2.2	4.5E-03	2.4	1.9	6.6E-03	2.2	0.3	1.5E-01	0.8
EPHA2	P29317	20	1.4	1.4E-02	1.9	-0.9	3.3E-02	1.5	2.3	1.4E-03	2.8
EPHB2	P29323	3	0.7	2.9E-01	0.5	-1.4	1.5E-02	1.8	2.0	1.8E-02	1.7
SPB3	P29508	9	-1.3	2.8E-01	0.6	1.0	3.7E-02	1.4	-2.3	8.5E-02	1.1
PML	P29590	4	1.3	5.1E-02	1.3	1.0	7.9E-02	1.1	0.3	4.0E-01	0.4
EF1D	P29692	5	0.2	4.6E-01	0.3	0.2	6.8E-01	0.2	0.1	6.5E-01	0.2
MARCS	P29966	6	-0.2	9.8E-01	0.0	0.0	9.6E-01	0.0	-0.2	9.9E-01	0.0
ATPD	P30049	2	-0.7	1.8E-01	0.7	0.7	1.9E-01	0.7	-1.4	3.6E-03	2.4
AMRP	P30533	4	-0.4	3.5E-01	0.5	0.3	4.3E-01	0.4	-0.7	1.1E-01	1.0
SORCN	P30626	6	-0.1	9.5E-01	0.0	0.8	1.4E-01	0.9	-0.9	3.0E-02	1.5
1433B	P31946	4	2.8	1.4E-02	1.8	3.0	2.3E-03	2.6	-0.2	3.0E-01	0.5
1433S	P31947	7	-0.9	3.7E-01	0.4	1.0	2.7E-01	0.6	-2.0	2.0E-01	0.7
CADH5	P33151	13	0.3	4.2E-01	0.4	-0.8	4.5E-02	1.3	1.1	9.8E-03	2.0
MRP1	P33527	11	0.3	3.1E-01	0.5	-2.1	4.4E-03	2.4	2.4	2.3E-03	2.6
CTNA1	P35221	16	0.7	1.1E-01	1.0	-0.3	2.2E-01	0.7	1.0	1.3E-02	1.9

CTNB1	P35222	6	0.3	5.4E-01	0.3	0.0	9.5E-01	0.0	0.3	2.9E-01	0.5
PHB	P35232	6	0.2	9.5E-01	0.0	-0.1	7.8E-01	0.1	0.3	9.7E-01	0.0
RADI	P35241	3	0.0	9.3E-01	0.0	0.4	5.5E-01	0.3	-0.4	1.3E-01	0.9
MYH9	P35579	43	1.1	1.1E-01	1.0	0.6	9.4E-02	1.0	0.5	4.5E-01	0.3
BASI	P35613	9	-0.8	1.4E-01	0.9	-0.9	2.9E-02	1.5	0.2	3.3E-01	0.5
VGFR2	P35968	2	0.3	8.7E-01	0.1	-2.5	2.9E-03	2.5	2.8	6.0E-02	1.2
GGT5	P36269	6	-1.3	7.8E-02	1.1	-1.7	3.7E-02	1.4	0.4	2.3E-01	0.6
SPB5	P36952	12	1.0	7.6E-01	0.1	1.2	1.4E-02	1.8	-0.3	4.1E-01	0.4
FDFT	P37268	14	0.8	1.0E-01	1.0	-1.5	1.4E-02	1.8	2.2	2.7E-03	2.6
TAGL2	P37802	10	0.6	1.3E-01	0.9	1.1	3.4E-02	1.5	-0.5	1.4E-01	0.9
IL6RB	P40189	15	0.1	6.6E-01	0.2	-0.8	4.4E-02	1.4	0.9	1.6E-02	1.8
GARS	P41250	2	0.4	2.7E-01	0.6	1.2	4.8E-02	1.3	-0.8	2.0E-01	0.7
S19A1	P41440	6	2.3	8.0E-03	2.1	0.0	9.4E-01	0.0	2.3	1.4E-03	2.8
LAP2B	P42167	2	-1.1	5.1E-02	1.3	-0.8	4.0E-02	1.4	-0.2	5.2E-01	0.3
ECE1	P42892	10	1.4	6.0E-02	1.2	0.7	1.9E-01	0.7	0.7	9.6E-02	1.0
LIS1	P43034	4	-0.1	5.5E-01	0.3	0.1	8.2E-01	0.1	-0.2	2.9E-01	0.5
MUC18	P43121	26	-0.9	7.3E-02	1.1	-0.8	7.6E-02	1.1	-0.2	6.1E-01	0.2
BTD	P43251	6	4.2	1.0E-02	2.0	2.2	1.6E-02	1.8	2.0	6.7E-02	1.2
NAMPT	P43490	8	1.9	1.4E-02	1.9	1.5	2.2E-02	1.7	0.3	3.2E-01	0.5
VDAC2	P45880	10	1.5	1.2E-02	1.9	1.8	8.2E-03	2.1	-0.3	1.9E-01	0.7
NOTC1	P46531	4	-0.6	3.3E-01	0.5	-2.0	3.6E-02	1.4	1.4	3.6E-03	2.4
LEG7	P47929	5	0.1	5.4E-01	0.3	1.5	4.0E-02	1.4	-1.3	2.4E-01	0.6
LIMS1	P48059	2	-0.4	7.1E-01	0.1	-0.2	4.6E-01	0.3	-0.2	9.6E-01	0.0
COPD	P48444	7	-0.4	2.7E-01	0.6	-0.3	3.5E-01	0.5	-0.1	6.2E-01	0.2
IDHP	P48735	10	-0.9	2.0E-01	0.7	0.3	4.3E-01	0.4	-1.2	3.6E-02	1.4
ACADV	P49748	6	-0.8	1.0E-01	1.0	0.0	9.7E-01	0.0	-0.7	5.5E-02	1.3
MMP14	P50281	5	0.2	5.9E-01	0.2	-0.5	5.1E-01	0.3	0.7	5.4E-02	1.3
GDIB	P50395	12	0.0	6.8E-01	0.2	0.3	2.6E-01	0.6	-0.3	1.6E-01	0.8
EMD	P50402	3	0.2	4.1E-01	0.4	0.5	1.9E-01	0.7	-0.2	5.2E-01	0.3
CPT1A	P50416	6	0.5	2.9E-01	0.5	-1.7	1.6E-02	1.8	2.2	8.7E-03	2.1
SERPH	P50454	17	-0.3	6.9E-01	0.2	0.2	5.1E-01	0.3	-0.5	2.9E-01	0.5
PPT1	P50897	2	0.5	8.7E-01	0.1	0.7	2.4E-01	0.6	-0.2	4.8E-01	0.3
TCPD	P50991	11	0.0	8.9E-01	0.1	0.3	3.0E-01	0.5	-0.3	2.8E-01	0.6
RAB5C	P51148	3	0.7	1.3E-01	0.9	-0.2	5.2E-01	0.3	0.9	3.5E-02	1.5
RAB7A	P51149	7	-0.6	1.4E-01	0.9	-0.3	4.0E-01	0.4	-0.3	2.4E-01	0.6
SSRD	P51571	3	-0.9	5.7E-02	1.2	0.3	3.3E-01	0.5	-1.2	1.4E-02	1.9
BAP31	P51572	4	0.0	9.9E-01	0.0	0.0	9.3E-01	0.0	0.1	8.8E-01	0.1
AL3A2	P51648	4	-0.3	4.7E-01	0.3	-1.2	4.4E-02	1.4	0.9	9.1E-01	0.0
COPB	P53618	9	1.0	4.9E-02	1.3	0.6	9.4E-02	1.0	0.3	2.9E-01	0.5
COPA	P53621	9	0.6	1.5E-01	0.8	0.0	9.5E-01	0.0	0.6	5.2E-02	1.3
CCHL	P53701	2	2.6	8.0E-02	1.1	0.4	3.8E-01	0.4	2.1	9.8E-02	1.0
MOT1	P53985	6	3.1	4.1E-03	2.4	-2.1	9.8E-03	2.0	5.2	5.0E-04	3.3
AT1B3	P54709	3	-1.9	1.4E-02	1.9	-0.6	9.2E-02	1.0	-1.3	2.1E-02	1.7
EPHB4	P54760	4	0.4	4.9E-01	0.3	-1.5	1.4E-02	1.8	1.9	3.8E-03	2.4
SNAA	P54920	4	-1.2	4.5E-02	1.3	-0.2	7.2E-01	0.1	-1.0	1.4E-02	1.9
MANF	P55145	5	-1.0	1.7E-01	0.8	-0.1	7.8E-01	0.1	-0.9	1.5E-01	0.8
CAD11	P55287	3	0.2	4.5E-01	0.3	-1.1	2.1E-02	1.7	1.3	1.4E-02	1.9
CAD13	P55290	6	-1.3	2.5E-02	1.6	-1.0	2.2E-02	1.7	-0.3	5.0E-01	0.3
SEC13	P55735	3	0.0	9.1E-01	0.0	0.8	7.6E-02	1.1	-0.8	4.5E-02	1.3
EPIPL	P58107	42	0.4	6.8E-01	0.2	2.1	8.1E-03	2.1	-1.7	1.6E-01	0.8
TPIS	P60174	16	-0.1	9.5E-01	0.0	0.8	1.2E-01	0.9	-0.9	1.4E-02	1.9
ACTG	P60709	7	0.4	9.3E-01	0.0	0.7	8.5E-02	1.1	-0.3	2.9E-01	0.5
CDC42	P60953	3	-0.4	6.9E-01	0.2	0.6	9.2E-02	1.0	-0.9	6.7E-02	1.2
RAB14	P61106	3	1.3	8.4E-01	0.1	0.0	9.6E-01	0.0	1.3	7.7E-01	0.1
RL15	P61313	6	-0.5	6.9E-01	0.2	0.7	1.9E-01	0.7	-1.2	6.1E-02	1.2
RHOA	P61586	6	-0.1	7.3E-01	0.1	0.7	1.2E-01	0.9	-0.7	3.0E-01	0.5
LYSC	P61626	4	-1.0	8.9E-02	1.1	0.8	9.3E-02	1.0	-1.9	8.9E-03	2.1
B2MG	P61769	4	0.4	3.7E-01	0.4	0.1	8.6E-01	0.1	0.3	2.9E-01	0.5
NPC2	P61916	3	-1.8	1.1E-02	1.9	-0.1	7.4E-01	0.1	-1.7	3.3E-03	2.5
HNRPK	P61978	14	-0.1	9.5E-01	0.0	0.7	5.8E-02	1.2	-0.8	7.4E-02	1.1
RRAS2	P62070	2	0.4	6.0E-01	0.2	1.6	8.9E-02	1.0	-1.2	1.6E-02	1.8
PRS4	P62191	3	0.0	7.4E-01	0.1	0.4	1.5E-01	0.8	-0.5	6.8E-02	1.2
RS8	P62241	8	-0.6	5.7E-01	0.2	0.6	8.5E-02	1.1	-1.2	9.6E-02	1.0
SMD2	P62316	4	-1.1	5.1E-02	1.3	0.1	7.4E-01	0.1	-1.2	5.8E-03	2.2
RB11A	P62491	6	-0.3	5.8E-01	0.2	0.2	5.5E-01	0.3	-0.5	1.4E-01	0.8
PPIA	P62937	11	-0.2	9.7E-01	0.0	0.5	1.3E-01	0.9	-0.7	1.8E-01	0.7
FKB1A	P62942	3	0.5	2.6E-01	0.6	0.7	1.2E-01	0.9	-0.2	9.7E-01	0.0
AP2B1	P63010	7	0.1	7.5E-01	0.1	-0.1	9.4E-01	0.0	0.2	3.0E-01	0.5
IF5A1	P63241	8	0.2	6.4E-01	0.2	0.8	5.9E-02	1.2	-0.6	7.4E-02	1.1
YBOX1	P67809	7	-0.4	3.0E-01	0.5	0.1	7.3E-01	0.1	-0.6	1.1E-01	1.0
EF1A1	P68104	16	0.0	9.5E-01	0.0	0.5	1.9E-01	0.7	-0.4	1.0E-01	1.0
TBA4A	P68366	2	0.9	7.5E-01	0.1	0.8	2.7E-01	0.6	0.1	5.0E-01	0.3
HBA	P69905	4	1.9	2.7E-02	1.6	0.6	2.4E-01	0.6	1.2	1.2E-02	1.9
NUCB2	P80303	5	-0.4	1.9E-01	0.7	0.1	6.8E-01	0.2	-0.5	5.3E-02	1.3
BASP1	P80723	4	-0.5	5.7E-01	0.2	-1.8	1.5E-01	0.8	1.3	1.2E-01	0.9
DCD	P81605	4	-0.4	3.4E-01	0.5	1.1	6.1E-02	1.2	-1.6	8.1E-03	2.1
DAB2	P98082	2	0.6	6.0E-01	0.2	-0.2	6.8E-01	0.2	0.8	3.0E-01	0.5
PGBM	P98160	67	0.7	7.4E-02	1.1	-0.2	5.4E-01	0.3	0.9	1.5E-02	1.8
EFNB1	P98172	7	-0.3	4.5E-01	0.3	-1.9	1.3E-02	1.9	1.6	6.9E-03	2.2
MPCP	Q00325	4	0.8	7.5E-02	1.1	1.1	3.6E-02	1.4	-0.3	2.5E-01	0.6
CLH1	Q00610	44	0.6	1.2E-01	0.9	0.2	5.1E-01	0.3	0.4	1.1E-01	1.0
HNRPU	Q00839	16	-0.1	8.8E-01	0.1	0.1	6.6E-01	0.2	-0.2	4.5E-01	0.3
SPTB2	Q01082	15	-0.3	3.7E-01	0.4	-0.5	1.8E-01	0.7	0.2	5.2E-01	0.3
FABP5	Q01469	4	-1.4	2.7E-01	0.6	0.6	1.5E-01	0.8	-2.1	1.1E-01	0.9
CAP1	Q01518	11	-0.2	5.7E-01	0.2	0.4	2.2E-01	0.7	-0.5	9.6E-02	1.0
PFKAP	Q01813	13	0.7	7.9E-02	1.1	0.3	3.7E-01	0.4	0.4	1.0E-01	1.0
SEMG2	Q02383	6	0.5	8.8E-01	0.1	3.7	1.8E-01	0.7	-3.2	3.8E-03	2.4
DSG1	Q02413	22	-1.2	8.6E-02	1.1	0.5	1.9E-01	0.7	-1.8	3.1E-02	1.5
TIE2	Q02763	7	0.2	9.5E-01	0.0	-1.5	1.0E-02	2.0	1.6	9.3E-03	2.0
NUCB1	Q02818	2	-0.8	4.9E-01	0.3	0.4	2.7E-01	0.6	-1.1	1.7E-01	0.8
LMNB2	Q03252	2	-0.3	4.2E-01	0.4	-0.5	1.9E-01	0.7	0.2	6.0E-01	0.2
UPAR	Q03405	4	-0.6	2.7E-01	0.6	-0.8	5.3E-02	1.3	0.1	4.5E-01	0.4
C1QBP	Q07021	5	-0.9	8.6E-02	1.1	0.3	4.0E-01	0.4	-1.2	8.1E-03	2.1
CKAP4	Q07065	19	-0.4	3.0E-01	0.5	0.1	8.0E-01	0.1	-0.5	9.6E-02	1.0
BAX	Q07812	4	0.4	2.5E-01	0.6	1.3	1.4E-02	1.8	-0.8	3.0E-01	0.5
PCDH1	Q08174	4	0.1	8.4E-01	0.1	-0.9	5.0E-02	1.3	0.9	3.2E-02	1.5
GOGA2	Q08379	2	0.7	3.3E-01	0.5	0.6	4.5E-01	0.3	0.1	5.6E-01	0.3
DSC1	Q08554	11	-2.0	6.2E-02	1.2	0.1	9.4E-01	0.0	-2.0	6.2E-02	1.2
FBLN3	Q12805	13	0.7	9.9E-02	1.0	0.4	2.1E-01	0.7	0.3	2.8E-01	0.5
SF3A3	Q12874	2	-0.3	8.0E-01	0.1	-0.2	5.6E-01	0.3	-0.1	8.4E-01	0.1

LMAN2	Q12907	4	-0.7	8.6E-02	1.1	0.1	7.9E-01	0.1	-0.8	2.3E-02	1.6
PRDX4	Q13162	3	0.1	9.9E-01	0.0	0.5	1.9E-01	0.7	-0.4	1.0E-01	1.0
MMRN1	Q13201	5	1.4	3.3E-02	1.5	0.2	5.6E-01	0.3	1.2	1.6E-02	1.8
ILK	Q13418	2	1.7	2.4E-01	0.6	0.2	6.6E-01	0.2	1.5	2.5E-01	0.6
ADAM9	Q13443	7	1.6	9.2E-02	1.0	-1.6	6.0E-02	1.2	3.2	2.6E-03	2.6
CD166	Q13740	20	-0.2	7.7E-01	0.1	-0.8	4.4E-02	1.4	0.6	4.1E-02	1.4
DAG1	Q14118	6	-2.4	4.0E-03	2.4	-1.4	1.4E-02	1.8	-1.0	1.7E-02	1.8
SREC	Q14162	2	-0.3	8.0E-01	0.1	-1.7	1.4E-02	1.8	1.4	7.3E-02	1.1
SRC8	Q14247	20	0.1	5.5E-01	0.3	0.6	1.2E-01	0.9	-0.5	2.1E-01	0.7
FLNC	Q14315	42	0.2	3.8E-01	0.4	0.5	1.5E-01	0.8	-0.2	9.6E-01	0.0
DSC3	Q14574	5	-1.7	9.3E-02	1.0	0.6	5.4E-01	0.3	-2.3	7.3E-02	1.1
ITIH4	Q14624	3	3.3	7.2E-02	1.1	-4.9	2.0E-02	1.7	8.2	1.2E-03	2.9
GANAB	Q14697	12	0.5	1.5E-01	0.8	0.3	3.5E-01	0.5	0.2	4.0E-01	0.4
LBR	Q14739	3	0.2	7.2E-01	0.1	0.3	4.2E-01	0.4	-0.1	6.0E-01	0.2
LTBP1	Q14766	8	1.6	1.7E-02	1.8	0.6	1.9E-01	0.7	1.0	8.1E-03	2.1
NUMA1	Q14980	3	-0.3	3.6E-01	0.4	0.8	5.8E-02	1.2	-1.1	3.6E-02	1.4
2-Sep	Q15019	5	-0.4	4.6E-01	0.3	-0.1	7.9E-01	0.1	-0.3	3.4E-01	0.5
POSTN	Q15063	27	1.3	3.4E-02	1.5	-0.2	6.4E-01	0.2	1.5	3.6E-03	2.4
EEA1	Q15075	8	-0.6	1.1E-01	0.9	-0.8	5.7E-02	1.2	0.3	3.0E-01	0.5
PDIA6	Q15084	9	-1.1	5.0E-02	1.3	-0.3	3.0E-01	0.5	-0.7	3.8E-02	1.4
PTPRK	Q15262	3	-0.9	1.1E-01	1.0	-1.8	2.2E-02	1.7	0.9	3.6E-02	1.4
RCN1	Q15293	14	-0.5	1.6E-01	0.8	0.3	3.5E-01	0.5	-0.7	2.4E-02	1.6
PCBP2	Q15366	4	0.1	9.8E-01	0.0	0.9	7.6E-02	1.1	-0.8	3.8E-02	1.4
CDSN	Q15517	2	-2.1	8.9E-02	1.1	-0.1	9.6E-01	0.0	-2.1	1.3E-01	0.9
NHRF2	Q15599	3	-0.7	1.5E-01	0.8	0.0	9.6E-01	0.0	-0.6	9.6E-02	1.0
AAAT	Q15758	2	-4.3	4.1E-03	2.4	-1.9	2.1E-02	1.7	-2.4	8.0E-03	2.1
DPYL2	Q16555	10	0.2	5.2E-01	0.3	0.6	9.0E-02	1.0	-0.4	3.2E-01	0.5
MIC60	Q16891	6	0.6	1.4E-01	0.9	-0.6	9.2E-02	1.0	1.1	9.6E-03	2.0
ECSCR	Q19T08	3	-2.8	1.4E-02	1.9	0.2	7.4E-01	0.1	-3.0	7.1E-04	3.1
FND3B	Q53EP0	3	3.1	4.0E-03	2.4	1.6	1.4E-02	1.9	1.4	9.5E-03	2.0
DHB12	Q53GQ0	8	1.1	2.7E-02	1.6	-0.4	2.1E-01	0.7	1.5	3.3E-03	2.5
FILA2	Q5D862	20	-1.1	1.8E-01	0.7	0.7	9.4E-02	1.0	-1.8	6.0E-02	1.2
TOIP1	Q5JTV8	2	0.2	7.4E-01	0.1	-0.3	3.4E-01	0.5	0.5	1.5E-01	0.8
ATLA3	Q6DD88	2	0.6	4.7E-01	0.3	-0.4	5.5E-01	0.3	1.0	8.0E-02	1.1
RETST	Q6NUM9	11	1.9	8.2E-03	2.1	-1.5	1.5E-02	1.8	3.4	9.2E-04	3.0
CAVN1	Q6NZI2	9	-0.1	8.9E-01	0.1	-0.1	7.3E-01	0.1	0.0	6.5E-01	0.2
SBSN	Q6UWP8	3	-0.9	1.2E-01	0.9	1.4	8.5E-02	1.1	-2.3	1.3E-02	1.9
CD109	Q6YHK3	2	-1.2	1.7E-02	1.8	-1.5	9.9E-03	2.0	0.3	1.7E-01	0.8
DDX46	Q7L014	12	-0.7	3.9E-01	0.4	0.0	9.6E-01	0.0	-0.7	2.7E-01	0.6
NEGR1	Q7Z3B1	2	-0.7	8.6E-02	1.1	-0.5	1.6E-01	0.8	-0.2	3.0E-01	0.5
CLC14	Q86T13	6	-1.9	1.3E-02	1.9	-1.3	2.5E-02	1.6	-0.6	8.1E-02	1.1
LYRIC	Q86UE4	4	-0.5	3.0E-01	0.5	-0.6	6.6E-02	1.2	0.1	3.9E-01	0.4
KTN1	Q86UP2	31	-0.5	3.0E-01	0.5	-0.1	6.6E-01	0.2	-0.3	3.0E-01	0.5
STX12	Q86Y82	3	-0.2	3.9E-01	0.4	0.1	7.9E-01	0.1	-0.3	1.3E-01	0.9
PLD3	Q8IV08	2	0.9	1.0E-01	1.0	0.9	1.4E-01	0.9	0.0	6.3E-01	0.2
SYNPO	Q8N3V7	2	0.8	6.6E-02	1.2	0.5	2.3E-01	0.6	0.4	2.3E-01	0.6
S43A3	Q8NBI5	2	1.7	1.4E-01	0.9	-2.5	6.3E-02	1.2	4.2	6.2E-04	3.2
ZNT7	Q8NEW0	6	-1.1	4.8E-02	1.3	-0.1	9.0E-01	0.0	-1.0	8.7E-03	2.1
S2540	Q8TBP6	4	2.9	4.0E-02	1.4	-2.3	4.2E-03	2.4	5.3	4.6E-03	2.3
C99L2	Q8TCZ2	2	-2.2	1.4E-02	1.8	-1.6	4.8E-02	1.3	-0.7	3.6E-02	1.4
SCRB1	Q8WTV0	2	0.9	7.1E-02	1.1	-1.9	1.4E-02	1.8	2.8	1.5E-03	2.8
PDC6I	Q8WUM4	12	0.0	8.7E-01	0.1	0.4	1.9E-01	0.7	-0.4	1.7E-01	0.8
S39A7	Q92504	2	-0.1	8.6E-01	0.1	1.8	6.1E-02	1.2	-1.9	3.0E-03	2.5
NECT2	Q92692	3	-0.2	6.2E-01	0.2	-1.3	2.1E-02	1.7	1.1	1.7E-02	1.8
HTRA1	Q92743	4	7.7	7.2E-02	1.1	9.0	1.2E-03	2.9	-1.2	3.2E-01	0.5
GGH	Q92820	3	1.8	1.3E-02	1.9	3.6	1.2E-03	2.9	-1.8	3.3E-03	2.5
NRCAM	Q92823	20	0.1	7.3E-01	0.1	-1.0	2.9E-02	1.5	1.1	8.7E-03	2.1
GSLG1	Q92896	5	1.2	7.9E-02	1.1	1.3	4.4E-02	1.4	-0.1	9.9E-01	0.0
RAB1C	Q92928	3	-0.5	1.7E-01	0.8	-0.6	6.6E-02	1.2	0.2	6.0E-01	0.2
MYDGF	Q969H8	2	-0.2	6.9E-01	0.2	0.0	9.4E-01	0.0	-0.2	4.8E-01	0.3
LRC59	Q96AG4	5	-0.3	5.4E-01	0.3	0.1	8.8E-01	0.1	-0.4	3.1E-01	0.5
ESAM	Q96AP7	6	0.8	8.6E-02	1.1	-0.9	8.1E-02	1.1	1.8	2.7E-03	2.6
FKB10	Q96AY3	5	0.4	2.2E-01	0.6	0.1	6.6E-01	0.2	0.3	2.7E-01	0.6
EFHD2	Q96C19	2	0.1	9.3E-01	0.0	0.3	5.7E-01	0.2	-0.2	3.2E-01	0.5
RCN3	Q96D15	6	-1.0	7.5E-02	1.1	0.1	8.5E-01	0.1	-1.0	1.6E-02	1.8
PDLI5	Q96HC4	19	0.3	3.6E-01	0.4	0.7	1.0E-01	1.0	-0.4	3.0E-01	0.5
DCBD2	Q96PD2	5	0.0	7.3E-01	0.1	-1.3	2.2E-02	1.7	1.3	1.5E-02	1.8
GSDMA	Q96QA5	5	-1.9	5.1E-02	1.3	0.4	1.9E-01	0.7	-2.3	1.7E-02	1.8
VPS35	Q96QK1	4	0.0	9.4E-01	0.0	0.4	4.3E-01	0.4	-0.4	1.7E-01	0.8
HHIP	Q96QV1	21	1.9	5.5E-03	2.3	0.6	9.2E-02	1.0	1.3	3.8E-03	2.4
SDF2	Q99470	2	-0.9	8.9E-02	1.1	0.2	6.5E-01	0.2	-1.2	1.5E-02	1.8
PHB2	Q99623	3	0.3	9.9E-01	0.0	-0.5	2.4E-01	0.6	0.8	5.1E-01	0.3
SGMR1	Q99720	2	-0.3	8.3E-01	0.1	0.9	3.4E-02	1.5	-1.2	1.0E-01	1.0
S29A1	Q99808	9	3.0	7.3E-03	2.1	-0.7	1.7E-01	0.8	3.7	7.5E-04	3.1
ESYT1	Q9BSJ8	4	1.1	7.4E-02	1.1	0.5	3.9E-01	0.4	0.7	9.6E-02	1.0
TMED9	Q9BVK6	2	-0.9	1.2E-01	0.9	0.5	2.3E-01	0.6	-1.5	8.1E-03	2.1
RFIP5	Q9BXF6	3	-1.2	4.5E-02	1.3	-0.5	1.3E-01	0.9	-0.7	8.8E-02	1.1
EHD4	Q9H223	11	-0.1	8.7E-01	0.1	-0.1	8.6E-01	0.1	0.0	6.5E-01	0.2
GAPR1	Q9H4G4	3	-0.5	7.2E-01	0.1	0.3	6.6E-01	0.2	-0.9	1.6E-01	0.8
EHD1	Q9H4M9	3	-0.8	6.8E-02	1.2	-0.8	6.1E-02	1.2	0.0	8.8E-01	0.1
MMRN2	Q9H8L6	17	0.8	5.6E-02	1.3	-0.4	1.9E-01	0.7	1.2	8.1E-03	2.1
GHC1	Q9H936	4	2.2	1.4E-02	1.8	-2.2	8.2E-03	2.1	4.4	1.2E-03	2.9
NET4	Q9HB63	8	2.4	8.2E-03	2.1	-0.7	1.4E-01	0.8	3.1	7.1E-04	3.1
AGRL4	Q9HBW9	3	-1.9	1.9E-02	1.7	-2.1	1.5E-02	1.8	0.2	5.5E-01	0.3
C1QR1	Q9NPY3	11	-0.5	1.4E-01	0.9	-1.0	2.1E-02	1.7	0.5	7.0E-02	1.2
RTN4	Q9NQC3	3	0.8	8.0E-02	1.1	0.9	6.3E-02	1.2	-0.1	6.0E-01	0.2
MIC19	Q9NX63	2	-0.1	8.9E-01	0.1	-0.1	6.6E-01	0.2	0.1	6.0E-01	0.2
STAB1	Q9NY15	2	-0.6	2.6E-01	0.6	-1.6	2.7E-02	1.6	0.9	9.6E-02	1.0
F120A	Q9NZB2	2	1.4	5.4E-02	1.3	1.1	7.3E-02	1.1	0.3	4.4E-01	0.4
MYOF	Q9NZM1	4	1.3	6.6E-02	1.2	-0.1	8.8E-01	0.1	1.4	1.4E-02	1.9
EHD2	Q9NZN4	11	-0.2	9.5E-01	0.0	0.2	4.0E-01	0.4	-0.5	5.3E-01	0.3
CRIM1	Q9NZV1	2	-0.6	3.0E-01	0.5	-1.8	8.2E-03	2.1	1.3	1.9E-01	0.7
VAPA	Q9P0L0	2	0.2	8.9E-01	0.1	-0.2	3.8E-01	0.4	0.5	4.5E-01	0.3
RRBP1	Q9P2E9	24	1.2	2.8E-02	1.6	0.3	3.9E-01	0.4	0.9	2.2E-02	1.7
GBG12	Q9UBI6	2	-0.4	6.8E-01	0.2	0.5	3.5E-01	0.5	-0.9	4.2E-02	1.4
CATZ	Q9UBR2	4	-0.6	4.6E-01	0.3	0.6	2.3E-01	0.6	-1.2	2.7E-02	1.6
DJB11	Q9UBS4	3	-1.9	8.0E-02	1.1	-1.1	1.9E-01	0.7	-0.7	1.5E-01	0.8
ZO2	Q9UDY2	9	-0.2	6.6E-01	0.2	0.2	5.0E-01	0.3	-0.4	1.5E-01	0.8
DNJB4	Q9UDY4	7	0.4	3.6E-01	0.4	0.7	6.2E-02	1.2	-0.3	7.4E-01	0.1
SWP70	Q9UH65	3	0.0	8.7E-01	0.1	0.1	7.4E-01	0.1	-0.1	9.8E-01	0.0

LIMA1	Q9UHB6	7	0.3	3.4E-01	0.5	0.3	4.0E-01	0.4	0.0	6.3E-01	0.2
ATS1	Q9UHI8	2	1.6	3.7E-02	1.4	-0.1	8.2E-01	0.1	1.8	2.7E-03	2.6
CBPA4	Q9UI42	3	-1.8	6.7E-02	1.2	0.5	3.3E-01	0.5	-2.3	2.3E-02	1.6
DBNL	Q9UJU6	3	0.2	7.4E-01	0.1	0.3	2.6E-01	0.6	-0.1	5.1E-01	0.3
EPCR	Q9UNN8	4	-1.9	1.1E-02	2.0	-0.4	1.5E-01	0.8	-1.5	9.6E-03	2.0
PA2G4	Q9UQ80	6	0.1	8.0E-01	0.1	0.8	9.2E-02	1.0	-0.7	1.9E-02	1.7
VDAC3	Q9Y277	2	2.3	1.1E-02	2.0	1.0	5.7E-02	1.2	1.3	1.8E-02	1.7
E41L3	Q9Y2J2	4	0.1	6.5E-01	0.2	-0.5	1.8E-01	0.7	0.6	1.2E-01	0.9
SHLB1	Q9Y371	4	-0.2	9.6E-01	0.0	0.8	7.6E-02	1.1	-1.0	1.4E-01	0.8
FIS1	Q9Y3D6	2	-2.4	4.8E-02	1.3	-2.0	7.6E-02	1.1	-0.4	3.4E-01	0.5
TLN1	Q9Y490	47	0.2	5.2E-01	0.3	0.0	9.4E-01	0.0	0.1	4.1E-01	0.4
PLXD1	Q9Y4D7	14	-1.4	1.3E-02	1.9	-0.4	1.5E-01	0.8	-1.0	1.2E-02	1.9
LOXL2	Q9Y4K0	24	1.6	1.5E-02	1.8	2.6	3.4E-03	2.5	-1.0	9.6E-03	2.0
HYOU1	Q9Y4L1	5	0.0	7.4E-01	0.1	-0.2	4.6E-01	0.3	0.2	8.8E-01	0.1
SRPRB	Q9Y5M8	2	-0.5	2.2E-01	0.7	0.0	9.1E-01	0.0	-0.5	2.0E-01	0.7
JAM1	Q9Y624	7	0.6	1.8E-01	0.8	0.0	9.4E-01	0.0	0.6	7.4E-02	1.1
NPTN	Q9Y639	3	-2.7	4.0E-03	2.4	-0.6	1.4E-01	0.9	-2.0	1.4E-03	2.9
COPG1	Q9Y678	5	1.0	7.9E-02	1.1	0.7	6.5E-02	1.2	0.3	3.9E-01	0.4
CLIC4	Q9Y696	4	-0.1	9.8E-01	0.0	0.2	5.9E-01	0.2	-0.3	6.3E-01	0.2
MTCH2	Q9Y6C9	4	2.6	3.2E-02	1.5	2.4	2.1E-02	1.7	0.2	4.0E-01	0.4
TX264	Q9Y6I9	12	4.6	4.0E-03	2.4	1.9	1.4E-02	1.8	2.7	2.0E-03	2.7

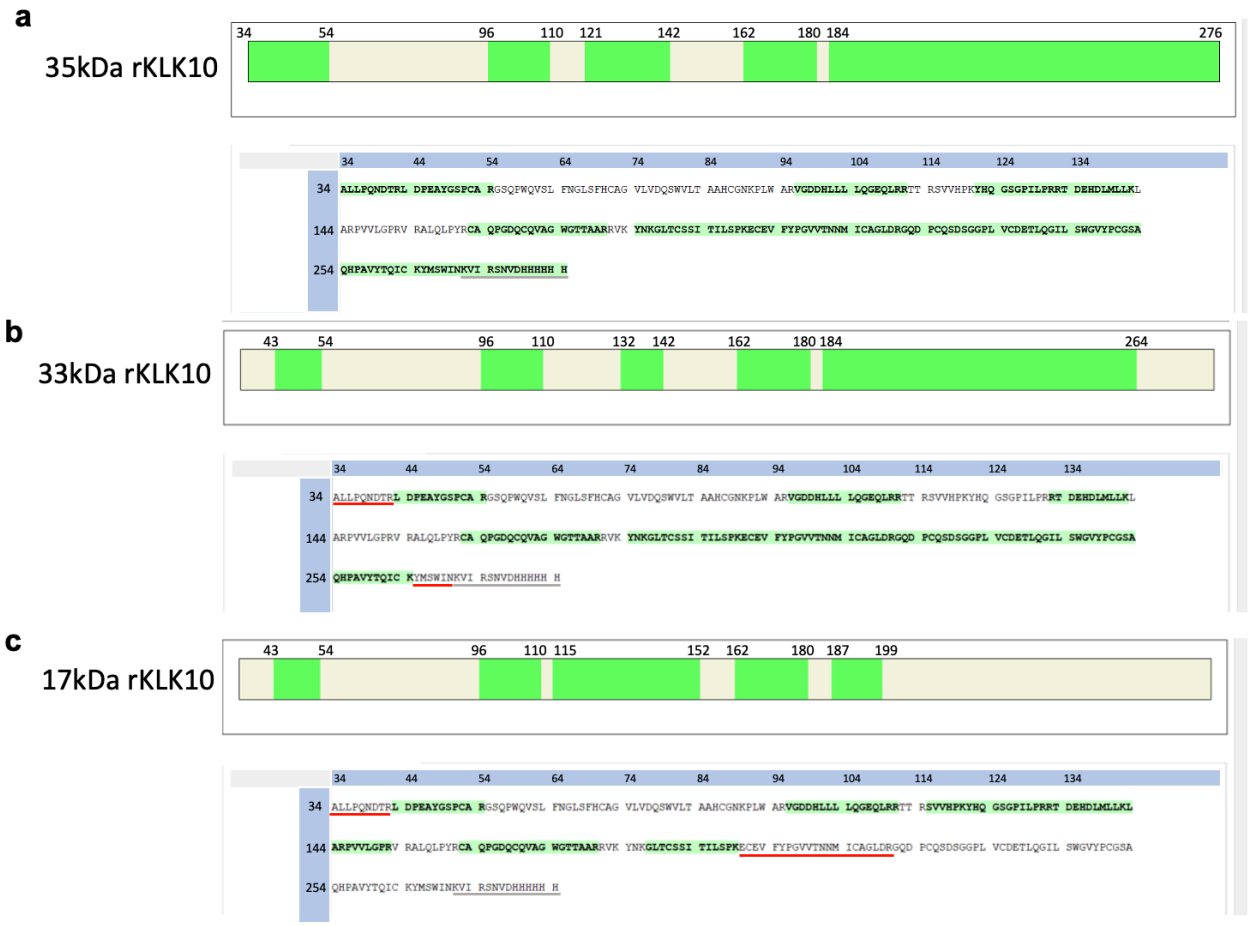

Figure A.1. **Tryptic peptide map of rKLK10 cleaved by HTRA1.** rKLK10 was incubated with WT or catalytically inactive HTRA1 (500 ng each) for 18hrs and resolved by SDS-PAGE. Coomassie-stained bands corresponding to 35kDa, 33kDa, and 17kDa rKLK10 were excised and digested with trypsin followed by tandem liquid chromatography mass spectrometry. Peptide sequences were analysed using Proteome Discoverer and were mapped against 35kDa rKLK10 (A34-N276) protein sequence. Tryptic sequences identified by the mass spectrometry are highlighted in green. Red lines indicate potential cleavage regions by HTRA1. For clarity, the signal peptide (M1-A33) is not included, and the C-terminal His-tag sequence is marked with a grey line.

REFERENCES

1. Ku KH, Subramaniam N, Marsden PA. Epigenetic determinants of flow-mediated vascular endothelial gene expression. *Hypertension*. 2019;74:467-476
2. Andueza A, Kumar S, Kim J, Kang D-W, Mumme HL, Perez JI, Villa-Roel N, Jo H. Endothelial reprogramming by disturbed flow revealed by single-cell rna and chromatin accessibility study. *Cell reports*. 2020;33:108491
3. Ni C-W, Qiu H, Rezvan A, Kwon K, Nam D, Son DJ, Visvader JE, Jo H. Discovery of novel mechanosensitive genes in vivo using mouse carotid artery endothelium exposed to disturbed flow. *Blood*. 2010;116:e66-e73
4. Nam D, Ni C-W, Rezvan A, Suo J, Budzyn K, Llanos A, Harrison D, Giddens D, Jo H. Partial carotid ligation is a model of acutely induced disturbed flow, leading to rapid endothelial dysfunction and atherosclerosis. *American Journal of Physiology - Heart and Circulatory Physiology*. 2009;297:H1535-H1543
5. Stefanini ACB, da Cunha BR, Henrique T, Tajara EH. Involvement of kallikrein-related peptidases in normal and pathologic processes. *Dis. Markers*. 2015;2015:946572-946572
6. Geovanini GR, Libby P. Atherosclerosis and inflammation: Overview and updates. *Clin Sci (Lond)*. 2018;132:1243-1252
7. Lusis AJ. Atherosclerosis. *Nature*. 2000;407:233-241
8. Libby P. Coronary artery injury and the biology of atherosclerosis: Inflammation, thrombosis, and stabilization. *Am J Cardiol*. 2000;86:3J-8J; discussion 8J-9J
9. Gimbrone MA, Jr., Garcia-Cardena G. Endothelial cell dysfunction and the pathobiology of atherosclerosis. *Circ Res*. 2016;118:620-636
10. Fruchart J-C, Nierman MC, Stroes ESG, Kastelein JJP, Duriez P. New risk factors for atherosclerosis and patient risk assessment. *Circulation*. 2004;109:III-15-III-19
11. Vaughan CJ, Gotto AM, Basson CT. The evolving role of statins in the management of atherosclerosis. *J. Am. Coll. Cardiol.* 2000;35:1-10
12. Sabatine MS, Leiter LA, Wiviott SD, Giugliano RP, Deedwania P, De Ferrari GM, Murphy SA, Kuder JF, Gouni-Berthold I, Lewis BS. Cardiovascular safety and efficacy of the pcsk9 inhibitor evolocumab in patients with and without diabetes and the effect of evolocumab on glycaemia and risk of new-onset diabetes: A prespecified analysis of the fourier randomised controlled trial. *The lancet Diabetes & endocrinology*. 2017;5:941-950
13. Kumar S, Kang D-W, Rezvan A, Jo H. Accelerated atherosclerosis development in c57bl6 mice by overexpressing aav-mediated pcsk9 and partial carotid ligation. *Lab. Invest.* 2017;97:935
14. Click RL, Holmes DR, Vlietstra RE, Kosinski AS, Kronmal RA. Anomalous coronary arteries: Location, degree of atherosclerosis and effect on survival—a report from the coronary artery surgery study. *J. Am. Coll. Cardiol.* 1989;13:531-537
15. Benjamin EJ, Muntner P, Alonso A, Bittencourt MS, Callaway CW, Carson AP, Chamberlain AM, Chang AR, Cheng S, Das SR. Heart disease and stroke statistics—2019 update: A report from the american heart association. *Circulation*. 2019;139:e56-e528
16. Pahwa R, Jialal I. Atherosclerosis. *Statpearls*. Treasure Island (FL); 2021.

17. Carey RM, Whelton PK. Prevention, detection, evaluation, and management of high blood pressure in adults: Synopsis of the 2017 american college of cardiology/american heart association hypertension guideline. *Ann. Intern. Med.* 2018;168:351-358
18. Ku DN, Giddens DP, Zarins CK, Glagov S. Pulsatile flow and atherosclerosis in the human carotid bifurcation. Positive correlation between plaque location and low oscillating shear stress. *Arterioscler. Thromb. Vasc. Biol.* 1985;5:293-302
19. Chiu J-J, Chien S. Effects of disturbed flow on vascular endothelium: Pathophysiological basis and clinical perspectives. *Physiol. Rev.* 2011;91:327-387
20. Zarins CK, Giddens DP, Bharadvaj BK, Sottiurai VS, Mabon RF, Glagov S. Carotid bifurcation atherosclerosis. Quantitative correlation of plaque localization with flow velocity profiles and wall shear stress. *Circ. Res.* 1983;53:502-514
21. Nam D, Ni C-W, Rezvan A, Suo J, Budzyn K, Llanos A, Harrison D, Giddens D, Jo H. Partial carotid ligation is a model of acutely induced disturbed flow, leading to rapid endothelial dysfunction and atherosclerosis. *American Journal of Physiology-Heart and Circulatory Physiology*. 2009;297:H1535-H1543
22. Dekker RJ, Van Soest S, Fontijn RD, Salamanca S, De Groot PG, VanBavel E, Pannekoek H, Horrevoets AJ. Prolonged fluid shear stress induces a distinct set of endothelial cell genes, most specifically lung kruppel-like factor (klf2). *Blood, The Journal of the American Society of Hematology*. 2002;100:1689-1698
23. Sangwung P, Zhou G, Nayak L, Chan ER, Kumar S, Kang D-W, Zhang R, Liao X, Lu Y, Sugi K, Fujioka H, Shi H, Lapping SD, Ghosh CC, Higgins SJ, Parikh SM, Jo H, Jain MK. Klf2 and klf4 control endothelial identity and vascular integrity. *JCI Insight*. 2017;2:e91700-e91700
24. Jo H, Song H, Mowbray A. Role of nadph oxidases in disturbed flow-and bmp4-induced inflammation and atherosclerosis. *Antioxidants & redox signaling*. 2006;8:1609-1619
25. Feng S, Bowden N, Fragiadaki M, Souilhol C, Hsiao S, Mahmoud M, Allen S, Pirri D, Ayllon BT, Akhtar S, Thompson AAR, Jo H, Weber C, Ridger V, Schober A, Evans PC. Mechanical activation of hypoxia-inducible factor 1α drives endothelial dysfunction at atheroprone sites. *Arterioscler. Thromb. Vasc. Biol.* 2017;37:2087-2101
26. Esmerats JF, Villa-Roel N, Kumar S, Gu L, Salim M, Ohh M, Taylor W, Nerem R, Yoganathan A, Jo H. Disturbed flow increases ube2c (ubiquitin e2 ligase c) via loss of mir-483-3p, inducing aortic valve calcification by the pvhl (von hippel-lindau protein) and hif-1α (hypoxia-inducible factor-1α) pathway in endothelial cells. *Arterioscler. Thromb. Vasc. Biol.* 2019;39:467-481
27. Xiao H, Lu M, Lin TY, Chen Z, Chen G, Wang WC, Marin T, Shentu TP, Wen L, Gongol B, Sun W, Liang X, Chen J, Huang HD, Pedra JH, Johnson DA, Shyy JY. Sterol regulatory element binding protein 2 activation of nlrp3 inflammasome in endothelium mediates hemodynamic-induced atherosclerosis susceptibility. *Circulation*. 2013;128:632-642
28. Wu C, Huang RT, Kuo CH, Kumar S, Kim CW, Lin YC, Chen YJ, Birukova A, Birukov KG, Dulin NO, Civelek M, Lusis AJ, Loyer X, Tedgui A, Dai G, Jo H, Fang Y. Mechanosensitive ppap2b regulates endothelial responses to atherorelevant hemodynamic forces. *Circ. Res.* 2015;117:e41-e53
29. Wang Y, Sun H-Y, Kumar S, Puerta MdM, Jo H, Rezvan A. Zbtb46 is a shear-sensitive transcription factor inhibiting endothelial cell proliferation via gene expression regulation of cell cycle proteins. *Laboratory Investigation*. 2019;99:305-318

30. Xu S, Xu Y, Liu P, Zhang S, Liu H, Slavin S, Kumar S, Koroleva M, Luo J, Wu X, Rahman A, Pelisek J, Jo H, Si S, Miller CL, Jin ZG. The novel coronary artery disease risk gene jcad/kiaa1462 promotes endothelial dysfunction and atherosclerosis. *Eur. Heart J.* 2019;40:2398-2408
31. Glaser SF, Heumuller AW, Tombor L, Hofmann P, Muhly-Reinholz M, Fischer A, Gunther S, Kokot KE, Hassel D, Kumar S, Jo H, Boon RA, Abplanalp W, John D, Boeckel JN, Dimmeler S. The histone demethylase jmjd2b regulates endothelial-to-mesenchymal transition. *Proc. Natl. Acad. Sci. U. S. A.* 2020;117:4180-4187
32. Boo YC, Hwang J, Sykes M, Michell BJ, Kemp BE, Lum H, Jo H. Shear stress stimulates phosphorylation of enos at ser635 by a protein kinase a-dependent mechanism. *American Journal of Physiology-Heart and Circulatory Physiology*. 2002;283:H1819-H1828
33. Son DJ, Kumar S, Takabe W, Woo Kim C, Ni C-W, Alberts-Grill N, Jang I-H, Kim S, Kim W, Won Kang S, Baker AH, Woong Seo J, Ferrara KW, Jo H. The atypical mechanosensitive microrna-712 derived from pre-ribosomal rna induces endothelial inflammation and atherosclerosis. *Nature Communications*. 2013;4:3000
34. Texon M, Imparato AM, Helpern M. The role of vascular dynamics in the development of atherosclerosis. *JAMA*. 1965;194:1226-1230
35. Nerem RM. Hemodynamics and the vascular endothelium. 1993
36. Heo KS, Fujiwara K, Abe J. Disturbed-flow-mediated vascular reactive oxygen species induce endothelial dysfunction. *Circ. J.* 2011;75:2722-2730
37. Steinman DA, Taylor CA. Flow imaging and computing: Large artery hemodynamics. *Ann. Biomed. Eng.* 2005;33:1704-1709
38. Davies PF, Polacek DC, Handen JS, Helmke BP, DePaola N. A spatial approach to transcriptional profiling: Mechanotransduction and the focal origin of atherosclerosis. *Trends Biotechnol.* 1999;17:347-351
39. Demos C, Tamargo I, Jo H. Chapter 1 - biomechanical regulation of endothelial function in atherosclerosis. In: Ohayon J, Finet G, Pettigrew RI, eds. *Biomechanics of coronary atherosclerotic plaque*. Academic Press; 2020:3-50.
40. Tzima E, Irani-Tehrani M, Kiosses WB, Dejana E, Schultz DA, Engelhardt B, Cao G, DeLisser H, Schwartz MA. A mechanosensory complex that mediates the endothelial cell response to fluid shear stress. *Nature*. 2005;437:426-431
41. Ingber DE. Cellular mechanotransduction: Putting all the pieces together again. *The FASEB journal*. 2006;20:811-827
42. Chiu JJ, Chien S. Effects of disturbed flow on vascular endothelium: Pathophysiological basis and clinical perspectives. *Physiological reviews*. 2011;91:327-387
43. Davies PF. Hemodynamic shear stress and the endothelium in cardiovascular pathophysiology. *Nature clinical practice. Cardiovascular medicine*. 2009;6:16-26
44. Tzima E, Irani-Tehrani M, Kiosses WB, Dejana E, Schultz DA, Engelhardt B, Cao G, DeLisser H, Schwartz MA. A mechanosensory complex that mediates the endothelial cell response to fluid shear stress. *Nature*. 2005;437:426-431
45. Demos C, Williams D, Jo H. Disturbed flow induces atherosclerosis by annexin a2-mediated integrin activation. 2020
46. Albarrán-Juárez J, Iring A, Wang S, Joseph S, Grimm M, Strilic B, Wettschureck N, Althoff TF, Offermanns S. Piezo1 and g(q)/g(11) promote endothelial inflammation

depending on flow pattern and integrin activation. *The Journal of experimental medicine*. 2018;215:2655-2672
47. Yamamoto K, Korenaga R, Kamiya A, Qi Z, Sokabe M, Ando J. P2x4 receptors mediate atp-induced calcium influx in human vascular endothelial cells. *American Journal of Physiology-Heart and Circulatory Physiology*. 2000;279:H285-H292
48. Coon BG, Baeyens N, Han J, Budatha M, Ross TD, Fang JS, Yun S, Thomas J-L, Schwartz MA. Intramembrane binding of ve-cadherin to vegfr2 and vegfr3 assembles the endothelial mechanosensory complex. *Journal of Cell Biology*. 2015;208:975-986
49. Conway DE, Breckenridge MT, Hinde E, Gratton E, Chen CS, Schwartz MA. Fluid shear stress on endothelial cells modulates mechanical tension across ve-cadherin and pecam-1. *Curr Biol*. 2013;23:1024-1030
50. Orr AW, Ginsberg MH, Shattil SJ, Deckmyn H, Schwartz MA. Matrix-specific suppression of integrin activation in shear stress signaling. *Molecular biology of the cell*. 2006;17:4686-4697
51. Mehta V, Pang K-L, Rozbesky D, Nather K, Keen A, Lachowski D, Kong Y, Karia D, Ameismeier M, Huang J, Fang Y, del Rio Hernandez A, Reader JS, Jones EY, Tzima E. The guidance receptor plexin d1 is a mechanosensor in endothelial cells. *Nature*. 2020;578:290-295
52. Erb L, Weisman GA. Coupling of p2y receptors to g proteins and other signaling pathways. *Wiley Interdiscip Rev Membr Transp Signal*. 2012;1:789-803
53. Bhullar IS, Li YS, Miao H, Zandi E, Kim M, Shyy JY, Chien S. Fluid shear stress activation of ikappab kinase is integrin-dependent. *The Journal of biological chemistry*. 1998;273:30544-30549
54. Sun X, Fu Y, Gu M, Zhang L, Li D, Li H, Chien S, Shyy JY, Zhu Y. Activation of integrin α5 mediated by flow requires its translocation to membrane lipid rafts in vascular endothelial cells. *Proc Natl Acad Sci U S A*. 2016;113:769-774
55. Zhang C, Zhou T, Chen Z, Yan M, Li B, Lv H, Wang C, Xiang S, Shi L, Zhu Y, Ai D. Coupling of integrin α5 to annexin a2 by flow drives endothelial activation. *Circulation research*. 2020
56. Simmons RD, Kumar S, Jo H. The role of endothelial mechanosensitive genes in atherosclerosis and omics approaches. *Arch Biochem Biophys*. 2016;591:111-131
57. Kumar S, Kim CW, Son DJ, Ni CW, Jo H. Flow-dependent regulation of genome-wide mrna and microrna expression in endothelial cells in vivo. *Scientific data*. 2014;1:140039
58. Kumar S, Kim CW, Simmons RD, Jo H. Role of flow-sensitive micrornas in endothelial dysfunction and atherosclerosis: Mechanosensitive athero-mirs. *Arterioscler Thromb Vasc Biol*. 2014;34:2206-2216
59. Simmons RD, Kumar S, Thabet SR, Sur S, Jo H. Omics-based approaches to understand mechanosensitive endothelial biology and atherosclerosis. *Wiley Interdiscip Rev Syst Biol Med*. 2016;8:378-401
60. Dunn J, Thabet S, Jo H. Flow-dependent epigenetic DNA methylation in endothelial gene expression and atherosclerosis. *Arterioscler Thromb Vasc Biol*. 2015;35:1562-1569
61. Dunn J, Qiu H, Kim S, Jjingo D, Hoffman R, Kim CW, Jang I, Son DJ, Kim D, Pan C, Fan Y, Jordan IK, Jo H. Flow-dependent epigenetic DNA methylation regulates endothelial gene expression and atherosclerosis. *J. Clin. Invest.* 2014;124:3187-3199

62. Ni CW, Qiu H, Rezvan A, Kwon K, Nam D, Son DJ, Visvader JE, Jo H. Discovery of novel mechanosensitive genes in vivo using mouse carotid artery endothelium exposed to disturbed flow. *Blood*. 2010;116:e66-73
63. Boo YC, Jo H. Flow-dependent regulation of endothelial nitric oxide synthase: Role of protein kinases. *American journal of physiology. Cell physiology*. 2003;285:C499-508
64. van Thienen JV, Fledderus JO, Dekker RJ, Rohlena J, van Ijzendoorn GA, Kootstra NA, Pannekoek H, Horrevoets AJ. Shear stress sustains atheroprotective endothelial klf2 expression more potently than statins through mrna stabilization. *Cardiovasc Res*. 2006;72:231-240
65. Hamik A, Lin Z, Kumar A, Balcells M, Sinha S, Katz J, Feinberg MW, Gerzsten RE, Edelman ER, Jain MK. Kruppel-like factor 4 regulates endothelial inflammation. *J Biol Chem*. 2007;282:13769-13779
66. Nam D, Ni CW, Rezvan A, Suo J, Budzyn K, Llanos A, Harrison D, Giddens D, Jo H. Partial carotid ligation is a model of acutely induced disturbed flow, leading to rapid endothelial dysfunction and atherosclerosis. *Am J Physiol Heart Circ Physiol*. 2009;297:H1535-1543
67. Magid R, Murphy TJ, Galis ZS. Expression of matrix metalloproteinase-9 in endothelial cells is differentially regulated by shear stress. Role of c-myc. *J Biol Chem*. 2003;278:32994-32999
68. Chatzizisis YS, Coskun AU, Jonas M, Edelman ER, Feldman CL, Stone PH. Role of endothelial shear stress in the natural history of coronary atherosclerosis and vascular remodeling: Molecular, cellular, and vascular behavior. *Journal of the American College of Cardiology*. 2007;49:2379-2393
69. Arroyo AG, Iruela-Arispe ML. Extracellular matrix, inflammation, and the angiogenic response. *Cardiovasc Res*. 2010;86:226-235
70. Kwak BR, Back M, Bochaton-Piallat ML, Caligiuri G, Daemen MJ, Davies PF, Hoefer IE, Holvoet P, Jo H, Krams R, Lehoux S, Monaco C, Steffens S, Virmani R, Weber C, Wentzel JJ, Evans PC. Biomechanical factors in atherosclerosis: Mechanisms and clinical implications. *Eur Heart J*. 2014;35:3013-3020, 3020a-3020d
71. Tarbell JM, Shi ZD, Dunn J, Jo H. Fluid mechanics, arterial disease, and gene expression. *Annual review of fluid mechanics*. 2014;46:591-614
72. Heo KS, Berk BC, Abe J. Disturbed flow-induced endothelial proatherogenic signaling via regulating post-translational modifications and epigenetic events. *Antioxid Redox Signal*. 2016;25:435-450
73. Le NT, Sandhu UG, Quintana-Quezada RA, Hoang NM, Fujiwara K, Abe JI. Flow signaling and atherosclerosis. *Cellular and molecular life sciences : CMLS*. 2017;74:1835-1858
74. Davies PF. Endothelial transcriptome profiles in vivo in complex arterial flow fields. *Ann Biomed Eng*. 2008;36:563-570
75. Chiu JJ, Usami S, Chien S. Vascular endothelial responses to altered shear stress: Pathologic implications for atherosclerosis. *Annals of medicine*. 2009;41:19-28
76. Bryan MT, Duckles H, Feng S, Hsiao ST, Kim HR, Serbanovic-Canic J, Evans PC. Mechanoresponsive networks controlling vascular inflammation. *Arterioscler Thromb Vasc Biol*. 2014;34:2199-2205
77. Abe J, Berk BC. Novel mechanisms of endothelial mechanotransduction. *Arterioscler Thromb Vasc Biol*. 2014;34:2378-2386

78. Simion V, Haemmig S, Feinberg MW. Lncrnas in vascular biology and disease. *Vascul Pharmacol*. 2018
79. . !!! INVALID CITATION !!! 78-84
80. Kumar S, Williams D, Sur S, Wang J-Y, Jo H. Role of flow-sensitive microrna and long noncoding rnas in vascular dysfunction and atherosclerosis. *Vascular Pharmacology*. 2019;114:76-92
81. Bartel DP. Micrornas: Target recognition and regulatory functions. *Cell*. 2009;136:215-233
82. Siomi H, Siomi MC. Posttranscriptional regulation of microrna biogenesis in animals. *Mol Cell*. 2010;38:323-332
83. Han J, Pedersen JS, Kwon SC, Belair CD, Kim YK, Yeom KH, Yang WY, Haussler D, Blelloch R, Kim VN. Posttranscriptional crossregulation between drosha and dgcr8. *Cell*. 2009;136:75-84
84. Yeom KH, Lee Y, Han J, Suh MR, Kim VN. Characterization of dgcr8/pasha, the essential cofactor for drosha in primary mirna processing. *Nucleic Acids Res*. 2006;34:4622-4629
85. Han J, Lee Y, Yeom KH, Nam JW, Heo I, Rhee JK, Sohn SY, Cho Y, Zhang BT, Kim VN. Molecular basis for the recognition of primary micrornas by the drosha-dgcr8 complex. *Cell*. 2006;125:887-901
86. Han J, Lee Y, Yeom KH, Kim YK, Jin H, Kim VN. The drosha-dgcr8 complex in primary microrna processing. *Genes Dev*. 2004;18:3016-3027
87. Kim VN. Microrna precursors in motion: Exportin-5 mediates their nuclear export. *Trends Cell Biol*. 2004;14:156-159
88. Lund E, Guttinger S, Calado A, Dahlberg JE, Kutay U. Nuclear export of microrna precursors. *Science*. 2004;303:95-98
89. Leuschner PJ, Martinez J. In vitro analysis of microrna processing using recombinant dicer and cytoplasmic extracts of hela cells. *Methods*. 2007;43:105-109
90. Ambros V, Bartel B, Bartel DP, Burge CB, Carrington JC, Chen X, Dreyfuss G, Eddy SR, Griffiths-Jones S, Marshall M, Matzke M, Ruvkun G, Tuschl T. A uniform system for microrna annotation. *RNA*. 2003;9:277-279
91. Valencia-Sanchez MA, Liu J, Hannon GJ, Parker R. Control of translation and mrna degradation by mirnas and sirnas. *Genes Dev*. 2006;20:515-524
92. Saxena S, Jonsson ZO, Dutta A. Small rnas with imperfect match to endogenous mrna repress translation. Implications for off-target activity of small inhibitory rna in mammalian cells. *J Biol Chem*. 2003;278:44312-44319
93. Hutvagner G, Zamore PD. A microrna in a multiple-turnover rnai enzyme complex. *Science*. 2002;297:2056-2060
94. Lai EC. Micro rnas are complementary to 3' utr sequence motifs that mediate negative post-transcriptional regulation. *Nat Genet*. 2002;30:363-364
95. Zhang C. Micrornas: Role in cardiovascular biology and disease. *Clin Sci (Lond)*. 2008;114:699-706
96. Wu F, Yang Z, Li G. Role of specific micrornas for endothelial function and angiogenesis. *Biochem Biophys Res Commun*. 2009;386:549-553
97. Davis-Dusenbery BN, Wu C, Hata A. Micromanaging vascular smooth muscle cell differentiation and phenotypic modulation. *Arterioscler Thromb Vasc Biol*. 2011;31:2370-2377

98. Santoro MM. "Fishing" for endothelial microrna functions and dysfunction. *Vascul Pharmacol*. 2011;55:60-68
99. Menghini R, Stohr R, Federici M. Microrna in vascular aging and atherosclerosis. *Ageing Res Rev*. 2014;17:68-78
100. Wojciechowska A, Braniewska A, Kozar-Kaminska K. Microrna in cardiovascular biology and disease. *Advances in clinical and experimental medicine : official organ Wroclaw Medical University*. 2017;26:865-874
101. Mozos I, Malainer C, Horbanczuk J, Gug C, Stoian D, Luca CT, Atanasov AG. Inflammatory markers for arterial stiffness in cardiovascular diseases. *Frontiers in immunology*. 2017;8:1058
102. Kowara M, Cudnoch-Jedrzejewska A, Opolski G, Wlodarski P. Microrna regulation of extracellular matrix components in the process of atherosclerotic plaque destabilization. *Clinical and experimental pharmacology & physiology*. 2017;44:711-718
103. Koroleva IA, Nazarenko MS, Kucher AN. Role of microrna in development of instability of atherosclerotic plaques. *Biochemistry. Biokhimiia*. 2017;82:1380-1390
104. Dlouha D, Hubacek JA. Regulatory rnas and cardiovascular disease - with a special focus on circulating micrornas. *Physiological research*. 2017;66:S21-S38
105. Fang Y, Shi C, Manduchi E, Civelek M, Davies PF. Microrna-10a regulation of proinflammatory phenotype in athero-susceptible endothelium in vivo and in vitro. *Proceedings of the National Academy of Sciences of the United States of America*. 2010;107:13450-13455
106. Lee DY, Lin TE, Lee CI, Zhou J, Huang YH, Lee PL, Shih YT, Chien S, Chiu JJ. Microrna-10a is crucial for endothelial response to different flow patterns via interaction of retinoid acid receptors and histone deacetylases. *Proceedings of the National Academy of Sciences of the United States of America*. 2017;114:2072-2077
107. Lee DY, Yang TL, Huang YH, Lee CI, Chen LJ, Shih YT, Wei SY, Wang WL, Wu CC, Chiu JJ. Induction of microrna-10a using retinoic acid receptor-alpha and retinoid x receptor-alpha agonists inhibits atherosclerotic lesion formation. *Atherosclerosis*. 2018;271:36-44
108. Qin X, Wang X, Wang Y, Tang Z, Cui Q, Xi J, Li YS, Chien S, Wang N. Microrna-19a mediates the suppressive effect of laminar flow on cyclin d1 expression in human umbilical vein endothelial cells. *Proceedings of the National Academy of Sciences of the United States of America*. 2010;107:3240-3244
109. Wang KC, Nguyen P, Weiss A, Yeh YT, Chien HS, Lee A, Teng D, Subramaniam S, Li YS, Chien S. Microrna-23b regulates cyclin-dependent kinase-activating kinase complex through cyclin h repression to modulate endothelial transcription and growth under flow. *Arterioscler Thromb Vasc Biol*. 2014;34:1437-1445
110. Iaconetti C, De Rosa S, Polimeni A, Sorrentino S, Gareri C, Carino A, Sabatino J, Colangelo M, Curcio A, Indolfi C. Down-regulation of mir-23b induces phenotypic switching of vascular smooth muscle cells in vitro and in vivo. *Cardiovasc Res*. 2015;107:522-533
111. Chen K, Fan W, Wang X, Ke X, Wu G, Hu C. Microrna-101 mediates the suppressive effect of laminar shear stress on mtor expression in vascular endothelial cells. *Biochem Biophys Res Commun*. 2012;427:138-142
112. Kim JH, Lee KS, Lee DK, Kim J, Kwak SN, Ha KS, Choe J, Won MH, Cho BR, Jeoung D, Lee H, Kwon YG, Kim YM. Hypoxia-responsive microrna-101 promotes

angiogenesis via heme oxygenase-1/vascular endothelial growth factor axis by targeting cullin 3. *Antioxid Redox Signal*. 2014;21:2469-2482
113. Zhang N, Lei J, Lei H, Ruan X, Liu Q, Chen Y, Huang W. Microrna-101 overexpression by il-6 and tnf-alpha inhibits cholesterol efflux by suppressing atp-binding cassette transporter a1 expression. *Experimental cell research*. 2015;336:33-42
114. Wang KC, Garmire LX, Young A, Nguyen P, Trinh A, Subramaniam S, Wang N, Shyy JY, Li YS, Chien S. Role of microrna-23b in flow-regulation of rb phosphorylation and endothelial cell growth. *Proceedings of the National Academy of Sciences of the United States of America*. 2010;107:3234-3239
115. Chen H, Li X, Liu S, Gu L, Zhou X. Mircrorna-19a promotes vascular inflammation and foam cell formation by targeting hbp-1 in atherogenesis. *Sci Rep*. 2017;7:12089
116. Ren ZQ, Liu N, Zhao K. Micro rna-19a suppresses il-10 in peripheral b cells from patients with atherosclerosis. *Cytokine*. 2016;86:86-91
117. Akhtar S, Hartmann P, Karshovska E, Rinderknecht FA, Subramanian P, Gremse F, Grommes J, Jacobs M, Kiessling F, Weber C, Steffens S, Schober A. Endothelial hypoxia-inducible factor-1alpha promotes atherosclerosis and monocyte recruitment by upregulating microrna-19a. *Hypertension*. 2015;66:1220-1226
118. Wu W, Xiao H, Laguna-Fernandez A, Villarreal G, Jr., Wang KC, Geary GG, Zhang Y, Wang WC, Huang HD, Zhou J, Li YS, Chien S, Garcia-Cardena G, Shyy JY. Flow-dependent regulation of kruppel-like factor 2 is mediated by microrna-92a. *Circulation*. 2011;124:633-641
119. Bonauer A, Carmona G, Iwasaki M, Mione M, Koyanagi M, Fischer A, Burchfield J, Fox H, Doebele C, Ohtani K, Chavakis E, Potente M, Tjwa M, Urbich C, Zeiher AM, Dimmeler S. Microrna-92a controls angiogenesis and functional recovery of ischemic tissues in mice. *Science*. 2009;324:1710-1713
120. Fang Y, Davies PF. Site-specific microrna-92a regulation of kruppel-like factors 4 and 2 in atherosusceptible endothelium. *Arterioscler Thromb Vasc Biol*. 2012;32:979-987
121. Loyer X, Potteaux S, Vion AC, Guerin CL, Boulkroun S, Rautou PE, Ramkhelawon B, Esposito B, Dalloz M, Paul JL, Julia P, Maccario J, Boulanger CM, Mallat Z, Tedgui A. Inhibition of microrna-92a prevents endothelial dysfunction and atherosclerosis in mice. *Circ Res*. 2014;114:434-443
122. Hinkel R, Penzkofer D, Zuhlke S, Fischer A, Husada W, Xu QF, Baloch E, van Rooij E, Zeiher AM, Kupatt C, Dimmeler S. Inhibition of microrna-92a protects against ischemia/reperfusion injury in a large-animal model. *Circulation*. 2013;128:1066-1075
123. Ni CW, Qiu H, Jo H. Microrna-663 upregulated by oscillatory shear stress plays a role in inflammatory response of endothelial cells. *Am J Physiol Heart Circ Physiol*. 2011;300:H1762-1769
124. Afonyushkin T, Oskolkova OV, Bochkov VN. Permissive role of mir-663 in induction of vegf and activation of the atf4 branch of unfolded protein response in endothelial cells by oxidized phospholipids. *Atherosclerosis*. 2012;225:50-55
125. Rayner KJ, Esau CC, Hussain FN, McDaniel AL, Marshall SM, van Gils JM, Ray TD, Sheedy FJ, Goedeke L, Liu X, Khatsenko OG, Kaimal V, Lees CJ, Fernandez-Hernando C, Fisher EA, Temel RE, Moore KJ. Inhibition of mir-33a/b in non-human primates raises plasma hdl and lowers vldl triglycerides. *Nature*. 2011;478:404-407

126. Tili E, Michaille JJ, Adair B, Alder H, Limagne E, Taccioli C, Ferracin M, Delmas D, Latruffe N, Croce CM. Resveratrol decreases the levels of mir-155 by upregulating mir-663, a microrna targeting junb and jund. *Carcinogenesis*. 2010;31:1561-1566
127. Sadeghi M, Ranjbar B, Ganjalikhany MR, F MK, Schmitz U, Wolkenhauer O, Gupta SK. Microrna and transcription factor gene regulatory network analysis reveals key regulatory elements associated with prostate cancer progression. *PLoS One*. 2016;11:e0168760
128. Korff T, Pfisterer L, Schorpp-Kistner M. Mir-663 and the miraculous vascular smooth muscle phenotypic switch. *Circ Res*. 2013;113:1102-1105
129. Li P, Zhu N, Yi B, Wang N, Chen M, You X, Zhao X, Solomides CC, Qin Y, Sun J. Microrna-663 regulates human vascular smooth muscle cell phenotypic switch and vascular neointimal formation. *Circ Res*. 2013;113:1117-1127
130. Son DJ, Kumar S, Takabe W, Kim CW, Ni CW, Alberts-Grill N, Jang IH, Kim S, Kim W, Won Kang S, Baker AH, Woong Seo J, Ferrara KW, Jo H. The atypical mechanosensitive microrna-712 derived from pre-ribosomal rna induces endothelial inflammation and atherosclerosis. *Nat Commun*. 2013;4:3000
131. Schober A, Nazari-Jahantigh M, Wei Y, Bidzhekov K, Gremse F, Grommes J, Megens RT, Heyll K, Noels H, Hristov M, Wang S, Kiessling F, Olson EN, Weber C. Microrna-126-5p promotes endothelial proliferation and limits atherosclerosis by suppressing dlk1. *Nature medicine*. 2014;20:368-376
132. Kim CW, Kumar S, Son DJ, Jang IH, Griendling KK, Jo H. Prevention of abdominal aortic aneurysm by anti-microrna-712 or anti-microrna-205 in angiotensin ii-infused mice. *Arterioscler Thromb Vasc Biol*. 2014;34:1412-1421
133. Kheirolomoom A, Kim CW, Seo JW, Kumar S, Son DJ, Gagnon MK, Ingham ES, Ferrara KW, Jo H. Multifunctional nanoparticles facilitate molecular targeting and mirna delivery to inhibit atherosclerosis in apoe(-/-) mice. *ACS Nano*. 2015;9:8885-8897
134. Hergenreider E, Heydt S, Treguer K, Boettger T, Horrevoets AJ, Zeiher AM, Scheffer MP, Frangakis AS, Yin X, Mayr M, Braun T, Urbich C, Boon RA, Dimmeler S. Atheroprotective communication between endothelial cells and smooth muscle cells through mirnas. *Nat Cell Biol*. 2012;14:249-256
135. Weber M, Baker MB, Moore JP, Searles CD. Mir-21 is induced in endothelial cells by shear stress and modulates apoptosis and enos activity. *Biochem Biophys Res Commun*. 2010;393:643-648
136. Zhou J, Wang KC, Wu W, Subramaniam S, Shyy JY, Chiu JJ, Li JY, Chien S. Microrna-21 targets peroxisome proliferators-activated receptor-alpha in an autoregulatory loop to modulate flow-induced endothelial inflammation. *Proceedings of the National Academy of Sciences of the United States of America*. 2011;108:10355-10360
137. Raitoharju E, Lyytikainen LP, Levula M, Oksala N, Mennander A, Tarkka M, Klopp N, Illig T, Kahonen M, Karhunen PJ, Laaksonen R, Lehtimaki T. Mir-21, mir-210, mir-34a, and mir-146a/b are up-regulated in human atherosclerotic plaques in the tampere vascular study. *Atherosclerosis*. 2011;219:211-217
138. Nam D, Ni CW, Rezvan A, Suo J, Budzyn K, Llanos A, Harrison DG, Giddens DP, Jo H. A model of disturbed flow-induced atherosclerosis in mouse carotid artery by partial ligation and a simple method of rna isolation from carotid endothelium. *J Vis Exp*. 2010
139. Li S, Fan Q, He S, Tang T, Liao Y, Xie J. Microrna-21 negatively regulates treg cells through a tgf-beta1/smad-independent pathway in patients with coronary heart disease. *Cell Physiol Biochem*. 2015;37:866-878

140. Kin K, Miyagawa S, Fukushima S, Shirakawa Y, Torikai K, Shimamura K, Daimon T, Kawahara Y, Kuratani T, Sawa Y. Tissue- and plasma-specific microrna signatures for atherosclerotic abdominal aortic aneurysm. *J Am Heart Assoc*. 2012;1:e000745
141. Tsai PC, Liao YC, Wang YS, Lin HF, Lin RT, Juo SH. Serum microrna-21 and microrna-221 as potential biomarkers for cerebrovascular disease. *Journal of vascular research*. 2013;50:346-354
142. Ji R, Cheng Y, Yue J, Yang J, Liu X, Chen H, Dean DB, Zhang C. Microrna expression signature and antisense-mediated depletion reveal an essential role of microrna in vascular neointimal lesion formation. *Circ Res*. 2007;100:1579-1588
143. Harmalkar M, Upraity S, Kazi S, Shirsat NV. Tamoxifen-induced cell death of malignant glioma cells is brought about by oxidative-stress-mediated alterations in the expression of bcl2 family members and is enhanced on mir-21 inhibition. *J Mol Neurosci*. 2015;57:197-202
144. Li Y, Yan L, Zhang W, Wang H, Chen W, Hu N, Ou H. Mir-21 inhibitor suppresses proliferation and migration of nasopharyngeal carcinoma cells through down-regulation of bcl2 expression. *Int J Clin Exp Pathol*. 2014;7:3478-3487
145. Yang Q, Yang K, Li A. Microrna-21 protects against ischemia-reperfusion and hypoxia-reperfusion-induced cardiocyte apoptosis via the phosphatase and tensin homolog/akt-dependent mechanism. *Mol Med Rep*. 2014;9:2213-2220
146. Yang Q, Yang K, Li AY. Trimetazidine protects against hypoxia-reperfusion-induced cardiomyocyte apoptosis by increasing microrna-21 expression. *Int J Clin Exp Pathol*. 2015;8:3735-3741
147. Weber M, Kim S, Patterson N, Rooney K, Searles CD. Mirna-155 targets myosin light chain kinase and modulates actin cytoskeleton organization in endothelial cells. *Am J Physiol Heart Circ Physiol*. 2014;306:H1192-1203
148. Wu XY, Fan WD, Fang R, Wu GF. Regulation of microrna-155 in endothelial inflammation by targeting nuclear factor (nf)-kappab p65. *J Cell Biochem*. 2014;115:1928-1936
149. Donners MM, Wolfs IM, Stoger LJ, van der Vorst EP, Pottgens CC, Heymans S, Schroen B, Gijbels MJ, de Winther MP. Hematopoietic mir155 deficiency enhances atherosclerosis and decreases plaque stability in hyperlipidemic mice. *PLoS One*. 2012;7:e35877
150. Zhu J, Chen T, Yang L, Li Z, Wong MM, Zheng X, Pan X, Zhang L, Yan H. Regulation of microrna-155 in atherosclerotic inflammatory responses by targeting map3k10. *PLoS One*. 2012;7:e46551
151. Nazari-Jahantigh M, Wei Y, Noels H, Akhtar S, Zhou Z, Koenen RR, Heyll K, Gremse F, Kiessling F, Grommes J, Weber C, Schober A. Microrna-155 promotes atherosclerosis by repressing bcl6 in macrophages. *J Clin Invest*. 2012;122:4190-4202
152. Du F, Yu F, Wang Y, Hui Y, Carnevale K, Fu M, Lu H, Fan D. Microrna-155 deficiency results in decreased macrophage inflammation and attenuated atherogenesis in apolipoprotein e-deficient mice. *Arterioscler Thromb Vasc Biol*. 2014;34:759-767
153. Sun HX, Zeng DY, Li RT, Pang RP, Yang H, Hu YL, Zhang Q, Jiang Y, Huang LY, Tang YB, Yan GJ, Zhou JG. Essential role of microrna-155 in regulating endothelium-dependent vasorelaxation by targeting endothelial nitric oxide synthase. *Hypertension*. 2012;60:1407-1414

154. Wang Y, Wang F, Wu Y, Zuo L, Zhang S, Zhou Q, Wei W, Wang Y, Zhu H. Microrna-126 attenuates palmitate-induced apoptosis by targeting traf7 in huvecs. *Mol Cell Biochem*. 2015;399:123-130
155. O'Connell RM, Chaudhuri AA, Rao DS, Baltimore D. Inositol phosphatase ship1 is a primary target of mir-155. *Proceedings of the National Academy of Sciences of the United States of America*. 2009;106:7113-7118
156. Costinean S, Sandhu SK, Pedersen IM, Tili E, Trotta R, Perrotti D, Ciarlariello D, Neviani P, Harb J, Kauffman LR, Shidham A, Croce CM. Src homology 2 domain-containing inositol-5-phosphatase and ccaat enhancer-binding protein beta are targeted by mir-155 in b cells of emicro-mir-155 transgenic mice. *Blood*. 2009;114:1374-1382
157. Tian FJ, An LN, Wang GK, Zhu JQ, Li Q, Zhang YY, Zeng A, Zou J, Zhu RF, Han XS, Shen N, Yang HT, Zhao XX, Huang S, Qin YW, Jing Q. Elevated microrna-155 promotes foam cell formation by targeting hbp1 in atherogenesis. *Cardiovasc Res*. 2014;103:100-110
158. Wei Y, Schober A, Weber C. Pathogenic arterial remodeling: The good and bad of microrna. *Am J Physiol Heart Circ Physiol*. 2013;304:H1050-1059
159. Yan H, Wang S, Li Z, Zhao W, Wang Z, Sun Z, Pan Y, Zhu J. Upregulation of mirna-155 expression by oxldl in dendritic cells involves jak1/2 kinase and transcription factors yy1 and myb. *International journal of molecular medicine*. 2016;37:1371-1378
160. Li X, Kong D, Chen H, Liu S, Hu H, Wu T, Wang J, Chen W, Ning Y, Li Y, Lu Z. Mir-155 acts as an anti-inflammatory factor in atherosclerosis-associated foam cell formation by repressing calcium-regulated heat stable protein 1. *Sci Rep*. 2016;6:21789
161. Dahlman JE, Barnes C, Khan OF, Thiriot A, Jhunjunwala S, Shaw TE, Xing YP, Sager HB, Sahay G, Speciner L, Bader A, Bogorad RL, Yin H, Racie T, Dong YZ, Jiang S, Seedorf D, Dave A, Sandhu KS, Webber MJ, Novobrantseva T, Ruda VM, Lytton-Jean AKR, Levins CG, Kalish B, Mudge DK, Perez M, Abezgauz L, Dutta P, Smith L, Charisse K, Kieran MW, Fitzgerald K, Nahrendorf M, Danino D, Tuder RM, von Andrian UH, Akinc A, Panigrahy D, Schroeder A, Koteliansky V, Langer R, Anderson DG. In vivo endothelial sirna delivery using polymeric nanoparticles with low molecular weight. *Nature Nanotechnology*. 2014;9:648-655
162. Nepal C, Coolen M, Hadzhiev Y, Cussigh D, Mydel P, Steen VM, Carninci P, Andersen JB, Bally-Cuif L, Muller F, Lenhard B. Transcriptional, post-transcriptional and chromatin-associated regulation of pri-mirnas, pre-mirnas and mornas. *Nucleic Acids Res*. 2016;44:3070-3081
163. Dykes IM, Emanueli C. Transcriptional and post-transcriptional gene regulation by long non-coding rna. *Genomics Proteomics Bioinformatics*. 2017;15:177-186
164. Man HSJ, Sukumar AN, Lam GC, Turgeon PJ, Yan MS, Ku KH, Dubinsky MK, Ho JJD, Wang JJ, Das S, Mitchell N, Oettgen P, Sefton MV, Marsden PA. Angiogenic patterning by steel, an endothelial-enriched long noncoding rna. *Proceedings of the National Academy of Sciences of the United States of America*. 2018;115:2401-2406
165. Chen G, Wang Z, Wang D, Qiu C, Liu M, Chen X, Zhang Q, Yan G, Cui Q. Lncrnadisease: A database for long-non-coding rna-associated diseases. *Nucleic Acids Res*. 2013;41:D983-986
166. Maass PG, Luft FC, Bahring S. Long non-coding rna in health and disease. *J Mol Med (Berl)*. 2014;92:337-346

167. Chen SLW, Z.M.; Hu, Z.Y.; Li, B. Genome-wide analysis of differentially expressed long noncoding rnas induced by low shear stress in human umbilical vein endothelial cells. *Integr Mol Med* 2015;2
168. Stanicek L, Lozano-Vidal N, Kwon H-B, Stainier D, Wittig I, Dimmeler S, Boon RA. Abstract 19863: The shear stress-induced human long non-coding rna lassie regulates endothelial cell-cell junctions. *Circulation*. 2017;136:A19863
169. Bell RD, Long X, Lin M, Bergmann JH, Nanda V, Cowan SL, Zhou Q, Han Y, Spector DL, Zheng D, Miano JM. Identification and initial functional characterization of a human vascular cell-enriched long noncoding rna. *Arterioscler Thromb Vasc Biol*. 2014;34:1249-1259
170. Boulberdaa M, Scott E, Ballantyne M, Garcia R, Descamps B, Angelini GD, Brittan M, Hunter A, McBride M, McClure J, Miano JM, Emanueli C, Mills NL, Mountford JC, Baker AH. A role for the long noncoding rna sencr in commitment and function of endothelial cells. *Mol Ther*. 2016;24:978-990
171. Madrigal-Matute J, Martin-Ventura JL, Blanco-Colio LM, Egido J, Michel JB, Meilhac O. Heat-shock proteins in cardiovascular disease. *Adv Clin Chem*. 2011;54:1-43
172. Fichtlscherer S, Zeiher AM, Dimmeler S. Circulating microrna: Biomarkers or mediators of cardiovascular diseases? *Arterioscler Thromb Vasc Biol*. 2011;31:2383-2390
173. Simionescu N, Niculescu LS, Carnuta MG, Sanda GM, Stancu CS, Popescu AC, Popescu MR, Vlad A, Dimulescu DR, Simionescu M, Sima AV. Hyperglycemia determines increased specific microrna levels in sera and hdl of acute coronary syndrome patients and stimulates microrna production in human macrophages. *PLoS One*. 2016;11:e0161201
174. Wang GK, Zhu JQ, Zhang JT, Li Q, Li Y, He J, Qin YW, Jing Q. Circulating microrna: A novel potential biomarker for early diagnosis of acute myocardial infarction in humans. *Eur Heart J*. 2010;31:659-666
175. Li T, Cao H, Zhuang J, Wan J, Guan M, Yu B, Li X, Zhang W. Identification of mir-130a, mir-27b and mir-210 as serum biomarkers for atherosclerosis obliterans. *Clinica chimica acta; international journal of clinical chemistry*. 2011;412:66-70
176. Liu X, Cheng Y, Yang J, Xu L, Zhang C. Cell-specific effects of mir-221/222 in vessels: Molecular mechanism and therapeutic application. *J Mol Cell Cardiol*. 2012;52:245-255
177. Cortez-Dias N, Costa MC, Carrilho-Ferreira P, Silva D, Jorge C, Calisto C, Pessoa T, Robalo Martins S, de Sousa JC, da Silva PC, Fiuza M, Diogo AN, Pinto FJ, Enguita FJ. Circulating mir-122-5p/mir-133b ratio is a specific early prognostic biomarker in acute myocardial infarction. *Circulation journal : official journal of the Japanese Circulation Society*. 2016;80:2183-2191
178. Andersson P, Gidlof O, Braun OO, Gotberg M, van der Pals J, Olde B, Erlinge D. Plasma levels of liver-specific mir-122 is massively increased in a porcine cardiogenic shock model and attenuated by hypothermia. *Shock (Augusta, Ga.)*. 2012;37:234-238
179. Shan K, Jiang Q, Wang XQ, Wang YN, Yang H, Yao MD, Liu C, Li XM, Yao J, Liu B, Zhang YY, J Y, Yan B. Role of long non-coding rna-rncr3 in atherosclerosis-related vascular dysfunction. *Cell Death Dis*. 2016;7:e2248
180. Reiss AB, Vernice NA, Siegart NM, De Leon J, Kasselman LJ. Exosomes in cholesterol metabolism and atherosclerosis. *Cardiovascular & hematological disorders drug targets*. 2017;17:185-194

181. Lu X. The role of exosomes and exosome-derived micrornas in atherosclerosis. *Current pharmaceutical design*. 2017;23:6182-6193
182. Loyer X, Vion AC, Tedgui A, Boulanger CM. Microvesicles as cell-cell messengers in cardiovascular diseases. *Circ Res*. 2014;114:345-353
183. Sohel MH. Extracellular/circulating micrornas: Release mechanisms, functions and challenges. *Achievements in the Life Sciences*. 2016;10:175-186
184. Vickers KC, Palmisano BT, Shoucri BM, Shamburek RD, Remaley AT. Micrornas are transported in plasma and delivered to recipient cells by high-density lipoproteins. *Nat Cell Biol*. 2011;13:423-433
185. Boon RA, Vickers KC. Intercellular transport of micrornas. *Arterioscler Thromb Vasc Biol*. 2013;33:186-192
186. Zernecke A, Bidzhekov K, Noels H, Shagdarsuren E, Gan L, Denecke B, Hristov M, Koppel T, Jahantigh MN, Lutgens E, Wang S, Olson EN, Schober A, Weber C. Delivery of microrna-126 by apoptotic bodies induces cxcl12-dependent vascular protection. *Science signaling*. 2009;2:ra81
187. Huang Y, Tang S, Ji-Yan C, Huang C, Li J, Cai AP, Feng YQ. Circulating mir-92a expression level in patients with essential hypertension: A potential marker of atherosclerosis. *J Hum Hypertens*. 2017;31:200-205
188. Faltejskova P, Bocanek O, Sachlova M, Svoboda M, Kiss I, Vyzula R, Slaby O. Circulating mir-17-3p, mir-29a, mir-92a and mir-135b in serum: Evidence against their usage as biomarkers in colorectal cancer. *Cancer biomarkers : section A of Disease markers*. 2012;12:199-204
189. Li M, Guan X, Sun Y, Mi J, Shu X, Liu F, Li C. Mir-92a family and their target genes in tumorigenesis and metastasis. *Experimental cell research*. 2014;323:1-6
190. Tian M, Ji Y, Wang T, Zhang W, Zhou Y, Cui Y. Changes in circulating microrna-126 levels are associated with immune imbalance in children with acute asthma. *Int J Immunopathol Pharmacol*. 2018;32:2058738418779243
191. Grimolizzi F, Monaco F, Leoni F, Bracci M, Staffolani S, Bersaglieri C, Gaetani S, Valentino M, Amati M, Rubini C, Saccucci F, Neuzil J, Tomasetti M, Santarelli L. Exosomal mir-126 as a circulating biomarker in non-small-cell lung cancer regulating cancer progression. *Sci Rep*. 2017;7:15277
192. Qi J, Wang J, Katayama H, Sen S, Liu SM. Circulating micrornas (cmirnas) as novel potential biomarkers for hepatocellular carcinoma. *Neoplasma*. 2013;60:135-142
193. Wei T, Ye P, Peng X, Wu LL, Yu GY. Prognostic value of mir-222 in various cancers: A systematic review and meta-analysis. *Clinical laboratory*. 2016;62:1387-1395
194. Song J, Ouyang Y, Che J, Li X, Zhao Y, Yang K, Zhao X, Chen Y, Fan C, Yuan W. Potential value of mir-221/222 as diagnostic, prognostic, and therapeutic biomarkers for diseases. *Frontiers in immunology*. 2017;8:56
195. Mirzaei HR, Sahebkar A, Mohammadi M, Yari R, Salehi H, Jafari MH, Namdar A, Khabazian E, Jaafari MR, Mirzaei H. Circulating micrornas in hepatocellular carcinoma: Potential diagnostic and prognostic biomarkers. *Current pharmaceutical design*. 2016;22:5257-5269
196. Fiorino S, Bacchi-Reggiani ML, Visani M, Acquaviva G, Fornelli A, Masetti M, Tura A, Grizzi F, Zanello M, Mastrangelo L, Lombardi R, Di Tommaso L, Bondi A, Sabbatani S, Domanico A, Fabbri C, Leandri P, Pession A, Jovine E, de Biase D. Micrornas as

possible biomarkers for diagnosis and prognosis of hepatitis b- and c-related-hepatocellular-carcinoma. *World journal of gastroenterology*. 2016;22:3907-3936
197. Ding S, Huang H, Xu Y, Zhu H, Zhong C. Mir-222 in cardiovascular diseases: Physiology and pathology. *Biomed Res Int*. 2017;2017:4962426
198. Zhang Z, Gao W, Long QQ, Zhang J, Li YF, Liu DC, Yan JJ, Yang ZJ, Wang LS. Increased plasma levels of lncrna h19 and lipcar are associated with increased risk of coronary artery disease in a chinese population. *Sci Rep*. 2017;7:7491
199. de Gonzalo-Calvo D, Kenneweg F, Bang C, Toro R, van der Meer RW, Rijzewijk LJ, Smit JW, Lamb HJ, Llorente-Cortes V, Thum T. Circulating long-non coding rnas as biomarkers of left ventricular diastolic function and remodelling in patients with well-controlled type 2 diabetes. *Sci Rep*. 2016;6:37354
200. Han D, Gao Q, Cao F. Long noncoding rnas (lncrnas) - the dawning of a new treatment for cardiac hypertrophy and heart failure. *Biochim Biophys Acta*. 2017;1863:2078-2084
201. Meng F, Yan J, Ma Q, Jiao Y, Han L, Xu J, Yang F, Liu J. Expression status and clinical significance of lncrna appat in the progression of atherosclerosis. *PeerJ*. 2018;6:e4246
202. Gangwar RS, Rajagopalan S, Natarajan R, Deiuliis JA. Noncoding rnas in cardiovascular disease: Pathological relevance and emerging role as biomarkers and therapeutics. *Am J Hypertens*. 2018;31:150-165
203. Buhrke A, Bar C, Thum T. [non-coding rna : Innovative regulators with therapeutic perspective]. *Herz*. 2018;43:115-122
204. Bitarafan S, Yari M, Broumand MA, Ghaderian SMH, Rahimi M, Mirfakhraie R, Azizi F, Omrani MD. Association of increased levels of lncrna h19 in pbmcs with risk of coronary artery disease. *Cell J*. 2019;20:564-568
205. Yan Y, Zhang B, Liu N, Qi C, Xiao Y, Tian X, Li T, Liu B. Circulating long noncoding rna uca1 as a novel biomarker of acute myocardial infarction. *Biomed Res Int*. 2016;2016:8079372
206. Viereck J, Thum T. Circulating noncoding rnas as biomarkers of cardiovascular disease and injury. *Circ Res*. 2017;120:381-399
207. Gao L, Liu Y, Guo S, Yao R, Wu L, Xiao L, Wang Z, Liu Y, Zhang Y. Circulating long noncoding rna hotair is an essential mediator of acute myocardial infarction. *Cell Physiol Biochem*. 2017;44:1497-1508
208. Cai Y, Yang Y, Chen X, Wu G, Zhang X, Liu Y, Yu J, Wang X, Fu J, Li C, Jose PA, Zeng C, Zhou L. Circulating 'lncrna otthumt00000387022' from monocytes as a novel biomarker for coronary artery disease. *Cardiovasc Res*. 2016;112:714-724
209. Bazan HA, Hatfield SA, Brug A, Brooks AJ, Lightell DJ, Jr., Woods TC. Carotid plaque rupture is accompanied by an increase in the ratio of serum circr-284 to mir-221 levels. *Circ Cardiovasc Genet*. 2017;10
210. Mitchell AJ, Gray WD, Hayek SS, Ko YA, Thomas S, Rooney K, Awad M, Roback JD, Quyyumi A, Searles CD. Platelets confound the measurement of extracellular mirna in archived plasma. *Sci Rep*. 2016;6:32651
211. Buschmann D, Haberberger A, Kirchner B, Spornraft M, Riedmaier I, Schelling G, Pfaffl MW. Toward reliable biomarker signatures in the age of liquid biopsies - how to standardize the small rna-seq workflow. *Nucleic Acids Res*. 2016;44:5995-6018
212. Zhao W, Zhao SP, Zhao YH. Microrna-143/-145 in cardiovascular diseases. *Biomed Res Int*. 2015;2015:531740

213. Rotllan N, Ramirez CM, Aryal B, Esau CC, Fernandez-Hernando C. Therapeutic silencing of microrna-33 inhibits the progression of atherosclerosis in ldlr-/- mice--brief report. *Arterioscler Thromb Vasc Biol*. 2013;33:1973-1977
214. Horie T, Baba O, Kuwabara Y, Chujo Y, Watanabe S, Kinoshita M, Horiguchi M, Nakamura T, Chonabayashi K, Hishizawa M, Hasegawa K, Kume N, Yokode M, Kita T, Kimura T, Ono K. Microrna-33 deficiency reduces the progression of atherosclerotic plaque in apoe-/- mice. *J Am Heart Assoc*. 2012;1:e003376
215. Ling H. Non-coding rnas: Therapeutic strategies and delivery systems. *Advances in experimental medicine and biology*. 2016;937:229-237
216. Chakraborty C, Sharma AR, Sharma G, Doss CGP, Lee SS. Therapeutic mirna and sirna: Moving from bench to clinic as next generation medicine. *Molecular therapy. Nucleic acids*. 2017;8:132-143
217. Bernardo BC, Ooi JY, Lin RC, McMullen JR. Mirna therapeutics: A new class of drugs with potential therapeutic applications in the heart. *Future medicinal chemistry*. 2015;7:1771-1792
218. Aryal B, Suarez Y. Non-coding rna regulation of endothelial and macrophage functions during atherosclerosis. *Vascul Pharmacol*. 2018
219. Deng L, Bradshaw AC, Baker AH. Role of noncoding rna in vascular remodelling. *Curr Opin Lipidol*. 2016;27:439-448
220. Gomes CPC, Spencer H, Ford KL, Michel LYM, Baker AH, Emanueli C, Balligand JL, Devaux Y, Cardiolinc n. The function and therapeutic potential of long non-coding rnas in cardiovascular development and disease. *Molecular therapy. Nucleic acids*. 2017;8:494-507
221. Hartmann P, Zhou Z, Natarelli L, Wei Y, Nazari-Jahantigh M, Zhu M, Grommes J, Steffens S, Weber C, Schober A. Endothelial dicer promotes atherosclerosis and vascular inflammation by mirna-103-mediated suppression of klf4. *Nat Commun*. 2016;7:10521
222. Emini Veseli B, Perrotta P, De Meyer GRA, Roth L, Van der Donckt C, Martinet W, De Meyer GRY. Animal models of atherosclerosis. *Eur. J. Pharmacol.* 2017;816:3-13
223. Getz GS, Reardon CA. Animal models of atherosclerosis. *Arterioscler. Thromb. Vasc. Biol.* 2012;32:1104-1115
224. Resnick N, Cimbrone Jr MA. Hemodynamic forces are complex regulators of endothelial gene expression. *The FASEB Journal*. 1995;9:874-882
225. Dewey CF, Jr., Bussolari SR, Gimbrone MA, Jr., Davies PF. The dynamic response of vascular endothelial cells to fluid shear stress. *J. Biomech. Eng.* 1981;103:177-185
226. Bussolari SR, Dewey CF, Jr., Gimbrone MA, Jr. Apparatus for subjecting living cells to fluid shear stress. *Rev. Sci. Instrum.* 1982;53:1851-1854
227. Franke RP, Gräfe M, Schnittler H, Seiffge D, Mittermayer C, Drenckhahn D. Induction of human vascular endothelial stress fibres by fluid shear stress. *Nature*. 1984;307:648-649
228. Go YM, Boo YC, Park H, Maland MC, Patel R, Pritchard KA, Jr., Fujio Y, Walsh K, Darley-Usmar V, Jo H. Protein kinase b/akt activates c-jun nh(2)-terminal kinase by increasing no production in response to shear stress. *J Appl Physiol (1985)*. 2001;91:1574-1581
229. Frangos JA, McIntire LV, Eskin SG. Shear stress induced stimulation of mammalian cell metabolism. *Biotechnol. Bioeng.* 1988;32:1053-1060

230. Frangos JA, Eskin SG, McIntire LV, Ives CL. Flow effects on prostacyclin production by cultured human endothelial cells. *Science*. 1985;227:1477-1479
231. Schaff UY, Xing MM, Lin KK, Pan N, Jeon NL, Simon SI. Vascular mimetics based on microfluidics for imaging the leukocyte–endothelial inflammatory response. *Lab on a Chip*. 2007;7:448-456
232. Ashpole NE, Overby DR, Ethier CR, Stamer WD. Shear stress-triggered nitric oxide release from schlemm's canal cells. *Invest. Ophthalmol. Vis. Sci.* 2014;55:8067-8076
233. Ganguly A, Zhang H, Sharma R, Parsons S, Patel KD. Isolation of human umbilical vein endothelial cells and their use in the study of neutrophil transmigration under flow conditions. *JoVE (Journal of Visualized Experiments)*. 2012:e4032
234. Sotiropoulou G, Pampalakis G, Diamandis EP. Functional roles of human kallikrein-related peptidases. *J. Biol. Chem.* 2009;284:32989-32994
235. Pavlopoulou A, Pampalakis G, Michalopoulos I, Sotiropoulou G. Evolutionary history of tissue kallikreins. *PLoS One*. 2010;5:e13781
236. Koumandou VL, Scorilas A. Evolution of the plasma and tissue kallikreins, and their alternative splicing isoforms. *PLoS One*. 2013;8:e68074-e68074
237. Prassas I, Eissa A, Poda G, Diamandis EP. Unleashing the therapeutic potential of human kallikrein-related serine proteases. *Nat Rev Drug Discov*. 2015;14:183-202
238. Clements J, Mukhtar A. Glandular kallikreins and prostate-specific antigen are expressed in the human endometrium. *The Journal of Clinical Endocrinology & Metabolism*. 1994;78:1536-1539
239. Emami N, Diamandis EP. Utility of kallikrein-related peptidases (klks) as cancer biomarkers. *Clin. Chem.* 2008;54:1600-1607
240. Schmitt M, Magdolen V, Yang F, Kiechle M, Bayani J, Yousef GM, Scorilas A, Diamandis EP, Dorn J. Emerging clinical importance of the cancer biomarkers kallikrein-related peptidases (klk) in female and male reproductive organ malignancies. *Radiology and oncology*. 2013;47:319
241. Diamandis EP, Yousef GM, Clements J, Ashworth LK, Yoshida S, Egelrud T, Nelson PS, Shiosaka S, Little S, Lilja H, Stenman UH, Rittenhouse HG, Wain H. New nomenclature for the human tissue kallikrein gene family. *Clin Chem*. 2000;46:1855-1858
242. Goyal J, Smith KM, Cowan JM, Wazer DE, Lee SW, Band V. The role for nes1 serine protease as a novel tumor suppressor. *Cancer Res.* 1998;58:4782-4786
243. Liu X-L, Wazer DE, Watanabe K, Band V. Identification of a novel serine protease-like gene, the expression of which is down-regulated during breast cancer progression. *Cancer Res.* 1996;56:3371-3379
244. Hu J, Lei H, Fei X, Liang S, Xu H, Qin D, Wang Y, Wu Y, Li B. Nes1/klk10 gene represses proliferation, enhances apoptosis and down-regulates glucose metabolism of pc3 prostate cancer cells. *Sci. Rep.* 2015;5:17426
245. Luo LY, Rajpert-De Meyts ER, Jung K, Diamandis EP. Expression of the normal epithelial cell-specific 1 (nes1; klk10) candidate tumour suppressor gene in normal and malignant testicular tissue. *Br J Cancer*. 2001;85:220-224
246. Zhang Y, Song H, Miao Y, Wang R, Chen L. Frequent transcriptional inactivation of kallikrein 10 gene by cpg island hypermethylation in non-small cell lung cancer. *Cancer Sci.* 2010;101:934-940

247. Luo L-Y, Katsaros D, Scorilas A, Fracchioli S, Bellino R, van Gramberen M, de Bruijn H, Henrik A, Stenman U-H, Massobrio M, van der Zee AGJ, Vergote I, Diamandis EP. The serum concentration of human kallikrein 10 represents a novel biomarker for ovarian cancer diagnosis and prognosis. *Cancer Res.* 2003;63:807-811
248. Yousef GM, White NM, Michael IP, Cho JC, Robb JD, Kurlender L, Khan S, Diamandis EP. Identification of new splice variants and differential expression of the human kallikrein 10 gene, a candidate cancer biomarker. *Tumour Biol.* 2005;26:227-235
249. Dorn J, Bayani J, Yousef GM, Yang F, Magdolen V, Kiechle M, Diamandis EP, Schmitt M. Clinical utility of kallikrein-related peptidases (klk) in urogenital malignancies. *Thromb. Haemost.* 2013;110:408-422
250. Tailor PD, Kodeboyina SK, Bai S, Patel N, Sharma S, Ratnani A, Copland JA, She J-X, Sharma A. Diagnostic and prognostic biomarker potential of kallikrein family genes in different cancer types. *Oncotarget*. 2018;9
251. Sidiropoulos M, Pampalakis G, Sotiropoulou G, Katsaros D, Diamandis EP. Downregulation of human kallikrein 10 (klk10/nes1) by cpg island hypermethylation in breast, ovarian and prostate cancers. *Tumour Biol*. 2005;26:324-336
252. Bharaj BB, Luo LY, Jung K, Stephan C, Diamandis EP. Identification of single nucleotide polymorphisms in the human kallikrein 10 (klk10) gene and their association with prostate, breast, testicular, and ovarian cancers. *The Prostate*. 2002;51:35-41
253. Dominek P, Campagnolo P, H-zadeh M, Kränkel N, Chilosi M, Sharman J, Caporali A, Mangialardi G, Spinetti G, Emanueli C. Role of human tissue kallikrein in gastrointestinal stromal tumour invasion. *Br. J. Cancer*. 2010;103:1422-1431
254. Stone OA, Richer C, Emanueli C, Van Weel V, Quax PH, Katare R, Kraenkel N, Campagnolo P, Barcelos LS, Siragusa M. Critical role of tissue kallikrein in vessel formation and maturation: Implications for therapeutic revascularization. *Arterioscler. Thromb. Vasc. Biol.* 2009;29:657-664
255. Borgoño CA, Diamandis EP. The emerging roles of human tissue kallikreins in cancer. *Nature Reviews Cancer*. 2004;4:876-890
256. Kryza T, Achard C, Parent C, Marchand-Adam S, Guillon-Munos A, Iochmann S, Korkmaz B, Respaud R, Courty Y, Heuzé-Vourc'h N. Angiogenesis stimulated by human kallikrein-related peptidase 12 acting via a platelet-derived growth factor b-dependent paracrine pathway. *The FASEB Journal*. 2014;28:740-751
257. Yousef GM, Diamandis EP. An overview of the kallikrein gene families in humans and other species: Emerging candidate tumour markers. *Clin. Biochem.* 2003;36:443-452
258. Yoon H, Laxmikanthan G, Lee J, Blaber SI, Rodriguez A, Kogot JM, Scarisbrick IA, Blaber M. Activation profiles and regulatory cascades of the human kallikrein-related peptidases. *J. Biol. Chem.* 2007;282:31852-31864
259. Yoon H, Blaber SI, Debela M, Goettig P, Scarisbrick IA, Blaber M. A completed klk activome profile: Investigation of activation profiles of klk9, 10, and 15. *Biol. Chem.* 2009;390:373-377
260. Debela M, Magdolen V, Schechter N, Valachova M, Lottspeich F, Craik CS, Choe Y, Bode W, Goettig P. Specificity profiling of seven human tissue kallikreins reveals individual subsite preferences*. *J. Biol. Chem.* 2006;281:25678-25688
261. Goettig P, Magdolen V, Brandstetter H. Natural and synthetic inhibitors of kallikrein-related peptidases (klks). *Biochimie*. 2010;92:1546-1567

262. Luo LY, Soosaipillai A, Grass L, Diamandis EP. Characterization of human kallikreins 6 and 10 in ascites fluid from ovarian cancer patients. *Tumor Biology*. 2006;27:227-234
263. Zhang Y, Bhat I, Zeng M, Jayal G, Wazer DE, Band H, Band V. Human kallikrein 10, a predictive marker for breast cancer. 2006
264. LeBeau AM, Singh P, Isaacs JT, Denmeade SR. Potent and selective peptidyl boronic acid inhibitors of the serine protease prostate-specific antigen. *Chem. Biol.* 2008;15:665-674
265. LeBeau AM, Banerjee SR, Pomper MG, Mease RC, Denmeade SR. Optimization of peptide-based inhibitors of prostate-specific antigen (psa) as targeted imaging agents for prostate cancer. *Bioorg. Med. Chem.* 2009;17:4888-4893
266. Evans DM, Jones DM, Pitt GR, Ashworth D, De Clerck F, Verheyen F, Szelke M. Synthetic inhibitors of human tissue kallikrein. *Immunopharmacology*. 1996;32:117-118
267. Debela M, Magdolen V, Bode W, Brandstetter H, Goettig P. Structural basis for the zn2+ inhibition of the zymogen-like kallikrein-related peptidase 10. *Biol. Chem.* 2016;397:1251-1264
268. Ni CW, Kumar S, Ankeny CJ, Jo H. Development of immortalized mouse aortic endothelial cell lines. *Vasc Cell*. 2014;6:7
269. Alberts-Grill N, Rezvan A, Son DJ, Qiu H, Kim CW, Kemp ML, Weyand CM, Jo H. Dynamic immune cell accumulation during flow-induced atherogenesis in mouse carotid artery: An expanded flow cytometry method. *Arterioscler Thromb Vasc Biol*. 2012;32:623-632
270. Rezvan A, Ni CW, Alberts-Grill N, Jo H. Animal, in vitro, and ex vivo models of flow-dependent atherosclerosis: Role of oxidative stress. *Antioxid Redox Signal*. 2011;15:1433-1448
271. Li L, Chen W, Rezvan A, Jo H, Harrison DG. Tetrahydrobiopterin deficiency and nitric oxide synthase uncoupling contribute to atherosclerosis induced by disturbed flow. *Arterioscler Thromb Vasc Biol*. 2011;31:1547-1554
272. Li L, Rezvan A, Salerno JC, Husain A, Kwon K, Jo H, Harrison DG, Chen W. Gtp cyclohydrolase i phosphorylation and interaction with gtp cyclohydrolase feedback regulatory protein provide novel regulation of endothelial tetrahydrobiopterin and nitric oxide. *Circ Res*. 2010;106:328-336
273. Ranieri VM, Thompson BT, Barie PS, Dhainaut J-F, Douglas IS, Finfer S, Gårdlund B, Marshall JC, Rhodes A, Artigas A, Payen D, Tenhunen J, Al-Khalidi HR, Thompson V, Janes J, Macias WL, Vangerow B, Williams MD. Drotrecogin alfa (activated) in adults with septic shock. *New England Journal of Medicine*. 2012;366:2055-2064
274. Griffin JH, Mosnier LO, Fernandez JA, Zlokovic BV. 2016 scientific sessions sol sherry distinguished lecturer in thrombosis: Thrombotic stroke: Neuroprotective therapy by recombinant-activated protein c. *Arterioscler Thromb Vasc Biol*. 2016;36:2143-2151
275. Griffin JH, Zlokovic BV, Mosnier LO. Activated protein c: Biased for translation. *Blood*. 2015;125:2898-2907
276. Mosnier LO, Sinha RK, Burnier L, Bouwens EA, Griffin JH. Biased agonism of protease-activated receptor 1 by activated protein c caused by noncanonical cleavage at arg46. *Blood*. 2012;120:5237-5246
277. Kumar S, Kang D-W, Rezvan A, Jo H. Accelerated atherosclerosis development in c57bl6 mice by overexpressing aav-mediated pcsk9 and partial carotid ligation. *Lab Invest*. 2017;97:935-945

278. Ni C-W, Qiu H, Jo H. Microrna-663 upregulated by oscillatory shear stress plays a role in inflammatory response of endothelial cells. *American Journal of Physiology-Heart and Circulatory Physiology*. 2011;300:H1762-H1769
279. Chang K, Weiss D, Suo J, Vega JD, Giddens D, Taylor WR, Jo H. Bone morphogenic protein antagonists are coexpressed with bone morphogenic protein 4 in endothelial cells exposed to unstable flow in vitro in mouse aortas and in human coronary arteries. *Circulation*. 2007;116:1258-1266
280. Kim CW, Song H, Kumar S, Nam D, Kwon HS, Chang KH, Son DJ, Kang D-W, Brodie SA, Weiss D, Vega JD, Alberts-Grill N, Griendling K, Taylor WR, Jo H. Anti-inflammatory and antiatherogenic role of bmp receptor ii in endothelial cells. *Arterioscler. Thromb. Vasc. Biol.* 2013;33:1350-1359
281. Tressel SL, Huang RP, Tomsen N, Jo H. Laminar shear inhibits tubule formation and migration of endothelial cells by an angiopoietin-2 dependent mechanism. *Arterioscler Thromb Vasc Biol*. 2007;27:2150-2156
282. Alberts-Grill N, Rezvan A, Son DJ, Qiu H, Kim CW, Kemp ML, Weyand CM, Jo H. Dynamic immune cell accumulation during flow-induced atherogenesis in mouse carotid artery: An expanded flow cytometry method. *Arteriosclerosis, thrombosis, and vascular biology*. 2012;32:623-632
283. Dubrovskyi O, Birukova AA, Birukov KG. Measurement of local permeability at subcellular level in cell models of agonist- and ventilator-induced lung injury. *Laboratory investigation; a journal of technical methods and pathology*. 2013;93:254-263
284. Liu R, Tang J, Xu Y, Dai Z. Bioluminescence imaging of inflammation in vivo based on bioluminescence and fluorescence resonance energy transfer using nanobubble ultrasound contrast agent. *ACS Nano*. 2019;13:5124-5132
285. Borden MA, Kruse DE, Caskey CF, Zhao S, Dayton PA, Ferrara KW. Influence of lipid shell physicochemical properties on ultrasound-induced microbubble destruction. *IEEE Trans Ultrason Ferroelectr Freq Control*. 2005;52:1992-2002
286. Shapiro G, Wong AW, Bez M, Yang F, Tam S, Even L, Sheyn D, Ben-David S, Tawackoli W, Pelled G, Ferrara KW, Gazit D. Multiparameter evaluation of in vivo gene delivery using ultrasound-guided, microbubble-enhanced sonoporation. *J Control Release*. 2016;223:157-164
287. Schägger H. Tricine–sds-page. *Nat. Protoc.* 2006;1:16-22
288. Rana S, Yang L, Hassanian SM, Rezaie AR. Determinants of the specificity of protease-activated receptors 1 and 2 signaling by factor xa and thrombin. *J Cell Biochem*. 2012;113:977-984
289. Mosnier LO, Sinha RK, Burnier L, Bouwens EA, Griffin JH. Biased agonism of protease-activated receptor 1 by activated protein c caused by noncanonical cleavage at arg46. *Blood*. 2012;120:5237-5246
290. Bae JS, Yang L, Rezaie AR. Lipid raft localization regulates the cleavage specificity of protease activated receptor 1 in endothelial cells. *J. Thromb. Haemost.* 2008;6:954-961
291. Frei AP, Moest H, Novy K, Wollscheid B. Ligand-based receptor identification on living cells and tissues using triceps. *Nat. Protoc.* 2013;8:1321-1336
292. Wingo TS, Duong DM, Zhou M, Dammer EB, Wu H, Cutler DJ, Lah JJ, Levey AI, Seyfried NT. Integrating next-generation genomic sequencing and mass spectrometry to estimate allele-specific protein abundance in human brain. *J. Proteome Res.* 2017;16:3336-3347

293. Kalluri AS, Vellarikkal SK, Edelman ER, Nguyen L, Subramanian A, Ellinor PT, Regev A, Kathiresan S, Gupta RM. Single-cell analysis of the normal mouse aorta reveals functionally distinct endothelial cell populations. *Circulation*. 2019;140:147-163
294. Sangwung P, Zhou G, Nayak L, Chan ER, Kumar S, Kang DW, Zhang R, Liao X, Lu Y, Sugi K, Fujioka H, Shi H, Lapping SD, Ghosh CC, Higgins SJ, Parikh SM, Jo H, Jain MK. Klf2 and klf4 control endothelial identity and vascular integrity. *JCI Insight*. 2017;2:e91700
295. Mestas J, Ley K. Monocyte-endothelial cell interactions in the development of atherosclerosis. *Trends Cardiovasc. Med.* 2008;18:228-232
296. Yoon CS, Park JH. Ultrasound-mediated gene delivery. *Expert Opin Drug Deliv*. 2010;7:321-330
297. Tomizawa M, Shinozaki F, Motoyoshi Y, Sugiyama T, Yamamoto S, Sueishi M. Sonoporation: Gene transfer using ultrasound. *World J Methodol*. 2013;3:39-44
298. Liu Z, Chen O, Wall JBJ, Zheng M, Zhou Y, Wang L, Ruth Vaseghi H, Qian L, Liu J. Systematic comparison of 2a peptides for cloning multi-genes in a polycistronic vector. *Sci. Rep.* 2017;7:2193
299. Wurm FM. Production of recombinant protein therapeutics in cultivated mammalian cells. *Nat. Biotechnol.* 2004;22:1393-1398
300. Newman CMH, Bettinger T. Gene therapy progress and prospects: Ultrasound for gene transfer. *Gene Ther.* 2007;14:465-475
301. Oikonomopoulou K, Hansen KK, Saifeddine M, Tea I, Blaber M, Blaber SI, Scarisbrick I, Andrade-Gordon P, Cottrell GS, Bunnett NW, Diamandis EP, Hollenberg MD. Proteinase-activated receptors, targets for kallikrein signaling. *J Biol Chem*. 2006;281:32095-32112
302. Oikonomopoulou K, Hansen KK, Saifeddine M, Vergnolle N, Tea I, Blaber M, Blaber SI, Scarisbrick I, Diamandis EP, Hollenberg MD. Kallikrein-mediated cell signalling: Targeting proteinase-activated receptors (pars). *Biol Chem*. 2006;387:817-824
303. Di Serio C, Pellerito S, Duarte M, Massi D, Naldini A, Cirino G, Prudovsky I, Santucci M, Geppetti P, Marchionni N, Masotti G, Tarantini F. Protease-activated receptor 1-selective antagonist sch79797 inhibits cell proliferation and induces apoptosis by a protease-activated receptor 1-independent mechanism. *Basic Clin. Pharmacol. Toxicol.* 2007;101:63-69
304. Sonin DL, Wakatsuki T, Routhu KV, Harmann LM, Petersen M, Meyer J, Strande JL. Protease-activated receptor 1 inhibition by sch79797 attenuates left ventricular remodeling and profibrotic activities of cardiac fibroblasts. *J. Cardiovasc. Pharmacol. Ther.* 2013;18:460-475
305. Hollenberg MD, Hooper JD, Darmoul D, Oikonomopoulou K. Volume 1 characterization, regulation, and interactions within the protease web: Characterization, regulation, and interactions within the protease web. In: Viktor M, Christian PS, Hans F, Manfred S, eds. *15 kallikrein-related peptidases (klks), proteinase-mediated signaling and proteinase-activated receptors (pars):*. De Gruyter; 2012:373-398.
306. Coughlin SR. Protease-activated receptors in hemostasis, thrombosis and vascular biology. *J Thromb Haemost*. 2005;3:1800-1814
307. Coughlin SR. Thrombin signalling and protease-activated receptors. *Nature*. 2000;407:258-264

308. Frei AP, Jeon O-Y, Kilcher S, Moest H, Henning LM, Jost C, Plückthun A, Mercer J, Aebersold R, Carreira EM. Direct identification of ligand-receptor interactions on living cells and tissues. *Nat. Biotechnol.* 2012;30:997
309. Hara K, Shiga A, Fukutake T, Nozaki H, Miyashita A, Yokoseki A, Kawata H, Koyama A, Arima K, Takahashi T, Ikeda M, Shiota H, Tamura M, Shimoe Y, Hirayama M, Arisato T, Yanagawa S, Tanaka A, Nakano I, Ikeda S-i, Yoshida Y, Yamamoto T, Ikeuchi T, Kuwano R, Nishizawa M, Tsuji S, Onodera O. Association of htra1 mutations and familial ischemic cerebral small-vessel disease. *N. Engl. J. Med.* 2009;360:1729-1739
310. Launay S, Maubert E, Lebeurrier N, Tennstaedt A, Campioni M, Docagne F, Gabriel C, Dauphinot L, Potier MC, Ehrmann M, Baldi A, Vivien D. Htra1-dependent proteolysis of tgf-beta controls both neuronal maturation and developmental survival. *Cell Death Differ.* 2008;15:1408-1416
311. Yang Z, Camp NJ, Sun H, Tong Z, Gibbs D, Cameron DJ, Chen H, Zhao Y, Pearson E, Li X, Chien J, Dewan A, Harmon J, Bernstein PS, Shridhar V, Zabriskie NA, Hoh J, Howes K, Zhang K. A variant of the htra1 gene increases susceptibility to age-related macular degeneration. *Science*. 2006;314:992-993
312. Lin MK, Yang J, Hsu CW, Gore A, Bassuk AG, Brown LM, Colligan R, Sengillo JD, Mahajan VB, Tsang SH. Htra1, an age-related macular degeneration protease, processes extracellular matrix proteins efemp1 and tsp1. *Aging Cell*. 2018;17:e12710-e12710
313. Chen CY, Melo E, Jakob P, Friedlein A, Elsässer B, Goettig P, Kueppers V, Delobel F, Stucki C, Dunkley T, Fauser S, Schilling O, Iacone R. N-terminomics identifies htra1 cleavage of thrombospondin-1 with generation of a proangiogenic fragment in the polarized retinal pigment epithelial cell model of age-related macular degeneration. *Matrix Biol.* 2018;70:84-101
314. Jiang J, Huang L, Yu W, Wu X, Zhou P, Li X. Overexpression of htra1 leads to down-regulation of fibronectin and functional changes in rf/6a cells and huvecs. *PLoS One*. 2012;7:e46115-e46115
315. Oka C, Tsujimoto R, Kajikawa M, Koshiba-Takeuchi K, Ina J, Yano M, Tsuchiya A, Ueta Y, Soma A, Kanda H, Matsumoto M, Kawaichi M. Htra1 serine protease inhibits signaling mediated by tgfbeta family proteins. *Development*. 2004;131:1041-1053
316. Oikonomopoulou K, Batruch I, Smith CR, Soosaipillai A, Diamandis EP, Hollenberg MD. Functional proteomics of kallikrein-related peptidases in ovarian cancer ascites fluid. *Biol. Chem.* 2010;391:381-390